Analysis and Synthesis of Wire Antennas

B. D. Popović, M. B. Dragović
and A. R. Djordjević

RESEARCH STUDIES PRESS

Analysis and Synthesis of Wire Antennas

ELECTRONIC & ELECTRICAL ENGINEERING RESEARCH STUDIES

ANTENNAS SERIES

Series Editor: **Professor J. R. James**
The Royal Military College of Science, Shrivenham, Wiltshire, England

1. Flat Radiating Dipoles and Applications to Arrays
   G. Dubost

2. Analysis and Synthesis of Wire Antennas
   B. D. Popović, M. B. Dragović *and* **A. R. Djordjević**

Analysis and Synthesis of Wire Antennas

B. D. Popović, M. B. Dragović *and* **A. R. Djordjević**

Department of Electrical Engineering,
University of Belgrade, Yugoslavia

RESEARCH STUDIES PRESS
A DIVISION OF JOHN WILEY & SONS LTD
Chichester · New York · Brisbane · Toronto · Singapore

RESEARCH STUDIES PRESS

Editorial Office:
58B Station Road, Letchworth, Herts. SG6 3BE, England.

Library of Congress Cataloging in Publication Data:

Popović, Branko D.
Analysis and synthesis of wire-antennas.
(Research studies on antennas series; 2)
Includes index.
1. Antennas (Electronics)
I. Dragović, M. B. II. Djordjević, A. R. III. Title
IV. Series
TK7871.6.P68 1982 621.38'.0283 82-11078
ISBN 0 471 90008 7

British Library Cataloguing in Publication Data:

Popvić, B. D.
Analysis and synthesis of wire antennas.
—(Research studies on antennas series; 2)
1. Antennas (Electronics)
I. Title II. Dragović, M. B. III. Djordjević A. R.
IV. Series 621.3841'1 TK656.A6

ISBN 0 471 90008 7

Printed in Great Britain

Editorial Preface

Wire dipole antennas and arrays have been extensively analysed for nearly a century yet a gulf has existed up until recently between the theory and practice. This came about because the exact theories could only be applied to the idealised geometries of dipoles and monopoles while engineering applications embraced a multitude of radiating wire configurations. The advent of computers promised to bridge this gulf since, in principle, the numerical methods enable engineers to calculate any arbitrarily shaped wire radiator. This has not always been achieved because computational techniques can introduce additional problems which obscure the value of computers as a design tool for engineers. In contrast, this present monograph presents the reader with an exhaustive computational treatment of wire antennas in their widest sense and clearly demonstrates the excellent results that can be obtained both by the numerical analysis and the synthesis of such radiating structures. A particularly interesting feature is the use of almost-entire domain polynomial representations of current instead of various subdomain basis function representations used elsewhere. Apart from the advantages of computational economy it does question the need for more complicated methods. The attention paid to the excitation region behaviour and the careful construction of practical antennas are some of the many notable aspects of the book that exhibit the sound physical appreciation the authors have for their research. Professor Popović and his colleagues have a high international reputation for their contributions to engineering electromagnetics and this book is a

culmination of many years of research. The text characteristically lays bare the essential details in an economic yet lucid manner and will appeal to postgraduates, research scientists and engineers alike, establishing beyond doubt that wire antennas can be designed by computer with confidence.

April 1982 *J. R. JAMES*

Preface

Thin-wire antennas, or similar antenna structures, were essentially the only antennas used for radio-communication purposes from the discovery of electromagnetic radiation by H. Hertz in 1887 until about the mid-thirties. At that time, utilization of higher frequencies made possible the design of other antenna types of practically acceptable sizes. However, wire antennas have remained in a wide use until today.

Analysis of wire antennas was first based on a sinusoidal approximation of current distribution along the wires. This approximation is known to predict fairly accurately the antenna radiation pattern, but it is usually quite insufficient for accurate determination of the antenna impedance. Although an integral equation for the current distribution along cylindrical wire dipoles was derived by H. E. Pocklington as early as in 1897,[1] a more accurate current distribution than sinusoidal along such dipoles was first obtained by E. Hallén in 1937,[2] who calculated a few terms of a series solution to another integral equation for current distribution along cylindrical antennas, which bears his name. R. W. P. King added considerably to our knowledge of wire antennas following, largely, Hallén's basic approach, culminating in his classical monograph in 1956.[3] About a decade later, wide usage of high-speed digital computers changed radically the methods of wire-antenna analysis. In addition, it opened the door for recent computer-aided design (synthesis) of such antennas by means of optimization

[1] The numbers refer to the List of References at the end of the monograph.

methods. At the present time, with adequate precautions and clear insight into the physical and numerical aspects of the problem, computer-aided analysis and synthesis of wire-antenna structures of electrically moderate sizes can be so accurate that experimental verification of the results thus obtained can almost be regarded more as a matter of custom than of necessity. Nevertheless, these powerful modern methods for analysis and synthesis of wire-antenna structures do not seem to be widely accepted and recognized by antenna design engineers. This is due, at least partly, to the fact that the modern ideas and numerical techniques underlying the analysis and, in particular, synthesis of wire-antenna structures are for the most part still to be found in the periodical literature. The present monograph, in which certain modern methods for wire-antenna analysis and synthesis are presented concisely and with the needs of design engineers and university educators in mind, is intended to fill this gap to some extent.

Essentially, the monograph represents a summary of over-a-decade long research activity on wire-antenna analysis and design at the University of Belgrade, Yugoslavia. The aim adopted in the very beginning was to develop accurate, but conceptually and computationally simple methods for analysis and, in the final stage, synthesis of general wire-antenna structures. It could be said that the aim has been largely reached, because in practically all cases which were considered the theoretical results were found to be in excellent agreement with experimental results, almost within the limits of experimental error. The principal objective of this monograph is to present, in an orderly and compact manner, the main results obtained at the University of Belgrade concerning the analysis and synthesis of diverse wire-antenna structures. Almost no attempt was made to present, discuss, compare and evaluate various methods for solving the wire-antenna problem proposed by other authors; that would have been a task of exceptional complexity. However, considerable care was exercised to make the monograph as self-contained and complete as possible.

Although some aspects of wire-antenna structures are not treated in the monograph explicitly (e.g., general wire-antenna arrays, antennas

made of circular wires with abrupt change in diameter, or of non-circular wires, etc.), most of them can be analysed and/or synthesized using the simple and accurate theory presented in the book with relatively little additional effort. On the other hand, many useful theoretical and experimental results (most often, coupled to each other) are presented throughout the monograph, as well as some practical data for design engineers, e.g., accurate graphs of conductance and susceptance of vertical monopole antennas above conducting ground plane driven by coaxial lines of various sizes (Appendix 5) and of unattenuated electric-field intensity of such antennas versus radiated power, their thickness and height (Appendix 6). It is believed, therefore, that the book might be of equal value to university professors, design engineers and graduate students interested in wire-antenna structures.

The monograph is divided into two parts: antenna analysis and antenna synthesis. The first part is devoted to the numerical determination of current distribution along various unloaded and loaded wire antennas in a vacuum or in homogeneous and inhomogeneous dielectric media (in general, lossy), and to the analysis of excitation regions and of wire junctions and ends. The second part constitutes an introduction to modern computer-aided design of wire-antenna structures by means of optimization methods.

Although much of the material, as presented, has not been published, a substantial part of the monograph was written by adapting, to a larger or smaller extent, articles published by the authors over the years in various journals and conference proceedings. In connection with this, the authors wish to express their sincere gratitude to the Institution of Electrical Engineers for permission to use the material published in the *Proceedings IEE* and in *Electronics Letters*, to the Institution of Electronic and Radio Engineers for permission to use the material published in *The Radio and Electronic Engineer*, and to Springer-Verlag for permission to use the material published in the *Archiv für Elektrotechnik*.

During the years of work which made this monograph possible, the authors had a permanent support from the Department of Electrical

Engineering of the Belgrade University, in the form of free use of computer, laboratory, workshop and other facilities. A part of the program was also supported by the Serbian Academy of Sciences and Arts and by the Serbian Research Foundation. Several faculty members at the Department participated in the project in one way or another, contributing greatly to a cheerful and stimulating working atmosphere. In this respect the authors are particularly indebted to Dr Dj. S. Paunović, an active member of the antenna group, for his cooperation in solving several problems, and to Professor A. S. Marinčić, for his permanent interest in the project and in the progress of this monograph. The larger part of the experimental results presented in the monograph were obtained by patient and reliable work of a number of the authors' students, and most of the antenna models and special parts of the measuring equipment were expertly made by the staff of the workshop of the Department.

The monograph was written during the stay of one of the authors (B.D.P.) as Visiting Professor at Virginia Polytechnic Institute and State University, Blacksburg, Virginia. The creative atmosphere at VPI & SU and, in particular, the understanding of Professors D. B. Hodge, Head, H. H. Hull, Assistant Head and I. M. Besieris, all of the Department of Electrical Engineering, were of substantial help in the complicated process of writing a book with co-authors on the two sides of the Atlantic.

The authors would also like to thank the Editor of the Research Studies on Antennas, Professor J. R. James, for his initiative which resulted in this monograph.

Blacksburg, Virginia, U.S.A.,
Belgrade, Yugoslavia,
April 1982

B. D. P.
M. B. D.
A. R. Dj.

Table of Contents

PART I: ANALYSIS OF WIRE-ANTENNA STRUCTURES

1. DETERMINATION OF CURRENT DISTRIBUTION IN ARBITRARILY EXCITED WIRE STRUCTURES

1.1. INTRODUCTION, 3

1.2. TWO-POTENTIAL EQUATION FOR CURRENT DISTRIBUTION IN ARBITRARY THIN-WIRE STRUCTURES, 5

1.2.1. Approximate solution of the two-potential equation, 10

1.3. SOME EQUATIONS FOR DETERMINING CURRENT DISTRIBUTION IN CYLINDRICAL CONDUCTORS, 13

1.3.1. The two-potential and vector-potential equations, 14

1.3.2. Hallén's equation, 16

1.3.3. Pocklington's equation, 18

1.3.4. Schelkunoff's equation, 18

1.4. CONCLUSIONS, 20

2. APPROXIMATIONS OF EXCITATION REGIONS

2.1. INTRODUCTION, 23

2.2. DELTA-FUNCTION GENERATOR, 25

2.2.1. Solution of Hallén's equation with delta-function generator, 29

2.3. APPROXIMATIONS OF COAXIAL-LINE EXCITATION, 34

2.3.1. TEM magnetic-current frill approximation of coaxial-line excitation, 35

2.3.2. Belt-generator approximation of coaxial-line excitation, 44

2.3.3. Higher-order approximations of coaxial-line excitation by means of wave modes, 48

2.4. APPROXIMATIONS OF TWO-WIRE LINE EXCITATION, 56

2.4.1. A method for measuring admittance of symmetrical antennas by reflection measurements in coaxial line, 63

2.5. CONCLUSIONS, 66

3. TREATMENT OF WIRE JUNCTIONS AND ENDS

3.1. INTRODUCTION, 69

3.2. CONSTRAINTS RESULTING FROM FIRST KIRCHHOFF'S LAW, 70

3.3. JUNCTION-FIELD CONSTRAINTS, 73

3.4. TREATMENT OF WIRE ENDS, 79

3.5. CONCLUSIONS, 90

4. WIRE ANTENNAS WITH DISTRIBUTED LOADINGS

4.1. INTRODUCTION, 91

4.2. EQUATIONS FOR CURRENT DISTRIBUTION ALONG ANTENNAS WITH SERIES DISTRIBUTED LOADINGS, 93

4.2.1. Examples of analysis of antennas with series distributed loadings, 96

4.3. WIRE ANTENNAS WITH DIELECTRIC OR FERRITE COATING, 100

4.4. CONCLUSIONS, 108

5. WIRE ANTENNAS WITH CONCENTRATED LOADINGS

5.1. INTRODUCTION, 109

5.2. MODIFICATION OF EQUATIONS FOR CURRENT DISTRIBUTION, 110

5.2.1. Examples of cylindrical antennas with concentrated resistive loadings, 114

5.2.2. Examples of cylindrical antennas with concentrated capacitive loadings, 118

5.3. NOTES ON MEASUREMENTS OF CONCENTRATED LOADINGS, 129

5.3.1. Compensation method for measuring lumped reactances, 129

5.3.2. Measurement of lumped reactances mounted on the antenna by means of a coaxial resonator, 132

5.4. WIRE ANTENNAS WITH MIXED LOADINGS, 139

5.5. CONCLUSIONS, 144

6. WIRE ANTENNAS IN LOSSY AND INHOMOGENEOUS MEDIA

6.1. INTRODUCTION, 145

6.2. WIRE ANTENNAS IN HOMOGENEOUS LOSSY MEDIA, 146

6.3. DETERMINATION OF CURRENT DISTRIBUTION ALONG WIRE ANTENNAS ON PLANE INTERFACE BETWEEN TWO HOMOGENEOUS MEDIA, 150

6.4. WIRE ANTENNAS ABOVE IMPERFECTLY CONDUCTING GROUND, 154

6.5. CONCLUSIONS, 164

PART II: SYNTHESIS OF WIRE-ANTENNA STRUCTURES

7. GENERAL CONSIDERATIONS OF WIRE-ANTENNA SYNTHESIS

7.1. INTRODUCTION, 167

7.2. GENERAL PRINCIPLES OF WIRE-ANTENNA SYNTHESIS, 169

7.2.1. Possible optimization functions, 170

7.2.2. Possible optimization parameters, 172

7.3. OUTLINE OF SOME OPTIMIZATION METHODS, 173

7.3.1. Complete search method, 175

7.3.2. A gradient method, 175

7.3.3. The simplex method, 177

7.4. CONCLUSIONS, 178

8. OPTIMIZATION OF ANTENNA ADMITTANCE

8.1. INTRODUCTION, 179

8.2. OPTIMIZATION OF ANTENNA ADMITTANCE BY VARYING DISTRIBUTED ANTENNA LOADINGS, 183

8.2.1. Some general examples of optimization, 186

8.2.2. Some remarks on loaded cylindrical antenna optimization, 187

8.2.3. Numerical examples, 188

8.3. SYNTHESIS OF PARALLEL LOADED CYLINDRICAL ANTENNAS WITH MINIMAL COUPLING, 192

8.3.1. Outline of the method, 194

8.3.2. Resistive cylindrical antennas with minimal coupling, 197

8.4. OPTIMIZATION OF ANTENNA ADMITTANCE BY VARYING CONCENTRATED LOADINGS, 202

8.4.1. Optimal broadband capacitively loaded cylindrical antennas, 206

8.4.2. Limits of VSWR for optimal broadband capacitively loaded cylindrical antennas versus their length, 212

8.5. OPTIMIZATION OF ADMITTANCE BY VARYING DISTRIBUTED AND CONCENTRATED LOADINGS, 214

8.6. OPTIMIZATION OF ADMITTANCE BY MODIFICATION OF ANTENNA SHAPE, 220

8.6.1. Synthesis of broadband folded monopole antenna, 223

8.6.2. Synthesis of broadband monopole antenna with parasitic elements, 224

8.6.3. Synthesis of cactus-like antenna matched to feeder at two frequencies, 228

8.6.4. Synthesis of vertical monopole antenna with susceptance-compensating element, 230

8.7. CONCLUSIONS, 232

9. OPTIMIZATION OF ANTENNA RADIATION PATTERN

9.1. INTRODUCTION, 235

9.2. OPTIMIZATION OF RADIATION PATTERN BY VARYING DRIVING VOLTAGES OF ANTENNA-ARRAY ELEMENTS, 239

9.3. OPTIMIZATION OF RADIATION PATTERN BY VARYING ANTENNA LOADINGS, 241

9.4. OPTIMIZATION OF RADIATION PATTERN BY VARYING ANTENNA SHAPE, 243

9.4.1. Synthesis of Uda-Yagi array with one and two directors and two reflectors, 244

9.4.2. Synthesis of inclined monopole antenna, 248

9.4.3. Synthesis of Uda-Yagi array with folded monopole as a driven element, 249

9.4.4. Synthesis of moderately broadband Uda-Yagi array, 252

9.5. CONCLUSIONS, 254

APPENDIX 1. NOTES ON EVALUATION OF INTEGRALS ENCOUNTERED IN ANALYSIS OF WIRE STRUCTURES ASSEMBLED FROM STRAIGHT WIRE SEGMENTS, 257

APPENDIX 2. NOTES ON HALLÉN'S EQUATION, 261

APPENDIX 3. EVALUATION OF THIN-WIRE ANTENNA RADIATION PATTERN AND INDUCED ELECTROMOTIVE FORCE, 263

A3.1. Evaluation of radiation pattern, 263

A3.2. Evaluation of electromotive force induced in a receiving wire antenna, 266

APPENDIX 4. NOTES ON TEM MAGNETIC-CURRENT FRILL APPROXIMATION OF COAXIAL-LINE EXCITATION, 269

A4.1. Near-zone field of TEM magnetic-current frill, 269

A4.2. Radiation field of TEM magnetic-current frill, 271

A4.3. Determination of antenna admittance from power generated by magnetic-current frill, 272

A4.4. Antenna admittance correction when boundary conditions are satisfied inadequately, 275

APPENDIX 5. ADMITTANCE OF MONOPOLE ANTENNAS DRIVEN BY COAXIAL LINE, 279

APPENDIX 6. FIELD INTENSITY VERSUS RADIATED POWER, HEIGHT AND THICKNESS OF A VERTICAL MONOPOLE ANTENNA ABOVE PERFECTLY CONDUCTING GROUND PLANE, 285

APPENDIX 7. SIMPLEX OPTIMIZATION PROCEDURE, 287

REFERENCES, 291

INDEX, 301

PART I
Analysis of Wire-Antenna Structures

CHAPTER 1

Determination of Current Distribution in Arbitrarily Excited Wire Structures

1.1. INTRODUCTION

This book deals with analysis and synthesis of wire-antenna structures assembled from arbitrarily interconnected wire segments. By the term "wire" we shall refer to metallic, highly conducting wires, but also to resistive wire-like structures (e.g., a dielectric rod covered with a resistive layer). We shall consider only electrically thin wires, i.e., wires the diameter of which is much smaller than the wavelength of a plane wave of the frequency considered propagating in the surrounding medium.

A wire structure can be constructed from a given number of wire segments in many ways, and the segments may in principle be straight or curved. Regions in which two or more segments are connected will be referred to as junctions. Junctions, wire ends, concentrated loadings along the wires and possible transition regions along the segments in which the diameter of the wire is changed will be referred to collectively as "discontinuities". In this chapter we shall not deal with discontinuities. They will be treated in detail in the third and fifth chapters.

A wire structure can be excited in many ways. If it is excited by the electric field of a wave propagating in the surrounding medium (e.g., the field of an incident plane wave), it behaves as a scatterer. If it is excited at one or more electrically small regions, it behaves as a transmitting antenna. The term "excitation region" will be used

to designate small regions of the antenna structure with any kind of impressed field. Excitation regions will be treated in more detail in the next chapter.

The definition of impressed field as will be used in this monograph differs somewhat from the usual definition. By the term "impressed field" we shall understand the field due to any type of *known* sources. For example, it may be the field of an incoming plane wave, the field due to known localised electric or magnetic currents, etc.

If a wire structure is used for receiving purposes, regarding the excitation field it can be treated as a combination of the cases of a scatterer and a transmitting antenna. It is well-known, however, that virtually all properties of interest of a receiving antenna (emf, impedance and radiation pattern) are known if the antenna transmitting properties are known. We shall not therefore treat receiving antennas separately. Actually, our main concern will be the transmitting wire-antenna structures. Some details of the theory of receiving antennas are presented in Appendix 3.

All the antenna properties can be deduced once the problem of determining current distribution along the wire segments of the structure has been solved. There is a number of possibilities how to approach that problem. As already mentioned in the Preface, the purpose of this monograph is not to present and discuss all of them. Instead, one particular method, which appears to be most suitable, is chosen, and general wire structures analysed using that method only. The starting point adopted for analysis is the so-called vector-scalar-potential equation, or briefly the two-potential equation, which will be derived in the next section.

When considering cylindrical wire antennas, or arrays of parallel cylindrical antennas, several integral equations are available which are in some respects more convenient than the two-potential equation. Since isolated and parallel coupled cylindrical dipoles are of very frequent occurrence, a brief survey of integral equations for current along such antennas will be presented later in this chapter and some numerical methods for their solution described.

1.2. TWO-POTENTIAL EQUATION FOR CURRENT DISTRIBUTION IN ARBITRARY THIN-WIRE STRUCTURES

Let us consider an arbitrary wire structure sketched in Fig.1.1, situated in a linear, isotropic and homogeneous dielectric medium, of permittivity ε and permeability μ. (Most often the medium will be a vacuum or air, of parameters equal or very close to ε_o and μ_o.*) For the moment we shall assume that all the segments of the structure have constant radius, that they are made of perfectly conducting wires and that no concentrated loadings are connected along the segments.

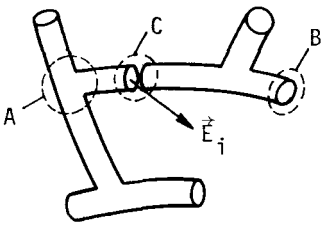

FIG.1.1. Arbitrary wire structure in impressed field $\vec{E}_i$. (A) wire junction, (B) wire end, (C) antenna terminals.

Let the structure be situated in a given time-harmonic impressed electric field of intensity $\vec{E}_i$ and of angular frequency ω. As a reaction to $\vec{E}_i$, currents and charges are induced along the segments of the structure, which are sources of the secondary electric field of intensity $\vec{E}$. These induced currents and charges are such that the tangential component of the total electric-field intensity vector is zero at all points of the (perfectly conducting) wire-structure surface:

$$(\vec{E}+\vec{E}_i)_{tang} = 0 \quad \text{on the wire surface.} \tag{1.1}$$

As $\vec{E}$ can be expressed in terms of currents and charges induced in the structure in the form of certain integrals, given below, and as currents and charges are interconnected through the continuity equation,

* If not stated otherwise, in all numerical examples presented in the monograph ε_o and μ_o will be used for permittivity and permeability of the medium.

eqn.(1.1) essentially represents an integral equation for current distribution along the wire structure.

Let us assume that a curvilinear s-axis, described by a vector function $\vec{r}_s(s)$ with respect to a convenient coordinate system, runs along the axis of a perfectly conducting wire segment, of radius a, as shown in Fig.1.2. Let the radius of curvature of the s-axis everywhere between s_1 and s_2 be much larger than a. The currents and charges in-

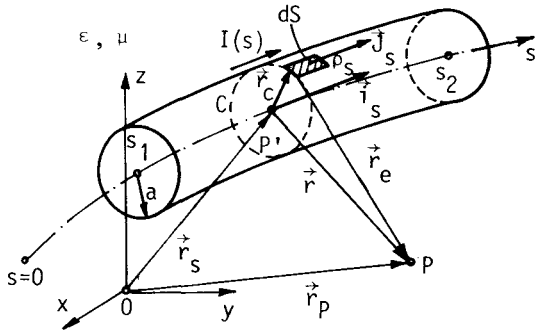

FIG.1.2. Curved current-carrying wire segment and the field point P. Not drawn to scale.

duced in this wire segment form an infinitesimally thin layer on the segment surface S. The surface-current density, $\vec{J}_s$, has, generally speaking, a component locally parallel to the wire axis and a circumferential component. In the case of thin wires the latter component is usually very small, except at the antenna discontinuities. As the problem of discontinuities will be treated in later chapters, we shall neglect here the circumferential component. Also, away from the discontinuities currents and charges are distributed practically uniformly around the circumference C of the segment local cross-section, for any s.[4] Thus we have approximately $\vec{J}_s = \frac{I(s)}{2\pi a}\vec{i}_s(s)$ and $\rho_s = \frac{Q'(s)}{2\pi a}$ along C, where I(s) is the segment current intensity, $\vec{i}_s(s)$ the unit vector locally tangential to the s-axis, ρ_s the surface-charge density and Q'(s) the segment charge per unit length. Since the conductor is perfect, there is no field inside it. We can, therefore, imagine that the inte-

rior of the segment is filled with any medium. If we imagine that it is a medium with parameters ε and μ, the medium is homogenized, and the usual expressions for the retarded potentials can be applied.[5] Thus, the electric field $\vec{E}$ due to this segment, at a point P, can be computed as

$$\vec{E} = -j\omega\vec{A} - \text{grad}\, V\,, \tag{1.2}$$

where

$$\vec{A} = \mu \int_S \vec{J}_s \; g(r_e) \; dS \tag{1.3}$$

is the magnetic vector-potential,

$$V = \frac{1}{\varepsilon} \int_S \rho_s \; g(r_e) \; dS \tag{1.4}$$

is the electric scalar-potential,*

$$g(r_e) = \frac{\exp(-jkr_e)}{4\pi r_e} \tag{1.5}$$

is Green's function for unbounded homogeneous medium,

$$\vec{r}_e = (\vec{r}_p - \vec{r}_s) - \vec{r}_c = \vec{r} - \vec{r}_c \tag{1.6}$$

is the exact distance between the segment surface element dS and the field point P, $\vec{r}$ is the distance between P and the point P' at the s-axis, and

$$k = \omega\sqrt{\varepsilon\mu} \tag{1.7}$$

is the phase coefficient. The integration around the segment circumference yields

$$\vec{A} = \mu \int_{s_1}^{s_2} I(s) \; \vec{i}_s(s) \; G(s) \; ds \tag{1.8}$$

* We assume that there are no concentrated charges at the segment ends, i.e., that at both ends the segment current is continuing into adjacent segment, or equals to zero, so that the first Kirchhoff's law is satisfied at these points.

and

$$V = \frac{1}{\varepsilon} \int_{s_1}^{s_2} Q'(s)\, G(s)\, ds \,, \tag{1.9}$$

where

$$G(s) = \frac{1}{2\pi a} \oint_C g(r_e)\, dl \,. \tag{1.10}$$

The integration around the circumference is very time consuming, and it is performed with difficulties when the field point P is at the segment surface (because the integrand is singular). In order to avoid this integration, G(s) is usually approximated by[6]

$$G(s) \simeq g(r_a) \,, \tag{1.11}$$

where

$$r_a = (r^2 + a^2)^{\frac{1}{2}} \tag{1.12}$$

is an approximate *average* distance between the field point P and the segment surface. Eqn.(1.11) yields *exact* values for the potentials along the s-axis of a *straight* segment. On the axis of a curved segment, and off the axis of a straight or curved segment, it represents a very good approximation provided that the radius of curvature of the s-axis is much larger than a, or that $r \gg a$ and $ka \ll 1$, respectively. The error introduced by using $g(r_a)$ instead of G(s) is largest for points close to the segment surface.

According to the equation of continuity, Q'(s) can be expressed in terms of I(s) as

$$Q'(s) = \frac{j}{\omega} \frac{dI(s)}{ds} \,. \tag{1.13}$$

Combining eqns.(1.2), (1.8), (1.9), (1.11) and (1.13) we find for the vector $\vec{E}$

$$\vec{E} = -j\omega\mu \int_{s_1}^{s_2} \left[I(s)\, \vec{i}_s(s) + \frac{1}{k^2} \frac{dI(s)}{ds} \mathrm{grad} \right] g(r_a)\, ds \,. \tag{1.14}$$

Consider now a structure consisting of N arbitrarily interconnected wire segments. Obviously, only the axial component of the total electric field is responsible for the axial current in the wires. Let $\vec{E}_i$ be the impressed electric field along the wires. From eqns.(1.1) and (1.14) and the concept of extended boundary conditions,[7,5] we easily obtain that current along the segments satisfies the integro-differential equation

$$\sum_{m=1}^{N} \int_{s_{1m}}^{s_{2m}} \left[\vec{i}_p \cdot \vec{i}_{sm} \, I_m(s_m) + \frac{1}{k^2} \frac{dI_m(s_m)}{ds_m} \vec{i}_p \cdot \mathrm{grad} \right] g(r_a) \, ds_m = \frac{\vec{i}_p \cdot \vec{E}_i}{j\omega\mu} , \quad (1.15)$$

where $\vec{i}_p$ is the unit vector at any point at the axis of the pth segment of the structure considered (p=1,2,...,N), locally tangential to the axis. Eqn.(1.15) is known as the *vector-scalar-potential equation* or *two-potential equation*. Note that it was derived assuming that the first Kirchhoff's law was satisfied at all junctions and wire ends.

In the case of general wire structures, the kernel in eqn.(1.15) has terms proportional to $1/r_a$ and to the first derivative of $1/r_a$ only. Other known integral equations for determining current distribution in the wire-antenna structures in the general case have in addition higher-order terms in $1/r_a$. Since r_a can be very small (for r=0 it equals a, the radius of the wire), the kernel in all equations is pseudo-singular, but has the lowest order pseudo-singularity in the case of eqn.(1.15). Since all the equations can be solved only numerically, the more weakly pseudo-singular is the kernel, the easier it is to evaluate the integrals encountered in the approximate solution of the equation. Therefore the authors consider eqn.(1.15) to be the most suitable starting point for analysis of wire-antenna structures of arbitrary shapes. Only in the case of cylindrical antennas and arrays of such parallel antennas can equations be derived having a more convenient kernel, containing terms proportional to $1/r_a$ alone, as will be explained in Section 1.3.

In the present discussion the problem of proper treatment of junctions, such as junction A in Fig.1.1, and the influence of ends, such

as B in Fig.1.1, were not included. These discontinuities will be treated in detail in Chapter 3.

There are several methods which have been used for numerical solution of eqn.(1.15). One of the methods, which appears to be particularly simple and can be used with computers of relatively moderate size and speed for analysis of wire-structures of reasonable complexity, will be presented in the following subsection. Some methods for determining current distribution along cylindrical wire antennas will be described in Section 1.3.

1.2.1. Approximate solution of the two-potential equation.* Numerical methods for solving eqn.(1.15) can be classified (a) according to possible mathematical manipulations with the equation prior to numerical solution (for example, further integration of the equation, with appropriate weighting functions, in accordance with the general approach of the method of moments[9]), and (b) according to the type of approximation of the current distribution, or so-called expansion or basis functions adopted. Broadly speaking, it seems that the results obtained by various methods and using different basis functions and sufficiently high order of approximations practically do not differ. However, amount of the computing time and computer storage requirements vary significantly from one procedure to another. Although at the present time limitations on both computer memory requirements and processing time usually almost do not exist for small structures, they tend to be quite pronounced when considering large structures or when using optimization procedures for computer-aided antenna synthesis. It is therefore useful to adopt a numerical method for solving eqn.(1.15) which is as fast as possible and has modest memory requirements.

In the authors' opinion, one of the most suitable methods in this sense for solving eqn.(1.15) is the point-matching method with entire or almost-entire-domain polynomial approximation for current distribution.

* This subsection is adapted from the material of Reference 8,

(In terms of the general method of moments, this amounts to Dirac's delta-function used as weighting or testing function, and powers in coordinates as basis or expansion functions.) According to this method, we divide the wire structure into N convenient segments, and approximate current distribution along the segments by power series[10,11]

$$I_m(s_m) = \sum_{i=0}^{n_m} I_{mi}\, s_m^i , \quad m=1,\ldots,N, \tag{1.16}$$

where n_m is the desired degree of polynomial approximation for current along the *m*th segment. We next substitute this approximate current distribution into integral equation (1.15), and stipulate that the equation be satisfied at a sufficient number of "matching points" along the wire structure in order to obtain a determined system of linear equations in unknown current-distribution parameters I_{mi}.

Obviously, the distribution of the matching points along the wire structure influences considerably accuracy of the solution. It is therefore useful to have a unique procedure for determining positions of the matching points which guarantees that in most cases an accurate solution would be obtained. The authors adopted the following rule: the matching points should be equidistantly spaced along each antenna segment, the distance between them being twice the distance between the segment end and the closest matching point. An example of this rule is shown in Fig.1.3.

Although, as already pointed out in the Preface, no attempt is made in this monograph to compare various existing methods for analysis of

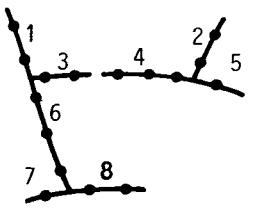

FIG.1.3. Illustration of the rule adopted for choice of matching points along wires of a wire structure. The segments are numbered 1 - 8, and the matching points designated by dots.

thin-wire antenna structures, the choice of the point-matching method combined with polynomial approximation of current warrants certain justifications and explanations.

The point-matching method for solving eqn.(1.15), with $I_m(s_m)$ substituted by the expression in eqn.(1.16), requires numerical evaluation of single integrals only. Other procedures for solving eqn.(1.15) by the moment method, corresponding to weighting functions different from Dirac's delta-function, require integration of double integrals, which is known to be numerically much more complicated and time-consuming, without yielding noticeable improvements in accuracy in almost all cases.

The polynomial expansion for current is very flexible and can sufficiently accurately approximate smooth functions (such as current distribution functions along wires of constant cross-section), as well as some of their derivatives, using only few terms. [The need of approximating the first derivative of current arises from explicit existence of the term dI/ds in eqn.(1.15). We shall see in Section 1.3 that some equations for the cylindrical antennas involve also d^2I/ds^2.] On the other hand, polynomials are simple and fast from the computational point of view. When compared with a sequence of simple rectangular or triangular pulses used to approximate current distribution along wire antennas,[12] polynomials require a substantially smaller number of unknown coefficients to be determined with only a moderate increase in complexity of the solving procedure. They are, therefore, particularly suitable for obtaining solutions using modern minicomputers.

It should be emphasized that the polynomial approximation of current is independent of the basis set used (for example, power functions as in eqn.(1.16), some special polynomials, such as Lagrange interpolation polynomials, etc.). The final results for the current distribution practically coincide, since they are simply rearrangements of each other. Therefore nothing seems to be gained except unnecessary complexity if any other polynomial basis functions are used instead of simple power functions given in eqn.(1.16).

The theory presented above is valid for wire structures assembled

from curved wire segments, provided that the radius of curvature of bent wires at any point is much larger than the wire radius. Such a general case can be solved numerically with relative ease, but usually it is not of interest. Instead, most often it is more convenient to have a computer program for numerical analysis of wire structures assembled from straight segments only, for the following reasons. Firstly, that is the most frequent case encountered in practice. Secondly, curved wire segments can always be approximated by a sufficient number of straight segments. Finally, numerical analysis of wire structures assembled from straight wire segments is simpler and faster than that for the general case. Therefore we shall consider only such wire structures.

In Appendix 1 several hints are given relating to numerical evaluation of integrals encountered in the point-matching solution of eqn. (1.15) with $I_m(s_m)$ given in eqn.(1.16) for the case of straight wire segments.

1.3. SOME EQUATIONS FOR DETERMINING CURRENT DISTRIBUTION IN CYLINDRICAL CONDUCTORS

As already mentioned, integral equations for current distribution along cylindrical antennas are available which are simpler than the two-potential equation, at least from the numerical point of view. This section is aimed at presenting some of these equations and at explaining certain numerical procedures for their approximate solution.

Consider a perfectly conducting cylindrical antenna of radius a and length b, situated in a homogeneous dielectric medium of parameters ϵ and μ. Let the z-axis of a coordinate system coincide with the antenna axis, and let the coordinates of the antenna ends be z_1 and z_2, as shown in Fig.1.4. Assume that the antenna is situated in an axially symmetric impressed time-harmonic electric field $\vec{E}_i$, of angular frequency ω, the z-component of which along the antenna axis is E_{iz} (generally a function of z). As already explained in Section 1.2, for such a structure we can use the usual expressions for the retarded potentials given by eqns.(1.3) and (1.4). Applying again the extended bound-

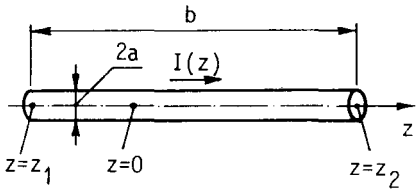

FIG.1.4. Cylindrical antenna.

ary conditions, we can begin the antenna analysis postulating that along the z-axis between z_1 and z_2

$$E_z = -E_{iz} \ , \tag{1.17}$$

where E_z is due to currents and charges induced in the antenna.

Due to axial symmetry, the antenna surface-currents and charges produce only axial electric field along the z-axis, which can be expressed in terms of the retarded potentials as

$$E_z = -j\omega A_z - \frac{\partial V}{\partial z} \ . \tag{1.18}$$

Note, however, that it is strictly not possible to consider a cylindrical antenna without taking into account the antenna ends. We shall see in Chapter 3 that the influence of the antenna ends in some instances is very pronounced and should be taken into account (e.g., for thicker antennas and resonant antenna lengths), while in some other instances it can be neglected without introducing a significant error.

Substituting eqn.(1.18) into eqn.(1.17) the general form of the integral equation for current distribution along the antenna is obtained. However, the final form of the equation depends on further steps in expressing A_z and V in terms of current I(z), which results in a number of equations for determining current distribution. Some of these equations are derived and briefly discussed below.

1.3.1. The two-potential and vector-potential equations. If A_z and V in eqn.(1.18) are substituted by their expressions in eqns.(1.8) and (1.9), the two-potential equation results. Since we already have the general form of the equation, eqn.(1.15), the special form valid for

cylindrical antennas is obtained simply if we let in the equation N=1, $\vec{i}_p=\vec{i}_s=\vec{i}_z$ and $\vec{i}_z\cdot\text{grad} = \partial/\partial z$. The result is

$$\int_{z_1}^{z_2} \left[I(z') + \frac{1}{k^2}\frac{dI(z')}{dz'}\frac{\partial}{\partial z}\right]g(r)\,dz' = \frac{E_{iz}}{j\omega\mu} . \tag{1.19}$$

Note that in eqn.(1.19)

$$r = \left[(z-z')^2 + a^2\right]^{\frac{1}{2}} \tag{1.20}$$

is the *exact* distance between the source point at the antenna surface and the field point at the z-axis. Differentiation of the equation kernel, g(r) [given by eqn.(1.5)], with respect to z results again in terms proportional to 1/r and $1/r^2$.

If, on the other hand, we first make use of the Lorentz condition for the retarded potentials,

$$\text{div}\,\vec{A} = -j\omega\varepsilon\mu\,V, \quad \text{i.e.,} \quad V = \frac{j}{\omega\varepsilon\mu}\,\text{div}\,\vec{A} , \tag{1.21}$$

and note that in the case considered everywhere $\vec{A}=A_z\vec{i}_z$, and thus along the z-axis $\text{div}\,\vec{A}=dA_z/dz$, eqn.(1.18) becomes

$$E_z = -j\omega\left(1 + \frac{1}{k^2}\frac{d^2}{dz^2}\right)A_z . \tag{1.22}$$

Combining eqns.(1.8), (1.11) and (1.22), with r_a replaced by r, we obtain from eqn.(1.17)

$$\left(1 + \frac{1}{k^2}\frac{d^2}{dz^2}\right)\int_{z_1}^{z_2} I(z')\,g(r)\,dz' = \frac{E_{iz}}{j\omega\mu} . \tag{1.23}$$

This integro-differential equation, for obvious reasons, might be termed the vector-potential equation. It is not convenient for numerical analysis of cylindrical antennas, because it implies numerical evaluation of the second derivative of the integral on the left side of the equation with respect to z.

1.3.2. Hallén's equation. Further branching is now possible starting with the vector-potential equation. One possibility is to rewrite eqn.(1.23) in a compact form,

$$\left(k^2 + \frac{d^2}{dz^2}\right) F(z) = k^2 S(z) \ , \quad z_1<z<z_2 \ , \tag{1.24}$$

and to determine F(z), which equals the integral in eqn.(1.23), in terms of the source function S(z), which stands for the right-hand side in eqn.(1.23). Solution of eqn.(1.24) is known to be

$$F(z) = C_1 \cos kz + C_2 \sin kz + k \int_{z_0}^{z} S(z') \sin k(z-z') \, dz' \ . \tag{1.25}$$

The first two terms on the right-hand side represent the solution of the homogeneous equation. The last term is the particular solution of eqn.(1.24). It can be obtained, for example, by the Lagrange method of varying constants.[13] In Appendix 2 it is proved that F(z) [eqn.(1.25)] satisfies eqn.(1.24) for an arbitrary constant z_0.

Thus, if we consider eqn.(1.23) as a differential equation in the integral shown, we obtain the following integral equation for current distribution along the antenna (the constants C_1 and C_2 have still to be determined, so that the sign in front of them is irrelevant):

$$\int_{z_1}^{z_2} I(z') \, g(r) \, dz' + C_1 \cos kz + C_2 \sin kz =$$

$$= \frac{k}{j\omega\mu} \int_{z_0}^{z} E_{iz}(z') \sin k(z-z') \, dz' \quad (z_1<z,z_0<z_2). \tag{1.26}$$

This equation is known as the Hallén equation.[2] Note that it has the kernel containing only 1/r terms. Therefore, from the computational point of view, it represents a very convenient equation, which has been widely used for analysis of cylindrical antennas and arrays of such parallel antennas. (It is quite simple to generalize Hallén's equation for the case of parallel cylindrical antennas, but we shall not do it here).

Eqn.(1.26) contains three constants (C_1, C_2 and z_0). As already mentioned, the constant z_0 can be adopted at will. The constants C_1 and C_2 can be determined in two ways. If the point-matching technique is used for determining I(z), we can simply adopt two matching points in addition to the number of matching points necessary for determining unknown coefficients in the finite series approximating the current, and consider C_1 and C_2 as additional unknowns. Alternatively, since eqn. (1.26) must be true for any z on the segment $[z_1,z_2]$, we can adopt two arbitrary values of z on the segment and require that the equation be satisfied for these two values of z. In this manner a system of two linear algebraic equations in C_1 and C_2 is obtained, from which they can be expressed in terms of certain integrals of I(z'). These integrals can be then introduced into eqn.(1.26). A more complicated expression under the integral sign is obtained, but for numerical solution of the equation it is irrelevant, except that programming is somewhat more complicated than in the first case. In the latter case, however, the order of the system of linear equations when using the point-matching technique is reduced by two, which in some instances can be advantageous.

As already pointed out, the end effects are not taken into account in this form of Hallén's equation. If we consider very thin antennas only (in terms of wavelength), we can stipulate that $I(z_1)=I(z_2)=0$, although this strictly is never the case. For example, if the antenna is in the form of a rod with flat ends, we have small radial currents on the flat caps, going to zero only at the center of the caps. A certain correction is obtained if the antenna is assumed to be for a/2 longer at each end in the case of flat caps, because such an additional antenna length has the same area as the antenna flat ends and, presumably, approximately the same charges are localized on the two surfaces. If the antenna ends are hemispherical, the real length of the antenna, including the caps, can be approximately taken as the antenna length in Hallén's equation, because the area of the hemispherical cap is exactly equal to that of the curved part of a right cylinder of radius a and length a. These corrections are only approximate, however, and cannot alleviate certain instabilities in the numerical solution of Hallén's equation,

which tend to be fairly pronounced for antennas of approximately resonant lengths. A much better remedy is to incorporate in the equation the field due to charges and currents at the antenna ends. However, this cannot be done in a simple manner with Hallén's equation.

1.3.3. Pocklington's equation. Another possibility for rearranging the vector-potential equation, eqn.(1.23), is to introduce the operator in parentheses under the integral sign. Since in the integrand g(r) alone is a function of z, this becomes

$$\int_{z_1}^{z_2} I(z') \left(1 + \frac{1}{k^2} \frac{\partial^2}{\partial z^2}\right) g(r)\, dz' = \frac{E_{iz}}{j\omega\mu} . \tag{1.27}$$

This equation is known as the Pocklington equation.[1] When the indicated differentiation is performed, the kernel of the equation turns out to have terms proportional to $1/r$, $1/r^2$ and $1/r^3$. As already explained, this is very inconvenient from the numerical point of view. Physically, this result follows from the fact that the integrand in eqn. (1.27) is proportional to the field of a Hertzian dipole. Thus, in this approach the antenna is implicitly envisaged as a chain of Hertzian dipoles. The $1/r^3$ term is a consequence of almost equal, but opposite charges at the adjacent ends of any two successive dipoles in the chain.

1.3.4. Schelkunoff's equation. Finally, consider again the two-potential equation, eqn.(1.19), for current distribution along cylindrical antennas. Note that $\partial g(r)/\partial z = -\partial g(r)/\partial z'$ because, from eqn. (1.20), $\partial r/\partial z = -\partial r/\partial z'$. Therefore the second term of the integral can be integrated by parts, to obtain

$$-\int_{z_1}^{z_2} \frac{dI(z')}{dz'} \frac{\partial}{\partial z'} g(r)\, dz' = -\frac{dI(z')}{dz'} g(r)\Big|_{z'=z_1}^{z_2} + \int_{z_1}^{z_2} \frac{d^2 I(z')}{dz'^2} g(r)\, dz' . \tag{1.28}$$

Thus the two-potential equation is transformed into

$$\int_{z_1}^{z_2} \left[I(z') + \frac{1}{k^2}\frac{d^2 I(z')}{dz'^2}\right] g(r)\, dz' - \frac{1}{k^2}\frac{dI(z')}{dz'} g(r)\Big|_{z'=z_1}^{z_2} = \frac{E_{iz}}{j\omega\mu} . \qquad (1.29)$$

This equation is known as the Schelkunoff equation.[14] It is very convenient for numerical analysis of cylindrical antennas. On the one side, it has the kernel of the most convenient type possible - depending on r as 1/r only. On the other side, this equation requires that the current distribution be approximated by a functional series which is twice differentiable, in order to find the second derivative in the brackets under the integral sign, as well as the values of $dI(z')/dz'$ at $z'=z_1$ and $z'=z_2$ on the left side of the equation. In that case it can be solved numerically as easily as the Hallén equation. In the authors' opinion, Schelkunoff's equation has not received an appropriate attention it deserves as the starting point for analysis of cylindrical antennas. For this reason we shall explain in more detail how it can be solved using numerical methods.

The simplest possibility is to use the point-matching technique combined with a convenient expansion for current. The expansion can be polynomial, in which case the process of solution closely parallels that described in connection with the general two-potential equation. However, another possibility is to approximate current distribution by a polynomial series in which the first two terms are replaced by trigonometric functions[15,16]

$$I(z) = C_1 \cos kz + C_2 \sin kz + \sum_{i=2}^{n} I_i z^i . \qquad (1.30)$$

If we substitute this expression for current into eqn.(1.29), the first two terms of the expansion vanish under the integral sign, because each makes the expression in the brackets equal to zero. Thus eqn.(1.29) reduces to approximate equation

$$\sum_{i=2}^{n} I_i \left\{ \int_{z_1}^{z_2} \left[z'^{i} + \frac{i(i-1)}{k^2} z'^{(i-2)} \right] g(r)\, dz' - \frac{i}{k^2} z'^{(i-1)} g(r) \Big|_{z'=z_1}^{z_2} \right\} +$$

$$+ \frac{C_1}{k} \sin kz'\, g(r) \Big|_{z'=z_1}^{z_2} - \frac{C_2}{k} \cos kz'\, g(r) \Big|_{z'=z_1}^{z_2} = \frac{E_{iz}}{j\omega\mu} . \quad (1.31)$$

As the next step we require that this equation be satisfied at (n-1) points along the antenna, which results in (n-1) complex linear equations in (n+1) unknown complex parameters C_1, C_2, $I_2,\ldots,I_n$. Two additional equations are obtained requiring that

$$I(z_1) = 0 \quad \text{and} \quad I(z_2) = 0 . \quad (1.32)$$

Expansion given by eqn.(1.30) is particularly useful when considering relatively long antennas (longer than about one wavelength). In this case the current distribution is well approximated by the trigonometric terms with a corrective polynomial term which is relatively small everywhere except in the vicinity of the antenna discontinuities (like excitation region and antenna ends). [This conclusion is valid provided that the origin, z=0, is sufficiently far from the antenna discontinuities, and if $z_1<0<z_2$ (see Fig.1.4).]

1.4. CONCLUSIONS

In the present chapter an integral equation was derived convenient for analysis of arbitrary wire structures and a method was explained for obtaining approximate solutions for current distribution along the structures. However, the problems of excitation region and various antenna discontinuities were not considered.

As a special, but important case, thin cylindrical antennas were analysed in more detail. A number of equations which can be used for their analysis was derived. A numerical procedure for determining current distribution in all the cases was outlined, but it was again assumed that excitation field was a continuous and relatively slowly varying function along the antenna.

The next four chapters are devoted to analysis of wire antennas in which the excitation field is close to that in the transmitting case, i.e., localized in a small region, and thus quasi-discontinuous, and along which discontinuities exist of various kinds. In this manner the theory presented in this chapter will be completed for analysis of a wide class of real transmitting and receiving wire-antenna structures.

CHAPTER 2
Approximations of Excitation Regions

2.1. INTRODUCTION

The approximate integral and integro-differential equations for current distribution along wire structures and cylindrical antennas derived in the preceding chapter are valid for any impressed electric field in which they might be situated, but simple numerical procedures suggested for their approximate solutions can be applied only if the impressed electric field is relatively slowly varying function along the wires of the structure. However, the impressed field is, often, concentrated in a relatively small region of the antenna structure (the so-called excitation region), in which it varies rapidly along the wires, as in the case of transmitting antennas. Rapid variations of the impressed field, and thus also rapid variations of the induced current and, especially, charge in this region, must be treated numerically with additional precautions. They usually require separate, rapidly varying expansion functions to be used in the excitation region, and specification of appropriate boundary conditions for these expansions. In order to be able to do that, a closer insight into variations of the impressed electric field along antennas in real circumstances is needed. This chapter is devoted to modelling of some systems used frequently for excitation of transmitting wire antennas and for connection between receiving wire antennas and the receiver.

Only rarely a wire antenna is connected to the terminals of a transmitter or receiver directly. Usually, this is done by means of a con-

venient transmission line (feeder). Coaxial lines and two-wire lines are used most often for that purpose. Almost without exceptions, the distance between conductors of a feeder in practice is small with respect to the wavelength of the wave radiated or received. An antenna connected to one end of a feeder has, therefore, two electrically close terminals, and can be considered as a two-terminal (one-port) network in the network theory sense. In the transmitting case, an antenna can be regarded as a lumped impedance element connected at the feeder end. In the receiving case, the antenna can be considered as an equivalent Thévenin's (or, alternatively, Norton's) generator connected to the feeder. It is well known that the internal impedance of the Thévenin generator equivalent to a receiving antenna is equal to the impedance of the same antenna when used for transmitting. Electromotive force of the receiving antenna can be determined in various ways, one of which is based on knowledge of the current distribution along the antenna in the transmitting case, in addition to orientation and distribution of the electric field of the received electromagnetic wave (see Appendix 3). For this reason we shall consider transmitting antennas only, as already mentioned in the introduction to the first chapter.

To be able to define an antenna as a two-terminal element, it is necessary to define two electrically close points in the excitation region in which the feeder terminates and the antenna begins. This can be done fairly arbitrarily if rough analysis only is needed, but considerable care has to be exercised if more accurate analysis is required.

In spite of the assumed electrically small volume occupied by the excitation region, its geometry has considerable influence on the antenna impedance or admittance, although it practically does not influence the antenna radiation pattern. Therefore precise modelling of the antenna excitation region is necessary for obtaining accurate theoretical values of the antenna impedance or admittance.

In this chapter several theoretical models of actual generating regions will be described and discussed, and the impressed field due to these models examined. This chapter, combined with the preceding chapter, represents a basis for accurate numerical analysis of cylindrical

and other wire-antenna structures without junctions and loadings along the wires. It contains also certain numerical results obtained using computer programs based on the theory presented so far, as well as comparison of these results with available experimental results.

2.2. DELTA-FUNCTION GENERATOR

The delta-function generator is the simplest - and the least accurate - theoretical model of the real excitation region of wire antennas. It can approximate to a certain degree any type of excitation, and has been widely used for analysis of wire antennas.

Without going into historical details, we shall only note that several forms of the delta-function generator have been used. In Fig.2.1 the generator is assumed in the form of an ideal voltage generator connected across a gap of negligible width along the antenna. The antenna admittance is defined in this case as $Y=I_g/V_g$, where V_g is the generator voltage, and I_g its current. As the gap width, d, is assumed to tend to zero, such a gap introduces an infinite capacitance across the generator terminals. This makes the antenna susceptance singular, which, of course, in reality is never the case.

In order to avoid in theoretical analysis the radial currents and charges in the gap, and to circumvent the gap capacitance, another representation of the delta-function generator is used, shown in Fig.2.2. This model can be deduced from that shown in Fig.2.1 by postulating

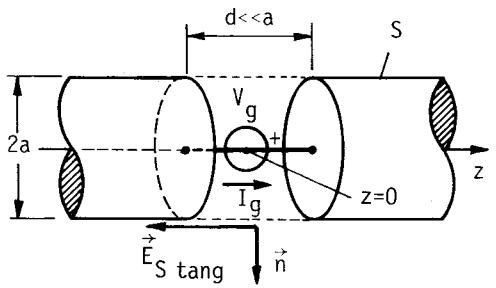

FIG.2.1. Ideal voltage generator connected across a narrow gap as approximation of excitation region. The gap width is not drawn to scale.

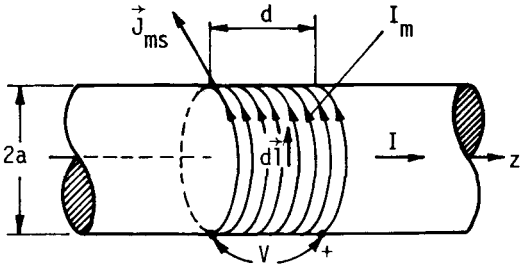

FIG.2.2. Magnetic-current ring as approximation of excitation region.

that the field in the gap be zero, while that in the exterior region (i.e., outside the surface S shown in Fig.2.1) be unchanged. This can be achieved by applying the general equivalence theorem.[5] Let $\vec{E}_S$ and $\vec{H}_S$ be the total fields on S, due to all the sources (i.e., to the generator current and to the antenna currents and charges). The sources inside S can be replaced with respect to the domain outside S by equivalent surface electric and magnetic current on S given by

$$\vec{J}_s = \vec{n} \times \vec{H}_S , \qquad \vec{J}_{ms} = - \vec{n} \times \vec{E}_S , \tag{2.1}$$

where $\vec{n}$ is the outward unit vector on S (see Fig.2.1). With these equivalent sources on S, the total field inside S is zero,[5] so that the medium can be homogenized. Note that the magnetic surface currents on S in Fig.2.1 exist only on the hatched surface shown in Fig.2.2, because the antenna is perfectly conducting.

The voltage across the magnetic-current ring can be defined as the integral of the total electric field along a path lying outside S (Fig. 2.2). This voltage is the same as that in Fig.2.1 (the fields outside S in the two cases are identical), and is very nearly equal to V_g, since a is small and thus the field essentially quasi-static. The antenna admittance is defined in this case as the ratio Y=I/V, where I is the antenna electric current at the antenna surface for z=0. This current is *not* equal to the current I_g of the ideal voltage generator in Fig. 2.1 (they differ for the displacement current in the gap). Therefore the antenna admittances as defined for the systems in Figs.2.1 and 2.2

are not equal.

If in Fig.2.2 we let the width d tend to zero, the surface magnetic-current layer degenerates into an infinitesimally thin magnetic-current ring of surface current $J_{ms}(z)=V\,\delta(z)$, the total current of the ring being $I_m=V$. As a consequence, a weakly (logarithmically) singular capacitance appears across the two sides of the ring, resulting again in an infinite antenna susceptance.

In the generator representation sketched in Fig.2.2 the magnetic-current ring is the source of the impressed electric field, $\vec{E}_i$. This field can be computed in terms of the electric vector-potential, $\vec{A}_e$, as

$$\vec{E}_i = -\frac{1}{\varepsilon}\,\mathrm{curl}\,\vec{A}_e \ , \tag{2.2}$$

where

$$\vec{A}_e = \varepsilon \int_S \vec{J}_{ms}\, g(r)\, dS \ , \tag{2.3}$$

S is the surface with magnetic currents, $\vec{r}$ the distance between the element dS and the field point, and g(r) Green's function, given by eqn. (1.5). Combining eqns.(2.2) and (2.3), introducing the "curl" operator under the integral in eqn.(2.3) and noting that it operates only on g(r), it can be easily obtained that

$$\vec{E}_i = \int_S \vec{J}_{ms} \times \mathrm{grad}\, g(r)\, dS = -\frac{1}{4\pi}\int_S (\vec{J}_{ms}dS)\times\Big[\vec{r}\,\frac{1+jkr}{r^3}\exp(-jkr)\Big] \ . \tag{2.4}$$

If d is assumed to be zero, $I_m\,d\vec{l}=V\,d\vec{l}$ should be introduced into eqn. (2.4) instead of $\vec{J}_{ms}\,dS$. In that case the impressed electric field $\vec{E}_i$ at the antenna surface exhibits the properties of a delta-function with respect to the z-coordinate. However, in order to apply the extended boundary conditions, the impressed field along the z-axis is required. Starting from eqn.(2.4), with $\vec{J}_{ms}\,dS$ substituted by $V\,d\vec{l}$, it is easy to show that, along the antenna axis,

$$E_{iz}(z) = \frac{Va^2}{2}\,\frac{1+jkr}{r^3}\exp(-jkr) \ , \tag{2.5}$$

where

$$r = (z^2 + a^2)^{\frac{1}{2}} . \tag{2.6}$$

From eqn.(2.5) it can be seen that the impressed field rapidly decays along the z-axis (actually, as $1/r^3$ in the near zone), and is thus practically confined only to a region the length of which is only several antenna radii. In this region $kr<<1$ since the antenna radius is assumed to be much smaller than the wavelength, and hence the integral of the impressed field in eqn.(2.5) along the z-axis in the excitation region is very closely equal to V. (For example, from $z=-4a$ to $z=4a$ this integral is equal to 0.97 V.) Therefore in some instances $E_{iz}(z)$ can be approximated by the Dirac delta-function, i.e., we can set $E_{iz}(z) \simeq V\,\delta(z)$, as discussed in the next subsection.

The impressed electric field given by eqn.(2.5) can be used when determining current distribution starting from the equations described in Chapter 1. However, if the point-matching method is used with any of these equations, except the Hallén equation, a relatively large number of matching points is necessary in the excitation region in order to properly sample the impressed field. Alternatively, the general method of moments can be applied for this region. For example, the integral constraint

$$\int_L (\vec{E} + \vec{E}_i)\cdot d\vec{l} = 0 \tag{2.7}$$

can be applied, where L is a short path along the z-axis in the vicinity of the ring. In this way the effect of the generator is taken into account integrally, neglecting the local variations of the impressed field. Such an approach yields reasonably stable numerical results for the antenna admittance for several reasons. Firstly, the model shown in Fig.2.2 introduces only a weakly singular capacitance across the ring. Secondly, any low-order expansion function for current distribution cannot adequately represent the rapid charge variations in the vicinity of the ring, and thus cannot account for the infinite capacitance. Thirdly, the application of the extended boundary conditions in

a numerical solution virtually eliminates this singularity since, viewed from the antenna axis, numerically it can be hardly distinguished whether the magnetic-current layer has a finite or zero width d. Finally, the integral constraint (2.7) introduces still further softening, by neglecting the local distribution of the electric field. However, computation of the integral in eqn.(2.7) can be done only numerically, which is time consuming. In addition, with almost the same computational effort more sophisticated approximations of the excitation regions can be utilized yielding more stable and reliable results for the antenna admittance. Therefore the delta-function generator is used primarily with the Hallén equation, because it can be very simply incorporated into the right-hand side of the equation, without any special numerical precautions, as will be explained in the following subsection.

2.2.1. Solution of Hallén's equation with delta-function generator. Let, for simplicity, in the Hallén equation [eqn.(1.26)] $z_0=0$ and the delta-function generator be at that location. The impressed electric field, given by eqn.(2.5), can be introduced into the integral on the right-hand side of eqn.(1.26). This impressed field practically exists only in the immediate vicinity of the point z=0, i.e., in the interval $z\in(-\zeta,\zeta)$, where ζ is of the order of few wire radii. Thus we have

$$\int_0^z E_{iz}(z')\sin k(z-z')\,dz' \simeq \left\{\begin{array}{l} \displaystyle\int_0^{-\zeta} E_{iz}(z')\sin k(z-z')\,dz' \,, \quad z<0 \\ \\ \displaystyle\int_0^{\zeta} E_{iz}(z')\sin k(z-z')\,dz' \,, \quad z>0 \end{array}\right\} \simeq$$

$$\simeq \sin k|z| \int_0^{\zeta} E_{iz}(z')\,dz' \qquad (2.8)$$

for $|z|>>\zeta$, because $k\zeta<<1$. Since the last integral in eqn.(2.8) is very nearly equal to V/2, according to the discussion in connection with eqn.(2.5), we have

$$\int_0^z E_{iz}(z') \sin k(z-z')\, dz' \simeq \frac{V}{2} \sin k|z| \,. \tag{2.9}$$

As ζ is very small compared with the antenna length, eqn.(2.9) is valid practically along the whole antenna. It is worth noting that eqn.(2.9) would be exact if the impressed electric field along the z-axis were taken to be a Dirac's delta-function, i.e.,

$$E_{iz}(z) = V\delta(z) \,. \tag{2.10}$$

With eqn.(2.9) substituted into eqn.(1.26), the Hallén equation reads:

$$\int_{z_1}^{z_2} I(z')\, g(r)\, dz' + C_1 \cos kz + C_2 \sin kz = \frac{kV}{2j\omega\mu} \sin k|z|$$

(asymmetrically driven antenna at z_0=0). (2.11)

If the antenna is symmetrically driven and its length is 2h, we have z_1=-h and z_2=h. In addition, C_2=0 in this case, because of symmetry. So we have

$$\int_{-h}^{h} I(z')\, g(r)\, dz' + C_1 \cos kz = \frac{kV}{2j\omega\mu} \sin k|z|$$

(symmetrically driven antenna at z_0=0). (2.12)

As already mentioned, eqns.(2.11) and (2.12) have been used extensively for analysis of cylindrical antennas. It is interesting to note that these equations physically *cannot have a solution*. This is easily understood if we have in mind that the last term in these equations exactly corresponds to the impressed electric field given by eqn.(2.10). Although eqn.(2.10) can be considered as an approximation of eqn.(2.5), such a singular impressed electric field can neither be obtained physically by any sources located at the antenna surface, nor can be compensated by any physically realisable distribution of antenna electric currents and charges located at that surface. This might explain relatively rapid ultimate divergence of the antenna susceptance with increasing order of the expansion functions when using eqns.(2.11) and

(2.12). However, if low-order expansion functions are used, this approximation yields fairly accurate results for the antenna admittance.

It is interesting to present some results obtained using eqn.(2.12) with polynomial approximation for current. Note first that the expansion for current along symmetrical dipoles must be an even function of z. For example, we may choose the expression

$$I(z) = \sum_{m=1}^{n} I_m \left(1 - \frac{|z|}{h}\right)^m , \tag{2.13}$$

as was done in Reference 10, to take the condition $I(\pm h)=0$ into account automatically. However, we can also adopt the simple power expansion[11]

$$I(z) = \sum_{m=0}^{n} I_m |z|^m , \tag{2.14}$$

with the constraint $I(\pm h)=0$ added to the point-matching equations. As mentioned in Chapter 1, the form of the polynomial approximation is irrelevant, since all are rearrangements of one another. The matching points should be distributed relatively evenly along one arm of the dipole. The simplest choice is to take them equidistantly, with one of the points at the antenna end (i.e., at z=h). Once we have determined the current distribution coefficients I_m, the antenna admittance is obtained, for V=1 V, as

$$Y = \frac{I(0)}{V} = \begin{cases} \sum_{m=1}^{n} I_m & \text{for expansion in eqn.(2.13)} \\ I_o & \text{for expansion in eqn.(2.14)} \end{cases} . \tag{2.15}$$

As a numerical example, Table 2.1 gives theoretical and experimental antenna admittances from Reference 10 for three antenna electrical lengths and fixed antenna radius. It is seen that the theoretical results remain relatively stable with increasing degree of approximation and that they are in good agreement with experimental results.

As the next example, Fig.2.3 presents two cases of theoretical and experimental current distributions. It is seen that the overall theo-

TABLE 2.1. Admittance of cylindrical dipoles of radius a=0.007022 λ for increasing degree of polynomial approximation of current, obtained as a solution to eqn.(2.12). (Ref.10)

h/λ	Admittance (mS) degree of polynomial approximation 2	3	4	measured[17]*
0.250	9.16 - j3.57	9.16 - j3.55	8.81 - j3.31	8.92 - j3.46
0.375	1.52 - j0.36	1.54 - j0.27	1.53 - j0.10	1.58 - j0.18
0.500	0.98 + j1.54	0.96 + j1.58	0.97 + j1.76	1.02 + j1.68

* In Reference 17 two sets of results for admittances of isolated monopole antennas driven by a coaxial line are given. The first set corresponds to admittances of antennas as elements terminating the coaxial line. In the second set these values are corrected as proposed by King to take approximately into account the influence on the antenna susceptance of the specific coaxial line used in measurements as contrasted to the delta-function excitation. In this section it was natural to use the latter set of results, but the first set was used with more accurate approximations of coaxial-line excitation (see Table 2.3). In both cases averaged measured values are shown (computed from a number of experimental results presented in Reference 17).

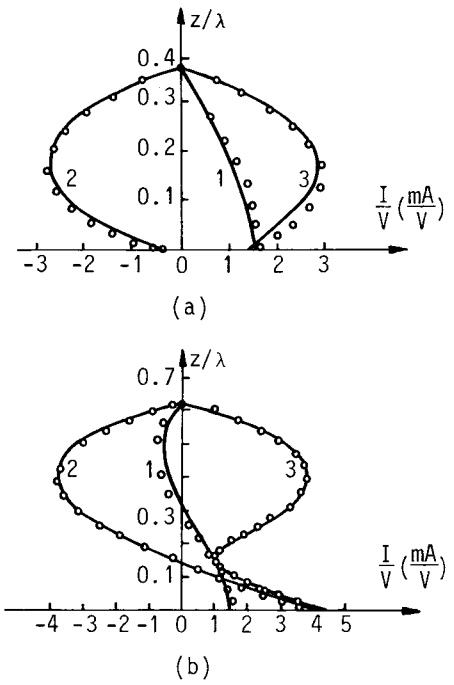

FIG.2.3. Current distribution along isolated dipoles of length (a) 2h=0.750 λ and (b) 2h=1.250 λ, of radius a=0.007022 λ; (1) real part, (2) imaginary part, (3) magnitude. o o o experiment[17], ——— theory, second degree polynomial approximation of current for case (a) and third degree for case (b), obtained as solution to eqn. (2.12). (Ref.10)

retical current distribution represents quite a good approximation, in spite of very low degree of polynomial approximation of current and the inaccurate model of the excitation region.

Finally, a rough sketch showing dependence of the antenna admittance versus the (half-length)/(wavelength) ratio, i.e., versus h/λ, presented in Fig.2.4, indicates that solutions of the Hallén equation with simple delta-function generator and polynomial approximation of current of quite low degree (second or third) predict fairly accurately the antenna admittance behaviour as a function of frequency. (In Appendix 5 more accurate curves are given for admittance of cylindrical antennas valid for a wide range of the ratios h/λ and a/λ.)

It is also shown in Reference 10 that Hallén's equation with the delta-function generator with polynomial approximation for current can efficiently be used for analysis of coupled cylindrical dipoles, and in References 18, 19 and 20 some results are given for isolated and coupled asymmetrical dipoles and for coupled symmetrical dipoles of unequal

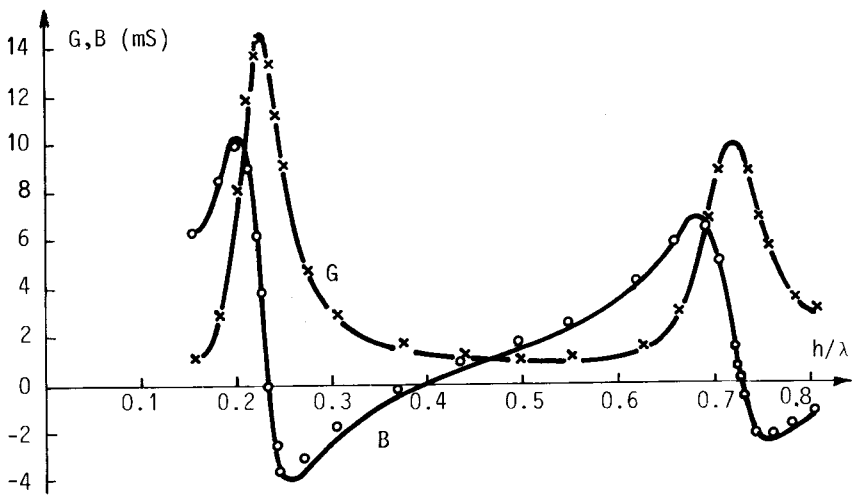

FIG.2.4. Conductance (G) and susceptance (B) of isolated dipoles of radius $a=0.007022\ \lambda$, for different ratios h/λ of dipoles. ××, oo experimental,[17] ——— polynomial approximation of current, second degree for $h/\lambda<0.5$, third degree for $h/\lambda>0.5$, obtained as a solution of eqn.(2.12). (Ref.10)

lengths. Thus, in spite of conceptual difficulties, the delta-function generator appears to be a convenient approximation for fairly accurate analysis of isolated and coupled cylindrical antennas. We shall see in the next sections that much better approximations of excitation regions are available, which yield accurate and reliable values of the antenna admittance, and which can be more efficiently incorporated into the two-potential equation for arbitrary wire structures.

2.3. APPROXIMATIONS OF COAXIAL-LINE EXCITATION

A frequently used system for feeding wire antennas is a coaxial line. Being inherently an asymmetrical structure, it is used mostly to feed asymmetrical antennas, like the monopole-antenna shown in Fig.2.5. The antenna is in the form of a simple protrusion of the inner coaxial-line conductor through the ground plane, at which the outer coaxial-line conductor terminates. In practice, the ground surface is usually made of a very good conductor. In shape and size it can be diverse: curved, flat, large or small in terms of the wavelength. Often, however, at least as far as the antenna admittance is concerned, the ground surface can be approximated by an infinite, perfectly conducting ground plane. This is the only case we shall consider in what follows.

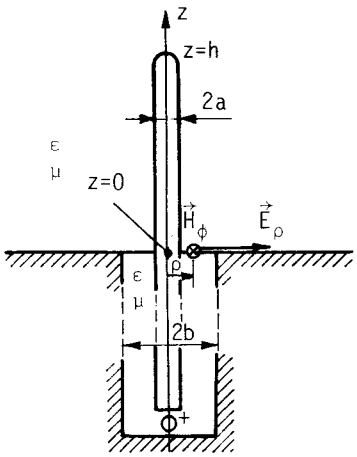

FIG.2.5. Sketch of a monopole antenna driven by coaxial line. Dielectric is assumed to be homogeneous everywhere.

In principle, the system shown in Fig.2.5 can be analysed if all currents and charges in the system are taken into account. These currents and charges are distributed on the antenna itself, on the ground plane, on the inner and outer coaxial-line conductors along the whole length of the line, and in the generator to which the antenna is connected. Obviously, such an approach would be extremely complicated but, fortunately, it is not necessary. It can be avoided if the coaxial-line excitation of the antenna is replaced by a suitable approximation which allows the half-space above the ground plane to be treated independently of the coaxial line and the image theory to be applied in order to reduce the problem to that of a symmetrical dipole driven by an equivalent generator. Three such approximations of the coaxial-line excitation are presented in the following subsections. They are all derived for the case of a vertical monopole, of the form shown in Fig.2.5, but they can also be applied successfully to arbitrary wire-antenna configurations situated above a perfectly conducting ground plane and fed in that plane by one or more coaxial lines.

Throughout the following discussion we shall assume that the operating frequency is sufficiently low so that TEM waves only can propagate along the coaxial line. In that case the electromagnetic field in the major part of the line is given practically as a sum of two TEM waves, propagating in opposite directions. At the line end, however, higher-order (TE and TM) modes must be taken into account. In connection with this, the antenna admittance is most often defined as the ratio of the coaxial-line current intensity and voltage, corresponding to the TEM mode, at the coaxial-line opening (i.e., in the plane z=0 in Fig.2.5). The antenna admittance thus defined uniquely determines the TEM-mode standing-wave pattern along the coaxial line.

2.3.1. TEM magnetic-current frill approximation of coaxial-line excitation. At frequencies for which, approximately, $kb<0.1$, very good results for the antenna admittance are obtained if the electromagnetic field at the coaxial-line opening in Fig.2.5 is approximated by the TEM mode only.[21,22] Therefore, we can set, for z=0,

$$\left.\begin{aligned} E_\rho(\rho) &\simeq E_{\rho TEM}(\rho) = \frac{V}{\rho \ln(b/a)} \\ H_\phi(\rho) &\simeq H_{\phi TEM}(\rho) = \frac{I(0)}{2\pi\rho} \end{aligned}\right\} \quad a<\rho<b \ , \tag{2.16}$$

where V is the voltage and I(0) current intensity at the coaxial-line opening, and ρ the distance of the point considered from the z-axis (see Fig.2.5).

According to the equivalence theorem,[5] the perfectly conducting ground plane can be extended to cover the coaxial-line opening, provided that an annular layer of surface magnetic currents is placed at the former opening, immediately above the plane, as shown in Fig.2.6(a). These magnetic currents are circular, and their density, with respect to the reference direction shown in Fig.2.6(a), is given by

$$J_{ms\phi}(\rho) = -E_\rho(\rho) \ . \tag{2.17}$$

If the coaxial-line voltage, V, is assumed to be known, from the first of eqns.(2.16) and eqn.(2.17) it follows that $J_{ms\phi}(\rho)$ is also known.

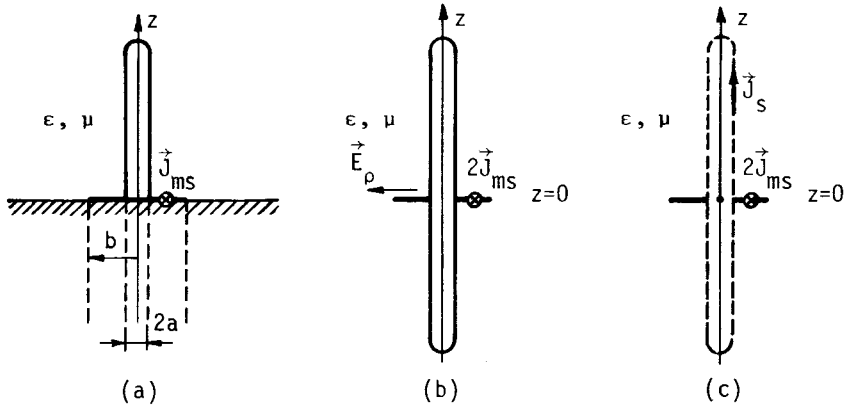

FIG.2.6. Equivalent systems for monopole-antenna driven by coaxial line sketched in Fig.2.5.

The image theory can now be applied to obtain the equivalent system sketched in Fig.2.6(b). In that system the magnetic-current density of the frill is twice that in Fig.2.6(a). These magnetic currents are the source of the impressed electric field for the symmetrical dipole antenna. Finally, we can apply once more the equivalence theorem to remove the perfectly conducting antenna, which leaves us with the magnetic-current frill and the induced currents and charges on the former antenna surface, situated in a homogeneous medium. A system is thus obtained in which the usual expressions for the retarded potentials can be applied.

The impressed electric field due to the TEM magnetic-current frill shown in Fig.2.6(c), at a point P(x,0,z) lying in the xOz plane (see Fig.A4.1 in Appendix 4), has the components

$$E_{ix}(x,z) = \frac{-4zV}{\ln(b/a)} \int_a^b \int_0^\pi \frac{\cos\phi}{r} \frac{dg(r)}{dr} \, d\phi \, d\rho \, , \tag{2.18}$$

and

$$E_{iz}(x,z) = \frac{-4V}{\ln(b/a)} \int_0^\pi g(r)\Big|_{\rho=a}^{b} \, d\phi \, , \tag{2.19}$$

where r is the distance between the source and the field points, and g(r) is the Green function. Details on derivation of these formulas can be found in Appendix 4.1. The integrals in eqns.(2.18) and (2.19) can be evaluated numerically without difficulties, except when the field point P is very close to the magnetic-current frill.

The expressions in eqns.(2.18) and (2.19) are important when analysing general wire-antenna structures. When considering a vertical monopole antenna, like that in Fig.2.5, we need to evaluate only the E_{iz} component along the z-axis, because $E_{ix}(0,z)=0$. This expression can be obtained from eqn.(2.19) noting that now $r=(\rho^2+z^2)^{\frac{1}{2}}$. It has the form

$$E_{iz}(0,z) = \frac{4\pi V}{\ln(b/a)} \left[g(r_a) - g(r_b) \right] \, , \tag{2.20}$$

where

$$r_a = (a^2 + z^2)^{\frac{1}{2}} \quad \text{and} \quad r_b = (b^2 + z^2)^{\frac{1}{2}} . \tag{2.21}$$

The equivalent dipole antenna shown in Fig.2.6(b) can next be analysed by any of the equations presented in Section 1.3 if E_{iz} is replaced by the expression in eqn.(2.20).

As a consequence of the annular magnetic-current frill excitation, current derivative has a discontinuity at the frill location. The value of the derivative $(dI/dz)|_{z=0+}$ is uniquely determined by the coaxial-line dimensions and the voltage at the line opening, as demonstrated below. This fact must be taken into account in a numerical solution for stable and accurate results in this case to be obtained.

To determine the value of $(dI/dz)|_{z=0+}$, note that at the antenna surface in Fig.2.6(b) the electric-field vector at z=0+ has only the radial component, E_ρ, which is tangential to the magnetic-current frill. According to the boundary conditions,

$$E_\rho(\rho=a,z=0+) - E_\rho(\rho=a,z=0-) = -2J_{ms\phi}(\rho=a) . \tag{2.22}$$

The antenna charge per unit length is related to the electric field as $Q'(z)=2\pi\varepsilon a\, E_\rho(\rho=a,z)$. The first current derivative and this charge are interrelated through the continuity equation, i.e., $dI(z)/dz=-j\omega Q'(z)$. From eqns.(2.16), (2.17) and (2.22) it hence follows that

$$\frac{dI(z)}{dz}\Big|_{z=0+} - \frac{dI(z)}{dz}\Big|_{z=0-} = -j\frac{4\pi\varepsilon\omega V}{\ln(b/a)} . \tag{2.23}$$

In the case considered the current derivative is an odd function of z. Therefore we finally have

$$\frac{dI(z)}{dz}\Big|_{z=0+} = -\frac{dI(z)}{dz}\Big|_{z=0-} = -j\frac{2\pi\varepsilon\omega V}{\ln(b/a)} = -jkY_c V , \tag{2.24}$$

where Y_c is the characteristic admittance of the coaxial line.

The conditions in eqns.(2.23) or (2.24) can easily be incorporated into any smooth approximation of the antenna current distribution, such as the polynomial approximation, resulting in very stable and accurate

results for current and charge distributions in the vicinity of the magnetic-current frill. However, these distributions are very rapidly varying along the z-axis in the excitation region, and special precautions must be taken in order to provide a sufficiently accurate approximation for these distributions near the magnetic-current frill, as will be discussed later in this section.

When using the magnetic-current frill with the Schelkunoff equation (see Subsection 1.3.4), care should be exercised when integrating by parts the integral shown on the left-hand side of eqn.(1.28). Namely, this integral should be split into two integrals, one of them being performed on the interval $(z_1,0)$, and the other on $(0,z_2)$, in order to avoid the discontinuity of dI/dz at z=0, where the magnetic-current frill is located. Thus instead of (1.28) we obtain

$$-\int_{z_1}^{z_2} \frac{dI(z')}{dz'} \frac{\partial}{\partial z'} g(r)\, dz' = -\frac{dI(z')}{dz'} g(r)\Big|_{z'=z_1}^{z_2} + \frac{dI(z')}{dz'}\Big|_{z=0-}^{0+} g(r)\Big|_{z=0} + \left(\int_{z_1}^{0-} + \int_{0+}^{z_2}\right) \frac{d^2I(z')}{dz'^2} g(r)\, dz' \,. \tag{2.25}$$

Eqn.(2.25) should now be introduced into eqn.(1.19), and E_{iz} substituted from eqn.(2.20). The second term on the right-hand side of eqn.(2.25) can be interpreted as the electric field due to the discontinuity in the first current derivative at z=0, multiplied by $-k^2/(j\omega\mu)$. Since the discontinuity is determined by eqn.(2.23), this field is known and can be treated as a part of the impressed electric field (as defined in Section 1.1). Therefore it should be moved to the right-hand side of eqn.(1.19), where it exactly cancels the first term of the impressed field given in eqn.(2.20). Thus we finally obtain the Schelkunoff equation for a cylindrical antenna driven by a magnetic-current frill:

$$\left(\int_{z_1}^{0-} + \int_{0+}^{z_2}\right)\left(I(z') + \frac{1}{k^2}\frac{d^2I(z')}{dz'^2}\right) g(r)\, dz' - \frac{1}{k^2}\frac{dI(z')}{dz'} g(r)\Big|_{z'=z_1}^{z_2} = \frac{j4\pi V}{\omega\mu \ln(b/a)} g(r_b) = \frac{E_{irz}}{j\omega\mu} \,. \tag{2.26}$$

Note that the resulting impressed field E_{irz} in eqn.(2.26) is less pseudo-singular along the z-axis than the field given by eqn.(2.20). It can be shown that the z-component of this resulting impressed electric field is singular only for (ρ=b,z=0), i.e., at the outer magnetic-current frill edge, while the field due to the frill alone, given by eqn. (2.19), is singular at the antenna surface also, i.e., for (ρ=a, z=0).

Once the antenna current distribution is determined, the monopole-antenna admittance, defined in terms of the coaxial-line TEM mode, is approximately given by*

$$Y = \frac{I(0)}{V} \quad , \tag{2.27}$$

where V is the assumed voltage at the coaxial-line opening, and I(0) the antenna current for z=0. Although based on the approximation of the electromagnetic field at the coaxial-line opening by the TEM mode only, eqn.(2.27) yields very accurate results at lower frequencies. At higher frequencies more accurate analysis of the electromagnetic field at the coaxial-line opening is necessary, as demonstrated in Subsection 2.3.3.

The monopole radiation pattern (in the upper half-space) can also be determined easily from the known current distribution, as shown in Appendix 3. The question arises, however, about the radiation field of the magnetic-current frill, which should be added to the antenna-current radiation field. This radiation field is, essentially, an approximation to the field radiated from the coaxial-line opening. Details on its computation are given in Appendix A4.2. It is usually negligibly small, except in cases when very short monopoles are considered (of lengths of the order of few outer coaxial-line radii) or when the coaxial-line circumference is a significant fraction of the wavelength. Determination of the radiation field from the coaxial-line opening is, therefore, required quite rarely.

The exact solution for the antenna current distribution results in

* Note that other approaches for determining the antenna admittance are possible, one of them being presented in Appendix A4.3.

zero total electric field in the interior of the monopole (dipole) surface, and zero total electric field tangential to that surface. However, an approximate solution does not satisfy these conditions, except, possibly, at some points. For gaining insight into the quality of a numerical solution, it is useful to compute the axial field due to the obtained approximate current distribution and to see how much it differs from $-E_{iz}(z)$.[23,24,25] As a specific example, shown in Fig.2.7 is the z-component of the total electric field, (E_z+E_{iz}), in the excitation region, for a point-matching polynomial solution of the two-potential equation for a quarter-wavelength cylindrical monopole sketched in Fig.2.5. The monopole radius was a=0.01 λ, the outer coaxial-line conductor radius b=2.3a, and the monopole had a hemispherical cap. In the analysis the monopole was divided into four segments: the excitation region (6a long), the hemispherical end cap (see Section 3.4), a 3a long segment adjacent to the end cap and the rest (central, main)

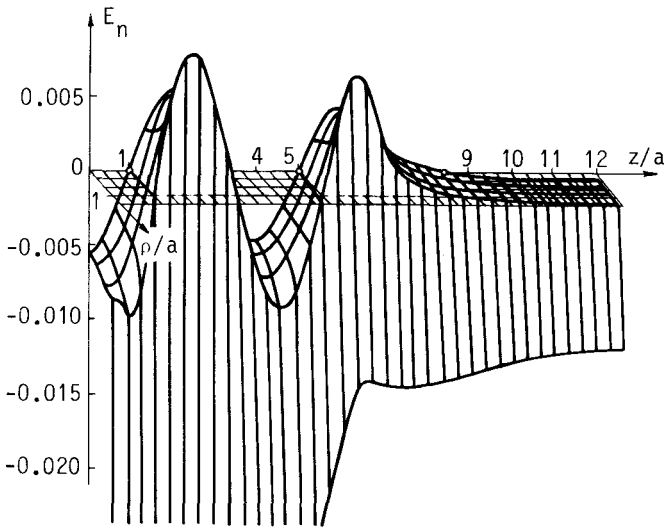

FIG.2.7. Real part of the axial component of the normalized electric field in the excitation region of a vertical monopole driven by a coaxial line. Small circles indicate the positions of matching points which are not masked by the graph. Imaginary part is several times smaller in magnitude. (Ref.25)

part of the monopole. Both the current and its first derivative were required to be continuous functions along the z-axis. The degrees of the polynomial approximation were 4 on all the segments except the end cap, where a third-degree polynomial was adopted. The matching points were distributed along the z-axis (i.e., the extended boundary conditions were used to formulate the equation). The total field is shown normalized with respect to the intensity of the excitation field at the origin, i.e., with respect to $E_{iz}(0)$.

As it can be seen from Fig.2.7, the total normalized electric field is practically zero at the matching points (where $|E_n|<10^{-6}$). In the excitation region this field is very small in magnitude ($|E_n|<0.01$) not only at the z-axis, but also everywhere within and on the monopole surface (i.e., for $\rho/a\leq 1$). This indicates that both the extended and the true boundary conditions are satisfied to a high degree. In the middle part of the monopole the total electric field in this case is for an order of magnitude smaller than in the excitation zone. Similar conclusions were found to be valid for any good solution for current distribution along a monopole of any dimensions. However, if the approximation of current distribution is poor (e.g., polynomial degree is inadequate, or the matching points are improperly distributed), the boundary conditions are also poorly satisfied. This results in significant error in the antenna admittance and even in the radiation pattern. In Appendix A4.4 a method is given for estimating and reducing the error in the antenna admittance in such a case.

For electrically thicker antennas ($ka\geq 0.01$) it suffices to take a fourth-degree polynomial approximation for current in the excitation region, a conclusion reached by extensive numerical experiments. The length of the excitation region should be between 3a and 10a (a length of 6a was adopted in the above example). However, in the case of electrically thinner antennas the second derivative of the antenna current (i.e., the z-component of the charge gradient) in the vicinity of the excitation region is also varying very rapidly along the antenna axis. In that case a different division of the antenna into segments was found (by numerical experiments) to be necessary. A segment several antenna

radii long is required at the monopole base in order that the excitation field can be sampled adequately, but one or more adjacent, progressively longer segments should be adopted in addition, in order to provide sufficiently accurate approximation of d^2I/dz^2 further from the first segment. This is essential for obtaining a good solution with the two-potential and other equations based directly on the boundary conditions for the electric field.

As an illustration, Table 2.2 presents the antenna admittance and the peak total normalized electric field along the z-axis (excluding the antenna cap) for a relatively thick quarter-wavelength monopole with a hemispherical cap, versus the polynomial degrees for the excitation region (which was adopted to be 20a/3 long) and for the major, middle part of the monopole. The antenna was analysed by the two-potential equation.

As can be seen from Table 2.2, very stable results for the monopole admittance, and the peak total normalized electric field strength smaller than 1% (excluding the end cap), are obtained for $n_1 \geq 4$ and $n_2 \geq 3$. Note, however, that this remarkable stability would not be obtained if the end effect were not properly included in the analysis. As a general rule, following from a large number of numerical experiments, the

TABLE 2.2. A quarter-wavelength monopole admittance (in mS) and peak normalized electric field strength along the monopole axis (in %, excluding the end cap), versus degrees of polynomial approximation n_1 (in the excitation region) and n_2 (along the main monopole part); a=0.01 λ, b/a=2.3.

n_2 \ n_1	2	3	4	5
2	21.92-j6.90 mS 30 %	19.14-j6.56 mS 7.2 %	18.32-j6.30 mS 0.9 %	18.40-j6.40 mS 0.5 %
3	21.42-j7.36 mS 30 %	18.24-j6.60 mS 7.2 %	17.70-j6.42 mS 1 %	17.70-j6.50 mS 0.2 %
4	21.64-j7.50 mS 30 %	18.12-j6.54 mS 7.2 %	17.72-j6.42 mS 1 %	17.76-j6.48 mS 0.1 %
5	21.86-j7.60 mS 30 %	18.10-j6.50 mS 7.2 %	17.74-j6.56 mS 1 %	17.80-j6.48 mS 0.1 %

density of the matching points along the main part of any thin-wire antenna (away from the excitation region, the end-cap regions and possible other discontinuities) should not be less than 6 points per wavelength in order to obtain reasonably accurate results for the antenna admittance.

2.3.2. Belt-generator approximation of coaxial-line excitation.[26]

Essentially, the belt generator is a modification of the generator model sketched in Fig.2.2. Instead of assuming that the width, d, of the generator tends to zero, as in the delta-function generator approximation, it is assumed to be finite. The belt generator thus resembles a belt of finite width wrapped around the antenna. In contrast to the approach presented in Subsection 2.3.1, where approximation of the impressed field sources (i.e., the magnetic currents) was sought, in the belt-generator theory approximation of the impressed field itself is considered. The main idea is to determine the size (length) of the excitation region and the distribution of the impressed field along it in such a way that the belt generator approximates as nearly as possible the actual excitation of the antenna. It is worth mentioning that the belt generator can take into account to some extent the higher-order modes near the coaxial-line opening, and not only the TEM mode as the approximation described in the preceding subsection. The details concerning the derivations can be found in Reference 26. Here, only the main idea will be explained and the final conclusions given, illustrated by some numerical examples.

Consider first the real coaxial-line excitation of a monopole antenna, sketched in Fig.2.8(a). In the domain bounded by the surface S_1, parts of the ground plane and the outer coaxial-line conductor, and the coaxial-line cross-section at $z=z_0$, the electromagnetic field is very complex. For example, in the coaxial line a multitude of modes exists in addition to the TEM mode, as indicated in the figure. In order to avoid the analysis of the electromagnetic field in the domain, we can approximate that domain with respect to both the antenna above $z=z_1$ and the coaxial line below $z=z_0$ by a simple network, extract non-TEM modes in the end section of the line and take their influence approximately

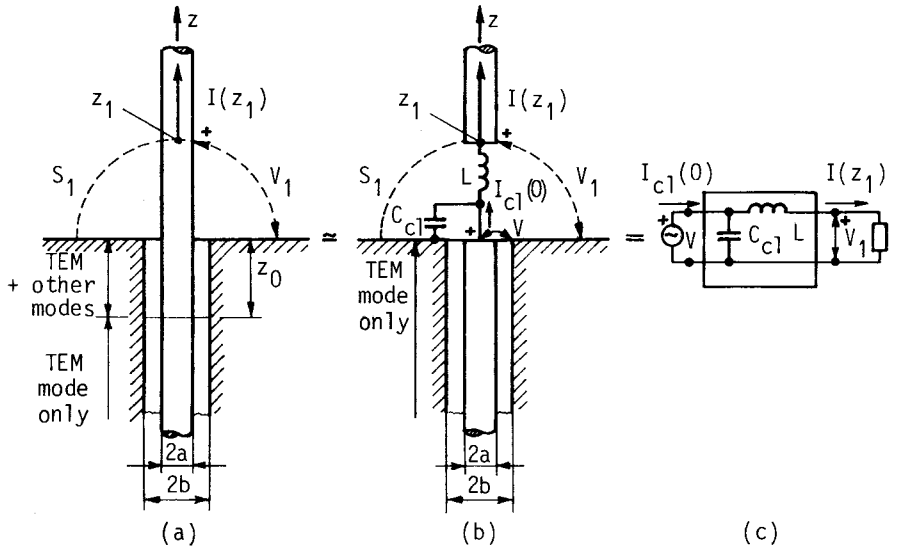

FIG.2.8. Excitation region of monopole antenna driven by coaxial line; (a) actual case, (b) approximation to actual case, (c) circuit-theory representation of case (b). (Ref.26)

into account by appropriately chosen network. Finally, we can assume that the TEM mode in the line extends up to the plane $z=0$.[27] This approximation is shown in Fig.2.8(b). (More complicated and more accurate approximating networks can, of course, be used if desired.) Thus the system in Fig.2.8(b) can be approximated with respect to the end of the coaxial line and the monopole above $z=z_1$ by the circuit-theory representation shown in Fig.2.8(c). The parameters C_{cl} and L were determined in References 26 and 28.

Consider now the same monopole antenna driven by a hypothetical belt generator, shown in Fig.2.9(a). Following similar reasoning as above, we obtain the approximation in Fig.2.9(b) and its circuit-theory representation, shown in Fig.2.9(c).

In order that the two excitation regions shown in Figs.2.8(b) and 2.9 (b) behave in the same way with respect to the antenna, the two-port networks in Figs.2.8(c) and 2.9(c) should be identical. In the approximation adopted this means that C_{bg} should be equal to C_{cl}. It is shown

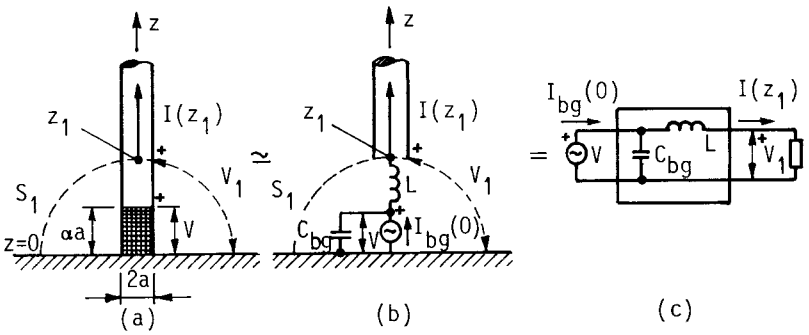

FIG.2.9. Excitation region of monopole antenna driven by finite-size belt generator; (a) actual case, (b) approximation to actual case, (c) circuit-theory representation of case (b). (Ref.26)

in Reference 26 that a very simple conclusion is reached in this manner under certain conditions. If the impressed field at the antenna surface in the excitation region is assumed to be of the form

$$E_{iz}(z) = \begin{cases} \frac{V}{\alpha a}\left(1+\cos\frac{\pi z}{\alpha a}\right) , & |z| \leq \alpha a \\ 0 , & |z| > \alpha a \end{cases} , \tag{2.28}$$

where V is the voltage across the coaxial-line opening, the coefficient α, determining the length αa of the belt generator on the monopole antenna approximately equivalent to coaxial-line excitation, is obtained from the following simple approximate equation:

$$\alpha = 2.18\left(\frac{b}{a}-1\right) . \tag{2.29}$$

In this manner the belt generator approximately equivalent to a given coaxial-line excitation can easily be found.

The image theory can now be applied to obtain the symmetrical system equivalent to that in Fig.2.9(a). The excitation field of the form given in eqn.(2.28) can be introduced into any equation for current distribution along symmetrically fed dipoles, and the approximate current distribution determined in a desired manner. A separate expansion for current needs to be adopted in the belt-generator region, because the

current is a rapidly varying function along the antenna in this region. For obvious reasons, the antenna current should be an even function of z satisfying the condition $dI(z)/dz\,|_{z=0}=0$. Since, most frequently, the width of the belt generator is larger than the antenna diameter, for application of the extended boundary conditions we can assume that, approximately, the impressed field given in eqn.(2.28) is the same along the antenna axis.

In the case of the vector-potential equation, the two-potential equation, Pocklington's equation and Schelkunoff's equation, $E_{iz}(z)$ given in eqn.(2.28) is used as it stands. Substituting the expression in eqn. (2.28) into the right-hand side integral of Hallén's equation (1.26), for symmetrical dipole antenna with $z_1=-h$ and $z_2=h$ that equation takes the form

$$\int_{-h}^{h} I(z')\, g(r)\, dz' + C_1 \cos kz = \frac{kV}{j\omega\mu}\, Cg(z)\ , \tag{2.30}$$

where

$$Cg(z) = \begin{cases} \frac{2}{K}\left[P^2 - 1 - \cos\frac{\pi z}{\alpha a} - (P^2-2)\cos kz\right], & 0\leq z\leq \alpha a \\ \frac{2}{K}\left[P^2 \cos k(z-\alpha a) - (P^2-2)\cos kz\right], & z>\alpha a \end{cases}\ , \tag{2.31}$$

$K=k\alpha a(P^2-1)$ and $P=\pi/(k\alpha a)$.

As a numerical example, given in Table 2.3 are values of admittances of several monopole antennas analysed using eqn.(2.30), corresponding to increasing degree of the polynomial approximation of current on the principal antenna part. The results are compared with those obtained with the delta-function generator (using the same division of the antenna into segments) and with experimental results. Agreement with experimental results is seen to be very good, while the delta-function generator solution exhibits the expected increase in susceptance with increased degree of the approximation (compare with Table 2.1).

Finally, it is interesting to note that the results for the monopole admittance and overall current distribution obtained with the magnetic-current frill and the belt-generator approximations of the excitation

TABLE 2.3. Theoretical and experimental admittance (in mS) of vertical monopoles above ground plane, with a=3.175 mm, b/a=3, at frequency f=663.5 MHz. (Ref.26)

h/λ	n_1	n_2	Theory, Hallén's equation: belt-generator approximation, α=4.36	Theory, Hallén's equation: delta-function-generator approximation	Experimental, coaxial-line excitation, b/a=3 (Ref.17*)
0.250	4	3	18.4 - j7.63	18.4 - j4.74	17.84 - j7.50
	4	4	18.1 - j7.74		
	4	5	17.5 - j7.64	17.6 - j4.75	
	4	6	17.4 - j7.78		
0.375	4	3	3.10 - j1.08	3.10 + j1.82	3.16 - j0.93
	4	4	3.10 - j1.04		
	4	5	3.08 - j0.96	3.08 + j1.95	
0.500	4	3	2.00 + j2.74	2.00 + j5.64	2.05 + j2.78
	4	4	1.97 + j2.72		
	4	5	1.97 + j2.73	1.97 + j5.64	
0.625	4	3	2.88 + j7.98	2.88 + j10.9	2.96 + j7.86
	4	4	2.78 + j7.71		
	4	5	2.80 + j7.75	1.80 + j10.7	
	4	6	2.84 + j7.87		

* Please see Table 2.1 for explanation concerning experimental results in Reference 17.

region are very close in all cases. If $kb \ll 1$, both yield results of sufficient accuracy for almost all practical applications. This is a consequence of very similar impressed electric fields due to these two generator models, as seen from Fig.2.10. If kb is not much smaller than 1, or if higher accuracy is needed, the theory presented in the following subsection may be used.

2.3.3. Higher-order approximations of coaxial-line excitation by means of wave modes.[29] We have seen that, at lower frequencies, the TEM approximation of both the electric and magnetic field at the coaxial-line opening, given in eqns.(2.16), yields relatively accurate re-

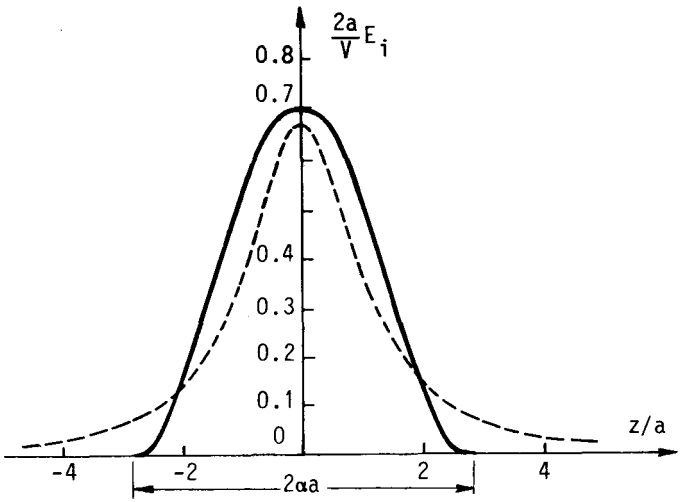

FIG.2.10. Impressed electric field in excitation region, for ka<<1 and b/a=2.3, due to belt-generator (solid line) and to TEM magnetic-current frill (dashed line) along the antenna axis.

sults for the antenna admittance (and, of course, for current distribution in general). However, if we consider the real electric and magnetic fields at the opening, it becomes obvious that a TEM wave alone cannot approximate the actual field distribution accurately, even at lower frequencies.[30] For example, at the outer coaxial-line conductor wedge, in reality both the radial (E_ρ) and axial (E_z) components of the electric field are singular and proportional to $(b-\rho)^{-1/3}$ when $\rho \to b$.[31] With the TEM approximation, however, E_ρ is regular everywhere between $\rho=a$ and $\rho=b$. Therefore, in an exact analysis higher-order wave modes at the coaxial-line opening should be taken into account in addition to the TEM mode.

Rigorous solution of the electromagnetic field for the whole system shown in Fig.2.5 is not known. As a boundary value problem this system is very complicated for direct numerical solution. Another approach is possible, however, which combines separate solutions for the electromagnetic fields in the upper half-space in Fig.2.5 (containing the monopole antenna), and in the lower half-space (i.e., in the coaxial line),

in terms of a functional series. The coefficients of the series are determined from the boundary conditions at the surface z=0, requiring that the tangential components of the electric and magnetic fields in the two half-spaces be equal at the coaxial-line opening. In principle, this approach can yield results which may have any desired accuracy, provided that a sufficient number of terms of the series expansion is taken into account. In practice, very accurate results can be obtained with several terms of the series only. The principal correction of the antenna admittance thus found at lower frequencies is in the susceptance, but at higher frequencies a significant correction of the monopole conductance results as well. In this subsection we shall describe this method briefly and present some numerical results.

The currents in the actual axially-symmetrical system shown in Fig.2.5 are only in the z-direction, or are radial (on the ground plane and the antenna end). Therefore the magnetic field cannot have the z-component, and TM modes alone can exist in the coaxial line in addition to the principal, TEM mode. Of all the TM_{mn} modes, the TM_{on} modes only are axially symmetrical, i.e., do not depend on the ϕ-coordinate. Therefore the solution must be sought in this case in the form of a series of TM_{on} modes.

The TM_{on} modes in the coaxial line, travelling in the direction of the (-z)-axis, are of the well-known form (see, for example, Reference 32):

$$\left.\begin{aligned} E_{zn}(\rho) &= -Z_{0n}(k_n\rho)\exp(\gamma_n z) \\ E_{\rho n}(\rho) &= (\gamma_n/k_n)\, Z_{1n}(k_n\rho)\exp(\gamma_n z) \\ H_{\phi n}(\rho) &= -(j\omega\varepsilon/\gamma_n)\, E_{\rho n}(\rho) \end{aligned}\right\} \quad z<0, \quad n=1,2,\ldots , \tag{2.32}$$

where

$$Z_{in}(x) = C_n J_i(x) + D_n N_i(x) , \tag{2.33}$$

$J_i(x)$ and $N_i(x)$ being the Bessel and Neumann functions, respectively, of order i, k_n, C_n and D_n coefficients to be determined, and

$$\gamma_n = (k_n^2 - k^2)^{1/2} \tag{2.34}$$

the propagation coefficient of the nth mode in the coaxial line. For determining the coefficients k_n, C_n and D_n we can use the boundary conditions $E_{zn}(a)=0$ and $E_{zn}(b)=0$, and normalize the amplitudes of the modes in a convenient manner. For example, we can adopt $Z_{1n}(k_n a)=1$ V/m. A system of three nonlinear equations in k_n, C_n and D_n, n=1,2,..., is thus obtained, which can be solved using any convenient procedure. As an example, given in Table 2.4 are values of these coefficients corresponding to the above normalization, for n=1,...,6, and for a coaxial line with b/a=2.3.

TABLE 2.4. Coefficients k_n, C_n (V/m) and D_n (V/m) of TM_{on} modes for a coaxial line with b/a=2.3 and n=1,...,6.

n	1	2	3	4	5	6
$k_n a$	2.396	4.822	7.242	9.661	12.079	14.496
C_n	1.923	-2.098	0.526	2.075	-4.176	4.326
D_n	-0.017	1.770	-3.328	3.294	-1.234	-2.011

Let us now represent the ρ-component, $E_\rho(\rho)$, of the total electric field strength at the coaxial-line opening as a sum of the E_ρ-field of the TEM mode and those for higher-order modes, i.e.,

$$E_\rho(\rho) = E_{\rho o}(\rho) + \sum_{n=1}^{\infty} w_n E_{\rho n}(\rho) , \quad z=0 , \tag{2.35}$$

where $E_{\rho o}(\rho)$ is the TEM-mode field, and $E_{\rho n}(\rho)$ is the TM_{on}-mode field, given in eqns.(2.32). Assuming the voltage at the coaxial-line opening, V, to be known, the TEM-mode field is given in eqn.(2.16), because the voltage across the coaxial-line opening due to any higher-order mode is zero, which can be proved from eqns.(2.32). The coefficients w_n in eqn.(2.35) are unknowns to be determined.

The equivalent system for a monopole driven by a coaxial line in this case is the same as before, sketched in Fig.2.6(a), except that now the total magnetic current of the frill is given as the sum

$$J_{ms\phi}(\rho) = -E_{\rho}(\rho) = -E_{\rho o}(\rho) - \sum_{n=1}^{\infty} w_n E_{\rho n}(\rho) . \tag{2.36}$$

Eqn.(2.36) ensures that the tangential component of the electric field at the coaxial-line opening in the systems shown in Figs.2.5 and 2.6(a) be equal.

We can now analyse the equivalent system shown in Fig.2.6(c) for every term of this series separately, yielding partial antenna currents, $I_n(z)$. Using the superposition principle we can find the total current $I(z)$ along the antenna as a sum of these partial currents,

$$I(z) = I_o(z) + \sum_{n=1}^{\infty} w_n I_n(z) . \tag{2.37}$$

Of course, all components of the electric and magnetic field due to this total current can similarly be represented as a sum of partial components (due to partial antenna currents).

According to the boundary conditions, the tangential component of the magnetic-field vector for z=0 in the systems shown in Figs.2.5 and 2.6(a,c) must be equal. On the other hand, from Ampère's law we obtain

$$2\pi\rho H_{\phi} = I + 2\pi j\omega\varepsilon \int_{a}^{\rho} \rho E_z(\rho)\, d\rho . \tag{2.38}$$

Hence we have an alternative, equivalent condition, that currents and the z-components of the electric field in both systems must be equal for z=0. This condition appears to be more convenient, because $E_z(\rho)$ is easier to compute and exhibits more rapid variations with ρ for z=0 than does $H_{\phi}(\rho)$. We thus obtain that the coefficients w_n must be such that the equation

$$\sum_{n=1}^{\infty} w_n E_{zn}(\rho) = E_{zIo}(\rho) + E_{zfo}(\rho) + \sum_{n=1}^{\infty} w_n \left[E_{zIn}(\rho) + E_{zfn}(\rho)\right] ,$$

$$a<\rho<b , \quad z=0 , \tag{2.39}$$

be satisfied. In this equation, the left-hand side is the z-component of the electric field in the coaxial line, given in terms of the field

of the higher-order modes [see eqns.(2.32)], $E_{zIo}(\rho)$ and $E_{zIn}(\rho)$ the fields of the antenna current due to excitation by the TEM and higher-order magnetic-current frills, and $E_{zfo}(\rho)$ and $E_{zfn}(\rho)$ the fields due to these frills themselves in the system of Fig.2.6(c).

In order to determine the coefficients w_n numerically, we must consider a truncated series instead of the infinite series in eqn.(2.39). We can then determine the coefficients of the truncated series approximately in various ways, of which the point-matching method appears to be the simplest. A suitable choice of the matching points is

$$\rho_p = a + \frac{b-a}{2m}(2p-1)\ , \quad p=1,\ldots,m\ , \tag{2.40}$$

for a series truncated with the *m*th term inclusive. In this manner the points $\rho=a$ and $\rho=b$ are avoided, which should be done, since at $\rho=a$ eqn.(2.39) is, theoretically speaking, identically satisfied, and at $\rho=b$ the total field is singular.

Once the first m coefficients w_n, $n=1,\ldots,m$, are determined, the problem is solved to the desired degree of approximation. Current distribution along the monopole is given in eqn.(2.37), truncated to the first m terms. This current for $z=0$ should be equal to the coaxial-line innner-conductor current for $z=0$, i.e.,

$$I(0) = I_o(0) + \sum_{n=1}^{m} w_n I_n(0) = I_{TEM}(0) + I_{\text{higher modes}}(0)\ , \tag{2.41}$$

where I_{TEM} is the current corresponting to the TEM mode and $I_{\text{higher modes}}$ to all the higher-order modes in the coaxial line. Note that $I_{TEM}(0)$ is *not* equal to either the total current $I(0)$, or to the current $I_o(0)$ due to the TEM-frill excitation alone, since currents in the antenna due to higher-mode frills and these frills themselves create an additional TEM magnetic field at $z=0$.

The monopole admittance is obtained as

$$Y = \frac{I_{TEM}(0)}{V}\ , \tag{2.42}$$

which corresponds to the definition of admittance when measured using

standard reflection measurements. To determine the current $I_{TEM}(0)$ from eqn.(2.41), note that the TM_{on} modes at z=0- are known, since w_n-coefficients are known and the modes propagate in the (-z)-direction only. Therefore we can easily determine the total current at z=0 corresponding to the higher-order modes in the coaxial line as the sum of line integrals of $H_{\phi n}(a)$ around the inner coaxial-line conductor at z=0,

$$I_{\text{higher modes}}(0) = 2\pi a \sum_{n=1}^{\infty} w_n H_{\phi n}(a) = -j2\pi a\omega\varepsilon \sum_{n=1}^{\infty} w_n \frac{Z_{1n}(k_n a)}{k_n} , \qquad (2.43)$$

according to eqns.(2.32). However, we have adopted the normalization $Z_{1n}(k_n a)$=1 V/m, so that, finally, we obtain for the monopole admittance computed with m higher-order modes

$$Y = \frac{I_o(0)}{V} + \frac{1}{V} \sum_{n=1}^{m} w_n \left[I_n(0) + j\frac{2\pi a\omega\varepsilon}{k_n} \right] . \qquad (2.44)$$

Note that the first term on the right of this equation is the monopole admittance computed with the TEM-frill approximation, according to eqn. (2.27), and the sum represents the correction.

As a numerical example, consider a monopole with hemispherical end cap, as in Fig.2.5, with a=3 mm, b=6.9 mm (i.e., b/a=2.3), at frequencies between 1 GHz (corresponding to b=0.023 λ) and 8 GHz (corresponding to b=0.184 λ). Given in Table 2.5 are the ratios $E_{\rho n}(a)/E_{\rho o}(a)$ for a quarter-wavelength monopole at 1 GHz (h/λ=0.25), and for a 0.8 λ monopole at f=8 GHz, obtained with m=6. This ratio is proportional to the coefficient w_n, and indicates how much the total field at the coaxial-line opening is influenced by a higher-order mode. It can be seen that it is almost real and only weakly frequency-dependent, which means that the field at the opening is very nearly quasi-static.

Shown in Table 2.6 are values of the corrective term of the monopole admittance, i.e., the sum in eqn.(2.44), for a quarter-wavelength monopole, a=3 mm, b/a=2.3 and at a frequency f=1 GHz, versus the number m of the higher-order modes used for correction. At this (relatively low) frequency, the correction is practically only in the antenna susceptance, for about -0.21 mS. Obviously, even with m=1 or m=2 the correc-

TABLE 2.5. Ratio $E_{\rho n}(a)/E_{\rho 0}(a)$ for b/a=2.3, a=3 mm and m=6, for f=1 GHz and h=75 mm, and for f=8 GHz and h=30 mm.

n	f=1 GHz	f=8 GHz
1	-0.1973 + j0.0041	-0.2128 + j0.0574
2	0.1347 - j0.0023	0.1411 - j0.0312
3	-0.1088 + j0.0017	-0.1149 + j0.0233
4	0.0981 - j0.0015	0.1021 - j0.0198
5	-0.0907 + j0.0013	-0.0955 + j0.0181
6	0.0453 - j0.0007	0.0471 - j0.0088

tion is sufficient for most purposes. At f=8 GHz, however, the correction was found to be as high as (-0.57 - j1.67) mS. It was found by numerical experiments that these values are almost independent of the monopole length. In general, numerical experiments have also indicated that the correction in susceptance is practically proportional to frequency (or, more precisely, to ka for b/a=constant), while the conductance increases with frequency much faster. Essentially, this takes into account radiation from the coaxial-line opening.

In conclusion, it may be said that the method presented above is the most accurate method available for analysis of antennas driven by a coaxial line. However, it is rather complicated and requires considerable numerical skill. Therefore it cannot be recommended for monopole analysis at lower frequencies (such that, approximately, kb<0.1), except if extremely high accuracy of the numerical results is required, but at higher frequencies (if kb is larger than about 0.1) it should be used if accurate and reliable results are desired.

TABLE 2.6. Corrective term, ΔY (mS), of monopole-antenna admittance for a quarter-wavelength monopole, a=3 mm, b/a=2.3, at 1 GHz, versus the number m of higher-order modes.

m	ΔY	m	ΔY
1	-0.021 - j0.181	4	0.003 - j0.214
2	0.012 - j0.229	5	0.002 - j0.211
3	-0.001 - j0.210	6	0.003 - j0.212

2.4. APPROXIMATIONS OF TWO-WIRE LINE EXCITATION

The two-wire-line excitation is used in practically all cases of symmetrical wire antennas. For example, a horizontal wire-antenna structure above ground, used for short-wave communications, is fed most frequently by a two-wire line. It is, therefore, of considerable practical interest to analyse this type of excitation in greater detail.

Shown in Fig.2.11 is a sketch of a symmetrical dipole antenna, which is connected to a distant generator by means of a two-wire line. The TEM wave propagating from the generator along the line is partially reflected from the line end (at which the antenna is connected). In addition to the reflected TEM wave, a multitude of evanescent higher-order modes is excited in the line near its end. Obviously, the reflection coefficient of the TEM wave depends on the line termination (i.e., on the antenna properties) and on the excited higher-order modes. Considering the antenna as one-port network connected at the line end, the antenna admittance is defined as the ratio of current and voltage of the TEM mode at the antenna terminals.

The antenna admittance thus defined depends to a certain extent on the transverse dimensions of the two-wire line. However, if these di-

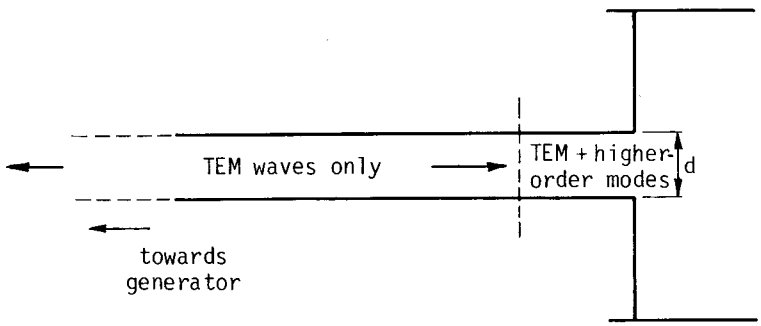

FIG.2.11. Sketch of a symmetrical wire antenna driven by very long two-wire line.

mensions are much smaller than the wavelength, this dependence is almost negligible, and the antenna admittance can be obtained approximately using any convenient approximation to the real excitation, such as the delta-function generator, the TEM magnetic-current frill or the belt generator. The delta-function generator approximation amounts to assuming that the distance d between the wires of the two-wire line tends to zero, and can be used with the same order of accuracy as in the case of the coaxial-line excitation. The other two representations are not physically obvious in this case, but they can yield stable solutions of reasonable accuracy if the two-wire line transverse dimensions and the antenna radius are sufficiently small. The outer radius of the magnetic-current frill and the belt-generator length are not critical parameters, because in the corresponding case of an electrically thin monopole antenna driven by a coaxial line the antenna admittance is practically independent of the coaxial-line dimensions.

However, if the two-wire line transverse dimensions are of the order of $0.001\,\lambda$ or larger, a more precise analysis is necessary. An approach to this problem was presented by King,[3] based on an equivalent L-C network between the two-wire line and the idealised antenna. Although yielding good agreement with experimental results, this method involves a somewhat artificial idea of the antenna intrinsic admittance. Another approach is to treat the wire antenna and the two-wire line sketched in Fig.2.11 together, as a unique wire structure, thus involving no approximation of the real excitation. Current distribution in this system can be determined using, for example, the method described in Section 1.2. In order to be able to analyse the system in this manner, it is necessary to introduce certain assumptions concerning the two-wire line.

One possibility is to consider the line to be straight and semi-infinite. We can then analyse the structure as having two progressive TEM waves along the two-wire line up to its end, with a corrective term in the end zone, requiring that boundary conditions for the electric field along the line and the antenna be satisfied. This procedure, using the Hallén equation with polynomial approximation for current along the an-

tenna and for the corrective term at the line end, was proposed in Reference 33, resulting in accurate antenna admittance. A disadvantage of this method is, perhaps, that rather complicated double integrals are involved in the analysis, which is inherent to the Hallén equation for non-cylindrical wire structures. This deficiency can be removed if the two-potential equation is used.

Another possibility is to consider the dipole to be driven by a line of relatively small length, as in Fig.2.12, and to solve the system as any other wire-antenna structure. In that case, however, the generator must be included into the analysis, which raises the question concerning the influence of the generator approximation on final results. Another question in this approach is the length of the two-wire line needed for obtaining accurate results for the antenna admittance and current distribution. Both problems can, fortunately, be solved quite simply, as outlined below.

To be able to obtain unique results for the antenna admittance, we have to assume that the section of the two-wire line in Fig.2.12 is of sufficient length, so that the coupling between the generator and the antenna exists only through the TEM waves along the line. On the other

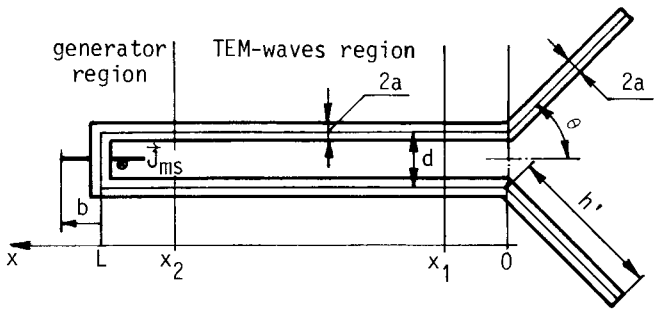

FIG.2.12. Sketch of symmetrical V-dipole antenna connected to generator by short segment of two-wire line. The generator is assumed to be a TEM magnetic-current frill.

hand, the shorter the section, the easier it is to analyse the problem numerically. By extensive numerical experiments it was found that the length of this section is not very critical, and that in some cases as little as 0.25 λ is sufficient to approximate accurately the two-wire-line excitation. This can be also verified from the example shown in Fig.2.13, where the admittance of a symmetrical dipole antenna is plotted versus the two-wire-line length, for various degrees of the polynomial approximation of current along the line.

What concerns the type of the generator to be used in representation shown in Fig.2.12, is obviously of little importance, provided that the line is of sufficient length. Therefore any desired approximation can be used, even the delta-function generator.

To solve for current distribution in the integral antenna-feeder system shown in Fig.2.12, we can, in principle, approximate current dis-

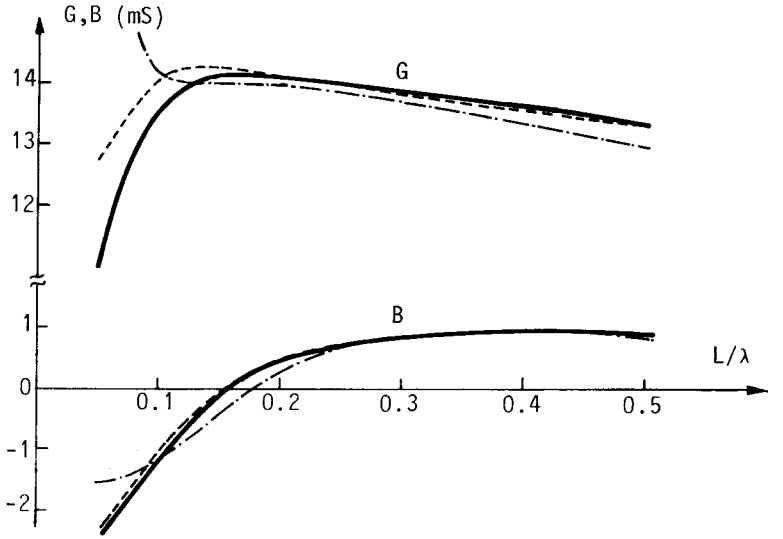

FIG.2.13. Conductance (G) and susceptance (B) of dipole antenna shown in Fig.2.12, for a=0.01 λ, θ=90°, h=0.2149 λ and d=0.03086 λ, versus the line length (L) for various degrees (n) of polynomial approximation of current along the line. — • — n=4; — — — n=5; ——— n=6.

tribution along the two-wire line by a sum of two TEM waves propagating in opposite directions, with unknown amplitudes, with additional terms in the vicinity of the line ends in order to approximate perturbation of the TEM regime in these regions. However, in the case of a short line it is much more convenient to use simple polynomial approximation along the whole line, because the line is then treated together with the antenna in a unique way and no significant adaptations of the program (in which polynomial approximation of current along all antenna segments is assumed) are necessary. Along the antenna itself, current expansion needs to be adopted according to the suggestions given in the preceding chapter. Naturally, continuity of current must be postulated at x=0 and x=L. What concerns the order of approximation along the two-wire line, it was found that it suffices to adopt a 4th-degree polynomial for the line segment if its length is of the order of $\lambda/4$, a 6th-degree polynomial being, however, sufficient for segments of lengths up to one wavelength (see Fig.2.13). If more precise current distribution is required near the line ends, separate subsegments can be taken in these regions.

Once the current distribution has been determined, the antenna admittance can be computed from any two values of current in the central two-wire-line part, using the formula

$$Y = jY_c \frac{I(x') \sin kx'' - I(x'') \sin kx'}{I(x'') \cos kx' - I(x') \cos kx''} , \quad x_1<x',x''<x_2 , \tag{2.45}$$

where

$$Y_c = \frac{\pi(\varepsilon/\mu)^{\frac{1}{2}}}{\ln \left\{d/(2a) + \left[d^2/(2a)^2 - 1\right]^{\frac{1}{2}}\right\}} \tag{2.46}$$

is the characteristic admittance of the two-wire line. Alternatively, the antenna admittance can be expressed in terms of current intensity and its derivative, dI(x)/dx, at a single point x, $x_1<x<x_2$, as follows:

$$Y = jY_c \frac{kI(x) \cos kx - I'(x) \sin kx}{I'(x) \cos kx + kI(x) \sin kx} , \quad x_1<x<x_2 , \quad I'(x) = \frac{dI(x)}{dx} . \tag{2.47}$$

Both formulas for the antenna admittance can easily be obtained from the well-known expression for current distribution along a transmission

line,

$$I(x) = j Y_c V_0 \sin kx + I_0 \cos kx \ , \tag{2.48}$$

where V_0 is the voltage and I_0 the current at x=0 corresponding to the TEM mode, and noting that $Y=I_0/V_0$.

It was found by extensive numerical experiments that eqns.(2.45) and (2.47) yield nearly the same results, provided that the points x' and x" in eqn.(2.45), i.e., the point x in eqn.(2.47), are within the limits of the TEM region along the line, and that x' and x" are not extremely close together. The latter case, obviously, may result in significant numerical errors when computing Y according to eqn.(2.45). An example is presented in Fig.2.14 for the case of a symmetrical dipole sketched

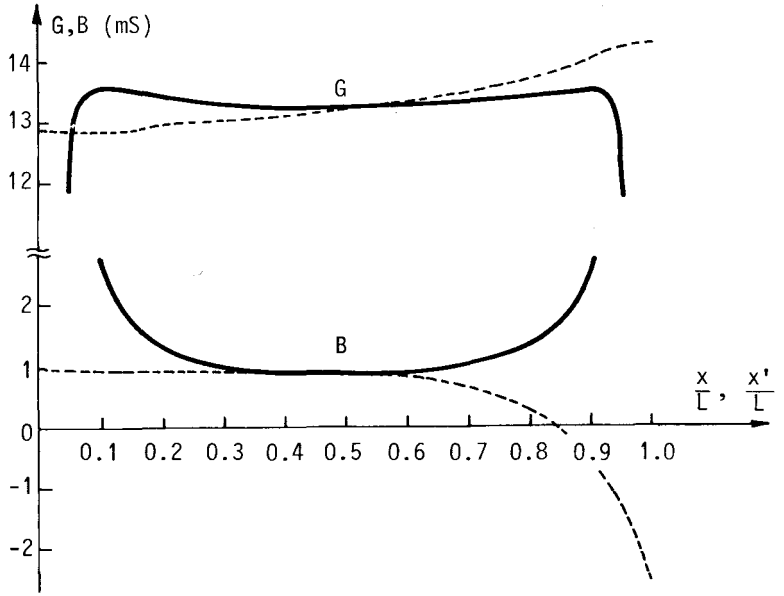

FIG.2.14. Conductance (G) and susceptance (B) of dipole antenna shown in Fig.2.12, for a=0.01 λ, θ=90°, h=0.2194 λ, d=0.03086 λ, L=0.5 λ and n=6, versus positions x' and x entering eqns.(2.45) and (2.47), with x"=L-x'. ——— G and B from eqn.(2.45); — — — G and B from eqn.(2.47).

in Fig.2.12. The antenna admittance was computed according to both formulas (2.45) and (2.47), but taking the points x' and x" symmetrically, i.e., x"=L-x'.

Finally, theoretical and experimental results for admittance of the V-dipole antenna sketched in Fig.2.12, for a=3 mm, $\theta=45^{o}$, d=12 mm and L=200 mm, are plotted in Fig.2.15 versus the antenna-arm length, h', at frequency f=883.3 MHz. Solid lines denote results obtained by the present theory, dashed lines (which almost coincide with the solid lines) denote results obtained in Reference 33 using Hallén's equation and an infinitely long two-wire line, while points represent experimental results, obtained according to the procedure outlined in the following

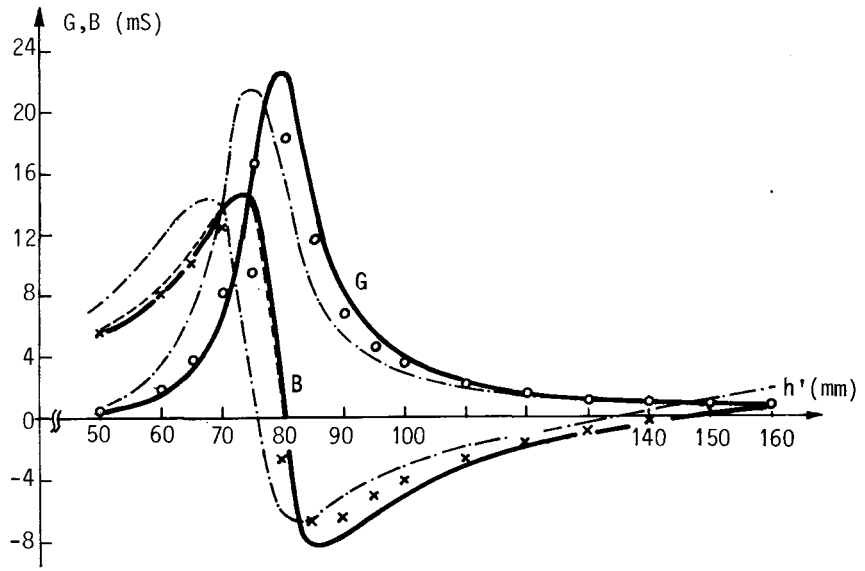

FIG.2.15. Conductance (G) and susceptance (B) of V-dipole antenna shown in Fig.2.12, for a=3 mm, $\theta=45^{o}$, d=12 mm and L=200 mm, at frequency f=883.3 MHz, versus antenna-arm length, h'. ——— present theory; — — — results obtained by Hallén's equation (Ref.33); oo,×× experimental results (Ref.34); — • — theoretical results for V-dipole antenna driven directly by a TEM magnetic-current frill.

subsection. Good agreement between theoretical and experimental results is observed. For comparison, theoretical results for admittance of a symmetrical V-dipole antenna are presented if the antenna is driven directly by a TEM magnetic-current frill with b/a=2 (which corresponds to L=0 in Fig.2.12). These results are in significant discrepancy with the results obtained for the two-wire-line excitation, showing that adequate modelling of the antenna excitation is indeed necessary in the present case.

2.4.1. A method for measuring admittance of symmetrical antennas by reflection measurements in coaxial line.[34] Direct measurements of input admittance of symmetrical antennas driven by symmetrical two-wire lines is a very difficult task. Firstly, there is no standard equipment for measurement of impedances of symmetrical systems the performance of which is comparable with that of the classical coaxial slotted line. Another problem is the influence of the antisymmetric wave mode which can be excited due to small asymmetries in the system caused by instrumentation situated in the electromagnetic field of the antenna and the two-wire line. The same problem is present when measurements are made by asymmetric coaxial-line instrumentation using standard balance-to-unbalance transformers, the accuracy of which is not high and is always influenced by the presence of antisymmetric wave modes.

The best way to overcome these difficulties is to perform the measurements on the asymmetrical system shown in Fig.2.16, which is an approximate asymmetric equivalent of the considered symmetrical antenna system. In this case the image theory applies, so that at a sufficient distance from the coaxial-line opening this situation is closely equivalent to the initial symmetrical antenna driven by a short segment of a two-wire line. The admittance measured at the reference plane 2-2' on the asymmetrical system shown in Fig.2.16 is twice the admittance of the symmetrical antenna considered.

Measurements can now be made using a standard slotted coaxial line connected behind the perfectly conducting plane (see Fig.2.16). In order to preserve high accuracy achieved by slotted-line measurements,

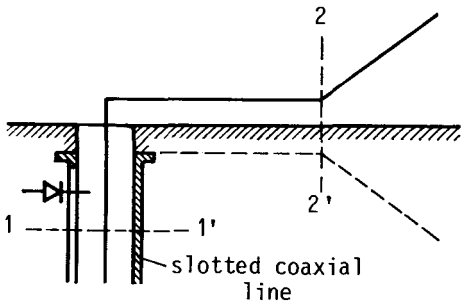

FIG.2.16. One half of a symmetrical antenna, together with a segment of a two-wire-line conductor, driven by a slotted coaxial line.

a special procedure must be adopted for calculating the impedance at the reference plane 2-2'. If we consider only TEM modes on both the coaxial line and the wire line, the system between reference planes 1-1' and 2-2' can be represented by a two-port network. The impedance Z_i seen at the reference plane 1-1' corresponding to the antenna terminating impedance Z_t at the reference plane 2-2' can be expressed in terms of the Z-parameters of this two-port network as

$$Z_i = \frac{Z_{11}Z_{22} - Z_{12}^2 + Z_{11}Z_t}{Z_{22} + Z_t} . \tag{2.49}$$

The parameters Z_{11}, Z_{22} and Z_{12} depend not only on the geometry of the coaxial line, the wire line and the transition region between these two, but also on the positions of the reference planes 1-1' and 2-2'. We can, therefore, adopt these positions in such a way that the transformation in eqn.(2.49) be as simple as possible.

One way to determine the Z-parameters accurately is to measure them on site by using three known reference impedances. The most reliable variable reference impedance at high frequencies is a movable short circuit and it was, therefore, used in the present measurements. If we fix the movable short circuit in the reference plane 2-2' (i.e., at the antenna terminal, so that $Z_t=0$), we can find the position of a voltage minimum along the slotted coaxial line and take this position as the reference plane 1-1'. If the two-port network is lossless, the voltage at the voltage minimum is zero, and therefore the impedance Z_i in this

reference plane is also zero. For this case we have from eqn.(2.49) that $Z_{11}Z_{22} - Z_{12}^2 = 0$, and eqn.(2.49) for arbitrary Z_t reduces to

$$Z_i = \frac{Z_{11}\, Z_t}{Z_{22} + Z_t} \,. \tag{2.50}$$

The parameters Z_{11} and Z_{22} can now be measured by extending the wire line beyond the reference plane 2-2' and by sliding the short circuit along the line, as shown in Fig.2.17. If we slide the short circuit to $x_2 = x_2' = \lambda/4$, we have $Z_t = Z_t' = \infty$. By locating the voltage minimum in the coaxial line at $x_1 = x_1'$, we can compute the input impedance as $Z_i' = j\, Z_{c1} \cdot \tan kx_1'$, where Z_{c1} is the characteristic impedance of the slotted coaxial line. From eqn.(2.50) we have immediately $Z_{11} = Z_i'$. By fixing the position of the slotted-line probe at $x_1 = x_1'' = \lambda/4$, we can now slide the short circuit to a new position $x_2 = x_2''$ which results in a voltage minimum at $x_1 = x_1''$, i.e., in $Z_i'' = \infty$ at the reference plane 1-1' (since current in that plane is then zero, and voltage is maximal). In this case we have, from eqn.(2.50), $Z_{22} = -Z_t'' = -jZ_{c2} \tan kx_2''$, where Z_{c2} is the characteristic impedance of the wire line, which is one half the characteristic impedance of the symmetrical two-wire line obtained if image theory is applied. Having thus determined the parameters Z_{11} and Z_{22}, we can now remove the short circuit and connect the desired antenna to the wire line, measure Z_i in the coaxial line and, from eqn.(2.50), then easily compute the antenna impedance Z_t at the reference plane 2-2'.

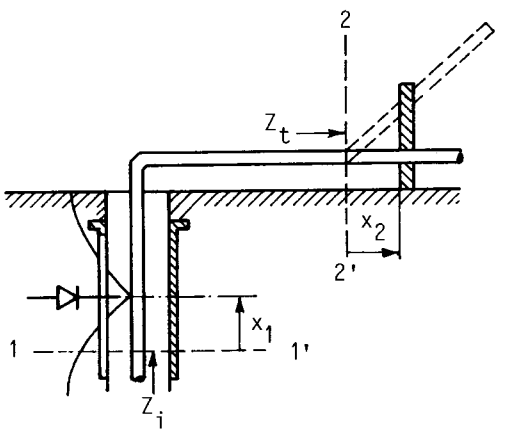

FIG.2.17. Measurement of equivalent-network Z-parameters.

2.5. CONCLUSIONS

Presented in this chapter were various approximations to actual excitations of wire-antenna structures. For practical applications it is useful to know which of these is most suitable in a given situation. Although this was mentioned when describing a specific approximation, it may be worth summarizing these suggestions at one place.

If radiation pattern of a wire-antenna structure alone is of interest, it suffices to use the simplest, delta-function generator approximation. The overall current distribution obtained with this approximation is quite accurate everywhere except near the generator itself (see Fig.2.3). The antenna radiation pattern obtained with this current distribution is very close to the actual pattern, so that this approximation suffices for practical applications. In addition, the delta-function generator approximation results in values of the antenna admittance which are good indications of the real values (see Table 2.1 and Fig.2.4). However, the antenna admittance, and particularly the susceptance, are substantially dependent on the order of approximation for current, so that they cannot be considered as reliable. In addition to this, the delta-function approximation can easily be incorporated only into the Hallén equation, and more sophisticated approximations are preferred with other types of equations.

If accurate value of the admittance of a wire-antenna structure driven by a coaxial line is desired, the TEM magnetic-current frill or the belt-generator approximations of the excitation should be used. The two approximations are of the same order of complexity and yield practically the same results, which are very accurate in most cases (see Table 2.3). It is important to note that for obtaining stable and reliable values of the antenna admittance using any approximation to the real excitation, it is essential, in particular for thicker antennas near resonance, to take into account the end effect.

The most accurate approximation of the coaxial-line excitation available is the magnetic-current frill which represents higher-order coaxial-line modes in addition to the TEM mode. The admittance correc-

tion term thus obtained (with respect to the TEM magnetic-current frill excitation) is relatively small at lower frequencies, and is practically imaginary (i.e., almost correction in susceptance only - see Table 2.6), but at higher frequencies the correction becomes substantial in both susceptance and conductance. Thus, at lower frequencies this relatively complicated procedure should be used only if extremely accurate theoretical values of admittance are required. At higher frequencies, however, when radiation from the coaxial-line opening becomes noticeable, this method should be used if accurate value of the antenna admittance is desired.

The two-wire-line excitation can be modelled very accurately by considering the antenna and a relatively short segment of the line as an integral wire structure. Note, however, that in the theory the structure is considered to be strictly symmetrical. In practice this is most often difficult to achieve, which may result in discrepancies between theoretical and experimental results.

CHAPTER 3
Treatment of Wire Junctions and Ends

3.1. INTRODUCTION

When dealing with wire-antenna structures having several interconnected wires, particular attention must be paid to the zones in which the wires are joined together, in order that a numerical solution for the antenna current distribution be accurate. Sharp bends along otherwise continuous wires fall into the same category, as well as abrupt changes of wire diameter, and can be treated using essentially the same technique. These three classes of discontinuities along wires of a wire-antenna structure we shall refer to as "junctions". As already pointed out in the previous chapters, wire ends deserve also special attention if stable and very accurate results for the antenna admittance are desired.

At wire junctions and ends and in their immediate vicinity the antenna current and charge distributions, as well as their fields, exhibit rapid variations. For example, the surface-current density vector, $\vec{J}_s$, has locally nonaxial components, which for some geometries can be very pronounced. On the other hand, the axial component in these regions may vary rapidly along the wire length or circumference, or may even be singular. Obviously, a rigorous treatment of junctions and ends is a complex problem. In principle, it can be solved by accurate approximations of current and charge distributions on the surface of the antenna junctions and ends and in their immediate neighbourhood. Fortunately, in most practical cases such an involved analysis is unnecessary if dimensions of these discontinuities are relatively small when compared

with the lengths of the wire segments interconnected at the junction and with the free-space wavelength. In these cases the local variations of current distribution can often be neglected if the integral effect of these variations is properly taken into account. This can be done efficiently by postulating some constraints on solutions of the integral equations for the antenna current distribution described in Chapter 1. Obviously, the manner in which the wire segments are interconnected in space (i.e., the antenna geometry) must be included appropriately into the antenna analysis, since this generally has appreciable influence on the antenna current distribution.

The constraints which include approximately the effects of junctions and of ends into the mathematical antenna model are established following the same general lines of reasoning. Therefore they are treated together in the following two sections. In Section 3.4 the rigorous treatment of wire ends is presented, showing its complexity and demonstrating to what extent such an analysis can improve accuracy of the approximate antenna current distribution.

3.2. CONSTRAINTS RESULTING FROM FIRST KIRCHHOFF'S LAW

If only thin-wire structures are considered, any linear dimension of junctions or wire ends is small compared with the wavelength. Therefore the fields in the domains of the junctions and wire ends are very nearly quasi-static, so that these discontinuities can be treated using a kind of circuit-theory relations. Hence, the wire segments should be regarded as branches, and the wire junctions and ends simply as the end points of these branches, i.e., as the nodes. In this way the actual shape of the junctions and ends is neglected, but an information about their geometry is retained.

In the formulation of some equations for current distribution in wire-antenna structures, the equation of continuity is implicitly taken into account by adopting the expressions for the vector and scalar potentials in the Lorentz gauge.[35] Therefore the exact solution of these equations would satisfy the equation of continuity automatically. In the derivation of the two-potential equation for arbitrary wire-antenna

structures, given in eqn.(1.15), as well as in the derivation of the special case of this equation for cylindrical antennas, eqn.(1.19), and the Schelkunoff equation, eqn.(1.29), the equation of continuity, eqn. (1.13), was used explicitly. However, it is assumed, in addition, that there are no excess charges at the ends of any antenna segment. This implies that the continuity equation for the wire currents at every node is *forced* to be in the form of the first Kirchhoff's law, i.e.,

$$\sum_{m=1}^{n} I_m = 0 \ , \tag{3.1}$$

where n is the number of wire segments meeting at the node, and the reference direction of a current is from the node outward. For a node representing a wire-segment end, this sum reduces to one term only, requiring that the current at the wire end vanishes. Since eqn.(3.1) was obtained from a basically artificial constraint, it *must* be used with eqns.(1.15), (1.19) and (1.29).

In reality, the distribution of charges accumulated at the antenna junctions and ends differs significantly from the charge distribution along the rest of the wire segments. Therefore, in a rigorous numerical solution these two distributions must be modelled separately. Fortunately, the charges accumulated at the antenna discontinuities are usually relatively small compared with the total charge along the rest of the wire segments. Therefore, the excess charges at the antenna nodes can often be neglected, and eqn.(3.1) is, indeed, approximately satisfied by the wire-structure currents. Note that if these charges were not neglected, their field should be incorporated into the two-potential and Schelkunoff's equation. Thus, for example, in eqn.(1.15) a term should be added to the left-hand side for every node, being essentially the electric field due to a point charge at the node.

Although it is not necessary to postulate the first Kirchhoff's law when using the equations based on the magnetic vector-potential only (i.e., the magnetic vector-potential, Pocklington's and Hallén's equations, given in Section 1.3), the use of eqn.(3.1) is always desirable in approximate numerical solutions, because this improves convergence

of the results, particularly with continuous approximations of the antenna current distribution.[11,36]

In some cases current distribution can be approximated in such a way that eqn.(3.1) be automatically satisfied at the antenna ends, e.g., by constructing special polynomials which vanish at wire ends,[10] or by using overlapping functions which are zero at the ends of their subdomains.[23] Explicit formulation of eqn.(3.1) can also be avoided by certain matrix manipulations.[36] However, we shall deal here only with simple polynomial approximation of current distribution, and therefore eqn.(3.1) needs always to be explicitly formulated and added to the point-matching equations.

In the theoretical analysis the antenna segments frequently coincide with the wire segments of the real antenna. However, in some cases a real antenna segment must be subdivided into two or more subsegments in order to obtain accurate solution for current distribution. This subdivision is necessary when current distribution is rapidly varying along one part of the physical antenna segment, while along the other part it is a slowly varying function. An example is the antenna excitation region, as pointed out in Chapter 2, with the only exception of the delta-function generator excitation, in which case such a subdivision is undesirable. When wire segments are very long in terms of the wavelength, they can be subdivided into subsegments in order to keep degrees of the polynomial approximation relatively low. An increase of the degree of the polynomial approximation requires a higher-order integration formula for evaluating the integrals encountered in the equation for the antenna current distribution, which somewhat complicates the programming. In addition, the lower-degree polynomials defined on shorter subsegments can be more flexible than a single higher-degree polynomial on the whole segment.

Obviously, a junction of two coaxial subsegments of equal radii does not represent a physical discontinuity in the real antenna structure. Therefore, both the current and charge distributions are continuous functions at such a node, so that, in addition to eqn.(3.1), the equation expressing continuity of the first current derivative at the node

may be added to the point-matching equations.[26] An exception of this rule are two subsegments on the two sides of a magnetic-current frill, as described in Section 2.3. In that case the discontinuity in the first current derivative is determined by eqn.(2.23). Formulation of equations for the first current derivative is not necessary except with the Schelkunoff equation, but it usually improves the convergence of the solution.

Eqn.(3.1) cannot be formulated for nodes lying in the ground plane for antennas driven by a coaxial line, because it is automatically satisfied in the equivalent symmetrical system. Only if there is a single antenna segment terminating at such a point at a right angle on the plane (or closely to that angle), current derivative can be set equal to zero, and this equation can replace eqn.(3.1). For other angles between the segment and the plane, or if there are more segments meeting at that node, junction-field constraints should be used.

3.3. JUNCTION-FIELD CONSTRAINTS

Consider a wire-antenna structure assembled from N_s segments (including in this number the wire subsegments), and having N_j junctions. Let the total number of unknown current-distribution coefficients be N_c. Hence, the total number of equations needed is also N_c. For such an antenna we can write N_j equations according to the first Kirchhoff's law. Thus, if only equations expressing the first Kirchhoff's law are formulated for the N_j antenna junctions, the number of the point-matching equations must be (N_c-N_j). It is easy to conclude that for a given number of antenna segments, N_s, the number of point-matching equations depends on the antenna topology. Therefore the matching points cannot be distributed along all the antenna segments in the same general manner. This is very inconvenient, because it prevents a unique choice of the number and positions of the matching points along all the antenna segments.

In addition to this disadvantage, postulating only the first Kirchhoff's law to be valid for a junction is not sufficient to obtain numerically stable solutions for the antenna current distribution if the

two-potential equation is used. This can be explained as follows. Neither the antenna theoretical model, described by eqn.(1.15), nor the approximation for current distribution, given in eqn.(1.16), can represent adequately the antenna junctions (as well as ends). Therefore the boundary conditions in the junction regions cannot be properly satisfied, so that by choosing the matching points arbitrarily and/or close to the antenna nodes might result in numerical instabilities.

Both problems can be solved by introducing additional constraints at every junction, which we shall refer to briefly as the junction-field constraints.[8] These constraints essentially minimize the influence of an improper current-distribution approximation in the vicinity of the junctions on the overall current distribution, by taking the integral effect of the approximate current distribution in the junction region to be the same as in a rigorous solution. In this way the effect of these inaccuracies is confined only to the junction and its immediate vicinity. At the same time these constraints enable a unique choice of the matching points along all segments of the wire-antenna structure.

The junction-field constraints represent, in a way, the second Kirchhoff's law for the antenna nodes. They can be deduced from the power considerations, as follows. In any numerical solution for current distribution in perfectly conducting antenna structures the boundary conditions are satisfied only approximately. Hence in the theoretical model the antenna electric currents are situated in a nonzero locally axial total electric field, and thus generate a nonzero complex power. The larger this power, the less accurate, on average, are the results for the antenna current distribution, admittance, radiation pattern, etc. The total locally axial electric field may be particularly large near the antenna junctions (as well as ends) because of inadequate modelling of current distribution in these regions. In order to keep this field low, one can try to better approximate current distribution in the vicinity of the junctions. However, this leads to a significant increase in the number of unknown current-distribution coefficients. If the specific surface distribution of currents in the vicinity of the junctions is ignored, as has been done in eqn.(1.15), this increase

might even fail to give any improvement.

The length of the zone of the junction is relatively small, of the order of a few radii of the thickest wire connected at the junction. Therefore current intensity in the wires interconnected at the junction does not vary significantly in this zone. The complex power generated by the antenna currents in the vicinity of a junction of n segments can hence be approximately evaluated as

$$S = - \sum_{m=1}^{n} U_m I_m^* , \tag{3.2}$$

where I_m is the current intensity at the junction node in the wire labelled "m" (Fig.3.1), the asterisk denoting the complex conjugate,

$$U_m = \int_{L_m} (\vec{E} + \vec{E}_i) \cdot d\vec{l} \tag{3.3}$$

is the voltage along the path L_m lying along the *m*th wire-segment axis (Fig.3.1), and $(\vec{E}+\vec{E}_i)$ is the total electric field. From eqn.(3.1) and Fig.3.1 it follows that

$$I_1^* = - \sum_{m=2}^{n} I_m^* , \tag{3.4}$$

so that eqn.(3.2) can be written in the form

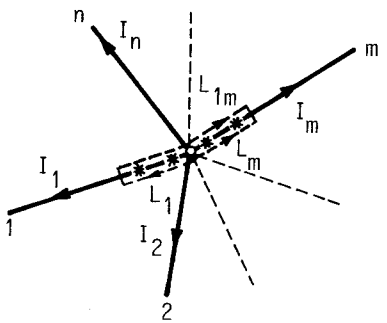

FIG.3.1. Symbolic representation of a junction of n wires.

$$S = -\sum_{m=2}^{n} (U_m - U_1)\, I_m^* \quad . \tag{3.5}$$

The difference $(U_m - U_1)$ is the integral of the total electric field along the path L_{1m} lying on the axes of the segments denoted by "1" and "m", as shown in Fig.3.1. The power generated by the antenna currents in the vicinity of the junctions will be zero if these differences are zero for m=2,3,...,n , i.e., if

$$\int_{L_{1m}} (\vec{E} + \vec{E}_i) \cdot d\vec{l} = 0 \quad , \quad m=2,3,\ldots,n \quad . \tag{3.6}$$

Eqns.(3.6) represent the junction-field constraints. In fact, they require that the total electric field along the wires in the vicinity of a junction oscillates around zero, so that its average value be zero, but they allow, in principle, that the electric field may have high local extrema.

By numerical trial-and-error method it was found that in most cases approximately optimal path length is about three to four wire radii along every segment. If radii of the wires interconnected at the junction are different, this path length is determined by the largest radius.

The integral in eqn.(3.6) can be approximately computed by using the repeated midpoint rule, i.e., by simply summing the integrand at midpoints of subsegments of equal lengths into which the path is subdivided. Eqn.(3.6) is thus reduced to summing (averaging) several point-matching equations. It was also found by numerical experiments that it suffices to take only two integration points per one arm of the path L_{1m} if the radii of the wires interconnected at a node do not differ more than about 2:1. These points are denoted by asterisks in Fig.3.1. For larger differences between the wire radii the number of the integration points should be correspondingly larger.

According to eqns.(3.6), for a junction of n wires we can formulate (n-1) equations resulting from the junction-field constraints. These equations, together with that obtained using the first Kirchhoff's law,

form a set of exactly n equations. This is true for the wire ends also (where n=1), but it should be noted that constraints in eqns.(3.6) need not be used for the ends. At these points the currents are postulated to be zero, and therefore complex power of these currents is usually negligible.

As a consequence, for the whole wire structure exactly two of these equations can be associated with every antenna segment. Hence, if the degree of the polynomial approximation is n_m, i.e., if there are (n_m+1) unknown current-distribution coefficients for that segment, (n_m-1) point-matching equations are required along it, which is a unique choice for all the antenna segments. For obvious reasons, the matching points should be distributed relatively uniformly along every segment, avoiding junctions and ends, at which the current distribution is relatively inaccurately approximated. Thus, if the segment local s_m-axis has the origin at one segment end, and if h_m is the segment length, a suitable choice of the matching points is

$$s_{mp} = \frac{2p-1}{2n_m-2} h_m , \quad p=1,2,\ldots,(n_m-1) . \tag{3.7}$$

Of course, for a junction of two coaxial wire segments of the same radius at which a magnetic-current frill is situated, instead of eqn.(3.6) the equation expressing discontinuity in the first current derivative should be used [see eqn.(2.23)].

As an example, shown in Fig.3.2 is a "top-loaded" monopole antenna driven by a coaxial line, which is modelled by the TEM magnetic-current frill. Depicted in Fig.3.3 is the total axial electric field along the axis of segments 1, 2 and 3 of the antenna, normalized with respect to the impressed electric field at the center of the magnetic-current frill. The matching points are denoted by circles in Fig.3.3. This example illustrates clearly practically all the conclusions of this section relating to the total axial electric field along the wires of a wire antenna resulting from the approximate numerical solution of the two-potential equation with polynomial approximation for current, subject to the constraints described above. If we note the scale of the relative total axial electric field, it may be concluded that the cur-

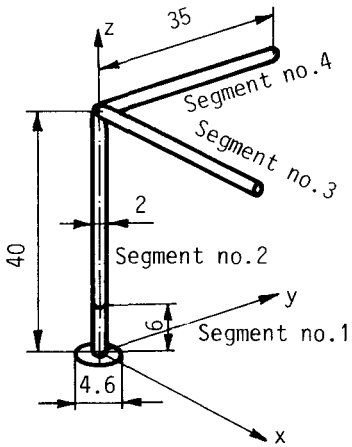

FIG.3.2. Sketch of top-loaded monopole antenna driven by coaxial line. All dimensions are in millimeters.

rent distribution obtained is quite accurate. According to the authors' best knowledge, no available method results in better satisfaction of boundary conditions with approximately the same order of current-distribution approximation.

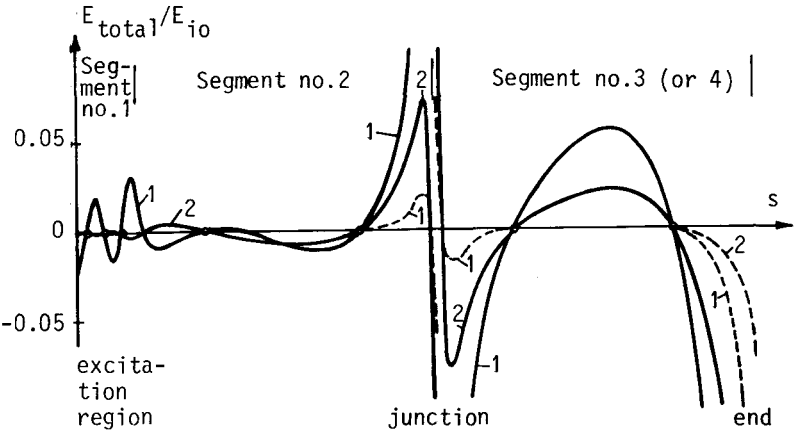

FIG.3.3. Real part (1) and imaginary part (2) of locally axial electric field along segments of antenna shown in Fig.3.2, normalized with respect to impressed electric field at center of magnetic-current frill, at frequency f=1 GHz. Adopted degrees of polynomial approximation of current were $n_1=4$, $n_2=3$ and $n_3=n_4=3$. End effects were neglected. ——— normal scale; — — — 10 times reduced scale. Small circles denote matching points.

3.4. TREATMENT OF WIRE ENDS[24,15,16]

As it can be concluded from Fig.3.3, improper treatment of wire ends results in a very large total electric field in the vicinity of these discontinuities. In many practical cases this does not introduce significant errors in antenna analysis, because the antenna current is forced to be zero at the wire ends and the power generated by this current is relatively small. Thus, in the case of electrically thin wires, this large electric field usually has little effect on the antenna current distribution away from the wire ends, as well as on the antenna admittance and radiation pattern, provided that there are no matching points very close to the ends. However, neglecting the end effect in the case of electrically thicker resonant antennas can lead to significant numerical instabilities, which cause the antenna admittance to diverge with increasing order of the current distribution approximation in the end region.

A rigorous treatment of the end effect must include precise approximation of the surface current and charge distribution at the antenna ends, taking into account the exact shape of the ends. Such a treatment is presented in this section for the case of cylindrical antennas (of circular cross-section) with hemispherical and with flat ends, because these are the simplest structures where there are neither circumferential currents, nor circumferential variations of currents and charges, and the problem is, in fact, that of finding one-dimensional current distribution. The precise treatment of the end effect requires an exact integral equation for the antenna current distribution. Therefore we shall first make some necessary comments on the integral equations for cylindrical antennas.

Let us consider a hollow, cylindrical, thin-walled antenna, sketched in Fig.3.4(a). The antenna currents and charges are localised only on the cylindrical surface, of radius a. If the antenna conductor is assumed to be perfect, the tangential component of the total electric field at the antenna surface must be zero. Due to symmetry, there is no circumferential component of the electric field, and only the axial,

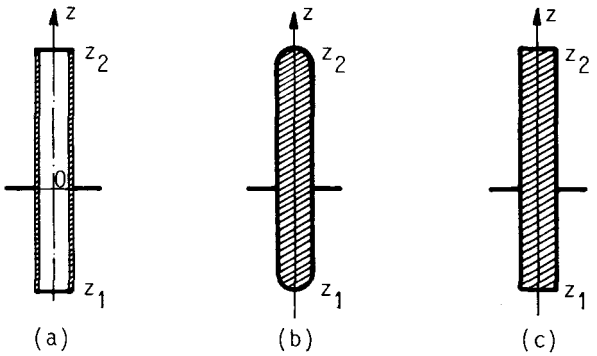

FIG.3.4. Sketch of (a) hollow, thin-walled cylindrical antenna, (b) cylindrical antenna with hemispherical end caps and (c) cylindrical antenna with flat end caps, driven by TEM magnetic-current frills.

z-component, should be considered. Thus the boundary conditions yield

$$E_z + E_{iz} = 0 \ , \tag{3.8}$$

where

$$E_z(z) = -j\omega\mu \int_{z_1}^{z_2} \left[I(s) + \frac{1}{k^2} \frac{dI}{ds} \frac{\partial}{\partial z} \right] G(z,s)\, ds \tag{3.9}$$

is the electric field along the antenna due to the antenna currents and charges, $\vec{E}_i$ is the impressed field (due, for example, to the TEM magnetic-current frill), and

$$G(z,s) = \frac{1}{2\pi} \int_{-\pi}^{\pi} g(r)\, d\phi \tag{3.10}$$

is the so-called exact kernel, where g(r) is Green's function, given in eqn.(1.5). The distance r between the source point $P'(z=s,\phi)$ and the field point $P(z,\phi=0)$ at the antenna surface is given as

$$r = \left[(z-s)^2 + 4a^2 (\sin \tfrac{\phi}{2})^2 \right]^{\frac{1}{2}} \ , \tag{3.11}$$

where a is the antenna radius. When eqn.(3.9) is substituted into eqn. (3.8), the *exact* form of the two-potential equation for the hollow cylindrical antenna is obtained. However, this equation contains a double integral with a logarithmic singularity,[37] which might be rather complex to handle. Thus, instead of using the exact kernel, the so-called reduced kernel is used almost without exception. It has the form

$$K(z,s) = g(r_a) \ , \tag{3.12}$$

where

$$r_a = \left[(z-s)^2 + a^2\right]^{\frac{1}{2}} \tag{3.13}$$

is interpreted as an approximate average distance (see also Section 1.2). Eqn.(3.12) should be substituted into eqn.(3.9) instead of G(z,s), yielding the already cited two-potential equation for cylindrical dipoles, eqn.(1.19). The reduced kernel in eqn.(3.12) is often interpreted as being only an approximation to more complex exact kernel given in eqn.(3.10) in connection with computing the electric field at the antenna surface due to the antenna currents and charges located at the surface. Alternatively, it is interpreted as the exact kernel if the currents and charges are assumed to lie along the antenna axis, and the field is computed at the antenna surface.[3] However, both of these approaches are misleading if one wants to find the source of instabilities associated with the reduced kernel.

If we imagine the field sources to be where they are in reality, i.e., at the antenna surface, and substitute eqn.(3.12) into eqn.(3.9), we obtain the *exact* expression for the electric field at the axis of the hollow-tube antenna. However, the electric field at the antenna axis is *not* equal to zero, because the antenna is hollow and its axis is not enclosed by a perfectly conducting surface. Therefore, forcing eqn. (3.8) to hold along the z-axis for such an antenna means imposing non-physical conditions, which, naturally, causes instabilities in the numerical solution. This is particularly pronounced when matching points are located in the immediate vicinity of the antenna ends, where the total field differs significantly from zero.

If the antenna is capped, eqn.(3.8) is rigorously satisfied along the z-axis, but the expression for E_z must include the field due to currents and charges located at the antenna ends [i.e., at the hemispheres in Fig.3.4(b), or the discs in Fig.3.4(c)]. It should be noted that with this correction eqn.(3.8) expresses the extended boundary conditions exactly, as discussed in Section 1.2.

If we consider a smooth, rotationally symmetrical antenna, the charge $Q'(z)$ per unit length measured along the antenna axis is related to the axial antenna current, $I(z)$, by the continuity equation (1.13), just as in the case of wires of constant cross-section. Therefore the electric field along the axis of such an antenna is essentially given by eqn. (1.14), and has the form

$$E_z(z) = -j\omega\mu \int_{z_1}^{z_2} \left[I(s) + \frac{1}{k^2} \frac{dI}{ds} \frac{\partial}{\partial z}\right] K(z,s)\, ds \ , \tag{3.14}$$

provided that the variable antenna radius, $a(s)$, is used in eqn.(3.13). When eqn.(3.14) is substituted into eqn.(3.8), the *exact* two-potential equation for the current distribution of a capped antenna is obtained.[38] This equation can be solved with almost no more problems than the "ordinary" two-potential equation, eqn.(1.19). However, one should bear in mind that the extended boundary conditions result in an inherently less stable equation than the exact boundary conditions, because in the first case the kernel is quasi-singular, and in the second it is singular.[39] As a consequence, the approximate current distribution obtained using the extended boundary conditions, being sensitive to location of the matching points, tends to oscillate when the spacing between the matching points becomes smaller than the distance between the matching points and the antenna surface.

As it can be seen from the above discussion, inclusion of the end effect in the analysis of cylindrical antennas does not represent a serious conceptual problem, except that it requires computation of a new type of quasisingular integrals (for the caps). Unfortunately, a number of extra terms is needed in order to approximate the antenna

current distribution in the vicinity of the antenna ends. This implies an increase in the computer storage requirements and execution time. However, visible improvements may be gained in the stability of the solution for the antenna current distribution, and particularly its admittance, as can be seen from the following example. Consider a quarter-wavelength monopole antenna, of radius a=0.007022 λ, driven by a coaxial line with b/a=3, sketched in Fig.2.5. According to the experimental results presented in Reference 17, the antenna admittance is Y=(17.84 - j7.50) mS. In the theoretical analysis the monopole antenna was first divided into two subsegments: the excitation region, and the rest of the monopole. The degree of the polynomial approximation in the excitation region was n_1, and along the rest of the monopole n_2. The antenna was analysed using the Hallén and the two-potential equations, with the belt-generator and the TEM magnetic-current-frill approximations of the coaxial-line excitation, without taking into account the end effect. In Table 3.1 the antenna admittance is presented for various degrees n_1 and n_2. It can be seen that the results do not seem to converge with increasing the polynomial degree n_2, although for n_2=4 or 5 the results are very close to the experimental ones. In order to locate the source of these instabilities, a third antenna subsegment, 6a long, was separated at the antenna end. The polynomial degree for this segment was n_3. The antenna admittance was quite in-

TABLE 3.1. Admittance (in mS) of quarter-wavelength monopole of radius 0.007022 λ, versus degrees of polynomial approximation for current distribution, without taking end effect into account.

n_1	n_2	Hallén's equation*	Two-potential equation	
		belt generator		TEM magnetic frill
3	3	18.04 - j7.61	19.80 - j7.49	19.61 - j7.33
3	4	17.65 - j7.68	18.39 - j7.62	18.33 - j7.59
4	4	17.61 - j7.66	18.41 - j7.58	18.24 - j7.48
4	5	17.35 - j7.73	17.84 - j7.50	17.89 - j7.42
4	6	17.10 - j7.74	17.32 - j7.64	17.30 - j7.58

* These results differ somewhat from those presented in Table 2.3 due to different arithmetic precision used in computation.

sensitive to variations of both n_1 and n_2, while changes of n_3 resulted in drastic variations of the admittance, as can be seen from the second column of Table 3.2 (n_4 is not applicable to this column). This points out to the improper treatment of the end effect as the source of the instabilities. If the end effect is rigorously analysed taking into account the hemispherical cap and approximating the antenna current distribution at the cap by a separate polynomial, the degree of which is n_4, and still retaining the short subsegment adjacent to the end, with the polynomial degree n_3, very stable and accurate results for the antenna admittance are obtained, presented in the last column of Table 3.2. The short subsegment adjacent to the hemispherical end improves very much the stability of the solution, because the antenna current is rapidly varying along it. The total electric field along the antenna axis, associated with this solution, is very small, as can be seen in Fig.3.5. For comparison, the total axial electric field at the antenna end obtained without taking the end effect into account is even stronger than the amplitude of the excitation field along the z-axis.

The antenna analysis which includes treatment of wire ends can be significantly expedited noting that the shape of the charge distribution in the vicinity of the ends practically does not vary with the antenna length and frequency. This will be demonstrated in the case of

TABLE 3.2. Admittance (in mS) of quarter-wavelength monopole of radius 0.007022 λ, versus degrees of polynomial approximation for current distribution, obtained by two-potential equation.

n_1	n_2	n_3	Without end effect	n_4	With end effect
4	4	3	17.00 - j7.60	3	17.74 - j7.47
				4	17.72 - j7.52
4	4	4	15.36 - j7.78	3	17.58 - j7.51
				4	17.60 - j7.50
4	4	5	16.50 - j7.66	3	17.68 - j7.48
				4	17.68 - j7.50
4	4	6	14.90 - j7.80	3	17.63 - j7.50
				4	17.66 - j7.52

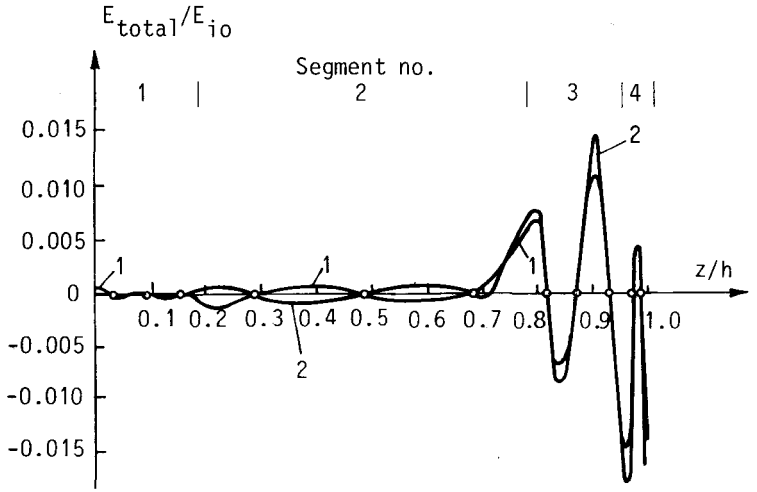

FIG.3.5. Real (1) and imaginary (2) parts of total axial electric field along z-axis of quarter-wavelength monopole of radius 0.007022 λ, normalized with respect to impressed electric field due to TEM magnetic-current frill at z=0. This field was computed from the solution of the two-potential equation which included end effect into account. Degrees of polynomial approximation were $n_1=n_2=n_3=4$ and $n_4=3$. Small circles denote matching points.

a cylindrical antenna with flat ends, like that sketched in Fig.3.4(c), although the procedure can also be applied to other shapes of the antenna ends.

In the case of antennas with flat ends eqn.(3.14) is not valid, because dI/ds is not defined at the end discs. In this case the electric field along the antenna axis due to the disc current is zero, as a consequence of symmetry. Therefore the total disc field is due only to its charge, of density $\rho_s(\rho)$. As this charge distribution is also symmetrical, its field along the antenna axis (see Fig.3.6) can be calculated from eqns.(1.2) and (1.4) as

$$E_{ds}(s) = -\frac{1}{\varepsilon}\int_0^a \rho_s(\rho)\,\frac{dg(r)}{ds}\,2\pi\rho\,d\rho\ , \qquad (3.15)$$

where $r=(s^2+\rho^2)^{\frac{1}{2}}$. The charge density $\rho_s(\rho)$ can be approximated by a polynomial with even degrees only,

$$\rho_s(\rho) = \sum_{k=0}^{n_d} D_k \left(\frac{\rho}{a}\right)^{2k} + D_r \delta(a-\rho) , \qquad (3.16)$$

in which case the integrals in eqn.(3.15) can be evaluated explicitly. The last term in eqn.(3.16) represents a line charge, i.e., a ring, which approximates the edge effect.

In what follows, the treatment of the end effect is included into the Schelkunoff equation, eqn.(1.29). In that case the discontinuity of the first current derivative, dI/ds, at the end of the antenna cylindrical part can be regarded as a source of a strong local electric field, E_e, given by the last left-hand term in eqn.(1.29). The field E_e is practically localised only in a region the length d of which along the s-axis is of the order of several antenna diameters (see Fig. 3.6). Therefore this zone will be referred to as the antenna end region. The charge distribution along the antenna cylindrical part (which is proportional to dI/ds) is a rapidly varying function in this region, so that its electric field, together with the field due to the disc charge, compensates the major part of the field E_e.

The charge distributions on the disc and on the antenna cylindrical part are proportional to dI/ds at the antenna end (i.e., at s=0). Being essentially quasi-static distributions, they depend practically only on the antenna end geometry, and not on the antenna length and frequency. Therefore they can be determined once for all antenna lengths and incorporated into the antenna current distribution.

The antenna current distribution along the antenna cylindrical part can now be represented as a sum of a slowly varying term, given in eqn. (1.30), valid along the whole antenna length, and a rapidly varying term, $I_1(s)$, defined only in the end region. This total current for s=0 must be equal to the disc current for $\rho=a$, which corresponds to the disc charge given by eqn.(3.16). The local current distribution $I_1(s)$ must also satisfy boundary conditions at the end of the end region

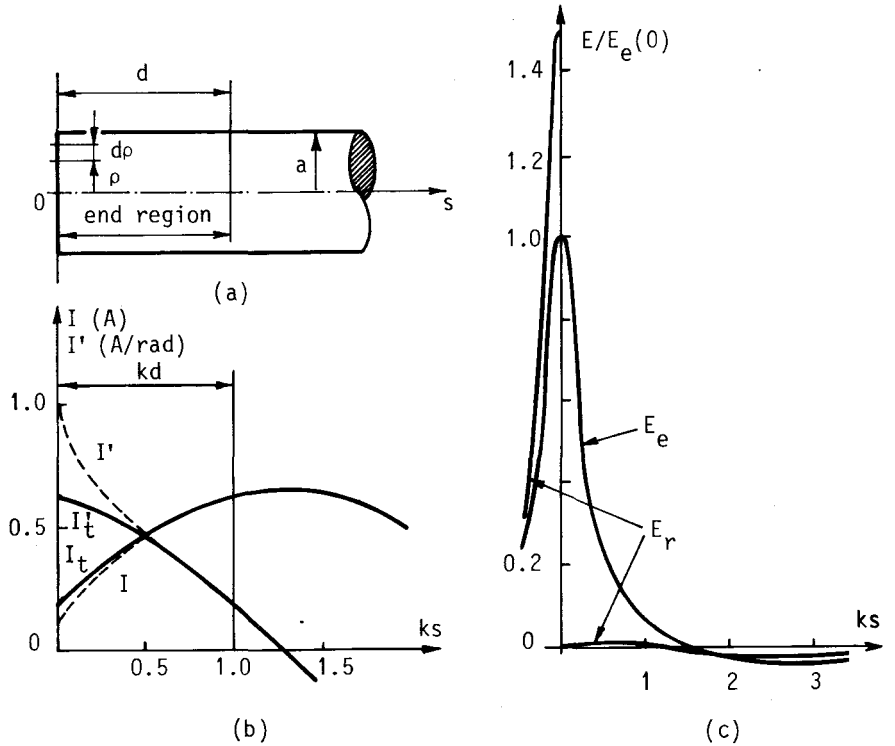

FIG.3.6. (a) Sketch of cylindrical-antenna end region. (b) Current and its first derivative in end region for ka=0.1321 and I'(0)=1 A/rad: I_t - main part of current, $I_t^!=dI_t/d(ks)$ - main part of the first current derivative, I - total current, I'=dI/d(ks) - the first derivative of total current. (c) Field distribution in end region: E_e - field due to discontinuity of the first current derivative, E_r - sum of E_e and fields due to local distributions on antenna cylindrical part and end discs. (Please see text for further explanations.)

(s=d). Therefore it is taken in the form of a special polynomial,

$$I_1(s) = \sum_{k=2}^{n_1} C_k (d-s)^k \quad , \tag{3.17}$$

so that $I_1=0$ and $dI_1/ds=0$ for s=d, thus automatically satisfying current and charge continuity conditions for s=d.

The coefficients C_k and D_k of the local distributions can be computed using the point-matching technique and requiring that the total electric field, E_r, which is the sum of E_e and the fields due to both local distributions, be a continuous and slowly varying function along the s-axis, and be zero at the antenna end (s=0+).[16]

Fig.3.6(b) gives an example of the antenna current and charge distributions along the cylindrical antenna part in the end region. I_t and I_t' are the main parts of the antenna current and its first derivative, which are in the present case approximated only by two trigonometric terms. Local current is superimposed on the main part, yielding the total current distribution along the antenna. Given in Fig.3.6(c) are the field E_e and the total field corresponding to the local distributions. Such a slowly varying electric field can now be easily compensated by a low-degree polynomial in the main part of the antenna current, requiring no more terms and matching points than on the rest of the antenna.

The method for analysis of cylindrical antennas described above is particularly suitable in the case of electrically long antennas.[15,16] As an example, Fig.3.7 shows conductance and susceptance of a monopole antenna with ka=0.1321, versus its electrical height, kh. In spite of the fact that the distance between successive matching points along the main antenna part was as large as 0.27 wavelengths, the theoretical results are seen to be remarkably accurate.

The above example is based on the Schelkunoff equation, but, obviously, the analysis of the local charge and current distributions can also be incorporated into other types of integral equations for cylindrical antennas. It should be noted that a similar analysis can be performed for local current distribution in the excitation region,[16] thus reducing the number of matching points and current distribution coefficients in that region, while retaining excellent results for the antenna admittance.

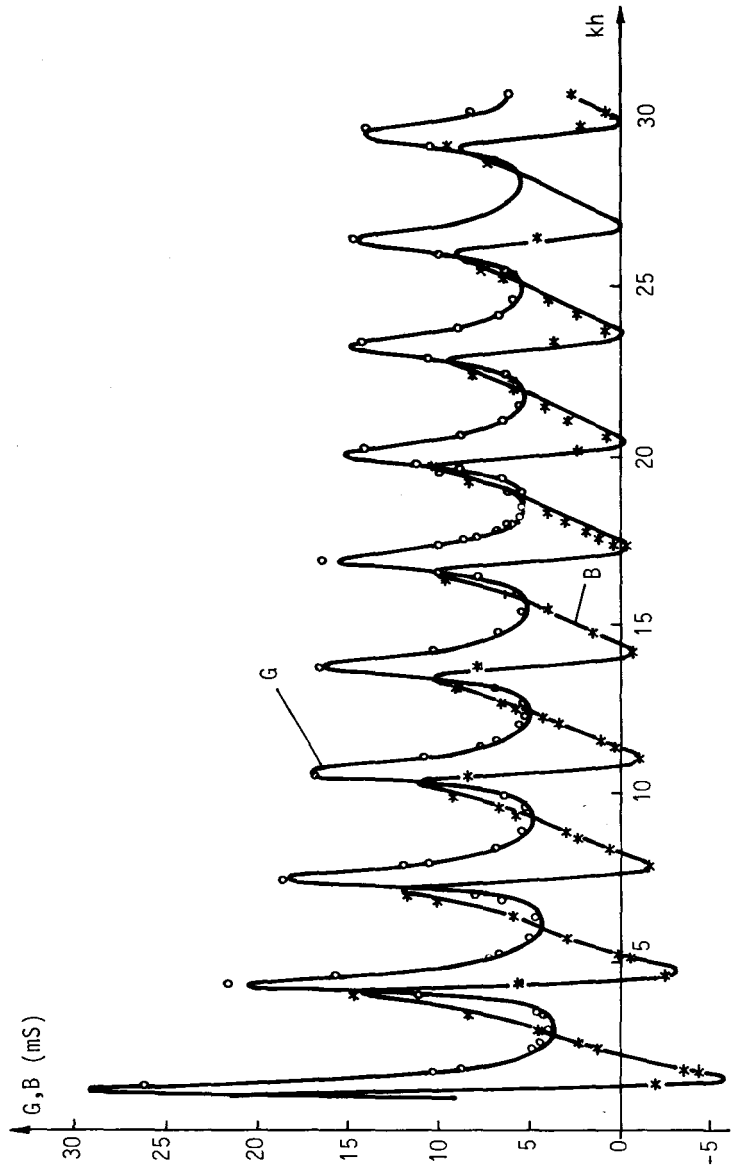

FIG.3.7. Conductance (G) and susceptance (B) of cylindrical monopole antenna of radius (in electrical units) ka=0.1321, versus its electrical height, kh. ——— theory, oo, ** experiment. (Ref.15)

3.5. CONCLUSIONS

Presented in this chapter were the approximate methods for treating wire junctions and ends. This treatment requires that the first Kirchhoff's law be postulated for every junction and end. In addition, junction-field constraints can be written for every junction, implicitly requiring that boundary conditions be satisfied, on average, in the junction region. These junction-field constraints are, in a sense, a representation of the second Kirchhoff's law. By requiring that all these constraints be satisfied for every junction and wire end it becomes possible to associate two of these equations with every antenna segment, so that (n_m-1) matching points can be chosen per segment. [Note that (n_m+1) is the number of unknown current-distribution coefficients for the segment considered.] This simple rule is valid for all the segments of a wire-antenna structure, which is very convenient, because it enables automatic choice of numbers and positions of the matching points in the antenna structure. These constraints yield relatively stable and sufficiently accurate solutions of the two-potential equation for arbitrary wire antennas for most practical purposes.

If more stable and reliable results for the antenna admittance are desired, in particular for resonant, or nearly-resonant, thicker antenna structures, it is necessary to model the antenna surface-current distribution more precisely. Such a treatment is very complicated and it was presented in this chapter only for the ends of cylindrical antennas. Very accurate numerical results for antenna current distribution and admittance of cylindrical antennas are thus obtained, which are approximately of the same order of accuracy as the most precise results that can be obtained by standard admittance measurements.

Using the technique described so far in this monograph, it is possible to analyse with remarkable accuracy any thin-wire antenna structure consisting of perfectly conducting wire segments. It was assumed in the analysis, however, that there are no loadings along the segments and that the whole structure is situated in a homogeneous perfect dielectric. These conditions are fulfilled frequently, at least approximately, but in practice loaded wire antennas and wire antennas in inhomogeneous and/or imperfect-dielectric media are also encountered. The problems associated with such cases are analysed in the next chapters.

CHAPTER 4
Wire Antennas with Distributed Loadings

4.1. INTRODUCTION

Electrical characteristics of an antenna made of a perfectly conducting material depend, at a given frequency, only on the antenna shape and size. In some cases it is convenient, or even necessary, to modify antenna current distribution for given antenna dimensions. This can be done by loading the antenna with a convenient type of loadings. In this way some of the antenna properties (such as admittance, radiation pattern, power gain, etc.) can be improved. A well-known example is the rhombic antenna. At its far end from the feeder a resistor is connected to decrease reflections from that end. In this way the antenna current distribution is changed from a standing wave to a travelling wave, which results in a remarkably broadband antenna in its admittance. Another well-known example is a medium-wave or short-wave vertical monopole antenna with an inductive coil inserted between two antenna sections, which improves to some extent radiation from the monopole. Finally, a dielectric, usually protective,cover over a wire antenna also represents a loading along the antenna.

The term "loaded wire antenna" is often used in a rather wide sense. For example, it is said frequently that a vertical monopole with an inverted-umbrella-like wire structure at its top is "capacitively loaded" (see also Fig.3.2). On the other hand, the same term is used for a vertical monopole consisting of two segments, the upper, short segment being connected to the base segment by means of a lumped capacitor. To

avoid this rather loose meaning of the word, in this and in the next chapter we shall use the expression "loaded wire antenna" in a more narrow sense. As loaded wire antennas we shall consider antennas having one or more of the following four general types of loadings:

a) If current in a wire segment or segments of the antenna can be associated with a continuous distribution of (locally) axial electric field which is a function of the current intensity at the point of the segment considered, we say that the segment is loaded with a *series distributed loading*. An example is an antenna made from a resistive rod.

b) If the voltage between two close points along a segment is a function of the current between these two points and remains finite if (theoretically) the two points become infinitely close, we say that there is a *series concentrated*, or *lumped loading* at that point of the segment. An example of this type of loading is an electrically small coil inserted between two antenna segments.

c) If a distributed current exists along the segment perpendicular to the local segment axis and is a function of the local radial electric field, i.e., of the local charge density on the antenna, we say that the antenna is loaded with a *shunt distributed loading*. A loading of this type is a thin protective dielectric coating over the wire.

d) If the preceding effect is localised to a very small part of a segment, but results in a finite radial current, we say that a *concentrated* (*lumped*) *shunt loading* exists at that point of the antenna. An example of this type of loading is a lumped capacitor, coil or resistor connected between two perpendicular segments, far from both ends of one of them, or a thin metallic disc mounted on the wire perpendicular to its axis.

In principle, the loading can be passive or active, linear or nonlinear, as in network theory. We shall consider here only cases of linear passive loadings. The present chapter is devoted to analysis of distributed loadings, and the next to analysis of lumped loadings.

4.2. EQUATIONS FOR CURRENT DISTRIBUTION ALONG ANTENNAS WITH SERIES DISTRIBUTED LOADINGS

Consider a cylindrical antenna with a linear distributed loading along its length, sketched in Fig.4.1. (It will be seen that generalization to an arbitrary wire-antenna structure is almost straightforward.) We assume that the loading is a smooth and slowly varying function of the z-coordinate (which, as earlier, coincides with the antenna axis).

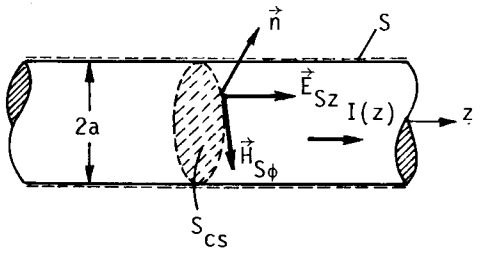

FIG.4.1. Part of cylindrical antenna with surface S enclosing it.

Let $\vec{E}$ be the electric field due to the antenna currents and charges, and $\vec{E}_i$ the impressed electric field. Hence, the total electric field on S, $\vec{E}_S=\vec{E}+\vec{E}_i$. The total magnetic field can be represented in a similar manner, $\vec{H}_S=\vec{H}+\vec{H}_i$. From the definition of the linear series distributed loading it follows that the total current through the antenna cross-section (equal to the sum of conduction and displacement currents through S_{cs}) must be proportional to the z-component of the total electric field at the antenna surface, i.e.,

$$E_{Sz}(z) = Z'(z)\, I(z) = Z'(z)\cdot 2\pi a H_{S\phi}(z) \quad . \tag{4.1}$$

$Z'(z)$ is known as the *internal impedance* per unit length, and is, essentially, *defined* by eqn.(4.1). It is an integral description of the antenna interior and can be determined, at least in principle, if we know the actual antenna composition.

In order to apply the usual expressions for the retarded potentials, the medium must be homogenized. This can be done using the equivalence theorem,[5] following the same procedure as in Section 2.2. Thus from

eqn.(2.1) we obtain the density of the equivalent surface electric current,

$$\vec{J}_s(z) = \frac{I(z)}{2\pi a} \vec{i}_z \ . \tag{4.2}$$

The density of the equivalent surface magnetic currents, $\vec{J}_{ms}$, is obtained from eqns.(2.1) and (4.1) as

$$\vec{J}_{ms}(z) = Z'(z)\, I(z)\, \vec{i}_\phi \ , \tag{4.3}$$

which means that the equivalent magnetic currents are circulating around the surface S.

It is interesting to note that eqn.(4.2) requires, essentially, that the total antenna electric current be assumed as a surface current on the antenna surface. This is identical with the perfect conductor case. However, now we have to assume that, in addition, a surface magnetic current, of density given in eqn.(4.3), exists simultaneously on the antenna surface. (Of course, for Z'=0 we obtain the perfect-conductor case.)

Current distribution I(z) must be such that the surface currents given in eqns.(4.2) and (4.3) make the z-component of the total electric field to be zero inside the domain occupied earlier by the antenna. It is simplest to require that this be true along the antenna axis, since the equations will be almost the same as those for perfectly conducting antenna obtained in Chapter 1, where we used the extended boundary conditions along the antenna axis to formulate the integral equations for the antenna current distribution.

The electric field due to the surface magnetic currents can be computed from eqn.(2.4). For the axial electric field along the z-axis we thus obtain

$$E_{mz} = -\int_{z_1}^{z_2} \frac{Z'(z')\, I(z')\, a^2}{2} \frac{1+jkr}{r^3} \exp(-jkr)\, dz' \ , \tag{4.4}$$

where z_1 and z_2 are the end-points of the loaded antenna segment, and

$$r = \left[a^2 + (z-z')^2\right]^{\frac{1}{2}} . \tag{4.5}$$

The field $E_{mz}(z)$ should now be simply added to the electric field produced by the electric currents and charges in any equation for determining current distribution along perfectly conducting antennas. Thus the extended boundary condition equation analogous to eqn.(1.17) now reads

$$E_z(z) + E_{mz}(z) = -E_{iz}(z) . \tag{4.6}$$

In the case of the two-potential equation for cylindrical structures, eqn.(1.19), the vector-potential equation, eqn.(1.23), the Pocklington equation, eqn.(1.27), and the Schelkunoff equation, eqn.(1.29), the term $-E_{mz}/(j\omega\mu)$ should be added to the left-hand sides of these equations. The Hallén equation, eqn.(1.26), can also be modified in a simple manner. Namely, in the integral on the right-hand side of this equation $E_{iz}(z')$ should be substituted by $\left[E_{iz}(z')+E_{mz}(z')\right]$, and the integral containing $E_{mz}(z')$ moved to the left-hand side of the equation.

Frequently both $Z'(z)$ and $I(z)$ are slowly varying functions along the antenna axis, such that they are practically constant along a distance of several wires' radii. In that case, provided that the wire is electrically thin, according to the duality theorem[5] we can consider the electric field $E_{mz}(z)$ to be approximately dual to the magnetic field on the axis of a very long, uniformly wound solenoid. Thus, on the antenna axis,

$$E_{mz}(z) \simeq -J_{ms}(z) = -Z'(z)\, I(z) . \tag{4.7}$$

This equation can easily be incorporated into the two-potential equation for arbitrary wire structures, eqn.(1.15), by merely adding the term $Z'_p(s_p)\, I_p(s_p)/(j\omega\mu)$ to the left-hand side of eqn.(1.15), where "p" is the index of the segment at the axis of which the field point is located.

Note that the approximate expression (4.7) strictly cannot be applied close to the antenna ends, because there it gives significantly different results from the exact eqn.(4.4). Fortunately, this is not a severe restriction, for the following reasons. In all the equations in

which $E_{mz}(z)$ enters directly (the two-potential equation, etc.), as a rule we do not choose matching points close to the antenna end (if the point-matching technique is used for obtaining the solution). In Hallén's equation expression (4.7) is integrated, so that the end error is smoothed out. All the results presented below and further in this monograph were obtained using the approximation of $E_{mz}(z)$ given in eqn. (4.7). For example, in the case of Hallén's equation the term

$$D(z) = \frac{k}{j\omega\mu} \int_{z_o}^{z} Z'(z')\, I(z')\, \sin k(z-z')\, dz' \tag{4.8}$$

should be added on the left side of the equation.

4.2.1. Examples of analysis of antennas with series distributed loadings. In practice, continuous series loading along wire antennas can be resistive, inductive or capacitive. Resistive loading is usually made in the form of a thin resistive layer over a dielectric rod.[40,41] Commercial surface-layer resistors can also be used to obtain step-like resistive loading.[42-44] Variable inductive distributed loading is obtained if the antenna is made in the form of a wire spiral with variable, slowly varying pitch. Continuous capacitive loading cannot be made easily. (For example, it can be realized if a molten dielectric is mixed with conducting powder, a thin cylinder made from this mixture, and left to solidify.) However, quasi-distributed loading can be obtained by making the antenna in the form of a row of many short metallic segments with dielectric discs between two successive segments.[45-48] This subsection presents some results for antennas with distributed resistive and quasi-distributed capacitive loading.

Fig.4.2 shows theoretical and experimental values of admittance of symmetrical dipoles with constant resistive loading, for $Z'(z)=700\ \Omega/m$ and $1400\ \Omega/m$, versus the electrical half-length kh of the dipoles.[49] The theoretical results were obtained using the delta-function generator and polynomial approximation for current in solving the Hallén equation given in eqn.(2.12) with the additional term in eqn.(4.8) at its left side. Agreement between theoretical and experimental results

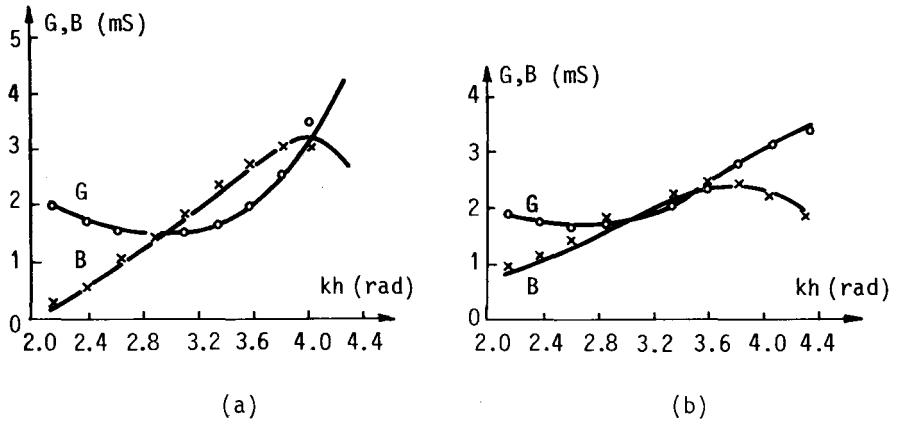

FIG.4.2. Conductance (G) and susceptance (B) of resistive dipoles with constant distributed loading versus their electrical length, kh; a=0.32 cm, h/a=71.3; (a) Z'(z)=700 Ω/m, (b) Z'(z)=1400 Ω/m. ——— theory (3rd-degree polynomial); oo , ×× experiment.[40] (Ref.49)

is seen to be very good.

Shown in Fig.4.3 is theoretical and experimental current distribution along dipole antenna of radius a=0.3175 cm and half-length h=0.5 m, with resistive loading approximately given by

$$Z'(z) = \frac{720}{1 - |z|/h} \ \Omega/m \ , \tag{4.9}$$

at f=450 MHz and f=900 MHz.[50] Again Hallén's equation with the delta-function generator was used. Agreement between theoretical and experimental results is seen to be quite good. It is worth mentioning that the loading in eqn.(4.9) in the experiments was approximated by step-like loading.[41] Shown in Fig.4.4 is dependence of conductance and susceptance of this antenna on frequency. Note excellent broadband properties in admittance of this antenna. From Fig.4.3 it may be concluded that there are practically no reflections from the dipole ends, which is precisely the reason for this broadband behaviour.[51,52] It was found that the dipole radiation pattern also does not change drastically with frequency.[50]

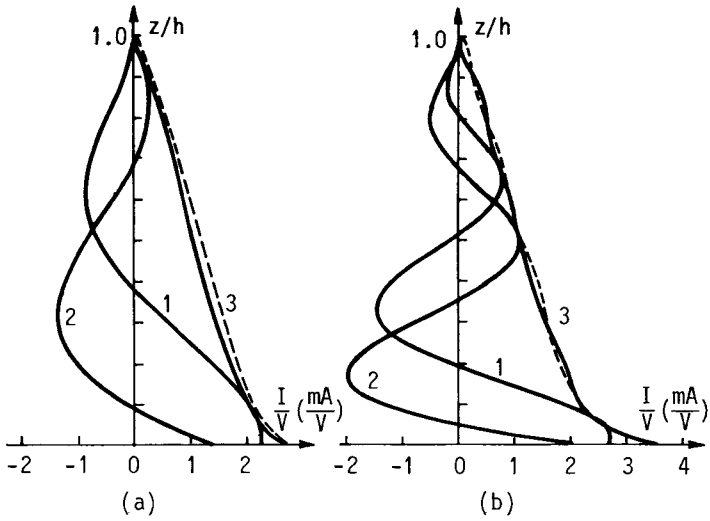

FIG.4.3. Current distribution (I) along resistive dipole antennas with a=0.3175 cm and h=0.5 m, loaded as given in eqn.(4.9), at (a) 450 MHz and (b) 900 MHz. (1) real part, (2) imaginary part, (3) magnitude. ——— theory (5th degree polynomial at 450 MHz, 7th degree at 900 MHz); — — — experiment (Ref.41, amplitude available only). (Ref. 50)

Fig.4.5 shows a monopole antenna with quasi-distributed capacitive loading.[47] It had altogether 16 rings, of wall thickness d=0.1 mm. The diameter of the supporting dielectric rod was D=8.16 mm, its relative permittivity ε_r=2.25, and the total monopole length was b=27 cm.

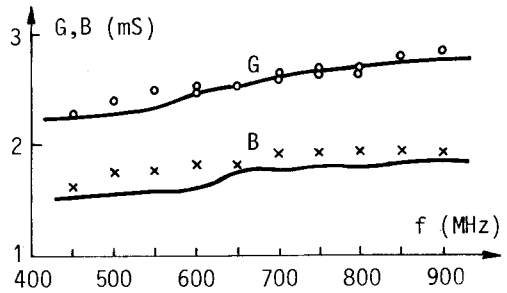

FIG.4.4. Dependence of conductance (G) and susceptance (B) of the antenna described in caption to Fig.4.3 on frequency. ——— 7th-degree polynomial approximation; oo, ×× experiment.[41] (Ref.50)

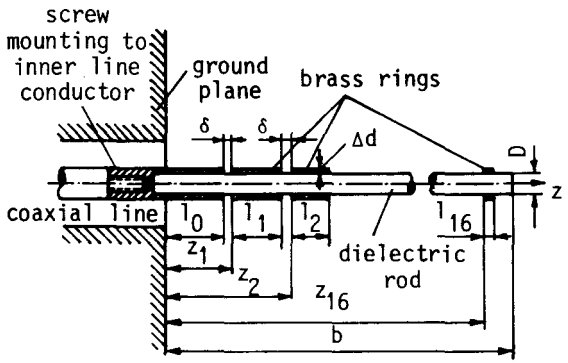

FIG.4.5. Schematic representation of capacitively loaded monopole. (Ref.47)

The lengths of the rings decreased towards the monopole end according to the relationship

$$l_k = 3\left[1 - (z_k/h)^2\right] \text{ cm} , \tag{4.10}$$

where $k=1,2,\ldots,16$, the z_k are as shown in Fig.4.5 and h was arbitrarily taken as 27.0 cm. The rings were set by appropriate gauges to approximately $\delta=0.1$ mm apart. If averaged, the impedance per unit length of the monopole can be represented as

$$Z'(z) \simeq -j \frac{X'_{f\text{ref}}(z)}{3\left[1 - (z/h)^2\right]} \frac{f_{\text{ref}}}{f} \ \Omega/\text{cm} , \tag{4.11}$$

where $X'_{f\text{ref}}(z)$ is the reactance per unit length at the reference frequency f_{ref}. After some estimates it is possible to write eqn.(4.11) in the approximate form

$$Z'(z) \simeq -j \frac{105}{\left[1 - (z/h)^2\right]\left[3 - 0.878(z/h)^2\right]} \frac{f_{\text{ref}}}{f} \ \Omega/\text{cm} . \tag{4.12}$$

Theoretical and experimental results for the monopole admittance are shown in Fig.4.6. The two sets of results are in reasonable agreement. Note that this antenna is also considerably broadband in its admittance.

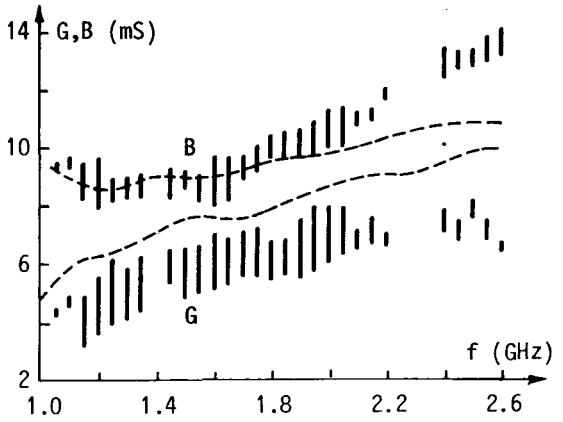

FIG.4.6. Conductance (G) and susceptance (B) of monopole with quasi-distributed capacitive loading as in eqn.(4.12), versus frequency. – – – theoretical; vertical lines indicate the ranges of measured values. (Ref.47)

4.3. WIRE ANTENNAS WITH DIELECTRIC OR FERRITE COATING[53,54]

Dielectric-coated wire antennas are used in many applications where direct contact of the metallic wire with the surrounding medium is undesirable. For example, the surrounding medium may be corrosive and/or conductive, and the dielectric coating may be protective and/or aimed at improving the antenna radiation properties. The thickness of the coating, in order to be efficient as a protection, is usually of the order of the wire radius. Such coatings influence the properties of the antenna to such an extent that bare-antenna theory cannot be applied for the antenna analysis. The influence of the coating is even more pronounced when the coating is made of a ferrite material.

There are only a few papers dealing with this interesting topic. Richmond and Newman[55] presented a general method for analysis of dielectric-coated wire antennas of arbitrary shape. However, their method is rather complicated, because it is based on the reaction integral which is solved by piecewise-sinusoidal approximation for current. In addition, it uses the delta-function generator model, so that values of the antenna susceptance should be considered only as approximate. James and Henderson[56,57] dealt with cylindrical antennas covered with a

thick layer of dielectric or ferrite material. Their method is based on cavity-type modes excited in the coating and the variational method. However, it was applied only to cylindrical structures and, being general, it is too complex when only thin coatings are considered. Extensive experimental results for dielectric-coated antennas were presented by Lamensdorf.[58]

In this section a simple method is proposed for analysis of antennas assembled from arbitrarily located and interconnected straight thin-wire segments, each of which may be covered, completely or partially, with a thin dielectric or ferrite coating (Fig.4.7). Essentially, these wires are loaded with distributed loading. It is of the shunt type if the coating is dielectric, and of the series type if it is magnetic. Therefore, coated antennas can be analysed using an approach similar to that presented in the preceding section. However, we shall use here a different approach.

The method is based on the quasi-static approximation of both the electric and magnetic field in the coating in planes transverse to the wire axis. The electric field is supposed to be radial, as it is in the case of an infinite, uniformly charged metallic cylinder in elec-

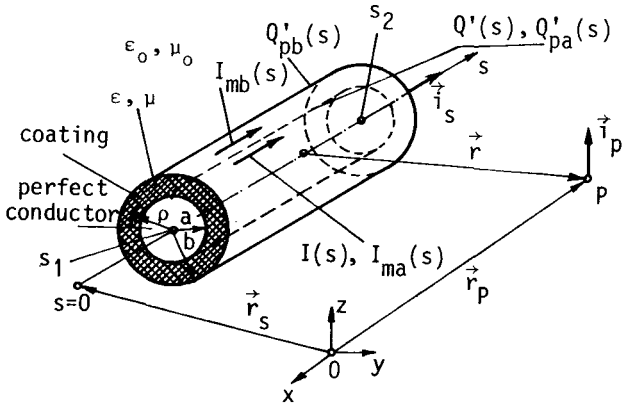

FIG.4.7. A current-carrying wire segment covered with a thin homogeneous dielectric or ferrite coating.

trostatics. If the free charge per unit length of the cylinder is Q', then in the dielectric coating

$$E_\rho(\rho) = \frac{Q'}{2\pi\varepsilon\rho}\ , \quad a<\rho<b\ . \tag{4.13}$$

The magnetic field has only the H_ϕ-component, the intensity of which is approximately the same as that due to an infinite current-carrying cylindrical conductor of radius a, i.e.,

$$H_\phi(\rho) = \frac{I}{2\pi\rho}\ , \quad a<\rho<b\ . \tag{4.14}$$

The approximate equations (4.13) and (4.14) are strictly valid for ρ= a+0, because at the metallic cylinder surface the axial electric field is zero. At points off this surface eqns.(4.13) and (4.14) are only approximate. They are valid if the axial electric field is much smaller than the radial field [in the case of eqn.(4.13)] and if the displacement current (i.e., the flux of $j\omega\vec{D}$) through the circle of radius ρ can be neglected when compared with the conduction current in the wire [in the case of eqn.(4.14)]. It was found that approximate equations (4.13) and (4.14) give sufficiently accurate results for coatings up to one, or even two wire radii thick, and for relative permittivity and permeability of the coating less than about 10.

The influence of the coating on the electromagnetic field can be reduced to that of the polarization charges and currents, and of the magnetization currents, situated in a vacuum.

From eqn.(4.13) it follows that the polarization vector is radial, of intensity $P_\rho(\rho)=(\varepsilon-\varepsilon_o)E_\rho(\rho)$. The polarization currents are hence radial and their density is $j\omega P_\rho$. The volume polarization charges in the coating do not exist, because the coating is homogeneous. At the inner surface of the coating the surface polarization charges exist, of density per unit length of the wire $Q'_{pa}=-Q'(1-1/\varepsilon_r)$. They combine with the adjacent free charges on the metallic cylinder, which yields a total charge per unit length at ρ=a equal to $Q'+Q'_{pa}=Q'_a=Q'/\varepsilon_r$. At the outer surface of the coating there are also surface polarization charges, of density per unit length $Q'_{pb}=Q'_b=Q'(1-1/\varepsilon_r)$.

From eqn.(4.14) it follows that the lines of the magnetization vector are circles centered at the conductor axis. Its intensity is $M_\phi(\rho)=(\mu/\mu_o-1)H_\phi(\rho)$. In the coating there exist radial magnetization currents, the density of which is $-\partial M_\phi/\partial s$. At the inner surface of the coating there are axial surface magnetization currents. Their intensity is $I_{ma}=(\mu_r-1)I$. Together with the wire conduction current, they form a tubular current of total intensity $I_a=\mu_r I$. At the outer surface of the coating there are magnetization surface currents of intensity $I_{mb}=I_b=-(\mu_r-1)I$.

The coating can now be removed, together with the wire segment, and the currents and charges I_a, I_b, Q'_a and Q'_b imagined to be situated in a vacuum. Within the cylinder of radius $\rho=a$ the electric field due to all these sources must be zero. Thus the two-potential equation can be formulated which includes all the charges and currents. If the extended boundary conditions are used, the total electric field is computed along the segment axis, where the electric field due to the radial polarization and magnetization currents is zero. When the electric field due to the coated segment considered is computed along the axis of any other antenna segment, the field due to the radial currents can be neglected, because these currents are uniformly distributed in all directions in a relatively small domain. Thus the radial currents can be disregarded altogether, and the field due to the wire and the coating currents and charges can be attributed only to two tubular layers of currents and charges: the inner, with a total current I_a and charge Q'_a per unit length, and the outer, with a total current I_b and charge Q'_b per unit length. (Of course, this approximation is less accurate when the field is computed in the coating itself.)

Following the reasoning of Section 1.2, the electric field due to these tubular distributions can be approximately computed by introducing approximate average distances, as in eqn.(1.11). Noting that the *wire* current I and charge Q' per unit length are related by the continuity equation (1.13), it is not difficult to derive the two-potential equation for an arbitrary thin-wire structure the segments of which may be covered with dielectric and/or ferrite coatings. It has the form

$$\sum_{m=1}^{N} \int_{s_{1m}}^{s_{2m}} \left\{ \left[\vec{i}_p \cdot \vec{i}_{sm} \mu_{rm} I_m(s_m) + \frac{1}{\varepsilon_{rm} k^2} \frac{dI_m(s_m)}{ds_m} \vec{i}_p \cdot \text{grad} \right] g(r_a) + \right.$$

$$\left. + \left[-\vec{i}_p \cdot \vec{i}_{sm} (\mu_{rm} - 1) I_m(s_m) + \left(1 - \frac{1}{\varepsilon_{rm}}\right) \frac{1}{k^2} \frac{dI_m(s_m)}{ds_m} \vec{i}_p \cdot \text{grad} \right] g(r_b) \right\} ds_m =$$

$$= \frac{1}{j\omega\mu} \vec{i}_p \cdot \vec{E}_i \quad , \qquad (4.15)$$

where $r_a=(r^2+a_m^2)^{\frac{1}{2}}$ and $r_b=(r^2+b_m^2)^{\frac{1}{2}}$. (This equation is valid for wire structures assembled from straight or curved segments.) It is very similar to eqn.(1.15) and can be solved in the same manner. Note that eqn.(4.15) is valid for segments with uniform coatings only, so that division of the wire structure into segments must be performed having that in mind.

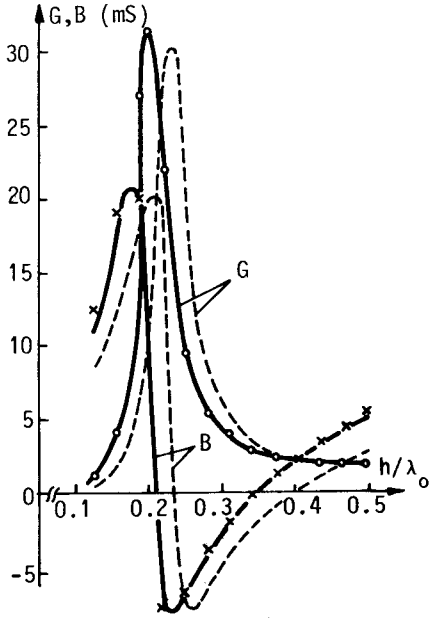

FIG.4.8. Conductance (G) and susceptance (B) of a bare and a dielectric-coated monopole antenna versus the normalized antenna length h/λ_o for λ_o=0.5 m, wire radius 3.18 mm, dielectric-layer thickness 3.18 mm and relative permittivity 3.2. ——— theory, with coating; — — — theory, without coating; oo , ×× experiment, with coating.[58] (Ref.53)

As the first example of analysis of coated wire antennas, shown in Fig.4.8 are theoretical and experimental results for the admittance of a vertical monopole antenna as a function of the normalized antenna length, and in Fig.4.9 theoretical and experimental current distributions along the same antenna. Very good agreement between theoretical and experimental results is observed.

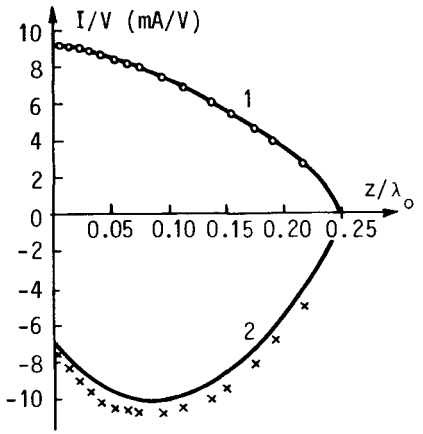

FIG.4.9. Current distribution along a dielectric-coated monopole antenna for h/λ_o= 0.25. Other data are the same as for Fig.4.8. (1) real part; (2) imaginary part. ——— theory; oo, ×× experiment.[58] (Ref.53)

As the next example, shown in Fig.4.10 are theoretical and experimental results for the admittance of a cactus-like antenna covered partially with dielectric coating (sketch of the antenna is given in the inset in the figure). Excellent agreement between theory and experiment is seen again.

As a further example, sketched in Fig.4.11 is an electrically small square loop with a ferrite coating. For ε_r=1 and μ_r=4, at the frequency f=100 MHz, the present method yields the loop inductance L_0=96 nH without the ferrite coating, and L=156 nH with the coating. The difference between these two results can be attributed to the increase of the magnetic energy in the coating, but can also be considered as a consequence of a series distributed inductive loading along the loop.

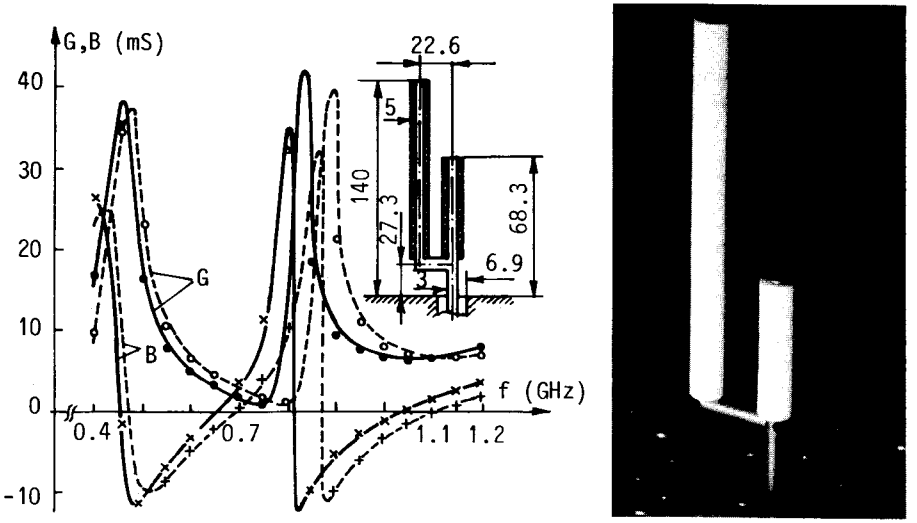

FIG.4.10. (a) Conductance (G) and susceptance (B) of cactus-like antenna shown in the inset, versus frequency. All dimensions are in millimeters. ——— theoretical, teflon coating (ε_r=2.1); — — — theoretical, without coating; ●● , ×× experimental, teflon coating; oo , ++ experimental, without coating. (Ref.54) (b) Photograph of the antenna.

The increase of inductance per unit length of the conductor due to the coating is

$$L'_f = \frac{\mu - \mu_o}{2\pi} \ln \frac{b}{a} , \qquad (4.16)$$

and the total increase of the inductance thus found is L_f=55 nH. This agrees well with the computed increase, $L-L_0$=50 nH. The inductance of the loop without coating calculated by means of the Neumann integral is found to be L_{0N}=91 nH, which is also in good agreement with L_0=96 nH obtained by the present method.

As the last example, Fig.4.12 shows the admittance versus frequency for a vertical monopole sketched in the figure inset for various types of the coating. The results for the coating with ε_r=1 and μ_r=4 are

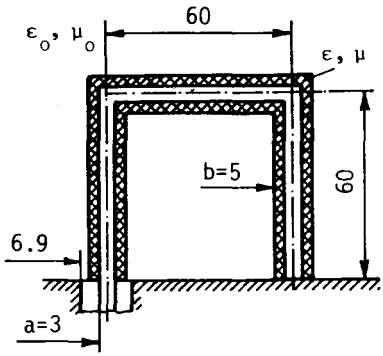

FIG.4.11. Sketch of a small square loop with a ferrite coating (ε_r=1, μ_r=4). All dimensions are in millimeters.

compared with the solution of Hallén's equation for a monopole of the same size with distributed inductive loading obtained according to eqn. (4.16). It is seen that the results practically coincide.

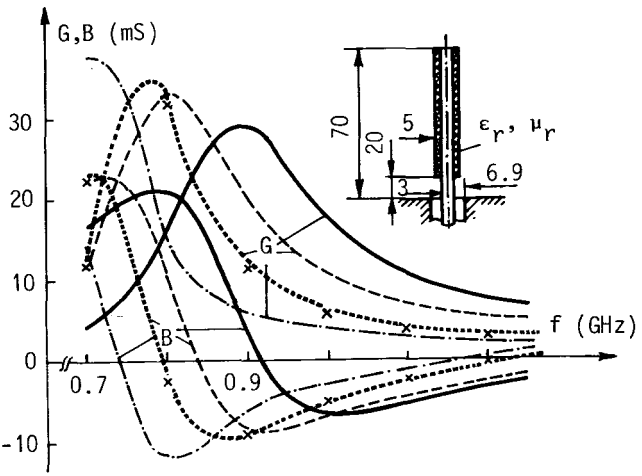

FIG.4.12. Theoretical conductance (G) and susceptance (B) of the monopole antenna shown in the inset, versus frequency. All dimensions are in millimeters. ——— ε_r=1, μ_r=1; — — — ε_r=4, μ_r=1; • • • ε_r=1, μ_r=4; — • — ε_r=4, μ_r=4; × × × results obtained from Hallén's equation and series loading given in eqn.(4.16), for ε_r=1, μ_r=4. (Ref.54)

As a general conclusion following from all the above examples, it is obvious that the dielectric or ferrite coating, even if quite thin, has an appreciable influence on the antenna properties. Purely dielectric coating ($\varepsilon_r \neq 1$, $\mu_r = 1$) can be regarded as a shunt capacitive loading, and purely ferrite coating ($\varepsilon_r = 1$, $\mu_r \neq 1$) as a series inductive loading. Both loadings have essentially the same effect: they apparently increase the antenna electrical length, shifting its resonances towards lower frequencies. However, variations of the antenna admittance become more pronounced when compared with those for the same antenna without coating.

The method presented in this section can obviously be applied also to analysis of antennas with lossy coatings, provided that losses are not very pronounced, by simply replacing the real permittivity ε and real permeability μ by complex values $\varepsilon=\varepsilon'-j\varepsilon''$ and $\mu=\mu'-j\mu''$, respectively.

4.4. CONCLUSIONS

Presented in this chapter were the methods for extending the integral equations for determining current distribution in perfectly conducting wire structures to structures containing wire segments with distributed impedance loadings. It was assumed that the loading was a smooth, relatively slowly varying function along the segments. A method was also presented for analysis of wire antennas with relatively thin dielectric or ferrite coating. It was pointed out that, although thin, such a coating can influence the antenna properties considerably.

Finally, it was mentioned that a continuous impedance loading is frequently approximated by a sequence of lumped loadings. An example which was given indicated that this approach is possible, but no criteria as to when and how such an approximation should be used were presented. The next chapter, dealing with antennas having concentrated loadings along their segments, among other questions treats that question also, and presents certain guidelines concerning approximation of distributed loading by lumped loadings.

CHAPTER 5
Wire Antennas With Concentrated Loadings

5.1. INTRODUCTION

Concentrated loadings along wire antennas can be considered as limiting cases of distributed loadings when the length of the loaded part of a segment becomes very small in comparison with the segment length and the wavelength, but its total impedance remains finite. As pointed out in the preceding chapter, in some instances only concentrated loadings can be made easily, in which cases distributed loadings are approximated by appropriate sequence of concentrated loadings. For example, this is the case with series capacitive loadings.

In practical realizations, concentrated loadings are easy to make at lower frequencies. At higher frequencies, however, it is difficult to realize desired loadings accurately, for mainly two reasons. Firstly, it is difficult to make the impedance elements themselves with some prescribed properties at high frequencies. Secondly, capacitance of the two segments between which a loading is connected represents a progressively important part of the total concentrated loading impedance as the frequency increases, which is very difficult to take into account. It is therefore virtually impossible to design theoretically a lumped loading at higher frequencies accurately. An experimental method which can help to obtain a desired loading is therefore presented in one section of this chapter.

However, the difficulties are not only encountered with the lumped loading realization, but also with its theoretical modelling. Precise

modelling is very complex even in the simplest cases, such as that of a capacitive loading in the form of a narrow gap between two cylindrical antenna parts. Fortunately, accurate modelling of a lumped impedance element along an antenna usually is not required. If the loading is taken into account correctly in an integral manner, the error in current distribution is localized practically in the immediate neighbourhood of the loading. Therefore this does not have a significant effect on either radiation properties of the antenna or on its admittance. For this reason the delta-function approximation of the loading and of the field due to the loading is sufficient for practically all purposes. Only rarely a more sophisticated approximation of lumped loadings is needed.

This chapter is devoted to analysis of wire antennas with lumped loadings along their segments. A description how such loadings can be realized in some instances is also given, and the effects which can be expected from introducing the loadings into the antenna structure are discussed. A full appreciation of the usefulness of lumped loadings will be possible, however, only in connection with wire-antenna synthesis, a topic treated in the last three chapters of this monograph.

5.2. MODIFICATIONS OF EQUATIONS FOR CURRENT DISTRIBUTION

Consider a wire segment containing an axially symmetrical concentrated loading of impedance Z_0, located at $z=z_0$, as sketched in Fig.5.1. In order to avoid a detailed analysis of the electromagnetic field in the interior of the surface S enclosing the wire segment, we can apply the same procedure as in Sections 2.2 and 4.2. For this we need the densities of the equivalent electric and magnetic surface currents, which are given by

$$\vec{J}_s(z) = \frac{I(z)}{2\pi a}\,\vec{i}_z \tag{5.1}$$

and

$$\vec{J}_{ms}(z) = E_{Sz}(z)\,\vec{i}_\phi \ , \quad z_1<z<z_2 \ , \tag{5.2}$$

where I(z) is the *total* current through the antenna cross-section, and

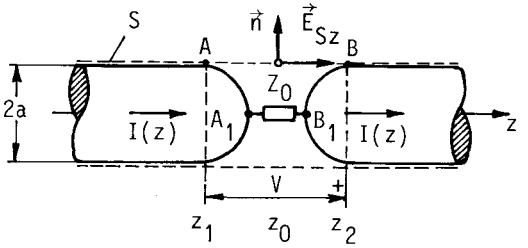

FIG.5.1. Short segment of wire antenna with a concentrated loading.

$\vec{E}_S$ is the total electric field at the surface S. This electric field depends primarily on the actual geometry of the gap at which the loading is connected and on the loading itself, and it cannot be computed in any simple manner. Therefore $\vec{E}_S$ is most often not known. Fortunately, in the case of concentrated loadings we do not need to know the actual distribution of this field, because practically only the integral effect of the loading (i.e., the voltage between its closely spaced terminals) is important. If $|z_2-z_1| \ll a \ll \lambda$, the total antenna current is practically constant for $z_1<z<z_2$ and equal to $I(z_0)$. Since E_S at any point between z_1 and z_2 is approximately proportional to this current, the circuit-theory approximations apply, so that we have

$$\int_{z_1}^{z_2} E_{Sz}(z')\,dz' \simeq Z_0\, I(z_0)\ , \tag{5.3}$$

provided that the capacitance between the loading terminals A_1 and B_1 in Fig.5.1 is included in Z_0. Note that the surface magnetic currents, $\vec{J}_{ms}$, are also proportional to the total current $I(z_0)$, so that from the circuit-theory standpoint they can be regarded collectively as an electric-current dependent voltage generator.

We can now use any convenient approximation for $E_{Sz}(z)$, subject to the constraint in eqn.(5.3). The simplest approximation is to let the gap width tend to zero, which results in a δ-function generator, discussed in Section 2.2, the voltage of which is $V=-Z_0 I(z_0)$. Hence for $E_{mz}(z)$, the electric field along the z-axis due to the magnetic currents, we obtain the same expression as that in eqn.(2.5), only with V

substituted by $-Z_0 I(z_0)$. This δ-function approximation of lumped loadings can be incorporated into any equation for the antenna current distribution in the same manner as the δ-function generator described in Section 2.2. Thus, with the two-potential integral equation the junction-field constraint

$$\int_L E_{\text{total } z}\, dz = 0 \tag{5.4}$$

should be applied for a short path (along the segment axis) containing the lumped loading. [Of course, for arbitrary wire structures the local s-axis should be used instead of the z-axis in eqn.(5.4).] Naturally, the field $\vec{E}_{\text{total}}$ in eqn.(5.4) includes the field $\vec{E}_m$ due to the magnetic-current ring which approximates the lumped loading.

With the Hallén equation the same approximation of E_{mz} is introduced as in Subsection 2.2.1, i.e.,

$$E_{mz} \simeq -Z_0\, I(z_0)\, \delta(z-z_0) \ . \tag{5.5}$$

Hence, for the symmetrical dipole antenna shown in Fig.5.2 the Hallén equation can easily be obtained in the form

$$\int_{-h}^{h} I(z')\, g(r)\, dz' + \frac{k}{2j\omega\mu} \sum_{i=1}^{n} Z_i\, I(z_i) \left[\sin k(z-z_i) + \sin k|z-z_i|\right] + C_1 \cos kz = \frac{k}{j\omega\mu} \int_0^z E_{iz}(z') \sin k(z-z')\, dz' \ , \tag{5.6}$$

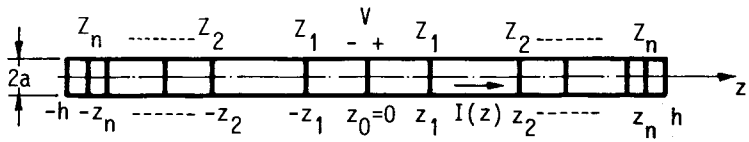

FIG.5.2. Symmetrical dipole antenna with delta-function concentrated impedance loadings.

with $z_0=0$ at the dipole center. The integral in the last term in eqn. (5.6) depends on the choice of the excitation approximation.

It is obviously possible to approximate a lumped loading in many other ways, although in some cases this may not have a physical counterpart. For example, we can approximate not the field E_{Sz} (i.e., the equivalent magnetic currents on S), but rather the field E_{mz} along the z-axis due to these currents, in the same way as with the belt-generator approximation of the antenna excitation (see Subsection 2.3.2). We can also approximate the concentrated impedance by a TEM magnetic-current frill, described in Subsection 2.3.1.[16] In both cases, when calculating the electric field along the z-axis, the voltage V in eqns. (2.28) and (2.20) should be replaced by $-Z_i\, I(z_i)/2$ and z replaced by $(z-z_i)$. The parameter α of the belt generator and the ratio b/a for the TEM frill can be chosen fairly arbitrarily, because they have no significant influence on the antenna current distribution when the antenna is electrically thin.

As already mentioned in the introduction to this chapter, a specific type of approximation of the lumped loadings has a pronounced effect only on the field and current distribution in the immediate neighbourhood of the loading. The overall current distribution and, in particular, the antenna admittance are almost unaffected by the type of approximation, provided that the radius of the wire and the length of the loading are much smaller than the wavelength. Therefore the simplest approximation from the numerical standpoint should be adopted, except for special cases when a more precise analysis of the loading is required. The delta-function approximation of the loadings can readily be incorporated into the analysis of general wire structures based on the two-potential equation, by introducing the junction-field constraint. Also, modification of the Hallén equation for cylindrical antennas to account for lumped loadings is simple and straightforward. The effect of the parasitic capacitance introduced between the loading terminals which is inherent to the delta-function approximation of the loading (see also Section 2.2) is practically not pronounced, for the same reasons as explained in Section 2.2, provided that the degrees of

polynomial approximation of current in the wire segments adjacent to the loading are not high. Therefore the delta-function approximation of the loadings will predominantly be used throughout this monograph.

5.2.1. Examples of cylindrical antennas with concentrated resistive loadings.[11] All the examples presented in this and the following subsection were analysed starting from eqn.(5.6), using the polynomial approximation for current combined with the point-matching method and adopting the delta-function approximation for the loadings. This subsection is devoted to examples of antennas with resistive, and the next subsection to examples of antennas with capacitive loadings. Resistive loadings are inconvenient because of losses they introduce, but they can produce some very useful effects, as already pointed out in Section 4.2. Capacitive loadings do not introduce losses, but are frequency-dependent. Therefore both types of loadings can be advantageously used in various situations.

As the first example of resistive loadings, consider so-called Altshuler's antenna.[59] Starting from the transmission-line theory, Altshuler predicted that a travelling wave could be maintained along a part of a thin cylindrical monopole, if a resistive loading of appropriate magnitude is inserted $\lambda/4$ from the monopole end. He verified this conclusion experimentally, on a monopole of radius a=0.3175 cm, at a frequency of f=600 MHz. The outer radius of the coaxial feeder to the monopole was equal to 8a. Altshuler found that a resistance of 240 Ω at $\lambda/4$ from the monopole end was the optimal loading, resulting in an essentially travelling current wave from the excitation point to the load, and a standing wave from the load to the monopole end. The monopole exhibited fairly constant admittance for practically any length of the monopole section from the ground plane to the load. This antenna was analysed starting from eqn.(5.6), with the delta-function approximation of the coaxial-line excitation.

Figure 5.3 shows dependence of conductance (G) and susceptance (B) of the antenna, versus the normalized half-length h/λ of the equivalent symmetrical dipole, as measured by Altshuler and as obtained theoretically. Agreement in conductance is seen to be very satisfactory. The

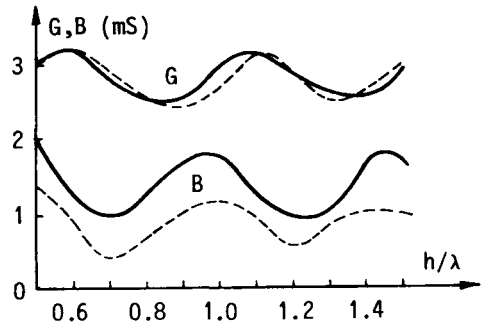

FIG.5.3. Conductance (G) and susceptance (B) of the symmetrical Altshuler antenna; a=0.3175 cm, f=600 MHz, Z_1=240 Ω at $\pm z_1 = \pm(h-\lambda/4)$. ——— theoretical; – – – experimental.[59] (Ref.11)

theoretical susceptance is higher than the experimental, although the shape of the susceptance curves in the two cases is very much alike. This discrepancy is due to poor approximation of the real driving conditions (coaxial line with outer-to-inner diameter ratio as large as 8) by the delta-function generator. The theoretical results were obtained by dividing the monopole into segments of lengths less than $\lambda/2$, and using the second-degree polynomial approximation for current along every segment.

As an example of current distribution, Fig.5.4 shows experimental and theoretical current distribution for $h/\lambda=5/8$. It is seen that agreement between theoretical and experimental curves is excellent.

It was interesting to analyse the possibility of approximating a continuous resistive loading by a sequence of lumped loadings. Therefore the following two cases were considered theoretically, using the delta-function generator excitation: (1) the total loading was evenly distributed along the antenna length, and (2) the total loading of equal magnitude was divided into several lumped loadings. We shall analyse the case of resistive antenna with constant continuous loading, for which experimental results are available.[49]

Consider a resistive dipole of half-length h=0.226 m and radius a= 0.3175 cm. Let the total loading along half of the dipole be 317 Ω, which is 1400 Ω/m, and let the frequency be f=663 MHz, i.e., $kh=\pi$. For the case of such a continuous loading theoretical and experimental

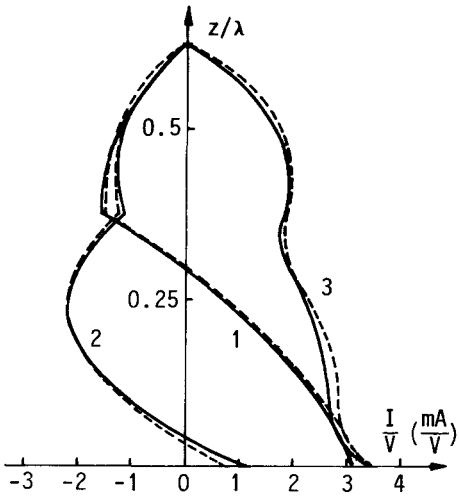

FIG.5.4. Real part (1), imaginary part (2) and magnitude (3) of current along one half of the symmetrical Altshuler antenna; a=0.3175 cm, h = 31.25 cm, f=600 MHz, Z_1=240 Ω at $\pm z_1=\pm(h-\lambda/4)=\pm 18.74$ cm. ——— theoretical; — — — experimental.[59] (Ref.11)

values of the admittance are presented in Reference 49. For convenience, these are given again in Table 5.1.

Let now the total loading be concentrated at n=1, 2, 3 and 4 equidistant points along the dipole arms. Values of G and B corresponding to

TABLE 5.1. Comparison of admittances of dipoles with continuous and lumped equidistant resistive loadings; a=0.3175 cm, h=0.226 m, f=663 MHz, total loading along one dipole arm = 317 Ω (i.e., 1400 Ω/m). In the case of lumped loadings, piecewise parabolic approximation of current has been adopted. (Ref.11)

Type of loading	Admittance (mS)
Single loading at ±h/2	3.70 + j2.11
Double loading, at ±h/3 and ±2h/3	2.48 + j2.73
Triple loading, at ±h/4, ±2h/4 and ±3h/4	2.15 + j2.70
Quadruple loading, at ±h/5, ±2h/5, ±3h/5 and ±4h/5	2.04 + j2.67
Continuous loading, theoretical, 3rd degree polynomial approximation for current[49]	1.90 + j1.91
Continuous loading, experimental[40]	1.9 + j2.2

these cases are also shown in Table 5.1. It is seen that as little as four loadings are sufficient to substitute the continuous resistive loading, at least as far as the dipole conductance is concerned. (Theoretical susceptance is, of course, increasing with n in the lumped loading case, as the same polynomial approximation for current is used for a progressively smaller segment of the antenna in the vicinity of the delta-function generator.) This indicates that about 10 concentrated loadings per wavelength are needed to approximate quite accurately a smooth, slowly varying continuous loading.

Compared in Fig.5.5 is the theoretical current distribution in the case of continuously loaded dipole of electrical half-length $kh=\pi$ with those corresponding to 2 and 4 lumped loadings. It is evident that as little as 4 lumped resistive loadings, i.e., 8 loadings per wavelength, can approximate the considered continuous resistive loading quite accurately. Note that this need not be the case if the loadings are not resistive.

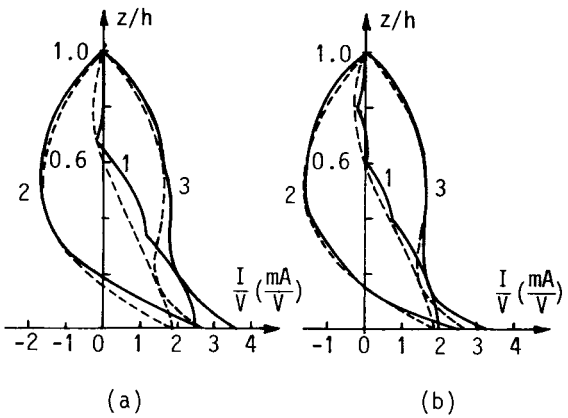

FIG.5.5. Theoretical current distribution along resistive dipoles; a=0.3175 cm, h=0.226 m, f=663 MHz, total loading along half of the dipole = 317 Ω. ——— lumped equidistant loadings, piecewise parabolic approximation of current; — — — continuous loading, 3rd-degree polynomial approximation of current. (1) real part, (2) imaginary part, (3) magnitude; (a) two lumped loadings, (b) four lumped loadings. (Ref.11)

5.2.2. Examples of cylindrical antennas with concentrated capacitive loadings.[60] Cylindrical antennas with lumped capacitive loadings along their length are known to offer interesting possibilities. Broadband cylindrical antennas[45,46,47] and cylindrical antennas sustaining a travelling wave along its major part[61,62] are examples of such structures. Due to a large number of parameters (positions and magnitudes of the loadings), antennas having a variety of properties can be obtained by appropriate choice of these parameters. This will be discussed in the next part of the monograph. In this subsection we shall present a number of examples for admittance and current distribution of these useful lossless structures.

For the theory to be applied successfully to capacitively loaded antennas, it is necessary that the real loadings be good approximations to delta-function loadings adopted in analysis. An excellent approximation of the delta-function loading is obtained if the loading is in the form of a narrow gap between two tubular parts of the antenna. Such a construction is shown in Fig.5.6(a). Briefly, the antenna is made in the form of a dielectric rod onto which metallic cylinders of desired lengths are mounted. A narrow longitudinal slot allows a cylinder to slide tightly over the dielectric rod. The desired amount of the capacitive loading is obtained by adjusting the width of the gap between the cylinders using appropriate gauges. The relation between the gap capacitance and the gap width, for different gap geometries, was obtained experimentally by the method described in the following section.

As the adjustment of the gap width by using gauges is not quite precise, another construction of the antenna, shown in Fig.5.6(b,c), was also used. Several elements with precisely determined fixed capacitance were made. (Here, the dielectric rod and the metallic cylinders were glued together.) In addition, a number of brass cylinders of different lengths were prepared, with a screw at one end and with a threaded hole at the other. The fixed gap, or gaps, could be positioned at the desired location along the antenna by an appropriate combination of the brass cylinders.

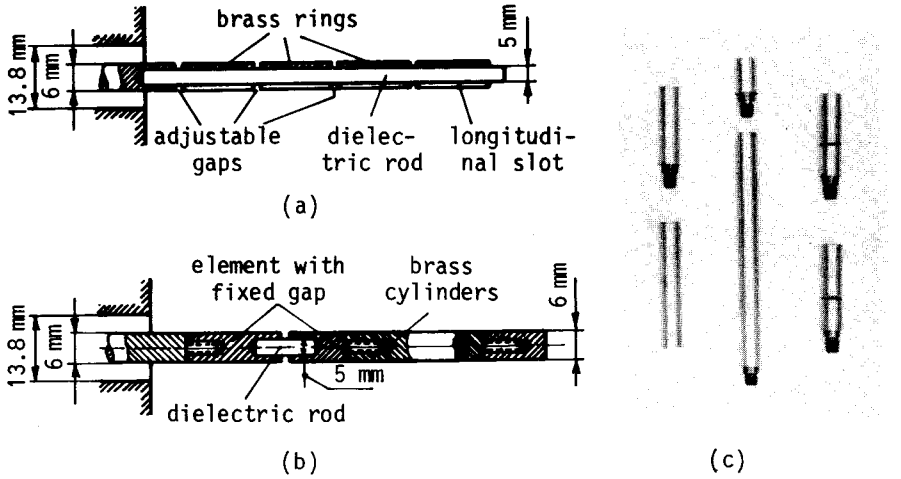

FIG.5.6. Two experimental models of the capacitively loaded monopole antenna: (a) model with variable gap widths; (b) model with a fixed gap width. (Ref.60) (c) Photograph of disassembled antenna with two capacitive loadings with fixed gap widths (on the extreme right side).

In order to verify the theoretical results, experimental setups were made for measurements of antenna admittance and radiation pattern (see Fig.5.7). These setups were used for obtaining all the experimental results presented in this monograph except those which are referenced to some other source.

The impedance measurements were made for monopole antennas mounted on a vertical ground plane. The ground plane was a square aluminium sheet of 2 m side. The hole in the plane through which the monopole was protruding was positioned somewhat off center, to eliminate possible resonances. The frequency range in which measurements were performed was from 1.1 GHz to approximately 2.6 GHz. Thus, at the lowest frequency used, the side of the square ground plane was longer than seven wavelengths.

The value of the apparent monopole admittance, i.e., the admittance referred to the end of the coaxial line, was measured by the standard reflection-measurement technique, using the GR 900 (General Radio Corp.)

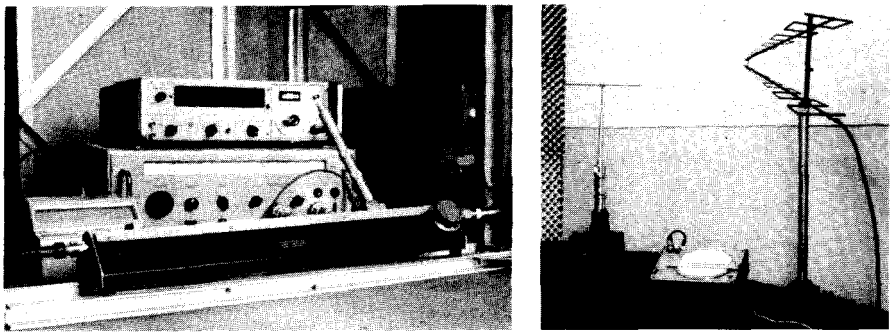

(a) (b)

FIG.5.7. (a) Photograph of part of the instrumentation used for measurements of antenna admittance: precision slotted line (General Radio 900-LB), sweep signal generator (Rohde Schwartz SWU BN 4246), frequency counter (Hewlett Packard 5246L with 5254C frequency converter) and galvanometer (Norma 251N) placed behind vertical ground plane. (b) Photograph of part of the equipment used for measurements of radiation pattern: antenna positioner (with a symmetrical dipole and detector), polar plotter, and transmitting log-periodic array.

slotted line. Although it was not possible to determine precisely the overall error of the measuring equipment, a maximum error of about 5% seemed to be a realistic estimate.

For measurements of the radiation pattern, dipole antennas were used. The antenna under investigation was mounted on a 10 m-high tower, and served as a receiving antenna. The distance between the transmitting and the receiving antennas was about 20 m. A detector, mounted at the antenna terminals, was designed to receive principally the symmetric mode. A small asymmetric component received by the detector was probably one of the causes of slight asymmetry of the radiation patterns presented below.

The available site was not clear, and considerable reflections were observed from nearby trees and buildings. The dipole was mounted horizontally, with a small distance (about 3 cm) existing between the dipole axis and the vertical axis of rotation of the antenna pedestal. These factors probably also added to the asymmetry of the measured ra-

diation patterns.

As mentioned above, in the general case a capacitively loaded antenna is a structure with many parameters. Therefore, only some representative examples of these structures are presented below. The simplest case is that of a monopole loaded with a single loading (or a dipole with two identical, symmetrically positioned loadings). A monopole antenna of the form shown in Fig.5.6(b) was made, of length h=15 cm (measured from the ground plane) and radius a=0.3 cm. In order to achieve good accuracy, gaps of fixed widths were used, and the capacitance of each loading was measured separately. Therefore, the best possible agreement between experimental and theoretical results was expected. The belt-generator approximation to coaxial-line excitation was used, so that accurate theoretical values of the antenna susceptance were also anticipated.

Consider first a monopole antenna with fixed value of the gap capacitance and variable position of the gap along the monopole. An example of conductance (G) and susceptance (B) of the monopole against frequency is shown in Fig.5.8. The theoretical results were obtained by using the measured value of the loading, -j197 Ω at 1 GHz.

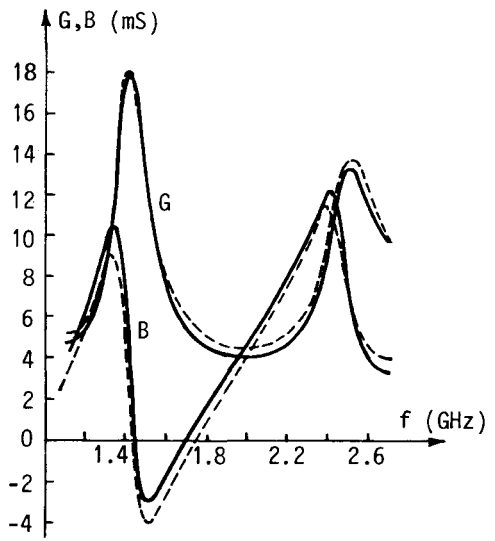

FIG.5.8. Conductance (G) and susceptance (B) of a monopole antenna with a single capacitive loading Z_l=-j197 Ω at 1 GHz, at a distance z_l= 6 cm from the ground plane. a=0.3 cm, h=15 cm. ——— theory; – – – experiment. (Ref.60)

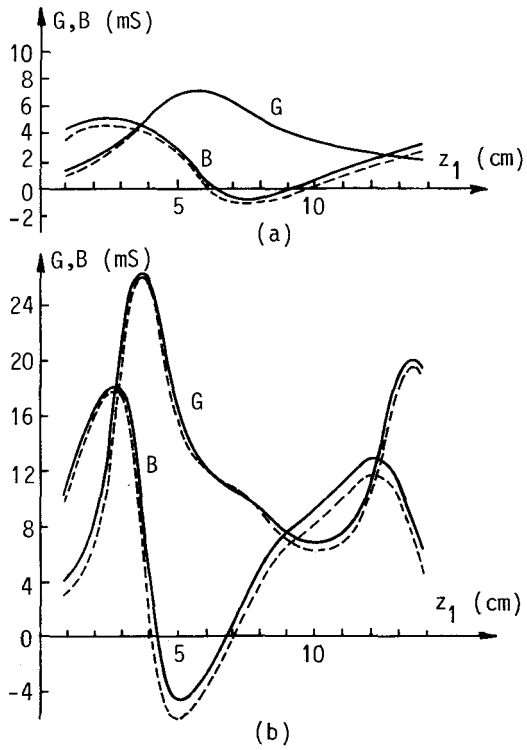

FIG.5.9. Conductance (G) and susceptance (B) of monopole antenna with a single capacitive loading Z_1=-j284 Ω at 1 GHz against distance z_1 of the loading from the ground plane; a=0.3 cm, h=15 cm. (a) f=1.0 GHz, (b) f=1.5 GHz. ——— theory; — — — experiment. (Ref.60)

Fig.5.9 shows the real and imaginary parts of the monopole admittance plotted against the position of a fixed capacitive loading of -j284 Ω at 1 GHz, at frequencies of 1 GHz and 1.5 GHz. Note that the influence of the loading position is much larger at 1.5 GHz than at 1 GHz. This is because the unloaded antenna at 1 GHz is approximately antiresonant, h=λ/2, and at 1.5 GHz is approximately resonant, h=3λ/4. Note, again, very good agreement of theoretical and experimental results.

Fig.5.10 shows a sequence of radiation patterns in the electric-field strength for a dipole antenna with two equal, symmetrically positioned loadings of values -j284 Ω, at 1 GHz, for different positions of the loadings. The frequency was 1.5 GHz. Note the considerable influence of the position of the loading on the radiation pattern.

Using again the construction shown in Fig.5.6(b), monopoles with two

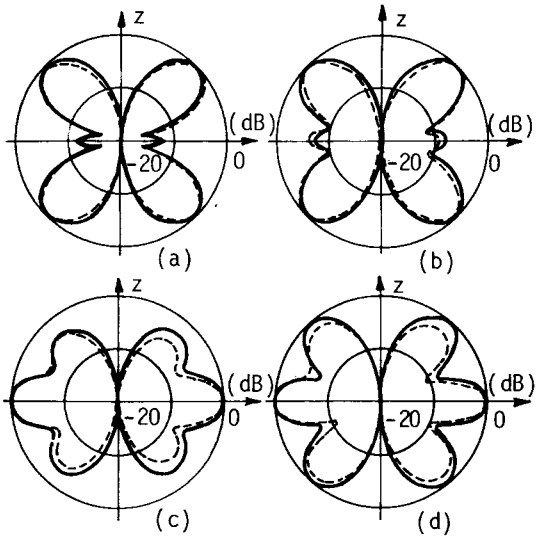

FIG.5.10. Radiation patterns in the plane containing the dipole axis for a dipole antenna with two loadings Z_1= -j284 Ω at 1 GHz, positioned symmetrically at $\pm z_1$; f=1.5 GHz, a=0.3 cm, h=15 cm. (a) z_1=3 cm, (b) z_1=6 cm, (c) z_1=9 cm, (d) z_1=12 cm. ——— theory; — — — experiment. (Ref.60)

capacitive loadings were investigated next. The two loadings were 185 Ω and 274 Ω at 1 GHz (measured values). They were positioned at different points along the monopole, and frequency dependence of the monopole admittance was measured and calculated. Fig.5.11 shows an example, in which loading Z_1=-j274 Ω at 1 GHz was positioned at z_1=6.0 cm, and loading Z_2=-j185 Ω at 1 GHz was positioned at z_2=10.1 cm from the ground plane. Note the considerable smoothing out of the curves when compared with those for a single loading (Fig.5.8). By interchanging the positions of the two loadings, similar curves were obtained, which, however, exhibited a somewhat more rapid change of admittance with frequency.

To gain some insight into the influence of the number of loadings along a monopole of fixed length on its properties, the following set of experiments and computations was performed. A monopole was made in the form of 25 rings of length 1 cm each. (In fact, the first ring was the protrusion of the inner cable conductor through the ground plane.) The gap capacitance against gap width has been measured and this value used in computations.

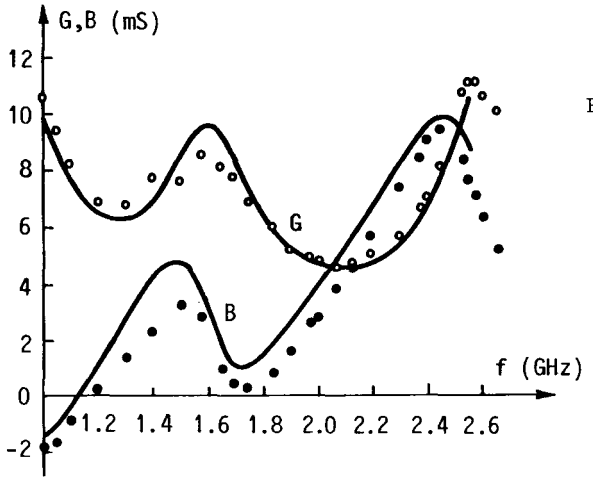

FIG.5.11. Conductance (G) and susceptance (B) against frequency of a monopole antenna with loadings Z_1=-j274 Ω and Z_2=-j185 Ω, at 1 GHz, positioned at z_1=6.9 cm and z_2=10.1 cm from the ground plane; a=0.3 cm, h=15 cm. ——— theory, o o, • • experiment. (Ref.60)

First, 24 gaps of approximately 0.1 mm width were left between the cylinders. Next, the second cylinder, counted from the ground plane, was pushed to come into contact with the third, the fourth to come into contact with the fifth, etc. Thus 12 gaps of approximately 0.2 mm width were obtained. This procedure was repeated to obtain 8, 6, 4, 3 and 2 gaps of widths 0.3 mm, 0.4 mm, 0.6 mm, 0.8 mm and 1.2 mm, respectively. Note that the first gap was always 1 cm from the ground plane. The frequency dependence of the monopole admittance in the range 1.1-2.6 GHz was both measured and computed in all these cases. Agreement between theory and experiment was found to be satisfactory. Fig.5.12 illustrates two representative cases. One reason for the discrepancy between theoretical and experimental results could be the very small, but non-zero, resistance between two rings pressed one against the other. It was found that the d.c. resistance betweem two such rings was not zero and, in addition, that it was sporadic from case to case.

An interesting feature of the admittance curves shown in Fig.5.12 can be seen: in both cases the antenna admittance is much less frequency sensitive than in the known case of the unloaded monopole antenna.

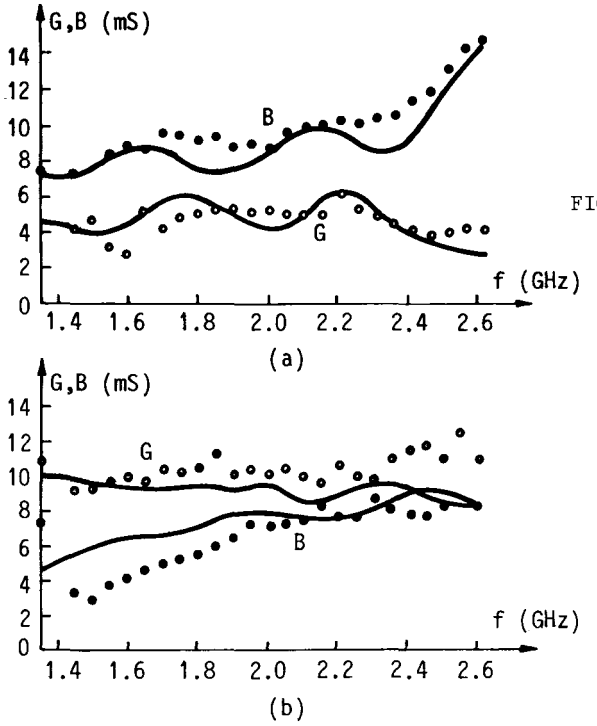

FIG.5.12. Conductance (G) and susceptance (B) of a monopole antenna with equal equidistant loadings, against frequency. The first loading was 1 cm from the ground plane; a=0.3 cm, h=25.4 cm. (a) four loadings, 380 Ω at 1 GHz each. (b) eight loadings, 280 Ω at 1 GHz each. ——— theory; oo, •• experiment. (Ref.60)

As an illustration, Fig.5.13 shows the theoretical current distribution for the monopole considered, for four and eight loadings, at a frequency of 2 GHz.

Let us consider now monopoles with a number of equal loadings, the distances between which become progressively smaller towards the monopole end. This construction was of interest because better broadband properties could be expected for tapered loadings than for equidistant loadings.[45] We shall restrict our attention to the monopoles shown in Fig.5.6(a), with the positions of the gap centers defined by

$$z_n = (n-0.5)\delta + \sum_{k=1}^{n} \left[3.2 - 0.2\,(k-1)\right] \text{ cm}, \quad n=1,2,\ldots,15, \tag{5.7}$$

where δ is the width of the gaps.

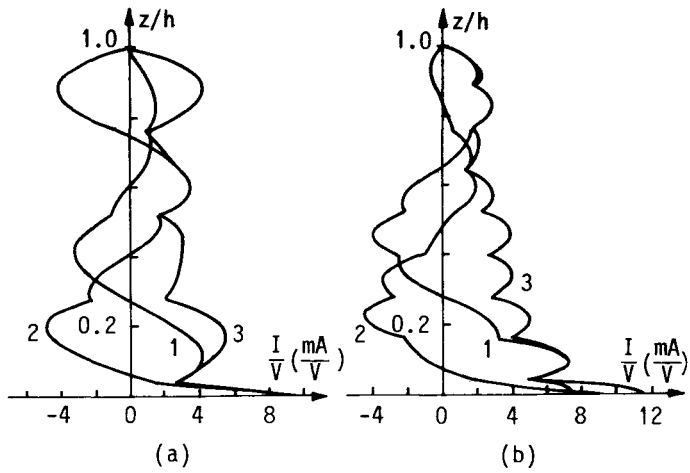

FIG.5.13. Theoretical current distribution along monopole antennas of Fig.5.12, at f=2 GHz; (1) real part, (2) imaginary part, (3) magnitude. (a) Four loadings. (b) Eight loadings. (Ref.60)

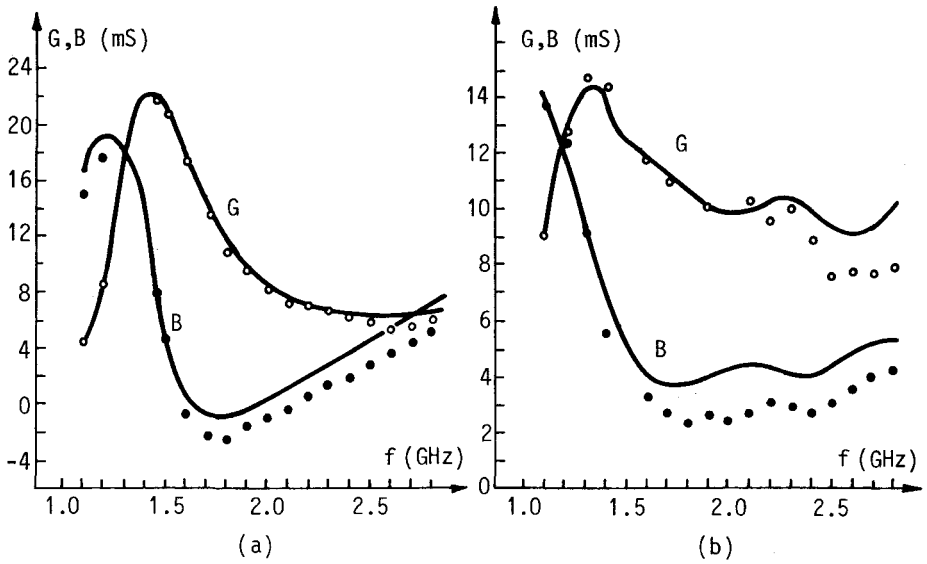

FIG.5.14. Conductance (G) and susceptance (B) of monopole antennas with n loadings of -j320 Ω at 1 GHz each, at distances from the ground plane given in eqn.(5.7); a=0.3 cm. (a) n=1, h=6.23 cm; (b) n=7, h=20.21 cm. ——— theory; oo, •• experiment. (Ref.60)

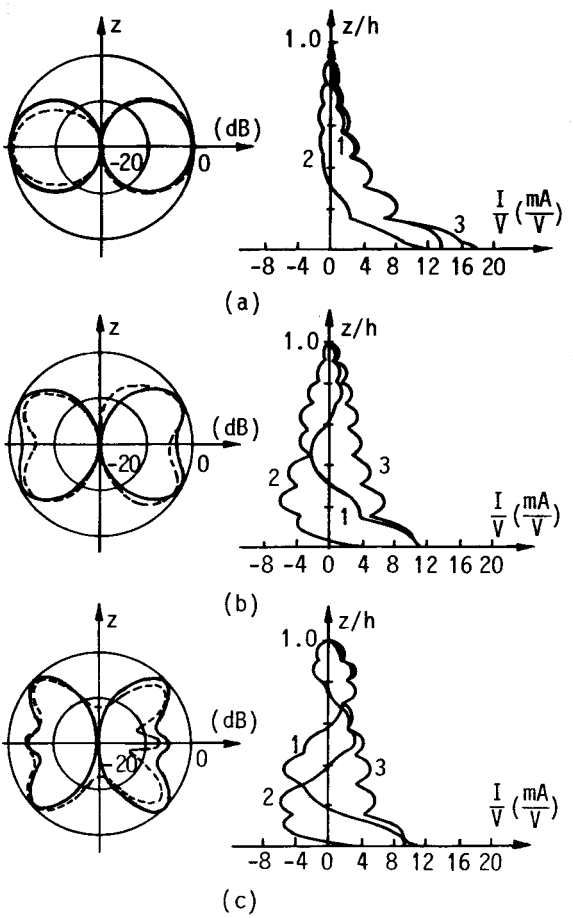

FIG.5.15. Radiation patterns in the plane containing the dipole axis and current distribution along a dipole antenna with arms the same as the monopole described in caption to Fig.5.14(b); (a) f=1.2 GHz, (b) f=1.8 GHz, (c) f=2.4 GHz; (1) real part, (2) imaginary part, (3) magnitude of current. ——— theory; — — — experiment. (Ref. 60)

Two representative examples are shown in Fig.5.14 of conductance and susceptance of the monopole admittance plotted against frequency, for Z_{load}=-j320 Ω at 1 GHz, and n=1 and 7. It is seen that the curves become flatter with increasing the number of the cylinders. (Note that the scale for n=1 is smaller than for the other case.) It is worth noting that, with only seven gaps, the antenna exhibits remarkable broadband properties. These are not improved considerably with additional cylinders, at least in the frequency range considered.

Finally, Fig.5.15 shows examples of the theoretical current distri-

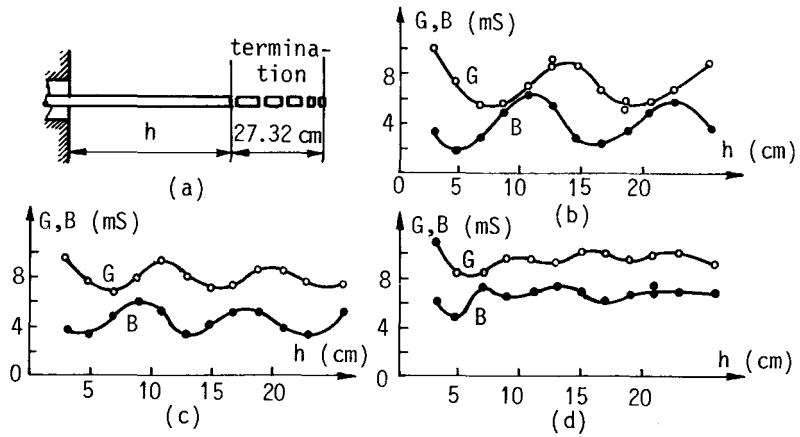

FIG.5.16. Conductance (G) and susceptance (B) of cylindrical antennas with nonreflecting capacitive termination, sketched in figure (a), versus the antenna length; (b) f=1.3 GHz, (c) f=1.7 GHz, (d) f=2.3 GHz. ——— theory; oo, •• experiment. (Ref.62)

bution and of the measured and calculated radiation pattern for an antenna having seven gaps, at frequencies of 1.2 GHz, 1.8 GHz and 2.4 GHz. The gap impedance was $-j320\ \Omega$ at 1 GHz. Note that the current distribution is in the form of a decaying progressive current wave with small standing waves between the loadings. The radiation patterns at 1.8 GHz and 2.4 GHz also clearly indicate the travelling-wave behaviour of the current. At 1.2 GHz the radiation region of the antenna is small, and the pattern resembles that of an electrically short antenna.

The reduction of the reflected wave along the antenna seen in the last figure suggested that a "nonreflecting" capacitive termination of unloaded monopoles could considerably increase their otherwise poor broadband properties. To that aim an antenna of the form shown in Fig. 5.16(a) was made and its admittance versus the length h of the monopole and frequency measured. The termination consisted of 15 rings of lengths $(30-k\cdot 2)$ mm, $k=0,1,\ldots,14$, with gaps of capacitances 1.2 pF left between successive rings. The results are shown in Figs.5.16(b)-(d).[62] It is seen that, indeed, the termination increases to a large extent the monopole broadband properties.

5.3. NOTES ON MEASUREMENTS OF CONCENTRATED LOADINGS

For a thin-wire antenna operating in the range up to few tens of megahertz , the problem of determining accurate value of the lumped-loading impedance is not complicated. In the simplest solution, the wire antenna is cut, and the loading is connected between the ends of the cut. The lumped-loading impedance can be obtained by standard bridge measurements, prior to introducing it into its place along the antenna. Impedance of the capacitor formed by the two wire antenna parts is usually much larger than that of the required lumped element, and can be neglected.

However, for frequencies of the order of 1 GHz and higher, the capacitor formed by two sections of an antenna itself may have impedance which is of the order of the required loading impedance. (Therefore, if a capacitive loading is desired, usually an additional capacitance need not be used at all.) This impedance should obviously be measured only as an integral part of the antenna structure. However, such a measurement will be difficult to carry out, and usually will have to be performed in some other, practically realisable, manner. Obviously, the results are then only approximate. For the results to be accurate (apart from the accuracy of the measurement itself), it is essential to measure the impedance in the operating frequency range of the antenna, and to realise a construction that is as close as possible to the real antenna structure.

This section describes two methods used by the authors for measuring concentrated reactive loadings mounted along wire antennas. The first method, outlined in the following subsection, is essentially a compensation method, and is particularly useful for determining impedance of a single loading, for example in measuring the dependence of the gap capacitance on its width. The second method, outlined in Subsection 5.3.2, is basically a resonant method, suitable for measuring reactances on an already assembled antenna.

5.3.1. Compensation method for measuring lumped reactances.[60] The most natural configuration for measurements of lumped antenna imped-

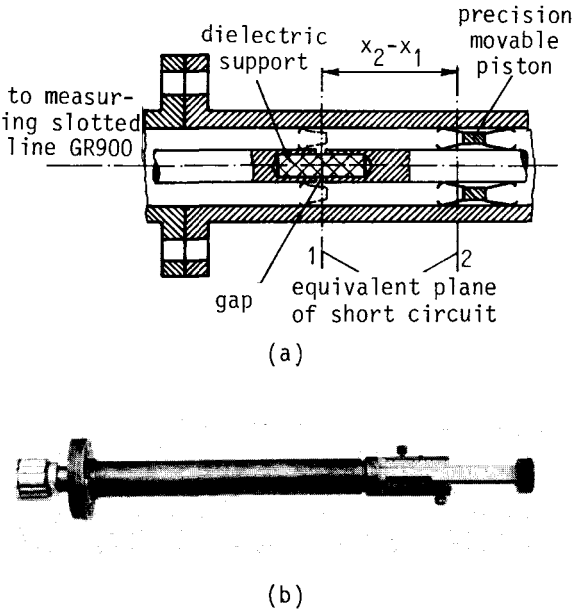

FIG.5.17. Schematic view (a) and photograph (b) of short-circuited coaxial line for measurement of concentrated loadings. (Ref.60)

ances appeared to be a coaxial line, with a part of the antenna itself replacing the inner line conductor. A 50 Ω air coaxial line was therefore made, having an inner-conductor diameter of 6 mm, and the inner diameter of the outer conductor of 13.8 mm. A precision movable piston with sliding contacts was an essential part of the coaxial line. The useful length of the coaxial line was 160 mm, and it was possible to set the movable piston with a precision of ±0.05 mm at any point within this region. The movable coaxial piston, together with the element which is being measured, is shown in Fig.5.17. For convenience, the loading in Fig.5.17(a) is shown as a capacitor in the form of a narrow gap between the two antenna parts (i.e., inner coaxial-line conductor parts.) To be more specific, we shall assume in further considerations that the loading is a capacitor, but the principle can be extended easily to any type of lumped reactive loading the size of which is of the order of the wire radius.

To eliminate possible errors due to connection discontinuities and supporting dielectric wafers on the measuring line, the following mea-

suring procedure was adopted. The short-circuited line was first checked without the capacitor shown in the figure, and the equivalent plane of the short circuit determined experimentally. The capacitor was then introduced into the line, and the piston moved until the equivalent plane of the short circuit coincided with the center of the gap of the capacitor. This position of the piston is designated by 1 in Fig.5.17(a). By means of the GR900 (General Radio Corp.) slotted coaxial line, the location of a minimum along the slotted line was detected. Note that, in this position of the piston, the capacitor is not connected in the circuit [Fig.5.17(a)]. Let us designate this position of the equivalent plane of the short circuit by x_1, with respect to an arbitrary reference plane.

The piston is next moved so that the capacitor is introduced into the circuit. As a result, the position of the minimum changes noticeably. The piston is then moved until the position of the minimum on the measuring line coincides with the earlier position (corresponding to position 1 of the piston). This obviously means that the total series impedance, referred to plane 1, is again practically zero. If x_2 is the position of the equivalent plane of the short circuit, it follows that the reactance of the capacitor is equal to the negative value of the reactance of the short-circuited coaxial line of length (x_2-x_1). The capacitance is hence obtained as

$$C = \frac{1}{\omega Z_c \tan k(x_2-x_1)} , \tag{5.8}$$

where Z_c is the characteristic impedance, and k the phase coefficient of the short-circuited coaxial line.

A comparison between the gap capacitance measured by the above method and the concept of a delta-function loading may need some comments at this point. As already explained, a rigorous analysis of this problem is intricate, but some comments relating to it can be given.

The proposed method enables us to measure certain reactance, and to refer it to a particular cross-section of the coaxial line. Provided that the gap width is small compared with the outer coaxial-line radius,

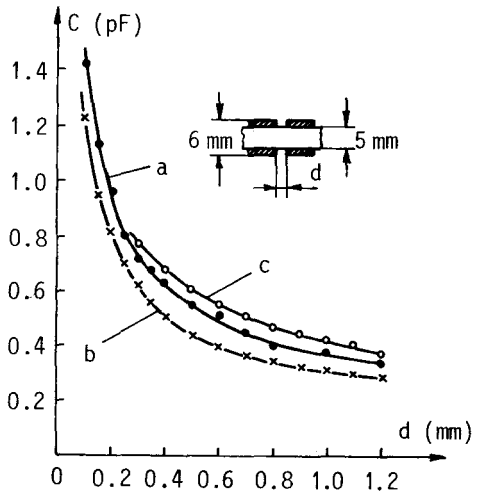

FIG.5.18. Measured gap capacitance against gap width, for three different dielectric supports; (a) acrylic rod, (b) air (acrylic rod with deep groove), (c) glass tube. (Ref.60)

the outer conductor does not influence the value of that reactance. (Although this could be proved experimentally, it requires making several short-circuited coaxial lines of different outer-conductor radius, and has not been done by the authors.) Thus this reactance can formally be ascribed to a delta-function loading, located on the inner-conductor surface, at the center of the gap.

As an example of application of the method, the capacitance was measured of the gap shown in the inset of Fig.5.18, for three different dielectric supports. Curve a, shown in the figure, refers to a solid acrylic cylinder of 5 mm diameter. Curve b corresponds to an acrylic cylinder with a deep groove around the gap, made to approximate the case of an air dielectric. Finally, curve c corresponds to a glass tube of outer and inner diameters 5 and 3 mm, respectively. These capacitances were used to obtain the theoretical results presented in the preceding section.

5.3.2. Measurement of lumped reactances mounted on the antenna by means of a coaxial resonator.[16] Using the compensation method described in the preceding subsection it is possible to measure isolated concentrated loadings. It cannot be used, however, for measuring a succes-

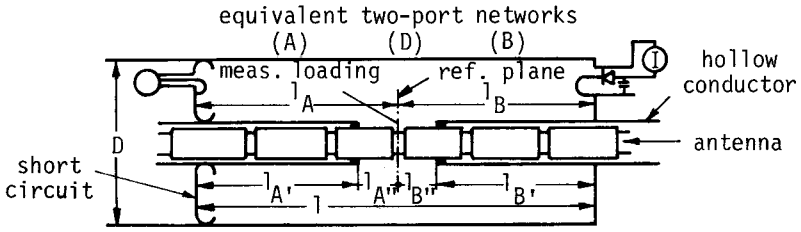

(a)

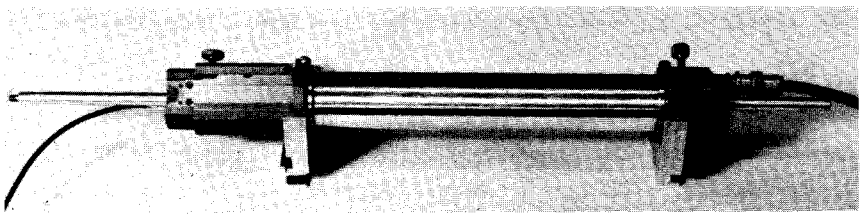

(b)

FIG.5.19. Schematic view (a) and photograph (b) of coaxial resonator used for measuring concentrated loadings along assembled antennas.

sion of loadings already mounted on an antenna, which is preferable in many cases. For example, by using gauges for fixing a gap width, only moderate accuracy can be achieved, so that short-circuited coaxial line shown in Fig.5.17 cannot be used for realising loadings of very accurate values. For this reason a special resonator was made which enabled precise measurements of prefixed loadings on an assembled antenna.

The measuring structure is shown in Fig.5.19. Basically, it is in the form of a coaxial resonator with the inner conductor made of two tubes with a short segment between them missing. By introducing the antenna into these tubes, any of the loadings can be positioned inside the resonator to represent a series loading of the inner coaxial-resonator conductor. To measure the loading impedance, we can bring the resonator into resonance by either varying the position of the short circuit, or by varying the frequency. The loading impedance can be

then computed from the frequency and the measured values of the lengths l_A and l_B or, if a more precise measurement is desired, of lengths $l_{A'}$, $l_{A''}$, $l_{B'}$ and $l_{B''}$ [see Fig.5.19(a)].

In addition to enabling measurements of loading impedances on assembled antennas, the method has another two useful properties. First, as a resonant method in which the measured quantity is obtained by measurements of length and frequency, it is a very accurate method. Second, it enables that actual parameters be determined of the loading considered as a two-port network, and thus check whether in reality it can be regarded, at least approximately, as a pure series element.

The particular resonator shown in Fig.5.19 was made for measurements on antennas of diameter 6 mm and 7 mm. The inner, tubular conductor of the resonator should differ in diameter as little as possible from the antenna diameter, to reduce the step-like transitions between them. Therefore it was made to be 7 mm, viz. 8 mm, for measurements of loadings on antennas having the two mentioned diameters.

The outer resonator diameter should be chosen so that its effect on the stray field due to the loadings being measured be as small as possible. However, it should not be too large, in order to eliminate the possibility of existence of higher coaxial-line modes. For the adopted value of the outer resonator diameter (28 mm), it was found that the effect of the outer conductor on the stray field due to the loading is negligible even if its length is several millimeters, and that the resonator can be used for frequencies up to about 5 GHz. There were other details concerning the construction of the resonator, but we shall not elaborate them here.

To determine the impedance of the loading introduced into the resonator, we shall consider the structure shown in Fig.5.19(a) as a series connection of three two-port networks: the two coaxial-line parts of the resonator, designated by A and B in Fig.5.19(a), and the measured loading between them, designated by D. We assume that D is a linear lossless reciprocal network (as are also the two coaxial-line parts), so that in the general case it is uniquely defined by three parameters, of either Y- or Z-type. (If the loading is geometrically symmetrical with

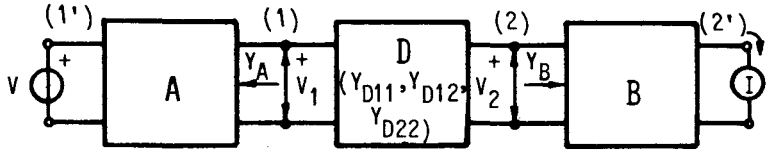

FIG.5.20. An equivalent circuit for the resonator sketched in Fig. 5.19(a).

respect to the median plane, two parameters suffice.) We shall adopt the Y-parameters for the analysis. One possible representation of the resonator is then as that shown in Fig.5.20. Due to a very weak coupling, the generator can be represented as an ideal voltage generator, and the diode used for detecting the resonance as an ideal current meter, i.e., the two-port networks A and B can be assumed to be short-circuited at their ports 1' and 2', respectively.

For a given loading, the lengths of the coaxial-line sections A and B of the resonator can always be adjusted so that the system in Fig. 5.19(a), i.e., in Fig.5.20, be in resonance. A resonance is detected by maximal current intensity in the current meter. We can always follow a measurement procedure to ensure that the first, lowest resonant frequency of the system be obtained. By measuring the lengths l_A and l_B, and frequency, it is possible to calculate the admittance of the two-port network A, at port 1 looking to the left, and that of network B, at port 2 looking to the right in Fig.5.20, as admittances of short-circuited coaxial lines of lengths l_A and l_B, respectively. (It is, of course, possible to take into account the different diameters of the inner line conductor, the lengths of which are designated in Fig. 5.19(a) by $l_{A'}$, $l_{A''}$, $l_{B'}$ and $l_{B''}$, if a more accurate representation is desired.) Let these admittances be Y_A and Y_B.

Resonance in Fig.5.20 is attained if input admittance to network D at port 1, looking to the right, equals $-Y_A$, and that at port 2, looking to the left, equals $-Y_B$. We thus obtain the equations

$$Y_{D11} + Y_{D12}\frac{V_2}{V_1} = -Y_A , \qquad Y_{D22} + Y_{D12}\frac{V_1}{V_2} = -Y_B . \tag{5.9}$$

Eliminating V_2/V_1 from these equations we get

$$Y_A Y_{D22} + Y_B Y_{D11} + (Y_{D11} Y_{D22} - Y_{D12}^2) = -Y_A Y_B . \tag{5.10}$$

(Of course, $Y_{D11}=jB_{D11}$, etc., since all the admittances in this equation are imaginary, the networks being lossless and passive.)

This is an equation in three unknowns, Y_{D11}, Y_{D22} and Y_{D12} (namely $Y_{D11}Y_{D22}-Y_{D12}^2$). To be able to determine these parameters of the D-network, we must calculate the admittances Y_A and Y_B for three different lengths l_A of the resonator, in which case eqn.(5.10) results in three linear equations for determining the three unknowns. To decrease measurement errors, it is advisable to perform several sets of such measurements, and to obtain the unknown parameters of the D-networks by some convenient procedure, for example by requiring that the solution be the best possible in the least-square sense. Note, however, that Y_{D11}, Y_{D22} and Y_{D12} are functions of frequency.

This method was applied to measure several types of concentrated loadings used in examples of antenna analysis and, in particular, of antenna synthesis. Two cases of importance for future reference are the experimental values of reactances of variable lumped capacitive and inductive loadings designed specifically to aid in verifying the results of the antenna synthesis (to be considered in the next part of this monograph). These two types of loadings are shown in Fig.5.21.

The value of the capacitive loading could be varied continuously by varying the distance δ, i.e., by screwing and unscrewing the movable part of the element. The screw pitch was only 0.25 mm, so that the distance between the capacitor electrodes was possible to adjust with accuracy of about 0.01 mm. Note that the physical length of the whole element is thereby not changed, so that the total antenna length is also not changed by adjusting one or more such capacitors on an assembled antenna. Dependence of the element capacitance and of susceptance at 1 GHz on the distance δ between the electrodes is shown in Fig.5.22.

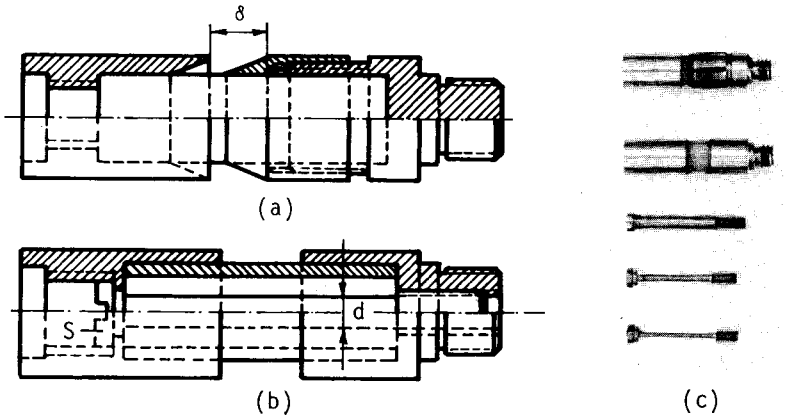

FIG.5.21. Variable lumped antenna loadings: sketch of (a) capacitive and (b) inductive loading; (c) photograph of both loadings and exchangeable inner conductors of the inductive loading.

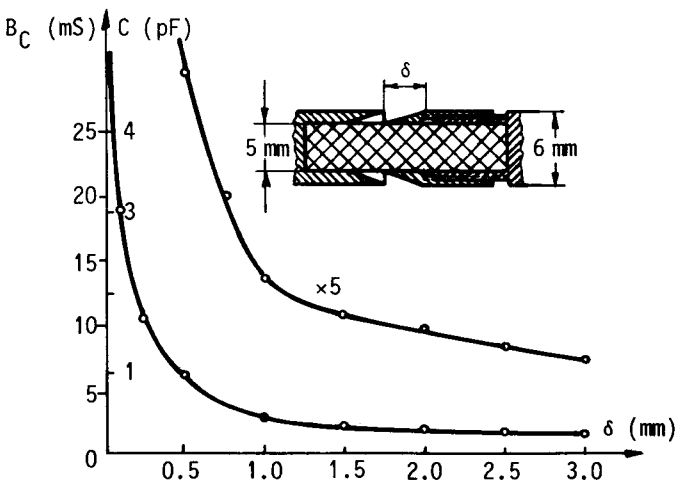

FIG.5.22. Capacitance (C) and susceptance at 1 GHz (B_C) of the capacitive loading shown in Fig.5.21(a) versus the distance δ between the electrodes. For upper curve the readings for C and B_C are to be divided by five.

Note that it was possible to realize with this capacitor capacitive loadings ranging from about 40 Ω to about 700 Ω at 1 GHz.

The value of the inductive loading shown in Fig.5.21(b) could be varied in steps by changing the diameter of the screw S shown in the figure (by replacing the screw), which was used as the inner conductor of the two short-circuited coaxial lines machined inside the element on both sides of the gap. The gap itself was left relatively wide (4 mm), in order to reduce the gap capacitance. Dependence of the element inductance and of its reactance at 1 GHz on the screw diameter is shown in Fig.5.23. Note that only a relatively limited range of values could be realized, due to small size of the element. This inductance was used primarily for compensation of the antenna susceptance by mounting the element in the excitation zone.

Finally, it was found experimentally that the elements described above cannot be strictly regarded as pure series elements, but that this is true with a relatively high accuracy. For example, in the case of the capacitive loading a shunt reactance of about 5 kΩ at 1 GHz existed in addition to the series capacitance, but it can be obviously neglected without significantly impairing accuracy.

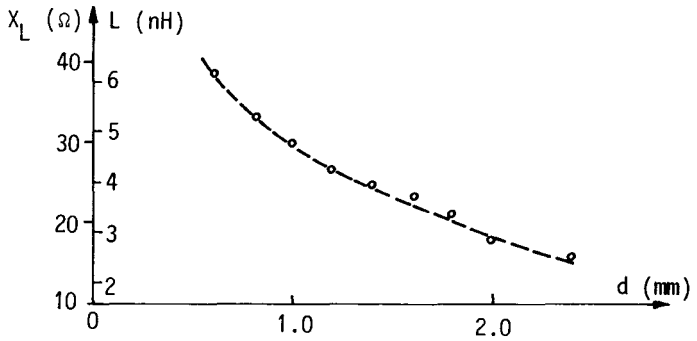

FIG.5.23. Inductance (L) and reactance at 1 GHz (X_L) of the lumped inductive loading sketched in Fig.5.21(b) versus the diameter of the screw representing the inner conductor of two short-circuited coaxial lines.

5.4. WIRE ANTENNAS WITH MIXED LOADINGS

It was shown in the preceding chapter that resistive antennas with distributed loading offer interesting possibilities, for example remarkable broadband properties. However, they exhibit losses, which in the case of the "travelling-wave" resistive antennas are such that efficiency is of the order of 50%.[51] On the other hand, antennas with lumped capacitive loading exhibited broadband properties inferior to those of resistive antennas, but did not have losses. These examples indicated that antennas with combined distributed and lumped loadings might be expected to have properties superior to those of antennas with only one type of loadings.

To analyse such antennas we have simply to combine the theory presented in Sections 4.2 and 5.2. For example, in the case of symmetrical cylindrical antennas the Hallén equation (5.6) should be modified by adding to the left side the term D(z) given in eqn.(4.8) with $z_0=0$. Such an equation could then be solved by any convenient procedure.

As an example of mixed distributed and lumped loadings we shall consider a cylindrical antenna with distributed resistive and concentrated capacitive loadings.[42] The first problem to be solved was that of designing a convenient model of cylindrical antenna with resistive and capacitive loadings. The antenna had to satisfy three basic requirements to be a useful model for investigations of such structures. Firstly, it had to be as simple as possible, for practical reasons. Secondly, it had to be flexible with respect to the amount and distribution of the loadings. Finally, the physical model had to be such that it can be analysed theoretically with sufficient accuracy.

After considering several possibilities, an antenna model which closely satisfied all the three requirements was made in the form of a row of commercially available high-quality resistors between which air gaps were left. The resistors were in the form of a thin resistive layer over a cylindrical ceramic body, with silver endings at both ends. A row of these resistors was placed in a groove made in a styrofoam dielectric support suspended in front of a vertical ground plane. The

air gaps between the resistors represented concentrated capacitors, the capacitance of which can be varied easily by varying the gap width. Such a construction is very simple and provides great flexibility in obtaining the desired distribution and magnitude of the loadings. Further, the structure very nearly satisfies the conditions for analysing the system by the approximate method described in this and the preceding chapters.

A monopole antenna of this form was made using resistors of lengths l=24 mm and radius a=3.5 mm. With regards to resistance, resistors of resistances 50, 100 and 200 Ω were used (which correspond to continuous resistive loadings of about 2080, 4170 and 8330 Ω/m, respectively). According to some known results[50,51] and to numerical computations performed by the authors, step-like resistive and lumped capacitive loadings were adopted, the magnitudes of which increased towards the antenna end. It was expected that such a loading should result in good broadband properties for frequencies between 1 and 2.5 GHz. Three resistive elements, each of length 4.8 cm (two connected resistors of the same resistance) were added to a segment which was 5.6 cm long and represented a simple protrusion through the ground plane of the inner coaxial-line brass conductor, of the same diameter as the resistors. The first resistive segment was made of two 50 Ω resistors, the second segment of two 100 Ω resistors and the third of two 200 Ω resistors. The air gap between the first and the second segment was 0.3 mm, corresponding approximately to 1.1 pF, the second gap was 0.5 mm, corresponding to 0.565 pF, and the last gap was 1 mm, corresponding to 0.34 pF, so that the total length of the monopole antenna was h=20.18 cm. A photograph of the antenna is shown in Fig.5.24.

Using the method described above and adopting the belt-generator mod-

FIG.5.24. Photograph of the resistive-capacitive monopole antenna, of radius a= 3.5 mm and length h=20.18 cm. (Ref.42)

el of the coaxial-line excitation, a program was prepared for analysing symmetrical dipole antennas with arbitrary continuous and concentrated impedance loadings along their lengths. The antenna admittance, radiation pattern and current distribution for the case described above were calculated in the frequency range 1.2-2.4 GHz. The solid lines in Fig.5.25 show the calculated conductance (G) and susceptance (B) of the antenna model against frequency.

To check the reproducibility of the antenna, measurements of the monopole admittance were performed several times. After every set of measurements the whole antenna was dismounted and then assembled again. The difference in the results was found to be practically within the limits of the experimental error. One typical set of measured results is presented in Fig.5.25.

A very good agreement between measured and theoretical values of G can be observed. Agreement between experimental and theoretical results is not so good for the imaginary part of the admittance. The measured and the computed B curves have practically the same shape, but there is a nearly constant difference between them. Three possible reasons for the discrepancy are (a) the capacitances of the concentrated capacitive loadings are not known exactly, (b) the mathematical model of the antenna is not sufficiently accurate, e.g., the influence of the silver resistor endings was not taken into account, and (c) the belt generator can also introduce some error.

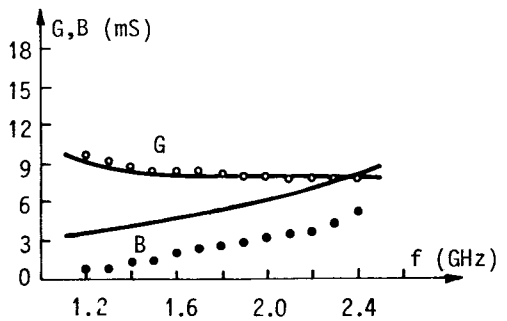

FIG.5.25. Conductance (G) and susceptance (B) of the antenna shown in Fig.5.24 against frequency. ——— theory; oo, •• experiment. (Ref.42)

It is evident that the described resistive-capacitive type of antenna has good broadband characteristics in admittance. For the average measured conductance of G_{av}=8.26 mS in the frequency range from 1.2 to 2.4 GHz, the average VSWR is only 1.38.

Measurement of current distribution in the present case is a very complicated task, and was not performed. However, theoretical analysis of such structures was proved to predict quite accurately not only the antenna admittance, but also the radiation pattern.[60] In other words, the theoretical current distribution should be very close to the actual distribution. The antenna efficiency, η, can therefore be determined theoretically with high accuracy as

$$\eta = \frac{P_{input} - P_{Joule\ along\ antenna}}{P_{input}} , \tag{5.11}$$

where

$$P_{input} = \frac{G}{G^2 + B^2} \left| I(0) \right|^2 , \tag{5.12}$$

and

$$P_{Joule\ along\ antenna} = \int_0^h R'(z) \left| I(z) \right|^2 dz , \tag{5.13}$$

I(z) representing the complex r.m.s. value of current intensity along the antenna and R'(z) the antenna resistance per unit length. The efficiency of the antenna described was found in this manner to be between 81 and 84% over the whole frequency range considered. This is much better than for purely resistive travelling-wave cylindrical antennas, for which, as mentioned, the efficiency is of the order of 50%. It should be noted that experimental determination of efficiency is extremely involved (it can be, for example, based on measured radiation pattern and gain) and probably less accurate than the theoretical estimate.

Finally, the theoretical current distributions exhibited a quasi-decaying travelling-wave property, and the corresponding radiation pat-

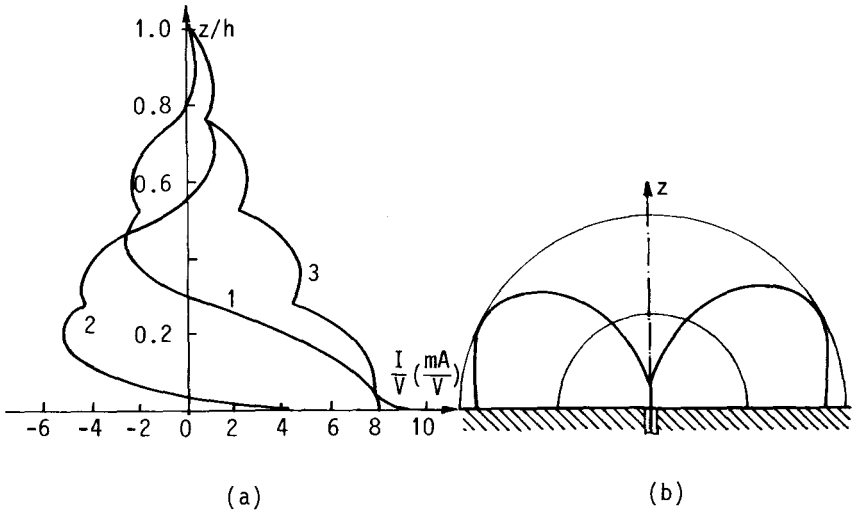

FIG.5.26. Theoretical current distribution (a) and radiation pattern in electric-field strength (b) of the antenna shown in Fig.5.24, at f=1.5 GHz; (1) real part, (2) imaginary part and (3) magnitude of current. (Ref.42)

terns had the expected shapes, typical for travelling-wave linear antennas. Examples of the current distribution and of the radiation pattern, in the electric-field strength, at f=1.5 GHz, are shown in Figs.5.26(a) and (b). The current magnitude had practically the same shape over the whole frequency range considered, and radiation patterns changed slowly from that of a Hertzian dipole at 1200 MHz to the shape similar to that shown in Fig.5.26(b), only with somewhat more pronounced radiation at approximately 45°, with respect to the ground plane, at 2400 MHz. Thus the antenna exhibits excellent broadband properties in the radiation pattern also.

In a later chapter a similar antenna will be considered as a system to be optimized. It will be seen that exceptionally broadband cylindrical antenna can be thus obtained, having very small VSWR in a remarkably wide frequency range.

5.5. CONCLUSIONS

In this chapter a method was presented for analysis of wire antennas with concentrated loadings. Although the loadings can be represented in various ways, the simplest, delta-function approximation of the loadings appeared to be of sufficient accuracy.

A number of examples of antennas with concentrated loadings analysed both theoretically and experimentally indicated satisfactory agreement between the two sets of results. Particular attention was devoted to concentrated capacitive loadings, because they are easy to realise accurately and are lossless. Most examples related to antennas with lumped capacitive loadings, and a section was devoted to describing several kinds of lumped capacitive loadings made by the authors and measurement of their capacitance in operating conditions. As an example of antennas with combined continuous and concentrated loadings, an RC cylindrical antenna was described and analysed, indicating some advantages of the combined type of loading over one type of loading only.

Inductive series lumped loadings were not considered as examples at all (although, of course, the method for analysis described in this chapter applies to that case also). The reason for this was the following. Such loadings result in essentially slow-wave structures. It is known that slow-wave structures are less efficient radiating systems than fast-wave structures (antennas with series capacitive loadings in our case), and that they usually have narrower bandwidth and smaller efficiency than the latter.

CHAPTER 6
Wire Antennas in Lossy and Inhomogeneous Media

6.1. INTRODUCTION

In deriving the equations for analysis of wire-antenna structures in previous chapters it was assumed that the antenna was situated in a homogeneous lossless medium. Although this assumption does approximate well the real situation frequently, e.g., in all instances in which an antenna is situated in air far from other objects or possibly adjacent to a large, theoretically perfectly conducting plane surface, in practice antennas in conducting, approximately homogeneous media are also encountered. Examples of such cases are numerous: antennas on space vehicles travelling through the ionosphere (neglecting sheaths around the antenna and the anisotropy of the ionosphere), antennas buried in the ground or immersed in the sea, or antennas used for measuring properties of media (i.e., plasma or the earth's crust). The next section of this chapter is devoted to analysis of wire antennas in such circumstances.

In reality, antennas are never operating in homogeneous media. For example, even if an antenna is situated high above the earth's surface, the presence of the supporting structure and the feeder certainly has certain influence on the antenna properties. A common case in which this kind of inhomogeneity is practically negligible is a large, plane conducting sheet through which a monopole antenna is fed by means of a coaxial line. In most instances, inhomogeneity of one kind or another is always present in the antenna vicinity, and has at least a small influence on the antenna properties.

Analysis of the influence of an inhomogeneity is, as a rule, a very difficult task. It is therefore often neglected even when this affects the final results considerably. There are two important cases of inhomogeneities, however, which can be analysed with high accuracy. One is that when a planar wire-antenna structure is located on the plane interface between two media. Approximately this situation is obtained if the antenna is laid on the flat surface of the earth or is floating on the surface of the sea. The other is that of antennas located above real, imperfectly conducting ground, a situation which is of very frequent occurrence in practice. These two cases will be considered in the third and fourth sections of this chapter.

6.2. WIRE ANTENNAS IN HOMOGENEOUS LOSSY MEDIA[63]

Consider a perfectly conducting wire-antenna structure situated in a homogeneous lossy medium of parameters $\varepsilon=(\varepsilon'-j\varepsilon'')$, μ and σ. Using exactly the same approach as in the case of antennas in lossless media, we can homogenize the medium and use the expressions for the retarded potentials. In the complex formalism the losses are incorporated in the equations (and in the solutions) by simply changing ε (real in the lossless case) to equivalent complex permittivity ε_{eq},

$$\varepsilon_{eq} = \varepsilon' - j(\varepsilon'' + \sigma/\omega) \ . \tag{6.1}$$

(Generally speaking, μ can also be complex, e.g., for a lossy, approximately linear ferrite material, but this case is rarely encountered in the antenna practice.) As a consequence, the propagation coefficient becomes complex also,

$$k = \omega\sqrt{\varepsilon_{eq}\mu} = \beta - j\alpha \ , \tag{6.2}$$

as well as the intrinsic impedance of the medium,

$$\zeta = \sqrt{\mu/\varepsilon_{eq}} = \zeta_r + j\zeta_i \ . \tag{6.3}$$

Thus, the presence of losses in a (homogeneous) medium leaves all the equations formally intact, but k and ζ become complex. Since the propagation coefficient k enters all the integrals which in a numerical solution of an antenna structure need to be evaluated numerically, a

computer program valid for their evaluation in the lossless case has to be modified. This, however, is a relatively easy task[64] and we shall not elaborate it here. Instead, we shall present some theoretical results for certain cases of cylindrical antennas for which experimental data are available.

Extensive experimental results were presented by Iizuka and King for admittance of, and current distribution along, monopole antennas immersed in a liquid conducting medium.[65-67] The monopole antennas analysed had a radius a=0.318 cm, and represented a simple protrusion of the inner coaxial-line conductor through the ground plane. The inner radius of the outer coaxial-line conductor was b=1.112 cm, so that the width of the equivalent belt generator, according to eqn.(2.29), was $\alpha a=5.45$ a.

In the experiments, the coaxial line was sealed at the ground plane with a lossless dielectric piece of polystyrene, which is not quite the same as the theoretical model that can be represented by the belt generator. However, it is not difficult to conclude that this cannot introduce significant error in theoretical results. The frequency in all the experiments was kept constant at 114 MHz, and $\sigma/\omega\varepsilon$ was varied from 0.036 to 8.8. The permittivity $\varepsilon=\varepsilon'-j0$ of the liquid solution used was in the range of $69\varepsilon_0$ to $78\varepsilon_0$.

For measurement of the admittance, the monopole antenna was made in two forms: (a) as a simple protrusion of the inner cable conductor (bare antenna), and (b) using an antenna partially covered with a dielectric cover (made of penton) to protect a small probe used to measure current distribution along the monopole. The two admittance curves differ considerably. Naturally, the first set of results, corresponding to the bare antenna, were considered.

Figs.6.1(a)-(c) display the theoretical and experimental curves showing conductance (G) and susceptance (B) of the corresponding symmetrical dipole antenna versus the antenna electrical halflength βh (measured in the conducting medium). The theoretical results were obtained using Hallén's equation and a single polynomial (of degree n) to approximate current distribution along the whole monopole-antenna length.

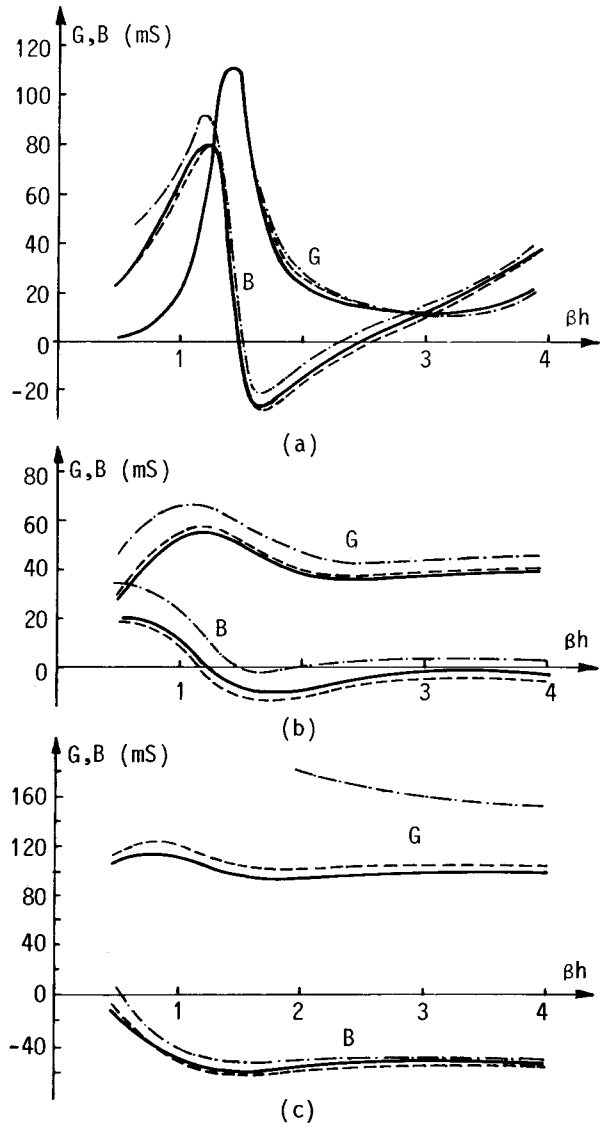

FIG.6.1. Conductance (G) and susceptance (B) of dipole antennas immersed in a conducting medium; a=0.318 cm, f=114 MHz; (a) ε_r=78, $\sigma/\omega\varepsilon$=0.036, (b) ε_r=77, $\sigma/\omega\varepsilon$=1.06, (c) ε_r=69, $\sigma/\omega\varepsilon$=8.8. ——— belt generator, n=5; — • — delta-function generator, n=3; — — — experiment.[65] (Ref.63)

The cases shown, with $\sigma/\omega\varepsilon$=0.036, 1.06 and 8.8, indicate again clearly the advantage of the belt generator (or, equivalently, of the TEM magnetic-current frill) over the delta-function generator. Already for $\sigma/\omega\varepsilon$=1.06, the conductance curve corresponding to the delta-function generator is in substantial error, an error that becomes rapidly larger as $\sigma/\omega\varepsilon$ increases further, in spite of the very low-order approximation for current used. It is interesting to note that, for $\sigma/\omega\varepsilon>1$, the more pronounced effect of the delta-function generator is on the antenna conductance rather than on susceptance, just as the converse is true for $\sigma/\omega\varepsilon<1$ (which, of course, should be expected).

As already mentioned, for measurements of current distribution Iizuka and King used a monopole partially covered along its length with a dielectric cover, protecting the probe from the liquid solution. Unfortunately, this arrangement obviously was radically different from the bare monopole antenna, as about 1/3 of the monopole circumference was not in direct contact with the liquid solution. Therefore, we cannot expect a close agreement of current distribution obtained by the present theory with experimental results of Iizuka and King.

The entire-domain polynomial used to approximate current distribution introduced some difficulties. By choosing closely spaced matching points in the belt-generator region, we can expect to obtain accurate values of current for small z, i.e., accurate value of the driving-point admittance; the results shown in Fig.6.1 clearly indicate that this reasoning is correct. However, if the mutual distance of the remaining matching points is much larger than the distance between the first three, we can expect certain unstable, oscillatory solutions about the true solution in that region. It is possible to avoid this difficulty in two ways. We can use either a higher-order approximation for current (thus increasing the number of the matching points and decreasing the distance between them), or divide the monopole into several subsegments. The first procedure was adopted here.

As an illustration of current distribution obtained by the present method, Fig.6.2 shows experimental distributions[65] (obtained with the monopole partially covered with a dielectric cover) for $\beta h=3\pi/4$ and for

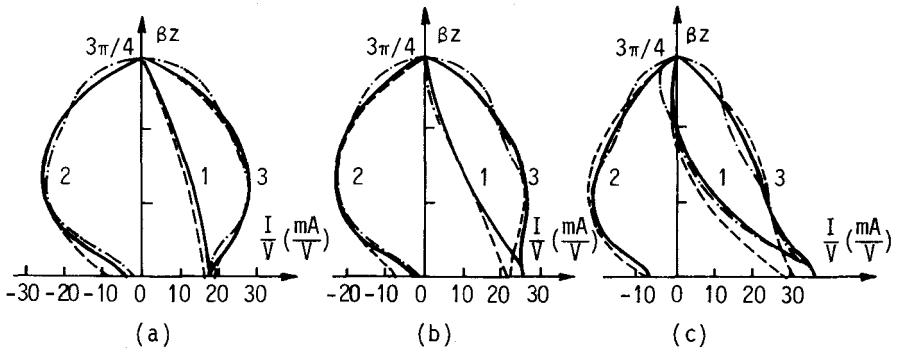

FIG.6.2. Current distribution along dipole antenna in a conducting medium; a=0.318 cm, βh=3π/4, f=114 MHz; (1) real part, (2) imaginary part, (3) magnitude; (a) ε_r=78, σ/ωε=0.036, (b) ε_r=78, σ/ωε=0.35, (c) ε_r=77, σ/ωε=1.06. ——— belt generator, n=8; — • — belt generator, n=5; — — — experiment.[65] (Ref.63)

σ/ωε=0.036, 0.35 and 1.06, together with the theoretical distributions for n=5 and n=8. It is evident that, for n=5, we have the aforementioned oscillatory solution, but that for n=8 this undesirable oscillatory character is lost. Both solutions are in a relatively good agreement with experiment.

Although the above examples relate to cylindrical antennas only, it can obviously be expected that the method for analysis of wire antennas described in the preceding chapters can successfully be extended to analysis of wire antennas of arbitrary shapes situated in homogeneous lossy media.

6.3. DETERMINATION OF CURRENT DISTRIBUTION ALONG WIRE ANTENNAS ON PLANE INTERFACE BETWEEN TWO HOMOGENEOUS MEDIA[68]

As mentioned in the introduction to this chapter, the problem of determining circuit and radiation properties of antennas located at or near the interface between two media arises in a number of practical situations. A wire antenna situated at or above a lossy ground, the so-called island antenna, and an antenna buried in the earth are ex-

amples of such structures. The problem is a very complex one. Rigorous solution of the problem implies determination of current distribution along the antenna, the electromagnetic field produced by which satisfies boundary conditions at the antenna surface and at the interface between the two media.

The problem of antennas located at the very interface between two media can be solved approximately, but in a simple manner, by dividing it into two quasi-independent problems: the first of determining (approximately) the current distribution along the antenna, and then determining the electromagnetic field in both media produced by this current distribution. The aim of the present section is to show that such an approximate two-step solution is possible, and to present a method for obtaining the first part of the solution, i.e., for determining approximate current distribution along a cylindrical antenna located at the interface between two media.

By a rigorous mathematical procedure it has been found that along thin, infinite straight wires parallel to the interface between two media, with time-harmonic current injected at a point along their length, there exists an exponential mode of propagation of current along the wire.[69] If the wire is located at a distance of several diameters from the interface, the propagation coefficient (in general complex) equals approximately the propagation coefficient of the medium in which the wire is situated. If the wire is located at the interface, the propagation coefficient is approximately given by

$$k^2 = \frac{k_1^2\mu_2 + k_2^2\mu_1}{\mu_1 + \mu_2} , \tag{6.4}$$

where k_1 and k_2 are the propagation coefficients of the two media, and μ_1 and μ_2 their permeabilities.

Consider a symmetrical dipole of radius a and length 2h, center-driven by a belt generator of convenient width to approximate a desired coaxial-line excitation, and situated (for the moment) in a homogeneous, generally lossy medium of complex parameters ε, μ and σ. From the

preceding section we know that any of the integral equations for current I(z) along the dipole is formally valid, except that the propagation coefficient k and the intrinsic impedance of the medium are now complex. The (complex) propagation coefficient k is given by

$$k^2 = \omega^2\varepsilon\mu(1 - j\sigma/\omega\varepsilon) \ , \tag{6.5}$$

where, of course, all the parameters may be complex.

Assume now that the antenna is located at the interface between media of parameters ε_1, $\mu_1=\mu_o$ and σ_1, and ε_2, $\mu_2=\mu_o$ and σ_2. Then the propagation coefficient along the dipole is approximately given by equation (6.4), i.e.,

$$k^2 \simeq \frac{k_1^2 + k_2^2}{2} = \omega^2\varepsilon_e\mu_o(1 - j\sigma_e/\omega\varepsilon_e) \ , \tag{6.6}$$

where

$$\varepsilon_e = 0.5(\varepsilon_1 + \varepsilon_2) \ , \quad \sigma_e = 0.5(\sigma_1 + \sigma_2) \ . \tag{6.7}$$

By comparing equations (6.4) and (6.7) we see that ε_e and σ_e can be considered as permittivity and conductivity of an equivalent medium. Thus, by simply substituting in eqn.(6.5) ε by ε_e and σ by σ_e, any integral equation for current distribution along the dipole situated in a homogeneous medium can be used for approximately determining current distribution along the dipole situated at the interface between the two media. It is also possible to show that with the concept of the equivalent medium the belt-generator approximation to coaxial-line excitation of the monopole remains valid, but we shall not consider that here.

Extensive experimental results are presented in Reference 70 for admittance and current distribution of monopole antennas driven by a coaxial line and located at or close to the interface between air and a water solution of sodium chloride. Theoretical results obtained by the above method were compared with those in Reference 70. In all the cases agreement was found to be good. As one example, Figs.6.3(a) and (b) display the theoretical and experimental curves for the monopole conductance (G) and susceptance (B) versus the ratio $\sigma/\omega\varepsilon$ for the solu-

tion, for a quarter-wave and half-wave monopole antenna (wavelength measured in the conducting medium). As the second example, Figs.6.4(a) and (b) show real and imaginary parts of current along a quarter-wave and a half-wave monopole (wavelength measured in the conducting medium) for $\sigma/\omega\varepsilon=1.06$ and $\varepsilon_r=77$. In all the cases agreement between theoretical and experimental results can be considered to be good.

It is obvious that the above approximate method for determining current distribution along symmetrical cylindrical dipole antennas can be used also for approximate analysis of arbitrary planar wire antennas situated at the plane interface between two media.

In the end, two remarks are necessary concerning the method just explained. First, note that, according to theoretical conclusions[69] (which were confirmed by measurements[70]), the antenna current distribution varies rapidly when it is moved into one or other medium, i.e.,

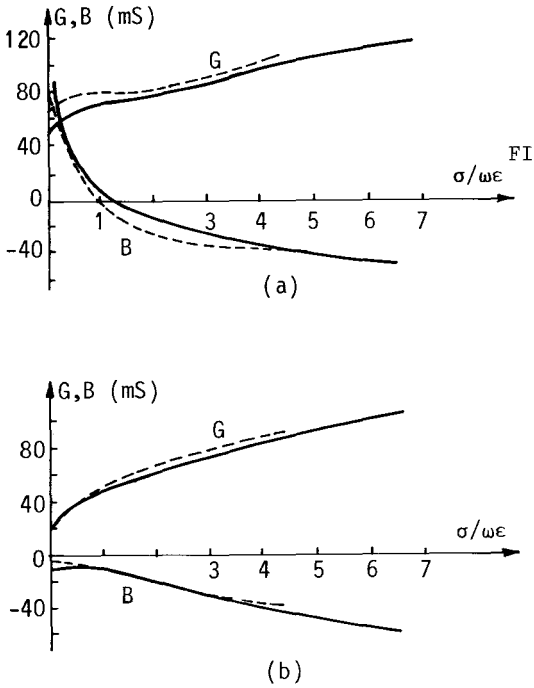

FIG.6.3. Conductance (G) and susceptance (B) of monopole antenna located at the interface of air and lossy medium, versus $\sigma/\omega\varepsilon$ of the medium; a=0.318 cm, b/a=3.5, f=114 MHz, ε_r varies from 69 to 78. – – – experimental;[70] ——— present method, 6th-degree polynomial approximation along (a) quarter-wavelength monopole, (b) half-wavelength monopole (wavelength measured in the conducting medium). (Ref.68)

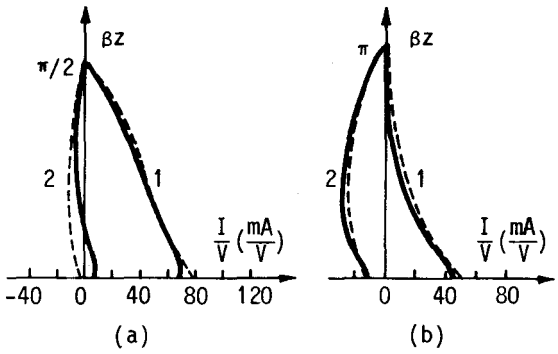

FIG.6.4. Real (1) and imaginary (2) parts of current distribution along monopole antennas at the interface of air and lossy medium; a=0.318 cm, b/a=3.5, f=114 MHz, $\sigma/\omega\varepsilon$=1.06, ε_r=77. – – – experimental;[70] ——— present theory, 9-th degree polynomial approximation for current; (a) quarter-wavelength monopole, (b) half-wavelength monopole (wavelength measured in the conducting medium). (Ref.68)

when it is not exactly at the interface. Second, as pointed out above, even if an antenna is at the interface and we know the current distribution along it, there still remains the problem of determining the field due to this antenna current in the two media. That problem we shall not consider here.

6.4. WIRE ANTENNAS ABOVE IMPERFECTLY CONDUCTING GROUND

In the case of an antenna placed in a homogeneous medium above a perfectly conducting ground plane, we know from the image theory that field due to currents and charges induced on the plane is the same as that of the antenna image situated in the homogeneous medium. The antenna analysis can be performed for the symmetrical equivalent system using any suitable method. However, no image theory is available if the antenna is placed relatively closely above an imperfectly conducting ground. Sommerfeld was the first author to analyse this complex problem, as early as in 1909,[71] and he was followed by many others. We shall present here a brief review of the basic principles of Sommer-

feld's theory, with slight modifications. For a more detailed treatment the reader may consult, for example, References 3 and 72.

In a homogeneous medium, the magnetic vector-potential due to an elemental current source of intensity $\vec{J}\,dv$ and the electric scalar-potential due to an elemental charge source of intensity ρdv are proportional to the respective source intensity and to the appropriate Green's function,

$$g(|\vec{r}-\vec{r}'|) = \frac{\exp(-jk|\vec{r}-\vec{r}'|)}{4\pi|\vec{r}-\vec{r}'|} \quad . \tag{6.8}$$

As usual, $\vec{r}$ defines the observation point, and $\vec{r}'$ the source point. This function can be interpreted as a spherical wave emanating from the source. Let us assume, for convenience, that the source is located at the origin of a rectangular coordinate system, so that $\vec{r}'=0$. According to Sommerfeld's theory,[71] this spherical wave can be mathematically represented as an integral of plane waves, as follows:

$$\frac{\exp(-jkr)}{r} = -\frac{jk}{2\pi}\int_0^{\pi/2+j\infty}\int_{-\pi}^{\pi} \exp\left[-jk(x\sin\theta\cos\phi + y\sin\theta\sin\phi + |z|\cos\theta)\right] \cdot \sin\theta\, d\phi\, d\theta \quad , \tag{6.9}$$

where $\vec{r}=x\vec{i}_x+y\vec{i}_y+z\vec{i}_z$, $r=|\vec{r}|$, and θ and ϕ can be interpreted as the angles of a spherical coordinate system determining the propagation vector of the elemental plane waves. The first part of the integration path in the complex θ-plane can be taken along the real axis, from the origin to $(\pi/2,0)$, and then parallel to the imaginary axis, from $(\pi/2,0)$ to $(\pi/2,+\infty)$. Hence, the following interpretation of eqn.(6.9) can be given. For $z>0$, along the first part of the integration path the exponential term of the integrand is an ordinary transversal plane wave, propagating in the direction determined by the angles θ and ϕ, $\sin\theta\, d\phi\, d\theta$ is the elemental solid angle, and the integration is performed over the whole upper half-space. However, along the second part of the integration path in the complex θ-plane the exponential term of the integrand is a generalized, non-transversal plane wave. This is possible to conclude if θ in the integrand is substituted by $(\pi/2+jt)$. The equiphase planes of that wave are perpendicular to the xy-plane and propagate in

a direction parallel to the xy-plane defined by the angle ϕ. The planes of equal amplitude are perpendicular to the z-axis, and the amplitude of the wave decays exponentially with increasing z. A similar interpretation of eqn.(6.9) is possible for $z<0$.

The integral over ϕ in eqn.(6.9) can be expressed in terms of the Bessel function of the first kind and order zero, to obtain

$$\frac{\exp(-jkr)}{r} = -jk \int_0^{\pi/2+j\infty} J_0(k\rho \sin\theta)\, \exp(-jk|z| \cos\theta) \sin\theta \, d\theta \,, \qquad (6.10)$$

where $J_0(t)$ is the Bessel function of the first kind and order zero, and $\rho=(x^2+y^2)^{\frac{1}{2}}$.

Let us now suppose that the elemental source is situated in a vacuum above flat surface of a homogeneous medium of permeability μ_0, as shown in Fig.6.5. The complex relative permittivity ε_r of the medium, which we consider to be the ground, is assumed to include in ε_r'' the ground conductivity. Each plane wave propagating in a direction characterized by an angle $\pi-\theta > \pi/2$ is incident on the ground surface at an angle θ with respect to the normal to the surface. This wave is partly reflected from the ground, and partly transmitted into it. Let us denote the angle of the reflected wave by θ_r, and the angle of the transmitted wave by θ_t (both with respect to the normal to the surface).

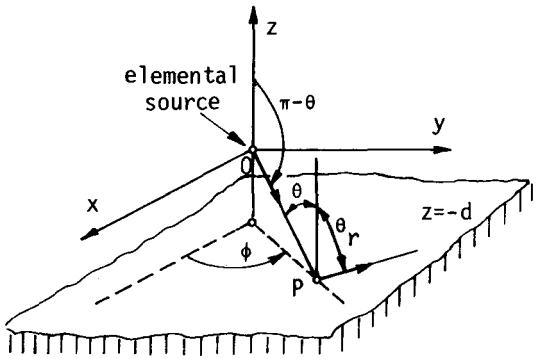

FIG.6.5. Elemental source above imperfectly conducting ground. P denotes the point of reflection of an elemental wave.

The reflection and transmission coefficients can be obtained from the boundary conditions at the plane z=-d:

$$E_x^i + E_x^r = E_x^t \,, \qquad E_y^i + E_y^r = E_y^t \,, \tag{6.11}$$

$$E_z^i + E_z^r = \varepsilon_r E_z^t \,, \tag{6.12}$$

$$B_x^i + B_x^r = B_x^t \,, \qquad B_y^i + B_y^r = B_y^t \,, \tag{6.13}$$

$$B_z^i + B_z^r = B_z^t \tag{6.14}$$

where the superscripts "i", "r" and "t" denote the incident, reflected and transmitted waves, respectively.

In his solution, Sommerfeld introduced at this point the Hertz potential. Since all the equations for current distribution presented in the preceding chapters were derived essentially on the basis of the Lorentz potentials, we shall use them instead of the Hertz potential, so that

$$\vec{E} = -j\omega\vec{A} - \text{grad}\, V \,, \tag{6.15}$$

$$\vec{B} = \text{curl}\, \vec{A} \,, \tag{6.16}$$

with

$$\text{div}\, \vec{A} = -j\omega\varepsilon\mu V \,. \tag{6.17}$$

The Lorentz scalar-potential V is a continuous function at all points of the system considered. Thus, according to eqn.(6.17),

$$\varepsilon_r \,\text{div}\, (\vec{A}^i + \vec{A}^r)\big|_{z=-d+0} = \text{div}\, \vec{A}^t\big|_{z=-d-0} \,. \tag{6.18}$$

Let us first assume that an elemental current source $\vec{J}\,dv = J_z\,dv\,\vec{i}_z$ (i.e., a z-directed Hertzian dipole) is placed at the origin (Fig.6.5). In that case $\vec{A}^i$ has only the z-component. The boundary conditions in eqns.(6.11)-(6.14) and (6.18) can be satisfied if both the reflected and transmitted vector-potentials are assumed to have only the z-component. The boundary conditions for the two potentials are obtained by inserting eqns.(6.15) and (6.16) into boundary conditions (6.11)-(6.14).

Eqns.(6.11) are satisfied automatically, because the magnetic vector-potential has no tangential component to the interface (z=-d) and the electric scalar-potential is a continuous function. Since the incident, reflected and transmitted vector-potentials are continuous functions of coordinates x and y on the boundary surface, eqns.(6.13) are satisfied if

$$A_z^i + A_z^r \Big|_{z=-d+0} = A_z^t \Big|_{z=-d-0} . \tag{6.19}$$

From eqn.(6.18) it follows that

$$\varepsilon_r \left(\frac{\partial A_z^i}{\partial z} + \frac{\partial A_z^r}{\partial z} \right) \Big|_{z=-d+0} = \frac{\partial A_z^t}{\partial z} \Big|_{z=-d-0} . \tag{6.20}$$

Conditions in eqns.(6.19) and (6.20) for the total magnetic vector-potential will be satisfied if they are satisfied by all the elemental plane-wave components of the incident, reflected and transmitted potentials. The local phase velocity of these waves along the ground surface must be equal on both sides of the surface, as in the case of plane waves, because the boundary conditions could not be otherwise satisfied at all time. Therefore we have that Snell's laws of reflection and refraction are valid in this case also, i.e., $\theta_r = \theta$ and

$$k \sin\theta = k_t \sin\theta_t , \quad \text{or} \quad \sin\theta = \sqrt{\varepsilon_r} \sin\theta_t , \tag{6.21}$$

where k and k_t are the propagation coefficients of the vacuum and the ground, respectively. Let R_{Azz} be the local reflection coefficient in this case for elemental incident plane-wave components of the total magnetic vector-potential, and T_{Azz} the local transmission coefficient. From eqn.(6.19) it follows that, locally,

$$1 + R_{Azz} = T_{Azz} . \tag{6.22}$$

The partial derivative with respect to z of the elemental plane wave reduces to multiplying that wave by $jk\cos\theta$ for the incident wave, by $-jk\cos\theta$ for the reflected wave and by $jk_t\cos\theta_t$ for the transmitted wave [see eqn.(6.9)]. Eqn.(6.20) therefore yields

$$\varepsilon_r (1 - R_{Azz})\, k \cos\theta = T_{Azz}\, k_t \cos\theta_t . \tag{6.23}$$

Eliminating T_{Azz} from eqns.(6.22) and (6.23) and noting that $k_t/k=\sqrt{\varepsilon_r}$, we obtain

$$R_{Azz} = \frac{\sqrt{\varepsilon_r}\cos\theta - \cos\theta_t}{\sqrt{\varepsilon_r}\cos\theta + \cos\theta_t} \quad , \tag{6.24}$$

or

$$R_{Azz} = 1 + F_{Azz} \quad , \quad F_{Azz} = -\frac{2\cos\theta_t}{\sqrt{\varepsilon_r}\cos\theta + \cos\theta_t} \quad . \tag{6.25}$$

The first term in R_{Azz} (i.e., 1) corresponds to the case when the ground conductivity tends to infinity. Therefore the other term, F_{Azz}, can be regarded to reflect the influence of the finite ground conductivity. The reflected magnetic vector-potential can thus be expressed as

$$A_z^r = \mu_o J_z dv \left\{ g(|\vec{r}+2d\vec{i}_z|) - \frac{jk}{4\pi} \int_0^{\pi/2+j\infty} F_{Azz} J_0(k\rho \sin\theta) \exp[-jk(z+2d)\cos\theta] \cdot \right.$$
$$\left. \cdot \sin\theta \, d\theta \right\} \quad (z>-d) \quad . \tag{6.26}$$

The electric scalar-potential in this case is proportional to $\partial A_z/\partial z$. Thus the reflection coefficient for the electric scalar-potential is simply

$$R_{Vz} = -R_{Azz} = -1 + F_{Vz} \quad , \quad F_{Vz} = -F_{Azz} \quad . \tag{6.27}$$

This result is obtained for a Hertzian dipole, i.e., for two closely spaced, opposite point charges. However, it is valid for *one* point charge as well, if properly associated with a z-oriented current element. Therefore the reflected electric scalar-potential due to an elemental charge ρdv is

$$V^r = \frac{\rho dv}{\varepsilon_o} \left\{ -g(|\vec{r}+2d\vec{i}_z|) - \frac{jk}{4\pi} \int_0^{\pi/2+j\infty} F_{Vz} J_0(k\rho \sin\theta) \exp[-jk(z+2d)\cos\theta] \cdot \right.$$
$$\left. \cdot \sin\theta \, d\theta \right\} \quad (z>-d) \quad . \tag{6.28}$$

Let us now assume that an elemental current source is placed again at the origin, but is now directed along the x-axis. In that case the incident magnetic vector-potential at the point P of reflection in Fig. 6.5 has only the x-component. However, for the boundary conditions to be satisfied, the reflected and transmitted potentials in general must have two components. A suitable choice is to take them to be the x- and z-components.[3] The reflection coefficient for the elemental plane-wave component of A_x is found in the analogous way to be given by

$$R_{Axx} = \frac{\cos\theta - \sqrt{\varepsilon_r}\cos\theta_t}{\cos\theta + \sqrt{\varepsilon_r}\cos\theta_t} = -1 + \frac{2\cos\theta}{\cos\theta + \sqrt{\varepsilon_r}\cos\theta_t} = -1 + F_{Axx}, \quad (6.29)$$

so that the reflected potential is

$$A_x^r = \mu_o J_x dv \left\{ -g(|\vec{r}+2d\vec{i}_z|) - \frac{jk}{4\pi} \int_0^{\pi/2+j\infty} F_{Axx} J_0(k\rho \sin\theta) \exp[-jk(z+2d)\cos\theta] \cdot \right.$$
$$\left. \cdot \sin\theta \, d\theta \right\} \quad (z>-d) . \quad (6.30)$$

It can be further shown that each of the reflected elemental plane-wave components of A_z is equal to the corresponding incident plane-wave component of A_x multiplied by

$$R_{Axz} = \frac{2(1-\varepsilon_r)\sin\theta\cos\theta\cos\phi}{(\cos\theta + \sqrt{\varepsilon_r}\cos\theta_t)(\sqrt{\varepsilon_r}\cos\theta + \cos\theta_t)\sqrt{\varepsilon_r}} =$$
$$= \frac{2\sin\theta\cos\theta\cos\phi\,(\cos\theta - \sqrt{\varepsilon_r}\cos\theta_t)}{\sqrt{\varepsilon_r}(\sqrt{\varepsilon_r}\cos\theta + \cos\theta_t)} = \cos\phi\, F_{Axz} . \quad (6.31)$$

The z-component of the reflected potential is

$$A_z^r = -\mu_o J_x dv \frac{k}{4\pi}\frac{x}{\rho} \int_0^{\pi/2+j\infty} F_{Axz} J_1(k\rho\sin\theta)\exp[-jk(z+2d)\cos\theta]\sin\theta\, d\theta$$
$$(z>-d) . \quad (6.32)$$

The incident electric scalar-potential is proportional to $\partial A_x^i/\partial x$, and the reflected to $(\partial A_x^r/\partial x + \partial A_z^r/\partial z)$. From these relationships, the re-

flection coefficient for the electric scalar-potential is found to be

$$R_{Vx} = -1 + \frac{2\cos\theta}{\sqrt{\varepsilon_r}(\sqrt{\varepsilon_r}\cos\theta + \cos\theta_t)} = -1 + F_{Vx} \,. \tag{6.33}$$

As before, this reflection coefficient can be associated with an elemental charge, instead of with a dipole, and the reflected potential due to the elemental charge ρdv is

$$V^r = \frac{\rho dv}{\varepsilon_o}\left\{ -g(|\vec{r}+2d\vec{i}_z|) - \frac{jk}{4\pi}\int_0^{\pi/2+j\infty} F_{Vx} J_0(k\rho\sin\theta)\exp[-jk(z+2d)\cos\theta]\cdot \right.$$
$$\left. \cdot \sin\theta \, d\theta \right\} \quad (z>-d) \,. \tag{6.34}$$

Eqns.(6.28) and (6.34) state essentially the same result as obtained in Reference 73 using a different approach.

If the elemental current source is arbitrarily oriented, the reflected magnetic vector-potential is obtained by applying eqns.(6.24)-(6.26) and (6.29)-(6.32) on the vertical and horizontal components of the incident potential. However, the reflection coefficient for the electric scalar-potential is rather complex, and the reflected potential can be found more easily from eqn.(6.17).

A similar procedure can be used for determining the reflected electric vector-potential due to possible magnetic currents above ground, but this will not be needed in the following example.

As an example, consider a symmetrical, horizontal dipole sketched in Fig.6.6. The excitation region of the dipole was approximated by a TEM magnetic-current frill, with b/a=2.3, according to Subsection 2.3.1. The field due to this frill is negligible at the ground surface with respect to the field due to electric current along the dipole. Therefore the reflected electric vector-potential due to these magnetic currents was not taken into account in what follows. To form the two-potential equation for the antenna current distribution, the x-component of the total electric field along the x-axis is of interest. If we denote, as usual, by x' the x-coordinate of the source point and by x

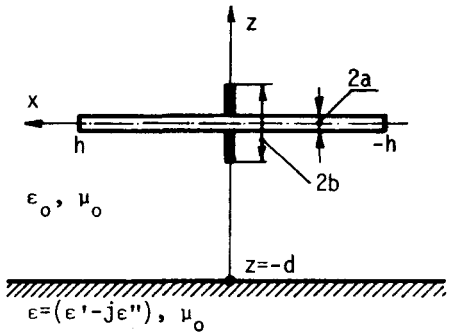

FIG.6.6. Horizontal dipole above imperfectly conducting ground.

that of the field point along the antenna, in all the expressions containing x the difference (x-x') appears only. In that case $\text{grad}_x V = \partial V/\partial x = -\partial V/\partial x'$, and the expression for grad V can be integrated by parts. Thus, the two-potential equation for the problem considered has the form

$$\int_{-h}^{h} \left\{ I(x') \left[g_d - g_r - \frac{jk}{4\pi} \int_0^{\pi/2+j\infty} F_{Axx} W(x,x',\theta)\, d\theta \right] + \right.$$

$$\left. + \frac{1}{k^2} \frac{d^2 I}{dx'^2} \left[g_d - g_r - \frac{jk}{4\pi} \int_0^{\pi/2+j\infty} F_{Vx} W(x,x',\theta)\, d\theta \right] \right\} dx' -$$

$$- \frac{1}{k^2} \frac{dI}{dx'} \left[g_d - g_r - \frac{jk}{4\pi} \int_0^{\pi/2+j\infty} F_{Vx} W(x,x',\theta)\, d\theta \right] \Bigg|_{x'=-h}^{h} =$$

$$= \frac{1}{j\omega\mu_o} E_{ix}(x) \,, \tag{6.35}$$

where

$$g_d = g(|x\vec{i}_x - x'\vec{i}_x + a\vec{i}_z|) \,, \tag{6.36}$$

$$g_r = g(|x\vec{i}_x - x'\vec{i}_x + 2d\vec{i}_z|) \tag{6.37}$$

and

$$W(x,x',\theta) = J_0(k|x-x'| \sin\theta)\exp[-jk(z+2d)\cos\theta]\sin\theta \ . \qquad (6.38)$$

A similar transformation is possible for a vertical dipole above imperfectly conducting ground.

As a numerical example, shown in Fig.6.7 is the impedance of the dipole sketched in Fig.6.6 versus the antenna height above ground, for $h=0.25\,\lambda$, $a=0.007\,\lambda$, $\varepsilon_r=10-j1.8$ and the degrees of the polynomial approximation $n_1=4$ in the excitation zone (which was taken to be 6a long) and $n_2=4$ on the rest of a dipole arm. The results obtained by the present method are compared with available theoretical results computed using also Sommerfeld's theory, but with Hallén's equation, the delta-function approximation of the generator and the second-degree polynomial approximation of current.[74] Excellent agreement between the two sets of results is seen. For comparison, also shown in Fig.6.7 is the antenna impedance for a perfectly conducting ground (i.e., for $\varepsilon''\to\infty$). These results clearly indicate that in the present case the approximation

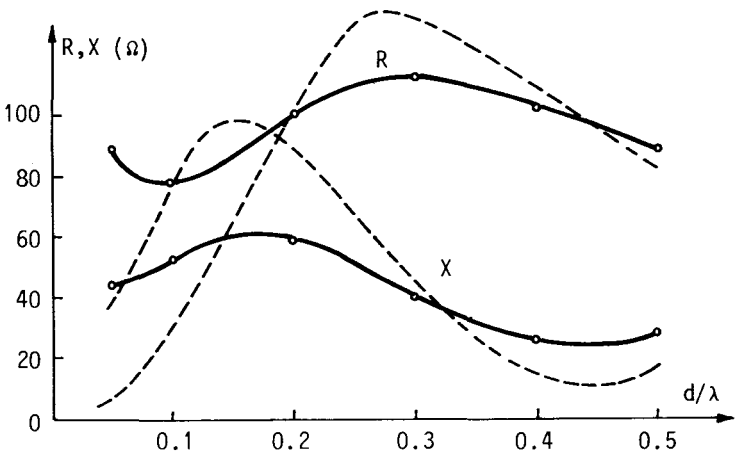

FIG.6.7. Resistance (R) and reactance (X) of the antenna sketched in Fig.6.6 versus the height, d, of the antenna above ground; $h=0.25\,\lambda$, $a=0.007\,\lambda$, $\varepsilon_r=10-j1.8$. ——— results obtained by the method described above; o o o results obtained using Hallén's equation;[74] — — — results for perfectly conducting ground.

that the ground is perfectly conducting is not adequate when computing the antenna current distribution and its impedance. Concerning the radiation pattern of the antenna shown in Fig.6.6 in the upper half-space, it can be computed using the above derived reflection coefficients once the antenna current distribution has been determined. We shall not, however, elaborate that here.

6.5. CONCLUSIONS

Although more difficult for analysis than wire antennas in homogeneous perfect dielectrics, we have seen that it is possible to analyse, approximately, three important cases of wire antennas in imperfect and inhomogeneous dielectrics: when the antenna is situated in a homogeneous lossy medium, when a planar antenna is situated at the plane interface between two homogeneous (possibly lossy) media and when a wire antenna is situated above real, lossy ground. The last case is probably the most important from the practical point of view, but also the most intricate.

With this chapter we are concluding the topics dealing with wire-antenna analysis. In engineering practice such an analysis is usually of interest only for antenna design purposes. The next part of the monograph is devoted to that important topic.

PART II
Synthesis of Wire-Antenna Structures

CHAPTER 7
General Considerations of Wire-Antenna Synthesis

7.1. INTRODUCTION

In the classical approach to designing a wire antenna or a wire-antenna structure, a certain prior knowledge of properties of a wide class of antennas, such as their admittance, radiation pattern, size, weight, rigidity, aerodynamic profile, etc., was indispensable. Using this knowledge and the designer's experience, an antenna was sought which satisfied the necessary requirements (including, possibly, only some of the mentioned antenna properties). Usually, a single step of this kind did not result in an antenna with the desired properties, and was, therefore, followed by several, or even many, similar corrective steps.

The trial-and-error method of the antenna design just described has been used for a long time. This is still a frequently utilised antenna design procedure, but it may not, obviously, be the optimal one. For example, in designing medium-wave arrays of vertical monopole antennas with a prescribed radiation pattern of the array in the horizontal plane, the procedure amounts to choosing one of the theoretical patterns available in antenna engineering handbooks (based on assumption of sinusoidal current distribution along the antennas) and then fulfilling the feeding conditions with which, theoretically, such a pattern is obtained. Experimental matching of the array elements to their respective feeders and the final experimental adjustment of the array follows, which is usually far from simple and, actually, may not result exactly in the pattern we wanted. As another example, we may design an Uda-Yagi array for a single frequency using available data, but no such

data can be found if we wish to design an Uda-Yagi antenna which can operate successfully at more than one frequency. Although experimental design in that case would be possible in principle, we would need at least some guidelines to make it both economical and feasible. These two examples indicate clearly that the classical antenna design, although it can be advantageously used in some cases, in many more cases is inconvenient or even virtually impossible.

With the advent of high-speed digital computers the design approach to many antenna structures changed radically. This trend started approximately between 1970 and 1975. Today, many antenna structures can be designed with such a high accuracy using the new, computer-aided design approach, that frequently an experimental model of the antenna resulting from the design, intended for possible corrections of theoretical results, is more a matter of tradition and scientific approach than of necessity.

This part of the monograph deals with computer-aided design of wire-antenna structures. Such a design may imply diverse procedures, but it is always based on a sequence of analyses of a more or less defined antenna structure with systematically perturbed parameters. This sequence is most often created automatically by the computer, although sometimes it might be advantageous to use the interactive process. It is terminated once an antenna is obtained which is considered to satisfy the desired requirements in "the best possible" manner. Thus, such a process creates, or synthesizes, an antenna with properties "as close as possible" to the desired properties. (We shall explain the meaning of the expressions "the best possible" and "as close as possible" as used in the antenna computer-aided design in the next section.) For this reason it is usual to refer to the computer-aided antenna design briefly as to the *antenna synthesis*. This chapter discusses the general principles of synthesis of wire-antenna structures, outlines some synthesis procedures and points out to possible general difficulties of the synthesis. More specific synthesis problems are then dealt with in the next two chapters.

7.2. GENERAL PRINCIPLES OF WIRE-ANTENNA SYNTHESIS

To synthesize a wire-antenna structure having certain desired properties, it is possible, in principle, to follow two procedures. The first procedure is that which is aimed at determining a unique solution, or a number of solutions, which satisfy certain conditions *exactly* (if such solutions exist). This approach is impractical for at least two reasons, even if solutions do exist. On the one hand, such solutions tend to be very unstable.[75,76] On the other hand, they may require quite impractical physical elements, e.g., negative inductances.[77]

The second procedure is based, essentially, on the engineering common sense: determine an antenna the properties of which are, if possible, so close to some desired properties that the solution can be accepted as the final solution. By appropriate constraints this approach can guarantee that the solution obtained be physically easily realizable (e.g., a cylindrical antenna with capacitive loadings only). It seems that, indeed, a meaningful synthesis method (in the engineering sense), which will *always* result in at least *some* realisable solution, can only be based on approaching a desired property (or a collection of properties) step by step, and not on requiring that it be reached exactly. We shall, therefore, follow in this monograph the second procedure, and by the term "antenna synthesis" we shall essentially imply any process which, on average, constantly improves the antenna properties (with respect to the desired properties) although, in principle, it may happen that the final result it reaches is rather far from the desired solution. The solution thus reached we shall term "the best possible solution" or "the solution as close as possible to the desired solution", although these expressions are not at all precise, since we shall see that the final solution often depends to a large extent on the initial conditions.

As formulated, the synthesis problem is, basically, a problem of nonlinear optimization. Therefore we construct a convenient real (usually positive definite or semidefinite) function which has a minimum when the desired antenna properties are reached (or, in some cases, when

the antenna properties are better than those desired). This function we shall refer to as the *optimization function*. Since the antenna properties depend on the antenna parameters, the optimization function is, essentially, a function of these parameters. We next use any convenient optimization method to minimize the optimization function.

Two preceding paragraphs define the main lines which the antenna synthesis must follow. However, there are many additional problems and dilemmas which have to be solved prior to starting a synthesis process. The following subsections deal briefly with some of them.

7.2.1. Possible optimization functions. Depending upon specific requirements on antennas which are synthesized, it is possible to construct many optimization functions. In this subsection we shall not present any specific optimization function - they will be introduced and justified in the next two chapters. Rather, we shall discuss some details relevant to these functions in general.

Once we know current distribution in an antenna, all the electrical quantities of interest, such as the antenna admittance, its radiation pattern, gain, efficiency (in the case of lossy structures), maximal electric field, etc., can be calculated relatively easily. Some of these quantities require a knowledge of current distribution along the whole antenna structure (e.g., the radiation pattern or efficiency), and some a knowledge of current intensity at a specific point along the antenna only (e.g., admittance or voltage across a lumped loading).

In one approach of the classical antenna synthesis, current distribution was sought which resulted in a desired radiation pattern. However, the more difficult part of the problem, that of *how* such a current distribution can be realized, was not considered. Also, in classical antenna synthesis, the problem of synthesizing an antenna having admittance close to a desired admittance was often not of interest, because it was assumed that it is always possible to match an antenna to the feeder by means of a matching network.

The antenna synthesis in the sense used in this monograph allows, however, the synthesis of wire antennas having *any* property (or a collec-

tion of properties) as close as possible to a desired value. For example, optimization functions can be constructed which result in the following antenna properties:

a) Antenna admittance as close as possible to a desired admittance, at a single frequency or at a number of frequencies.

b) Radiation pattern of an antenna or of an antenna array as close as possible to a desired pattern, at a single frequency or at a number of frequencies.

c) Antenna admittance and radiation pattern simultaneously as close as possible to some desired value, viz. some desired shape.

d) Antenna as broadband as possible in its admittance and/or radiation pattern.

e) Coupled antennas with minimal coupling.

In the next two chapters possible optimization functions corresponding to most of these cases will be described and utilized for wire-antenna synthesis.

Two additional general remarks might be added at this point. First, it is very important to understand that the range of properties of antennas of given dimensions is inherently limited. For example, a distributed resistive loading along a cylindrical antenna of given dimensions can result only in certain range of the antenna admittance and radiation pattern when the amount and distribution of the resistive loading are varied. As another example, by adding lumped capacitive loadings along a cylindrical antenna of given dimensions it can be made broadband with respect to its admittance only to certain extent. It is essential that the optimization function be constructed having in mind these limitations.

Second, if we wish to optimize simultaneously two or more antenna properties, it should be kept in mind that they might be to a lesser or larger extent contradictory. For example, to synthesize a loaded cylindrical antenna having a prescribed radiation pattern in the plane containing the antenna axis and simultaneously a prescribed admittance

is often not possible, except if a large tolerance in the radiation pattern and admittance is allowed. An insight into such situations should be obtained in any possible manner prior to constructing the optimization function and running the optimization program.

7.2.2. Possible optimization parameters. Any parameter characterizing an antenna in any sense can be varied in the optimization process in order to achieve desired antenna properties. We shall restrict here our considerations only to those antenna parameters which characterize its dimensions and its electrical properties. Thus, the optimization parameters may characterize the antenna shape, size, concentrated or distributed loadings, driving voltages of array elements, current distribution along the antenna, etc.

In principle, there is no limitation concerning the number of optimization parameters. For example, in the case of a loaded cylindrical antenna we may simultaneously vary its radius, length, positions of the loadings, their kind and their magnitudes. However, this is usually not done for three reasons. First, most often variations of some parameters have much more pronounced influence on the optimization function than variations of the rest. Second, any optimization parameter prolongs the optimization time considerably. Therefore optimization parameters with only a small influence on the antenna properties should be avoided. Finally, from the practical point of view only those parameters should be varied (i.e., should be taken as the optimization parameters) which in practice can be easily adjusted to any value which might be required by the result of the optimization process.

Variation of some antenna optimization parameters requires complete new solution of the equation for the antenna current distribution. For example, if we change the antenna length, the antenna diameter or the positions of the concentrated loadings in the case of a cylindrical antenna, the complete process of solution for the equation must be repeated, including the time-consuming integrations involved. In some instances, however, this is not necessary. For example, if we have lumped loadings at fixed positions along a wire antenna, no integrations need to be repeated if only magnitudes (and even the kind) of the

loadings are varied, and complete solutions for different values of the loadings are obtained with little more computational effort than that needed for solving again the basic linear system of equations. Such cases should always be considered as a possibility, at least at an initial stage of synthesis, because that can save a large amount of computing time. Several such examples will be presented in the following chapters.

7.3. OUTLINE OF SOME OPTIMIZATION METHODS

It is well-known that there is no best optimization method for all the problems of optimization. A variety of optimization methods are at our disposal for synthesis of wire-antenna structures, but some may be more convenient than the others. It is not possible, however, to say much about the effectiveness of an optimization method in a specific case by theoretical considerations alone. It seems that the only means to choose an optimization method for a problem at hand, like that of synthesis of a wire antenna, is to try how it works, to compare it with few other methods, and possibly to choose one of them on some rational basis. It should be pointed out, however, that if we need to perform the optimization relatively rarely, there is usually no need to try to find a faster optimization method if the one used gives satisfactory results.

An optimization method can be defined as a specific procedure for determining successive points in the parameter space in which the optimization function should be computed in order that a (usually local) minimum be reached. Only rarely the number of feasible points in the parameter space is finite, in which case we can make a complete search and find the global minimum. Most often the search is incomplete, and there is no guarantee that the global minimum is reached. Rather, possibly only a local minimum can be approached (with some prescribed accuracy).

All the optimization methods can roughly be divided into two groups: (1) those which use only the values of the optimization function itself for determining the next point of the process, and (2) those which use the gradient (i.e., partial derivatives) of the optimization function

for that purpose. The first are frequently referred to as the direct methods, and the second as the gradient methods. (It should be noted that in the case of antenna synthesis the optimization function is not an explicit function of the antenna parameters, and the derivatives of the optimization function must be computed numerically.) A special case which cannot be classified into these two groups is the random search, in which successive points are determined by the use of a random-number generator.

In our case the values of the optimization parameters are limited by practical possibilities. These constraints must be introduced into the optimization process, i.e., all the optimization methods used for wire-antenna synthesis are methods with constraints.

In any optimization procedure there exist two additional problems: that of the choice of the starting point for the process, and that of the decision on termination of the process. In order to expedite, or even to ensure convergence of the optimization procedure, the starting point should be located as closely as possible to a local minimum of the optimization function. This requires some prior knowledge about behaviour of the optimization function, which can be gained if some systematic data are available (or can be computed) of the properties of the antenna type considered. If such data are missing, it may be convenient to make a random search in the parameter space and to adopt the best point thus found as the starting point for a direct search or gradient optimization procedure.

The decision on termination of an optimization procedure depends both on the method used for optimization and on the goal of the antenna synthesis process. Basically, the procedure is terminated automatically if a minimum of the optimization function is presumably located with a sufficient accuracy (which depends upon our requirements). The decision can be thus based on testing increments of the parameters and/or of the optimization function in two successive iterations of the optimization procedure. In some cases, especially in early stages of the optimization, the interactive procedure might be desirable, whereby the optimization process can be directed or terminated according to the

designer's judgement.

This section is devoted to a very brief presentation of three optimization methods the authors used and found useful in synthesis of wire-antenna structures. Since the descriptions of the three methods given below are intended as a rough information only, the reader is referred to specialized literature for a more detailed treatment (see, for example, References 78 and 79).

7.3.1. Complete search method. The complete search method is one of the conceptually simplest optimization methods. Essentially, it consists in determining the optimization function at nodes of a (regular or irregular) multidimensional grid in the space of the optimization parameters and searching for the optimal solution among these.

A serious disadvantage of this method in the case of a large number of parameters is the need for computation of a large number of values of the optimization function. However, in some cases (e.g., antennas with concentrated loadings at fixed positions) evaluation of the optimization function can be greatly expedited if the optimization parameters are successively varied only one at a time. Thus, if the total number of parameters varied is small, the number of evaluations of the optimization function can be greatly increased without increasing the c.p.u. time required for the optimization. Therefore the complete search in these cases can be used efficiently.

This method can also be used with a coarse grid to obtain an idea where to start the optimization process, i.e., from which point in the multidimensional parameter space to trigger another, more convenient optimization process, which, however, cannot easily locate the position of, possibly, the global optimum.

7.3.2. A gradient method. The gradient methods are also known as the steepest-descent methods. The most rudimentary form of the method consists in adopting a starting point, determining the direction in the multidimensional parameter space at that point in which the optimization function decreases most rapidly, adopting a new starting point in that direction at a desired distance from the old starting point,

and repeating the process until a minimum of the optimization function is found. This amounts to calculating the components of the gradient of the optimization function, and then decreasing all the parameters by the corresponding gradient component multiplied by a suitable basic step "length". Let s be the basic step length, $F(x_1,x_2,\ldots,x_n)$ the optimization function ($x_1,x_2,\ldots,x_n$ are the optimization parameters) and $P_0(x_1^0,x_2^0,\ldots,x_n^0)$ the starting point in the parameter space. The components of grad F at P_0 are

$$\text{grad}_1^0 F = (\partial F/\partial x_1)^0, \ldots, \text{grad}_n^0 F = (\partial F/\partial x_n)^0 . \tag{7.1}$$

As in our case $\text{grad}_k^0 F$, k=1,2,...,n, cannot be determined analytically, we must calculate them approximately as $(\Delta F/\Delta x_k)^0$, k=1,2,...,n which requires at each point computation of (n+1) values of the optimization function. We then determine the next starting point as

$$x_k^1 = x_k^0 - s\cdot(\Delta F/\Delta x_k)^0 , \quad k=1,2,\ldots,n , \tag{7.2}$$

and repeat the procedure until the new value of F is larger than (or possibly equal to) the old value. Presumably, a local minimum of F is thus obtained.

The brief sketch of the well-known basic steepest-descent method was given here in order to point out some obvious difficulties in its application to our problems. (These difficulties are, actually, present in any application of the method and in most other optimization methods.) First, the process requires a relatively large number of evaluations of the optimization function. Second, the step length s has to be chosen appropriately, which can be done only if we already have a certain insight into the behaviour of the optimization function considered. Finally, the increments Δx_k for determining numerically the components of the gradient of the optimization function should be small, but large enough that the increment ΔF can be computed accurately, a problem the solution of which usually requires some prior numerical experiments.

Many improvements of this basic steepest-descent method are available. One of these is to follow the negative gradient at the starting

point as long as the optimization function decreases, and even to increase the basic step in the successive points along this line. The complete gradient is computed only when we reach a minimum along this straight line in the space of optimization parameters. This minimum can be located in various ways. In all the examples in later chapters which use this optimization method, this minimum was determined by quadratic interpolation based on the values of the optimization function at three successive points (which are nonequidistant) along the line. This procedure reduces the number of gradient evaluations considerably, and thus expedites the optimization process.

As most optimization methods, all gradient methods may end up in a local optimum, rather than in the desired global optimum in the domain of the optimization parameters considered. If the number of parameters is relatively large, it is virtually impossible to judge in any way whether the optimum found is the global optimum or not. The only procedure to check this seems to be the following. We adopt at random several starting points in the domain and repeat the optimization process. We can be fairly certain that the optimum is the global one if all the optimizations result in approximately the same optimum. However, it should be noted that, from the engineering point of view, we are usually not interested in the global optimum if the solution obtained can be considered satisfactory.

7.3.3. The simplex method. The term "simplex" is used as the name for a body in multidimensional space which is a generalization of the tetrahedron in three dimensions. The simplex optimization method computes the values of the optimization function at the vertices of a simplex in the parameter space, and on the bases of these values chooses a new, presumably smaller simplex within which an optimum should be situated. The simplex polyhedron rolls itself down towards the optimization function valley, elongates itself in the direction of the steepest fall of the function, and contracts itself near the minimum. The process is repeated until a simplex of sufficiently small size is obtained which locates an optimum with a desired accuracy. The authors used for optimization of some antenna structures the simplex optimiza-

tion algorithm as proposed by Nelder and Mead.[80] This algorithm is briefly described in Appendix 7.

It is fairly obvious that the simplex optimization method might, but also might not, be able to find the global optimum. This depends on both the initial simplex, and the way how it shrinks as the process progresses. The authors did find, however, that the simplex method, on average, required less time to reach an optimum than the gradient method.

7.4. CONCLUSIONS

This chapter summarized the basic ideas and procedures used by the authors in synthesis of wire-antenna structures. It was pointed out that many optimization functions can be constructed and that many antenna parameters can be used as the optimization parameters, but that only those parameters should be varied which can be realized in practice easily. Otherwise the antennas synthesized might be purely theoretical structures.

Concerning possible optimization methods, the three methods used by the authors were briefly explained and discussed. Except for the complete search method, the others cannot guarantee to find the global optimum of the optimization function in the domain of the optimization parameters considered. However, if the solution thus obtained is satisfactory from the engineering point of view, we are usually not interested whether a better solution does exist. In addition, from the engineering point of view, a relatively broad, stable optimum is obviously preferred to an optimum of the "deep-well" type in the parameter space, the latter solution being unstable in practical realizations. Therefore, even if in the optimization we miss such an optimum, this can be considered as positive rather than as negative.

The next two chapters present a relatively large number of examples of wire-antenna synthesis, in which the methods for antenna analysis presented earlier and the methods of synthesis outlined in this chapter are combined in the computer-aided antenna design.

CHAPTER 8
Optimization of Antenna Admittance

8.1. INTRODUCTION

If we consider an isolated wire antenna of relatively small electrical length or an array of such antennas, it is usually easy to roughly estimate their radiation pattern. This is possible because, at any frequency for which the antenna is electrically small, radiation pattern of one element is relatively independent of the antenna size and change in frequency, and the array pattern can be then determined using the classical array theory. However, the antenna admittance is a quantity which is very sensitive to variations in the antenna size and the operating frequency and can hardly be predicted without precise numerical analysis. It is, therefore, possible to vary certain parameters of an antenna and thus to obtain antennas having a broad range of values of admittance and simultaneously a relatively constant radiation pattern (or approximately known in the case of an array).

This chapter is devoted to examples of synthesis of wire antennas with admittance as close as possible to a desired admittance by varying various antenna parameters, one or several of them at a time. Examples of these parameters are distributed loadings, concentrated loadings, possible lumped loadings in the antenna excitation zone, and the antenna size and shape. It may be desired to optimize the antenna admittance at a single frequency, or in a certain frequency range. The latter is usually done if a broadband antenna to a lesser or larger extent is desired.

Optimization functions used in optimizations of wire-antenna admittance depend on the desired antenna properties. In most instances these functions are quite simple. However, the authors found that if an antenna broadband in its admittance is desired, a specific optimization function appears to be particularly convenient. We shall consider now that optimization function because it requires certain justifications and explanations. The other optimization functions which we shall use are fairly obvious, and will be introduced as needed.

The antenna admittance is optimized in order to match the antenna as closely as possible to its feeder. A measure of the level of the match can be described by various quantities. However, for at least three reasons to be explained below, the reflection coefficient at the antenna terminals, or a quantity closely related to it, appears to be a very convenient optimization function.[16]

Assume that the antenna is connected to a feeder of a real characteristic admittance Y_c. Let the maximal power which can be transmitted by the feeder (determined by the maximal admissible electric field in the feeder) in the case of a matched load be $(P_{max})_{Y=Y_c}$. It is well-known that if the load is not matched to the line, the maximal power which can be transmitted by the line is smaller than $(P_{max})_{Y=Y_c}$. If we denote the reflection coefficient by R,

$$R = \frac{Y_c - Y}{Y_c + Y} , \tag{8.1}$$

and its magnitude by $|R|$, the maximal power which can be transmitted by the line when not matched is given by

$$(P_{max})_{Y\neq Y_c} = (P_{max})_{Y=Y_c} \frac{1 - |R|}{1 + |R|} = \frac{(P_{max})_{Y=Y_c}}{\Gamma} , \tag{8.2}$$

where Γ is the voltage standing-wave ratio. Thus, the reflection coefficient R determines the maximal power which can be transmitted by the line. (This is, of course, important only in cases when the line is used at its full power-transmitting capacity, which is not always the case.)

The second important parameter depending directly on the reflection coefficient is the efficiency of power transfer to a nonmatched load. Provided that the line is lossless, i.e., that its characteristic admittance is real, the efficiency is given by

$$\eta = 1 - |R|^2 \ . \tag{8.3}$$

The third important quantity proportional to $|R|$, more precisely to $|R|^2$, is intermodulation noise due to feeder mismatch.[81] This is very important parameter if extreme sensitivity of a receiving system is desired, for example in radio surveillance systems.

For these reasons it seemed that a convenient quantity to be minimized when optimizing the antenna admittance is $|R|^2$, the square of the modulus of the reflection coefficient of the antenna with respect to a given feeder. Note that, for $Y \approx Y_c$, this is approximately equivalent to requiring that $|Y-Y_c|^2$ be minimal.

When optimizing the antenna admittance to be broadband, following the above reasoning it is logical to request that the integral

$$R_{eff}^2(f_1,f_2) = \frac{1}{f_2-f_1} \int_{f_1}^{f_2} |R(f)|^2 \, df \tag{8.4}$$

be minimal, where (f_2-f_1) is the frequency range. The quantity R_{eff} can be termed "the effective reflection coefficient". The integral in eqn.(8.4) can be evaluated only numerically. The simplest way of doing this is to approximate the integral by a finite sum,

$$R_{eff}^2(f_1,f_2) \simeq \frac{1}{n_f} \sum_{i=1}^{n_f} |R(f_i)|^2 \ , \tag{8.5}$$

where n_f is the adopted number of equidistant frequencies in the range (f_1,f_2). Note that computation of $R(f_i)$ is often time-consuming, because it requires evaluation of the antenna admittance. Therefore n_f should be adopted as small as possible.

According to eqns.(8.1) and (8.2), R_{eff} can be made smaller also by

varying Y_c, the characteristic admittance of the feeder. Although Y_c cannot be varied in a wide range (e.g., for commercial coaxial feeders between 50 Ω and 90 Ω), it is always possible to use broadband transformers to increase this range considerably. Therefore the admittance Y_c can be taken almost at will, except that it should be real, and can be considered as another variable for obtaining a better match. This admittance we shall term "the reference admittance" and denote by Y_{cref}.

There always exists an optimal reference admittance which gives the smallest effective reflection coefficient R_{eff}. If Y in the frequency range considered does not differ from Y_c considerably, this optimal reference admittance can be determined as follows. Note first that

$$\frac{x-1}{x+1} \simeq \frac{1}{2} \ln x \quad \text{for} \quad x \simeq 1 \ , \tag{8.6}$$

because the first two terms of the Taylor series at x=1 of the two functions are equal. We can thus approximate R in eqn.(8.1) by

$$R \simeq \frac{1}{2} \ln \frac{Y_c}{Y} = \frac{1}{2} \ln \frac{Y_c}{|Y|} - j \frac{1}{2} \arg Y \ , \quad \text{if} \quad Y \simeq Y_c \tag{8.7}$$

(we assume Y_c to be real). Introducing this approximation for R into equation (8.4), we obtain

$$R_{eff}^2(f_1,f_2) \simeq \frac{1}{4(f_2-f_1)} \int_{f_1}^{f_2} \left[\ln^2 \frac{Y_c}{|Y|} + (\arg Y)^2 \right] df \ . \tag{8.8}$$

Requiring now that $d(R_{eff}^2)/dY_c=0$, we get that the minimum of the effective reflection coefficient is obtained if

$$\ln Y_c \simeq \frac{1}{f_2-f_1} \int_{f_1}^{f_2} \ln |Y| \, df \ . \tag{8.9}$$

If the integral in eqn.(8.9) is approximated by a sum over n_f frequencies, as we approximated R_{eff}^2 in eqn.(8.5), we obtain that the optimal reference admittance is given by the geometric mean of the values of $|Y|$ at the n_f frequencies, i.e.,

$$(Y_{cref})_{opt} \simeq (|Y_1| \cdot |Y_2| \cdot \ldots \cdot |Y_{n_f}|)^{1/n_f} . \tag{8.10}$$

This optimal value of the reference admittance will be used in several examples of optimization later in this chapter. Of course, in order to obtain the smallest possible effective reflection coefficient, we need to require also that the arguments of Y_i, $i=1,2,\ldots,n_f$, be as close to zero as possible. If these arguments are close to zero, $(Y_{cref})_{opt}$ can be approximated by the geometric mean of the antenna conductances, $G_i = \mathrm{Re}(Y_i)$, $i=1,2,\ldots,n_f$. Another approximation can be obtained when the admittances Y_i are close to each other replacing the geometric by the arithmetic mean value.

8.2. OPTIMIZATION OF ANTENNA ADMITTANCE BY VARYING DISTRIBUTED ANTENNA LOADINGS[76]

In this section a method is presented for determining continuous impedance loading along a cylindrical antenna of given dimensions, which approximately results in certain desired input characteristics of the antenna. The essence of the method consists in assuming a dependence of the impedance loading on the length along the antenna, in the form of power series with unknown coefficients, and determining these coefficients by minimizing a convenient optimization function involving the antenna admittance. The method can easily be extended to arbitrary wire-antenna structures.

Although a continuously varying loading along an antenna is relatively difficult to realize, the method is of considerable practical value. On the one hand, continuous loading can efficiently be approximated by either step-like loading, or by concentrated loadings. On the other hand, the results obtained by the present simple method can be used as a starting point for optimization of antennas with a large number of concentrated loadings, which tends both to be very time-consuming and to end up in an undesired, local optimum if the initial values of the loadings are not reasonably close to the optimal values.

Consider a thin symmetrical cylindrical dipole of length 2h and ra-

dius a (with h>>a), driven at the center by a generator of voltage V and angular frequency ω. Let the dipole be situated in a lossless homogeneous medium of parameters ε and μ, and let the internal impedance per unit length along the dipole be $Z'(z)$, which we assume to be an arbitrary, but differentiable function of the coordinate z for $0<z<h$. The current distribution $I(z)$ along the dipole may be then determined from the integral equation obtained by combining eqns.(2.30) and (4.8), which has the form

$$\int_{-h}^{h} I(z')\, g(r)\, dz' + \frac{k}{j\omega\mu} \int_{0}^{z} Z'(z')\, I(z') \sin k(z-z')\, dz' + C_1 \cos kz = \\ = F_g(z) \,, \qquad (8.11)$$

$F_g(z)$ representing the adopted model of the generator driving the dipole. We can next eliminate the constant C_1 by requiring that the equation be satisfied at z=0.

To solve eqn.(8.11) for $I(z)$, assume that $I(z)$ can be approximated by a series with complex coefficients I_i to be determined,

$$I(z) = \sum_{i=1}^{n} I_i\, f_i(z) \,, \qquad (8.12)$$

with

$$\sum_{i=1}^{n} I_i\, f_i(h) = 0 \,. \qquad (8.13)$$

Let us assume that $Z'(z)$ can also be represented in a similar way as

$$Z'(z) = \sum_{j=1}^{m} Z_j\, g_j(z) \,. \qquad (8.14)$$

With eqns.(8.12)-(8.14) the integral equation (8.11) for current takes the following approximate form:

$$\sum_{i=1}^{n} I_i\, A_i(z) + \sum_{i=1}^{n} \sum_{j=1}^{m} I_i\, Z_j\, B_{ij}(z) = D(z) \,. \qquad (8.15)$$

Assuming that $f_n(h)\neq 0$, using eqn.(8.13) we can eliminate the coefficient I_n, to obtain

$$\sum_{i=1}^{n-1} I_i A'_i(z) + \sum_{i=1}^{n-1}\sum_{j=1}^{m} I_i Z_j B'_{ij}(z) = D(z) , \qquad (8.16)$$

where $A'_i(z)$ and $B'_{ij}(z)$ are simple expressions involving $A_i(z)$ and $A_n(z)$, namely $B_{ij}(z)$ and $B_{nj}(z)$, respectively.

To determine the coefficients I_i, i=1,2,...,(n-1), the point-matching method may be used. This results in a system of (n-1) linear equations in (n-1) unknowns I_i, i=1,2,...,(n-1), of the form

$$\sum_{i=1}^{n-1} \left[A'_i(z_k) + \sum_{j=1}^{m} Z_j B'_{ij}(z_k)\right] I_i = D(z_k) , \quad k=1,2,...,(n-1) . \qquad (8.17)$$

Solutions of the last system of equations can be considered as functions of the m parameters Z_j. We can construct an optimization function which includes the current-distribution parameters I_i, and minimize it by varying the values of the impedance parameters Z_j. Note that the square matrix $[A'_{ik}]$ and the 3-dimensional matrix $[B'_{ijk}]$ in eqn.(8.17) are independent of the values of Z_j [A'_{ik} and B'_{ijk} stand for $A'_i(z_k)$ and $B'_{ij}(z_k)$, respectively]. Therefore, for a given problem, these matrices can be computed once, and their values used in all subsequent solutions of eqns.(8.17). This is extremely important, because just evaluation of these matrices requires the larger part of the computing time necessary for solving eqns.(8.17). During an optimization process these equations are solved many times, and therefore any saving in the computing time necessary for a single step becomes worthwhile.

Finally, it is usually necessary to introduce some constraints on the values of Z_j, imposed by practical possibilities and the desired type of the loading.

We shall adopt that

$$f_i(z) = |z/h|^{i-1} , \qquad (8.18)$$

and

$$g_j(z) = |z/h|^{j-1} . \tag{8.19}$$

In that case the integrals $A_i(z_k)$ can be integrated numerically, and thus all the elements of the $[A'_{ik}]$ matrix determined. The integrals $B_{ij}(z_k)$ with the adopted $g_j(z)$ can be evaluated explicitly using a recurrence formula, and so the elements of the $[B'_{ijk}]$ matrix evaluated easily.

8.2.1. Some general examples of optimization. As already indicated, it is possible to optimize an antenna with impedance loading in many ways. In this subsection we shall mention as examples a few of these, for which numerical results will be presented in Subsection 8.2.3.

Perhaps the simplest case is that of requiring that the admittance, conductance or susceptance of an antenna of given dimensions and at a given frequency be as close as possible to a given value. For example, if we wish the admittance of the antenna to be as close as possible to a desired admittance Y_0, we construct the optimization process which will determine the loading along the antenna so that the expression

$$F(Z_1,Z_2,\ldots,Z_m) = |I_1/V - Y_0| \tag{8.20}$$

be minimal. (V represents the voltage of the generator, and the antenna admittance equals I_1/V.) Similarly, if we wish the susceptance to be as close as possible to zero, we may minimize $|\mathrm{Im}(I_1)|$.

Next, we can require, for example, that the current wave along an electrically long antenna of given dimensions and at a given frequency be as close as possible to a decaying travelling wave from some $h=h_1$ to $z=h$. A possible expression to be minimized in this case is

$$F(Z_1,\ldots,Z_m) = \frac{1}{V^2}\int_{h_1}^{h} \left\{ \left| I(h_1) \right| \frac{(1-z/h)^p}{(1-h_1/h)^p} - \left| \sum_{i=1}^{n} I_i (z/h)^{i-1} \right| \right\}^2 dz . \tag{8.21}$$

Here, $p \geq 1$. Of course, instead of the desired amplitude function of the form $(1-z/h)^p$ it is possible to use any other that decreases smoothly from the value $|I(h_1)|$ at $z=h_1$ to zero at $z=h$. Such an antenna will by necessity be broadband to a certain extent both in the admittance

and in the radiation pattern, because the above requirement minimizes, essentially, the waves reflected from the antenna ends.

A truly broadband antenna in either admittance or in radiation pattern, or in both, can be synthesized by the following optimization process. We first compute the $[A'_{ik}]$ and $[B'_{ijk}]$ matrices at a number n_f of frequencies in the desired frequency range. The function to be optimized must now include values of the admittance or a measure of the shape of the radiation pattern at all of these frequencies. For example, we may wish to minimize the expression

$$F(Z_1,\ldots,Z_m;f_1,\ldots,f_{n_f}) = \sum_{k=1}^{n_f} |I_1(f_k)/V - Y_{cref}|^2 , \tag{8.22}$$

where Y_{cref} is the desired reference admittance in the frequency range considered.

These few cases indicate how the function to be minimized can be constructed, but obviously they do not exhaust the possibilities for optimization of cylindrical antennas with continuous impedance loading.

8.2.2. Some remarks on loaded cylindrical antenna optimization. A cylindrical antenna of given dimensions can have only a restricted range of properties. For example, it is clear that we cannot have a cylindrical antenna with a maximum in the radiation pattern in the direction of the antenna axis, or an antenna with a negative value of conductance. However, very often we are not able to tell in advance whether we are requiring an antenna property (or a collection of properties) which can be closely approximated. For example, is it at all possible to have a thin cylindrical antenna with the main beam at an angle $\theta=45^o$ with respect to the z-axis and simultaneously with an admittance close to $Y_0=(4+j0)$ mS? Unfortunately, it does not seem possible to answer such questions in any simple manner, but by the method described above we can always find how closely the desired properties can be approached.

Whichever initial values of the Z_j-parameters we adopt to reach a certain solution, no method seems to be available to check whether it

is the best one. Fortunately, this is unimportant, in as far as the obtained solution satisfies the desired requirements. Also, as mentioned in Section 7.4, a minimum of the optimization function at the bottom of a deep, narrow well in a multidimensional space does not represent a desirable engineering solution. Such a solution is by necessity very sensitive to a change of parameters, i.e., it is unstable. Therefore for the present purpose any simple optimization method capable of locating a satisfactory minimum of the optimization function suffices.

The results in the following subsection were obtained by either the plain or the modified steepest descent method, briefly explained in Subsection 7.3.2. In all the cases the gradient was determined by varying the coefficients for $|\Delta Z_j|=10$ Ω/m. It was found that this represented a safe minimal increment of the coefficients to ensure accurate gradient computation when working with about 7 decimal digits. The step size $|\Delta Z_j|$ in Z_j was adopted to be 100 Ω/m if not stated otherwise.

8.2.3. Numerical examples. Although any type of generator representation can be used, all the numerical examples presented below were obtained with the delta-function generator. This appeared to be the simplest and sufficiently accurate generator representation for the present purpose of checking the method of synthesis.

Probably the simplest case of cylindrical antenna synthesis is that of determining the loading along an antenna of given dimensions which ensures that, at a given frequency, the antenna admittance be as close as possible to a desired value. From the practical point of view this is not of much interest, but it is useful as a means of comparing the theory with the experimental evidence and for estimating the convergence of the optimization process in a simple case.

An antenna was considered with h=11.44 cm and a=0.32 cm at a frequency f=667 MHz. When the antenna is loaded with a constant resistive loading $Z'(z)=700$ Ω/m, it is found theoretically[49] that the admittance of the antenna is $Y_0=(5.356 + j0.030)$ mS. In order to estimate the convergence of the process, the values of all the Z_j-parameters were

set to zero, and a search was made by the plain steepest descent method for real Z_j such that $|I_1/V-Y_0| \leq 0.1$ mS. The values of the Z_j-parameters converged very rapidly for all the values of m considered (m=1,2,...,6). For example, for m=1 after only 3 iterations it was found that $Z'(z)=$ 683 Ω/m; for m=2 after 10 iterations the result was

$$Z'(z) = 616 + 190\,(z/h)\ \Omega/m\,, \tag{8.23}$$

and for m=6 the optimization after 20 iterations resulted in

$$Z'(z) = 611 + 160\,(z/h) + 67\,(z/h)^2 + 35\,(z/h)^3 + 21\,(z/h)^4 + 13\,(z/h)^5\ \Omega/m\,. \tag{8.24}$$

A much more important practical problem of optimization is to find the loading which ensures a travelling current wave along the antenna. As mentioned, in this way an antenna which is to some extent broadband should be obtained automatically.

First an antenna was considered of half-length h=50 cm and radius a=0.3175 cm. A resistive loading was searched for such that the expression given in eqn.(8.21) with p=1 and h_1=0.25 h, be minimal at a frequency f=450 MHz. It has been shown both theoretically[51] and experimentally that if this antenna is loaded with a resistive loading of the form $Z'(z)=Z_0/(1-z/h)$, where Z_0 is a certain real constant, a travelling-wave antenna is obtained with I(z) proportional approximately to (1-z/h). In this example comparison was made between the results obtained by the present theory with those obtained theoretically by Wu and King[51] and verified experimentally by Shen.[41]

It was reasonable to assume that for a travelling-wave antenna the loading should increase towards the antenna ends. Arbitrarily, the initial values of the Z_j-parameters were adopted to be Z_1=1000 Ω/m, Z_2=2000 Ω/m, etc. With n=8 and m=4, using the second mentioned optimization method, after 30 gradient determinations with step size $|\Delta Z_j|=$ 100 Ω/m, then 25 gradient determinations with $|\Delta Z_j|$=50 Ω/m, and finally 25 gradient determinations with $|\Delta Z_j|$=20 Ω/m, the optimal loading was found to be

$$Z'(z) = 492 - 509\,(z/h) + 2749\,(z/h)^2 + 5017\,(z/h)^3\ \Omega/m\,. \tag{8.25}$$

For this Z'(z) the optimization function given in eqn.(8.21) was less than 0.0062 $(mA/V)^2 \cdot m$. Current distribution in this case is shown in Fig.8.1. The solution is quite close to that proposed by Wu and King and obtained experimentally by Shen (see Fig.4.3).

The two previous examples can be considered as a proof that the proposed optimization method yields results which are in agreement with available experimental results. The two following examples are illustrative numerical examples for which, unfortunately, experimental data do not exist.

It was interesting to discover whether a travelling-wave antenna can also be obtained with tapered capacitive loading. Arbitrarily, an antenna with h=15 cm and a=0.3 cm was considered, and the aim was to synthesize a capacitive loading which will result in a travelling current wave of the form given in eqn.(8.21), with p=1 and h_1=0.25 h, at a frequency f=1600 MHz. The fourth-degree polynomial approximation for current (n=5) and the third-degree polynomial for loading distribution (m=4) were adopted. The initial values of all the four parameters Z_j at 1 GHz were taken to be -j3000 Ω/m. After 17 gradient determinations

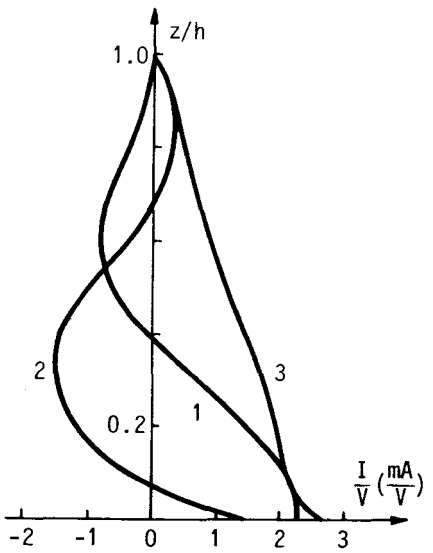

FIG.8.1. Current distribution along optimal travelling-wave cylindrical dipole antenna with resistive loading given in eqn.(8.25); a=0.3175 cm, h=50 cm, f=450 MHz, n=8, m=4, (1) real part, (2) imaginary part, (3) magnitude. (Ref.76)

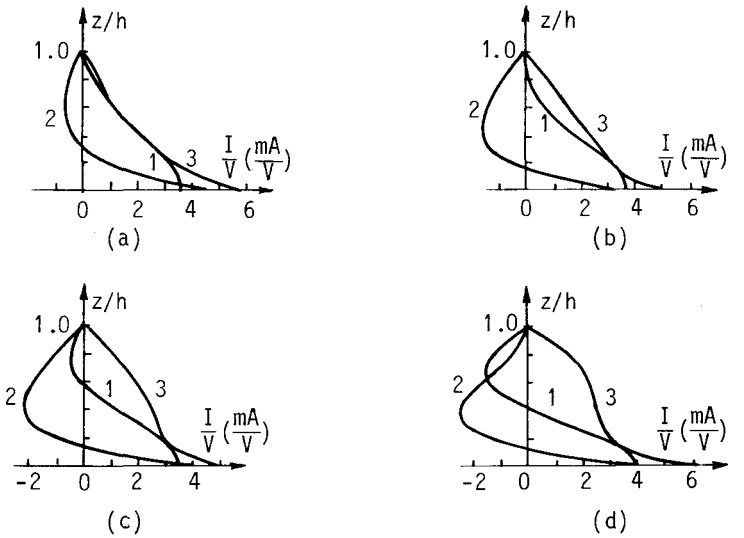

FIG.8.2. Current distribution along capacitively loaded cylindrical dipole antenna with loading given in eqn.(8.26), which results in travelling current wave at 1.6 GHz; a=0.3 cm, h=15 cm, n=5, m=4; (a) f=1.4 GHz, (b) f=1.6 GHz, (c) f=1.8 GHz, (d) f=2.0 GHz; (1) real part, (2) imaginary part, (3) magnitude. (Ref.76)

it was found with the modified steepest descent method that the expression given by eqn.(8.21) reduces to less than 0.006 $(mA/V)^2 \cdot m$, with

$$Z'(z) = -\frac{j}{f_{GHz}} \left[4894 + 4093(z/h) + 3696(z/h)^2 + 3465(z/h)^3\right] \ \Omega/m \,. \quad (8.26)$$

Current distributions along the antenna at f=1.4, 1.6, 1.8 and 2.0 GHz are shown in Fig.8.2, and variation of the antenna conductance and susceptance with frequency in Fig.8.3. A relatively good broadband antenna in admittance is obtained, and at 1.4 GHz and 1.6 GHz there seems to be only a small reflected wave from the antenna end.

As the final example, consider a capacitively loaded antenna of the same dimensions as in the preceding example, and let us determine the capacitive loading which minimizes the expression in eqn.(8.22) at frequencies f_1=1.4 GHz, f_2=1.6 GHz and f_3=1.8 GHz (i.e., n_f=3), with Y_{cref} in eqn.(8.22) given by

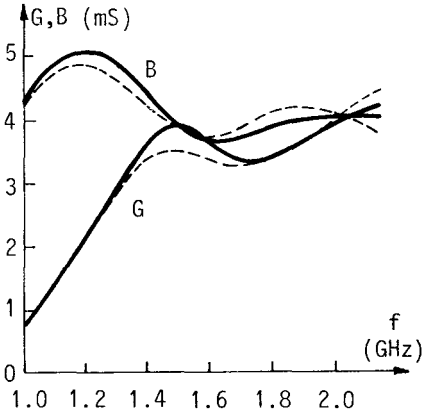

FIG.8.3. Dependence of conductance (G) and susceptance (B) of optimal capacitively loaded dipole antenna on frequency; a=0.3 cm, h=15 cm, n=5, m=4; ——— optimal travelling-wave antenna at 1.6 GHz with loading as in eqn.(8.26) and — — — optimal broadband antenna described in the text with loading as in eqn.(8.28). (Ref.76)

$$Y_{cref} = \frac{1}{n_f} \sum_{k=1}^{n_f} I_1(f_k)/V \ . \qquad (8.27)$$

By the modified steepest descent method, after 10 gradient searches it was found that with

$$Z'(z) = -\frac{j}{f_{GHz}}\left[5205 + 2535(z/h) + 2430(z/h)^2 + 2530(z/h)^3\right] \ \Omega/m \qquad (8.28)$$

the expression in eqn.(8.22) is reduced to less than 0.2 $(mS)^2$. Dependence of real and imaginary parts of the antenna admittance for this loading is shown in Fig.8.3 in dashed lines. We note considerable similarity of the G and B curves, those corresponding to the present example being somewhat flatter in the range of optimization (1.4-1.8 GHz), as expected.

8.3. SYNTHESIS OF PARALLEL LOADED CYLINDRICAL ANTENNAS WITH MINIMAL COUPLING[82,83]

If we consider an array of wire antennas, there is always certain coupling between the elements of the array. For a pair of elements, the closer their spacing, the stronger is the coupling. The elements can-

not be widely separated, however, for two reasons. On the one side, this would increase the dimensions of the array, and on the other side radiating properties of arrays with widely spaced elements most often are not suitable, because radiation patterns of such arrays have several beams. Therefore, coupling between elements of antenna arrays always exists in practice.

Because of the coupling, properties of individual elements are modified, with respect to both the behaviour of the elements as two-terminal networks, and to their radiation characteristics. In the classical array theory the coupling is neglected, which results in a very simple array analysis and synthesis. It turns out, however, that coupling cannot be neglected if a more precise analysis of an array is desired. For example, in the case of large periodic arrays the properties of all array elements except those quite close to the array edges are practically the same in spite of coupling, because in usual operating conditions of the array all such elements are situated in a very similar "electrical environment", but in determining these properties coupling cannot be neglected. In the case of smaller or aperiodic arrays properties of all their elements are different due to different influence on them of mutual coupling.

It seems that no attempt has been made to reduce coupling between elements of an antenna array by a convenient construction of the elements. This section is aimed at demonstrating that in the case of antenna arrays consisting of parallel, nonstaggered cylindrical elements coupling can be substantially reduced by appropriate impedance loading along the elements. This particular distribution of the loading can be determined by an optimization procedure, in which the loading along the antenna is varied until coupling between the elements as a function of the distance between them or of frequency, or of both quantities in a certain range, becomes minimal. As an example, two parallel nonstaggered resistive antennas are considered. It is shown numerically and verified experimentally that by means of the proposed method coupling between the antennas can be practically eliminated for distances between the antenna axes larger than about 0.2 wavelengths

and for a frequency range wider than 2:1. Antenna arrays consisting of such elements can be driven as if the elements were isolated, and the radiation properties of the array determined with relatively high accuracy according to the simple classical array theory, in which coupling between the array elements is neglected. The authors anticipate application of such and similar elements with minimal coupling for antenna arrays with a small number of elements, for aperiodic arrays in which the geometry of the array and/or frequency need to be varied, and for space-periodic arrays with elements in nonuniform electrical environments.

8.3.1. Outline of the method. Consider two identical parallel nonstaggered cylindrical antennas 1 and 2, of length 2h, radius a (a<<h) and distance between their axes b. Let the dipoles, for simplicity, be driven by ideal voltage delta-function generators of angular frequency ω and voltages V_1 and V_2, respectively. Let the z-axis of a coordinate system coincide with the axis of dipole no.1, and let the origin coincide with the dipole center, as shown in Fig.8.4. Finally, assume that the dipoles are situated in a homogeneous lossless medium and that the impedance per unit length along the dipoles, Z'(z), is a continuous, differentiable and even function of the coordinate z.

The system being linear, current distributions along the dipoles for

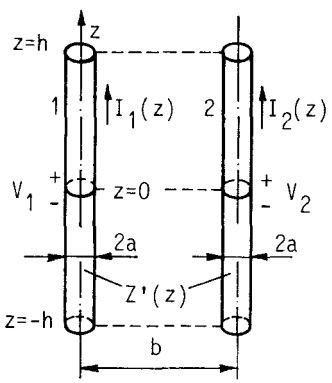

FIG.8.4. Two parallel symmetrical nonstaggered dipoles with continuous impedance loading.

arbitrary driving voltages V_1 and V_2 are given by

$$I_1(z) = V_1 Y_s(z) + V_2 Y_m(z) , \tag{8.29}$$

$$I_2(z) = V_1 Y_m(z) + V_2 Y_s(z) . \tag{8.30}$$

If $V_1=V_2=V_s$ (symmetric excitation), then $I_1(z) = I_2(z) = I_s(z)$, and if $V_2=-V_1=-V_a$ (antisymmetric excitation), then $I_2(z)=-I_1(z)=-I_a(z)$. The functions $Y_s(z)$ and $Y_m(z)$ can thus be expressed as

$$Y_s(z) = \frac{1}{2}\left[\frac{I_s(z)}{V_s} + \frac{I_a(z)}{V_a}\right] , \tag{8.31}$$

$$Y_m(z) = \frac{1}{2}\left[\frac{I_s(z)}{V_s} - \frac{I_a(z)}{V_a}\right] . \tag{8.32}$$

Therefore current distribution along the two antennas corresponding to any driving voltages V_1 and V_2 can be calculated if symmetric and antisymmetric current distributions are known. Note that the self and mutual admittances of the dipoles, Y_s and Y_m, are simply equal to $Y_s(0)$ and $Y_m(0)$, respectively.

Symmetric and antisymmetric current distribution along the antennas can easily be calculated by solving one of several existing integral equations. If we consider the Hallén-type equation, it is only necessary to substitute g(r) in eqn.(8.11) by

$$G^{(p)}(z,z') = g(r_s) + (-1)^{p+1} g(r_m) , \quad p=1,2 , \tag{8.33}$$

where

$$r_s = \left[(z-z')^2 + a^2\right]^{\frac{1}{2}} , \quad r_m = \left[(z-z')^2 + b^2\right]^{\frac{1}{2}} , \tag{8.34}$$

in order to obtain the integral equation from which the symmetric, viz. the antisymmetric current distribution can be calculated. The case p=1 corresponds to the symmetric, and p=2 to the antisymmetric driving conditions.

Solutions of these integral equations can be obtained in the same manner as those of eqn.(8.11) in the preceding section. As before,

these solutions can be considered as functions of the impedance parameters Z_j, j=1,2,...,m. Among these solutions we can search for those which correspond to the minimal coupling between the antennas. As the mutual admittance Y_m (or Y_{12} as is labelled frequently) of the antennas is given by

$$Y_m = \frac{1}{2}[Y^{(1)} - Y^{(2)}] , \tag{8.35}$$

where

$$Y^{(p)} = \frac{1}{V} \sum_{i=1}^{n} I_i^{(p)} f_i(0) , \quad p=1,2 , \tag{8.36}$$

the coefficients $I_i^{(p)}$ should be determined in such a way that a convenient real function $F(Y_m)$ be minimal.

In this manner the problem of determining a convenient loading along the antennas is reduced again to the problem of nonlinear optimization. The optimization function $F(Y_m)$ can be formed in many ways. Several possible forms of the optimization function $F(Y_m)$ for the case of minimization of coupling between the two antennas are the following:

a) $F_1(Y_m) = |Y_m|$, in which case it is required that the magnitude of the mutual admittance be as small as possible;

b) $F_2(Y_{m1},\ldots,Y_{mN}) = (|Y_{m1}| + \ldots + |Y_{mN}|)/N$, in which case it is required that the mean value of the magnitudes of mutual admittances in a certain range (in the frequency domain, space domain, or both at the same time) be as small as possible;

c) $F_3(Y_{m1},\ldots,Y_{mN}) = \max(|Y_{m1}|,\ldots,|Y_{mN}|)$, in which case it is required that the mutual admittance of largest magnitude in a certain range (in frequency domain, space domain or in both at the same time) be as small as possible;

d) $F_4(Y_{m1},\ldots,Y_{mN}) = \max(|Y_{m1}/Y_{\infty 1}|,\ldots,|Y_{mN}/Y_{\infty N}|)$, where $Y_{\infty k}$ denotes the self-admittance of such isolated antenna, in which case it is required that the mutual admittance of the largest magnitude in a certain range (in frequency domain, space domain or in both at the same time), with respect to the admittance of the antenna when isolated, be as

small as possible.

8.3.2. Resistive cylindrical antennas with minimal coupling. As an example of the method, distribution of the loading was determined along two thin cylindrical resistive antennas, i.e., antennas for which $Z'(z)=R'(z)+j0$, which ensures that the mutual admittance between the antennas be minimal. The function $F_4(Y_{m1},\ldots,Y_{mN})$ was adopted as the optimization function, in which Y_{mi}, $i=1,2,\ldots,N$, were values of the mutual admittance for different distances between the antennas. For determining the local minimum of the optimization function the modified method of steepest descent was used. Current and resistance distribution functions were adopted to be polynomials, as in the preceding section.

The antennas considered were of dimensions a=0.3 cm and h=15 cm, at a frequency f=1600 MHz. During the optimization process two natural tendencies were observed:

a) If the loading was assumed in the form

$$R'(z) = R_0 + R_1x + R_2x^2 + \ldots , \quad x=|z/h| , \tag{8.37}$$

minimization of coupling led to increasingly larger values of the first term, R_0. This could be expected, since in that case current intensities entering the expression (8.35) for mutual admittance tend to zero, so that Y_m tend also to zero.

b) If the loading was assumed in the form

$$R'(z) = R_1x + R_2x^2 + \ldots , \quad x=|z/h| , \tag{8.38}$$

there was a tendency during the optimization process towards negative resistance values $[R'(z)<0]$. This could also be expected, since by active loading it is possible to cancel the influence of one antenna on the other.

In order to eliminate these two tendencies, constraints were introduced into the computer program in values of the loading $R'(z)$. On the one side, it was requested that the loading $R'(z)$ at all points be smaller than a certain maximal loading. On the other side, it was re-

quested that the loading be passive for all z, by stipulating that $R'(z)>0$.

Three out of several results obtained by the optimization process with different polynomials representing the distribution of the loading are the following (as before, x stands for $|z/h|$):

$$R_1'(x) = 2777 + 1172\,x + 2147\,x^2 + 4162\,x^3 \quad \Omega/m\,, \tag{8.39}$$

$$R_2'(x) = 4000\,x + 6000\,x^3 + 7000\,x^4 \quad \Omega/m\,, \tag{8.40}$$

$$R_3'(x) = 1515\,x^2 + 3865\,x^3 + 6000\,x^4 + 8056\,x^5 \quad \Omega/m\,. \tag{8.41}$$

Although it is difficult to realize in practice resistive loading varying continuously along the antenna, it can be approximated either by a stepwise function (as was done in the case considered), or by a certain number of lumped loadings.

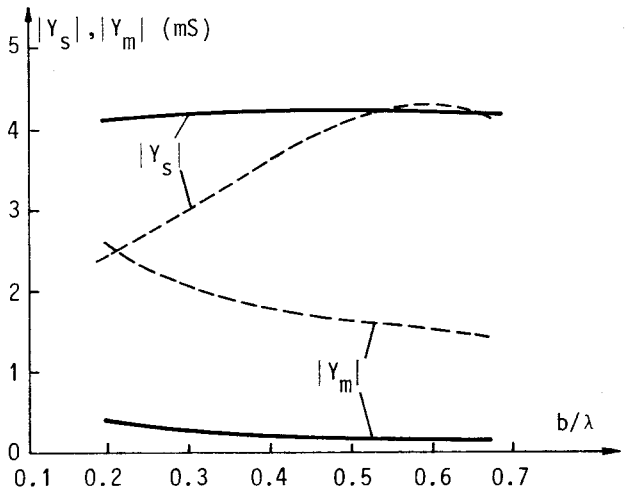

FIG.8.5. Magnitude of self and mutual admittance of two identical nonstaggered cylindrical dipoles versus normalized distance between their axes; a=0.3 cm, h=15 cm, f=1.6 GHz; ——— optimally loaded antenna as in eqn.(8.39); — — — unloaded antenna of the same size.

Fig.8.5 shows the magnitudes of self and mutual admittances for antennas with the loading as in eqn.(8.39), versus the distance between the antenna axes. For comparison, shown in the figure also are magnitudes of self and mutual admittances of unloaded antennas of the same size. In this case it is found that efficiency of the loaded antennas, defined by eqn.(5.11), is about 74 per cent. With some other distributions of the loading this efficiency, which is quite satisfactory for most purposes, can even be improved.

Distribution of current along such loaded antennas varies very little if driving conditions of the dipoles are changed from symmetric to antisymmetric, and it is almost identical with current distribution which would exist along an isolated antenna (i.e., if $b\to\infty$). As an example, Fig.8.6 shows real and imaginary parts of currents corresponding to symmetric and antisymmetric cases for the optimally loaded antenna with

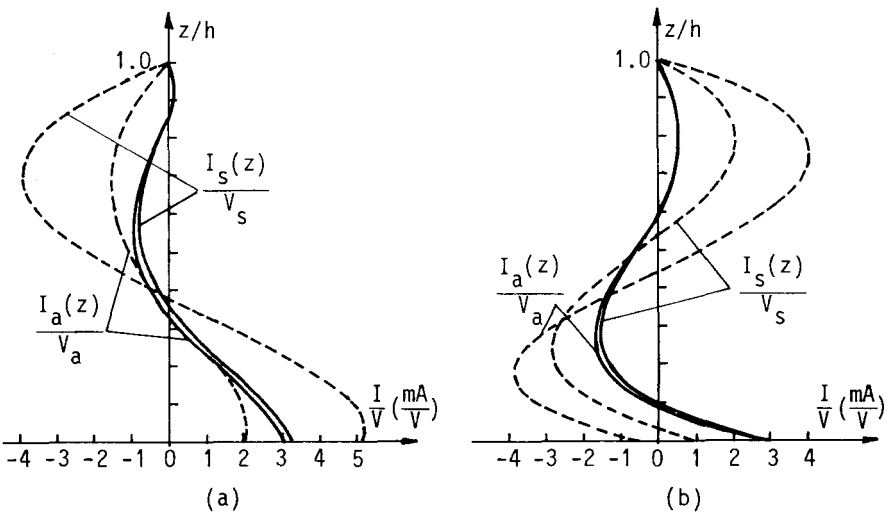

FIG.8.6. Symmetric and antisymmetric current distribution along optimal resistive antennas with loading as in eqn.(8.39) and along unloaded dipoles of the same size for distance between the dipoles b= 0.4λ; (a) real part, (b) imaginary part; ——— loaded antennas, — — — unloaded antennas.

loading as in eqn.(8.39), for distance between the dipole axes b=0.4λ. For comparison, shown also in the figure are analogous cases for unloaded antennas. The fourth-degree polynomial approximation for current along the antennas was used.

Shown in Fig.8.7 are magnitudes of self and mutual admittances of optimally loaded and of unloaded antennas versus frequency, for a distance between the antenna axes b=0.4λ. Important property of loaded antennas optimized for minimal coupling is seen clearly: coupling between such antennas is quite small in a wide frequency range, which is larger than 2:1 in the case shown in the figure.

According to eqns.(8.30) and (8.32), if only dipole no.1 is driven and dipole no.2 is short-circuited ($V_2=0$), then

$$I_2(z)|_{V_2=0} = \frac{1}{2}[I_s(z) - I_a(z)] , \tag{8.42}$$

for $V_1=V_s=V_a$. This indicates that magnitude of current in the short-circuited parasite can be a measure of coupling between the two antennas. This conclusion was used for checking theoretical results in a

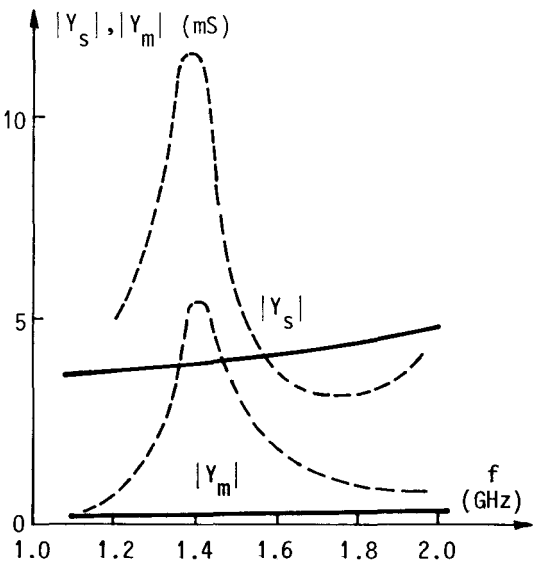

FIG.8.7. Magnitudes of self and mutual admittances versus frequency of two parallel coupled dipoles; a=0.3 cm, h=15 cm, b=0.4λ; ——— dipoles with loading as in eqn.(8.39), – – – unloaded dipoles.

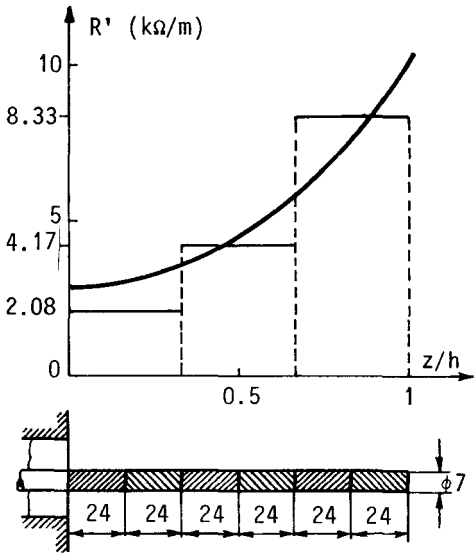

FIG.8.8. Synthesized optimal loading and stepwise approximation of the loading. The model was made in the form of a row of resistors. Dimensions are in millimeters. Note a slight difference in size of the experimental model when compared with the theoretical.

simple manner.

The optimally loaded cylindrical antenna with loading as in eqn. (8.39) was first approximated by an antenna with stepwise loading, as sketched in Fig.8.8, and its properties then checked theoretically. After concluding that the antennas with stepwise loading have properties which are quite similar to those of antennas with continuous loading, such antennas were made and some of their properties measured. Note that the experimental antenna in Fig.8.8 had a radius a=0.35 cm (as compared with a=0.3 cm used for the theoretical model with continuous loading) and length 14.4 cm (as compared with 15 cm).

From Fig.8.6 and eqn.(8.42) we see that very small current should be expected in a parasitic element optimized for minimal mutual coupling. This conclusion was verified experimentally in two ways. First, admittance of the optimally loaded monopole antenna was measured in the presence of identical, short-circuited monopole, versus frequency and for a wide range of distances between the antennas (from 2 cm to 16 cm). The results are shown in Fig.8.9. It is seen that the influence of the parasitic element on the admittance of the driven element is re-

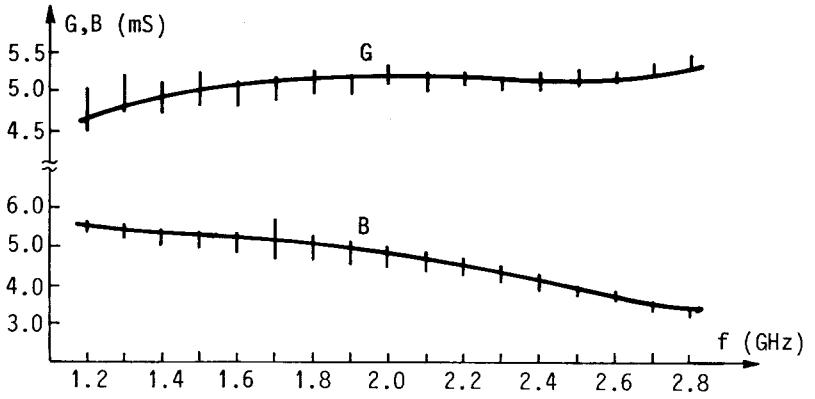

FIG.8.9. Conductance (G) and susceptance (B) of the optimal antenna shown in Fig.8.8 in the presence of identical short-circuited antenna, versus frequency, for different distances (in the range from 2 cm to 16 cm) of the parasitic element. ||| range of measured G and B values; ——— isolated antenna (measured).

markably small. Second, radiation pattern of such a system of dipole antennas was measured for a number of frequencies and distances between the elements, and compared with that of a single dipole with the same loading along its length. Some of the results are shown in Fig.8.10. It is seen that the optimally loaded parasite has quite small influence on the radiation pattern of optimally loaded antenna, while this is known not to be the case at all frequencies if the antennas are unloaded. In the case of optimally loaded antennas the influence of the parasitic element is small for practically all distances and a wide range of frequencies.

8.4. OPTIMIZATION OF ANTENNA ADMITTANCE BY VARYING CONCENTRATED LOADINGS[16]

Wire antennas with concentrated loadings are much more important than those with distributed loadings, because they can be realized more easily. We have seen in Chapter 5 that, in addition, with a relatively small number of concentrated loadings we can approximate quite accu-

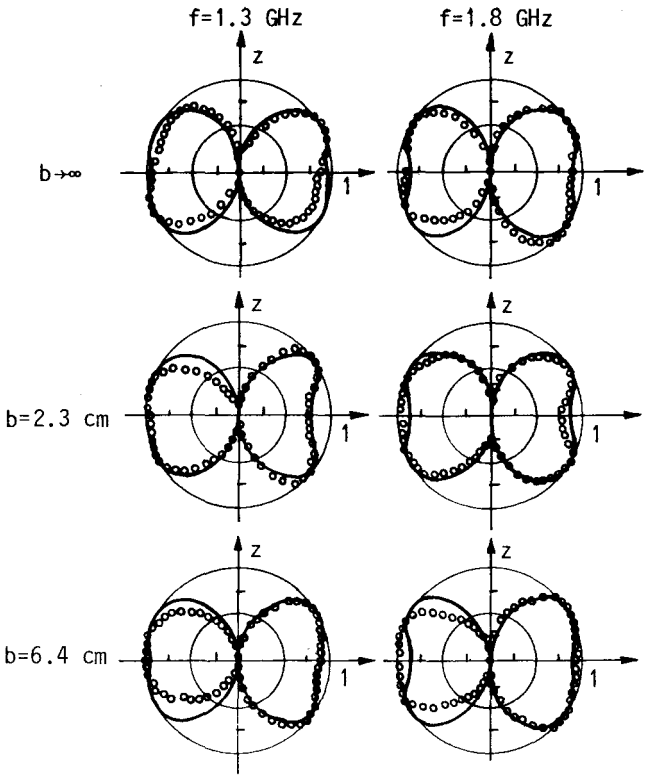

FIG.8.10. Measured radiation pattern in electric-field strength of optimally loaded symmetrical equivalent of the antenna shown in Fig. 8.8 with identical short-circuited parasitic element and theoretical pattern of isolated antenna with the same loading, in the plane containing the antenna axes; o o o experiment, ——— theory.

rately a distributed loading.

Synthesis of antennas with concentrated loadings, however, is in general very lengthy numerical procedure. Namely, if we allow the positions of the loadings to represent optimization parameters in addition to their impedances, the number of optimization parameters becomes relatively large even for a small number of the loadings. What makes it still more time-consuming is the fact that if we move a single loading along the antenna, we essentially have to analyse the antenna practi-

cally from the very beginning. On the other hand, we shall show below that if we fix the positions of the loadings and vary only their impedances, it is possible to analyse the antenna essentially only once, all subsequent analyses being reduced to a single matrix inversion. If, in addition, we have in mind that by variation of the impedance loadings at a sufficient number of fixed locations we can to some extent obtain effects analogous to physical displacement of the loadings along the antenna, it is obvious that the general synthesis case for antennas with variable loadings at variable locations need not be considered, except, possibly, in some very special cases. Therefore in this section we shall restrict our attention to synthesis of wire antennas with fixed geometry, having variable concentrated loadings at fixed positions along the wire structure.

Fig.8.11 shows a schematic representation of such an antenna, driven by a single generator of voltage V_0 and having n concentrated loadings of admittances $Y_1, Y_2, \ldots, Y_n$ (at the operating frequency). The antenna can be considered as (n+1)-port linear network, so that the following equations can be written for the structure:

$$\sum_{j=0}^{n} Y_{ij} V_j = I_i , \quad i=0,1,\ldots,n , \tag{8.43}$$

where V_0 is the generator voltage, I_0 its current and

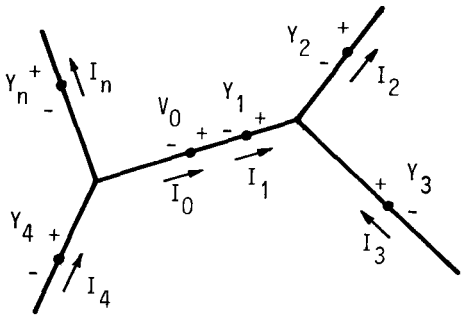

FIG.8.11. Schematic representation of wire-antenna structure driven by a single generator and loaded by n concentrated loadings.

$$I_i = -Y_i V_i , \quad i=1,\ldots,n \tag{8.44}$$

(with respect to the reference directions shown in Fig.8.11).

The self and mutual admittances of the structure, Y_{ii} and Y_{ij}, respectively, depend only on frequency and the antenna geometry. They can be computed from eqns.(8.43) if we know voltages V_i and currents I_i, i=0,1,...,n, for (n+1) independent driving conditions. For example, we can short circuit all the antenna ports except that labelled by "j", at which a voltage generator V_j is connected. We next solve for the antenna current distribution for these driving conditions. The currents I_i known, we can compute elements of one column of the admittance matrix as $Y_{ij}=I_i/V_j$, i=0,1,...,n. Performing this procedure (n+1) times (for j=0,1,...,n) we can compute all the elements Y_{ij}. Note that changing driving conditions in this case amounts to changes of the antenna excitation only, which enables great savings of the computer time in solving the integral equation for current distribution.

Once the Y-parameters of the structure are known, we can substitute eqns.(8.44) into eqns.(8.43) to obtain

$$\sum_{j=0}^{n} (Y_{ij} + \delta_{ij}Y_i) V_j = \delta_{0i} I_0 , \quad i=0,1,\ldots,n , \quad Y_0=0 . \tag{8.45}$$

Here, δ_{ij} is the Kronecker delta ($\delta_{ii}=1$ and $\delta_{ij}=0$ if $i\neq j$). Assuming that the generator voltage V_0 is known, from eqns.(8.45) we can compute the voltages V_j, j=1,...,n, at the loading terminals, and, in particular, the generator current I_0, for any values of the loading admittances Y_i. Obviously, in order to compute the antenna input admittance for a given set of loadings we do not have to repeat solutions of the integral equation for the antenna current distribution, which greatly expedites the optimization process.

The admittance Y_0 has no influence on the antenna current distribution and its radiation characteristics, and from this standpoint it can be discarded. However, its influence on the antenna input characteristics is very strong because it is connected in parallel to the antenna input terminals. This admittance can thus be very efficiently

used for compensation of the antenna input susceptance. Of course, similar effect can be obtained with a series impedance element. Therefore, either the parallel or the series compensating element should be included into an optimization of the antenna admittance. In the case of capacitively loaded antennas, which are the easiest to make and which will be considered as examples below, without compensating element the antenna susceptance tends to have quite large positive values.[16,47,60,84,85,86] Therefore we shall include a series compensating inductive element, of impedance Z_0, in all the examples of this section.

8.4.1. Optimal broadband capacitively loaded cylindrical antennas.[87]

Due to their simple construction, unloaded cylindrical antennas are of considerable practical importance. However, we know that their admittance varies very much with frequency, so that they cannot be used to operate in a wide frequency range. Basically, this property can be considered to stem from the fact that they radiate only from discontinuities, such as the antenna ends and the excitation zone.[14] They do not radiate along their length, because phase velocity of the antenna current wave is equal to the velocity of propagation of electromagnetic disturbances in the surrounding medium.[5,88]

In order to enhance radiation, it is necessary to produce a fast wave along the antenna. This can be achieved most easily by introducing lumped series capacitive loadings along it. Such loadings represent additional discontinuities along the antenna, which radiate just like the antenna ends and excitation region. An increase in number of these discontinuities results in increasingly better broadband antenna properties.[60,86]

As the optimization function, square of the effective reflection coefficient, R_{eff}^2, given in eqn.(8.5), will be used in all examples, and the reference admittance given in eqn.(8.10) will be adopted in evaluating R_{eff}. The self and mutual admittances Y_{ii} and Y_{ij} are determined by solving the Schelkunoff integral equation with combined trigonometric and polynomial approximation for current.[15] For the optimization process itself, a modification of the complete search is used. Namely,

taking two of the loadings as the optimization parameters (the others being fixed) a complete search is made and the optimal values of these two loadings determined. This procedure is repeated successively for other pairs of loadings, taken cyclically. In the case of five or six variable loadings an optimum is thereby reached typically in 5 to 20 cycles. It was found that, due to the particular analysis method described above, this optimization procedure enabled a significant increase of efficiency in determining the optimal lumped loadings along the antenna, when compared with other optimization methods.[16]

In order to further increase efficiency of the optimization process, the loading $Z_0=jX_0$ in the excitation zone (which compensates the antenna reactance) was treated separately. It can be optimized very simply if use is made of the following approximation, valid for small values of the reflection coefficient:

$$R_i \simeq \frac{Z_{ai} + jX_{0i} - Z_c}{2Z_c} , \tag{8.46}$$

where Z_{ai} is the antenna impedance and X_{0i} the reactance of the series compensating element (both at frequency f_i). Optimization of the reactance X_0 is thereby reduced to a linear fit, which expedites the optimization process noticeably, since this, in fact, reduces the number of optimization parameters by one.

A check of the optimization procedure described above was performed by comparing theoretical and experimental results. As the experimental model, an antenna with 6 concentrated loadings was adopted, shown in Fig.8.12(a,b). The radius, a, of the antenna was 3 mm, and its length, h, 163 mm. For the present purpose, only the monopole version of the antenna was used. The compensating element in the excitation zone (of reactance X_0 at a reference frequency) was made in the form of a series inductance shown in Fig.5.21(b), the reactance of which can be varied from 12 to 40 Ω (at 1 GHz). Five lumped capacitive loadings were positioned at unequal mutual distances, in order to minimize possible resonances. They were also made as variable elements, of the form shown in Fig.5.21(a), of capacitance ranging from 0.22 to 4 pF,

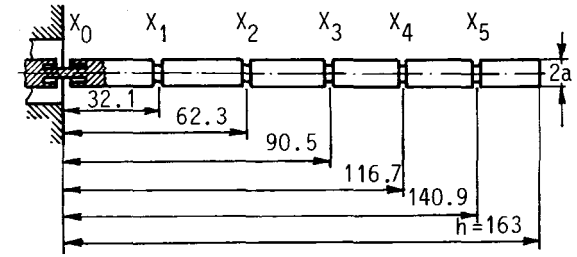

(a)

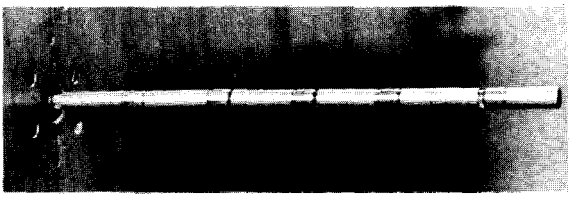

(b)

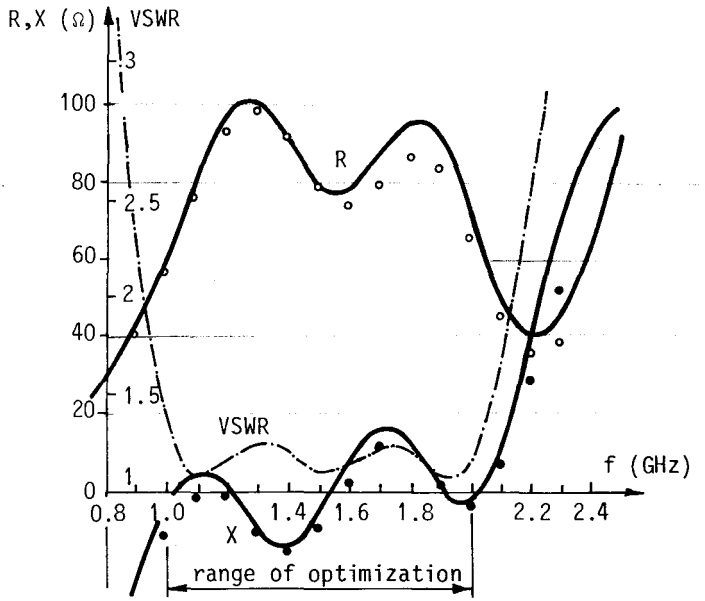

(c)

FIG.8.12. (a) Sketch of the experimental antenna; the dimensions are in millimeters. (b) Photograph of the experimental antenna. (c) Resistance (R) and reactance (X) and VSWR for the optimal octave antenna with h/a=54.3 in the range 1-2 GHz, with values of lumped reactances X_i given in Table 8.1. ———, — • — theory, oo, •• experiment.

which corresponds to reactance of about 700 Ω to about 40 Ω at 1 GHz.

In order to check accuracy of the adopted optimization procedure, a number of theoretically optimized antennas were examined experimentally. As an example, Fig.8.12(c) shows resistance, reactance and VSWR for an antenna optimized in a frequency range from f_1=1 GHz to f_2=2 GHz. It is seen that agreement between theoretical and experimental results is very good. It is interesting to note that VSWR is less than 1.25 in the whole range except in the small region near the lower frequency limit, in spite of the monopole length being only 0.542 wavelengths at 1 GHz.

A systematic analysis of optimal loaded broadband antennas was performed on a theoretical model of the same length and loading positions as in Fig.8.12(a). In order to analyse the influence of the antenna thickness on matching, antennas of radii a=3 mm, 1.5 mm and 0.75 mm were considered, which corresponds to the ratio h/a of 54.3, 108.7 and 217.3, respectively. For such antennas mutual and self admittances were first determined in the frequency range from 0.5 to 3 GHz, in steps of 0.1 GHz. Synthesis of a large number of broadband antennas of various properties was then performed, of which only some characteristic examples will be presented here.

As the first example, antennas with h/a=54.3 were optimized, with a constant frequency range of 500 MHz. With increasing f_1, the effective reflection coefficient, R_{eff}, decreased quite rapidly (from 0.3463 at 0.5 GHz to 0.0166 at 1.5 GHz). Such a rapid decrease in the reflection coefficient is partly due to decrease of the relative frequency band. In order to obtain a clearer insight into relative antenna properties, two cases with constant relative bandwidth were considered, the octave antennas (i.e., f_2/f_1=2), and approximately half-octave antennas (i.e., f_2/f_1=1.5).

In the case of octave antennas, analysis of influence of h/a on the reflection coefficient was performed on over 20 antenna types. Table 8.1 shows the values of the effective reflection coefficient (R_{eff}), the reference impedance $(Z_{cref})_{opt}=1/(Y_{cref})_{opt}$, labelled for short as

TABLE 8.1. Optimal octave antennas; f_1 and f_2 are given in GHz, Z_c in Ohms and X_i in Ohms at 1 GHz; rows for the same f_1 and f_2 correspond to h/a=54.3, 108.7 and (in the last three cases) to 217.3, respectively. The antenna dimensions are given in Fig.8.12(a).

f_1	f_2	R_{eff}	Z_c	X_0	X_1	X_2	X_3	X_4	X_5
0.6	1.2	0.2919	91	66	-75	-25	-100	0	0
		0.3505	102	79	-75	-125	-25	0	-25
0.8	1.6	0.1381	83	25	-100	-100	-150	-100	0
		0.2246	117	20	-75	-100	-275	-25	0
1.0	2.0	0.0966	88	29	-150	-25	-300	-175	0
		0.1397	112	34	-200	-25	-400	-175	0
		0.2012	135	39	-275	0	-570	-175	0
1.2	2.4	0.0659	90	17	-150	-175	-175	-325	-175
		0.0978	107	18	-250	-150	-275	-400	-150
		0.1382	130	18	-325	-175	-300	-600	-50
1.4	2.8	0.0315	98	15	-150	-250	-175	-525	-200
		0.0614	128	16	-210	-285	-230	-600	-205
		0.0920	157	13	-300	-300	-325	-700	-350

Z_c, and the optimal reactances of the lumped loadings, for a number of typical examples of optimal antennas with different ratios h/a. It is seen that magnitudes of the loadings do not differ considerably as the ratio h/a is increased.

Fig.8.13(a) shows VSWR versus frequency for three types of octave antennas with h/a=54.3. It is seen that the optimization results in a large decrease of VSWR in the passband (solid lines) when compared with that outside the passband (dashed lines). [Note the case of the 1-2 GHz antenna, the VSWR of which is very similar to that of a passband filter; this is the same graph as that in Fig.8.12(c)]. The largest VSWR is most often obtained at the lower frequency limit, f_1, which means that there it is most difficult to achieve matching, a result to be expected.

In order to analyse the influence of the relative bandwidth on matching, approximately half-octave antennas were also optimized, as already

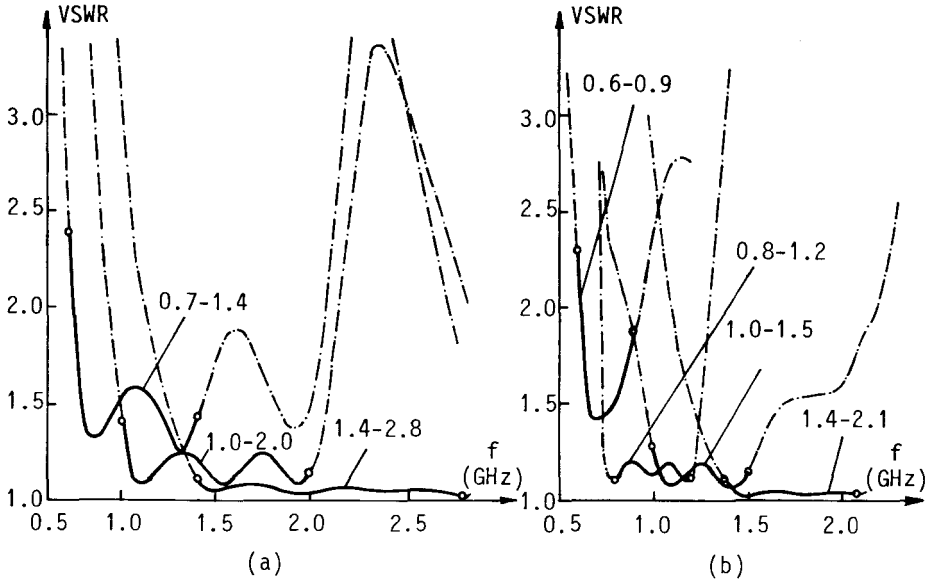

FIG.8.13. VSWR versus frequency for optimal broadband antennas sketched in Fig.8.12(a) with h/a=54.3. (a) Octave antennas. (b) Half-octave antennas.

mentioned. Table 8.2 gives the values of the reference impedance and optimal reactances of the lumped loadings for such antennas, and in Fig.8.13(b) the VSWR for several "half-octave" antennas is plotted versus frequency.

TABLE 8.2. Optimal "half-octave" antennas, i.e., $f_2/f_1=1.5$; h/a=54.3, f_1 and f_2 are given in GHz, Z_c in Ohms and X_i in Ohms at 1 GHz. The antenna dimensions are given in Fig.8.12(a).

f_1	f_2	R_{eff}	Z_c	X_0	X_1	X_2	X_3	X_4	X_5
0.6	0.9	0.2872	112	0	0	-75	-50	0	0
0.8	1.2	0.0728	68	61	-200	-75	-125	0	0
1.0	1.5	0.0775	89	25	-125	-50	-400	-25	0
1.2	1.8	0.0447	98	21	-150	-75	-450	-75	-100
1.4	2.1	0.0216	93	19	-200	-125	-425	-175	-200

8.4.2. Limits of VSWR for optimal broadband capacitively loaded cylindrical antennas versus their length.[87] In this subsection the influence of the antenna length and thickness on reflection coefficient of cylindrical antennas with concentrated capacitive loadings is analysed, and some diagrams are given indicating the antenna extremal possibilities. The analysis is based on a large number of results for antennas of the form shown in Fig.8.12(a) optimized with respect to their admittance in a prerequired frequency range.

Fig.8.14(a) shows the effective reflection coefficient, $(R_{eff})_1$, of optimal octave antennas, as compared with that for unloaded antenna,

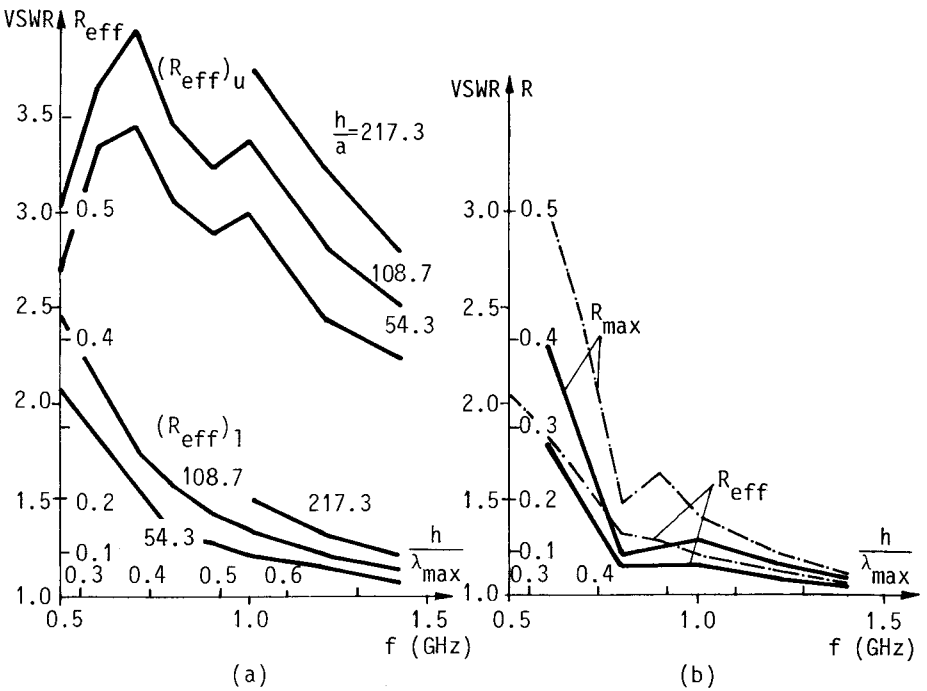

FIG.8.14. VSWR and reflection coefficient versus lower frequency limit, f_1 (or h/λ_{max}), for antenna sketched in Fig.8.12(a). (a) Effective reflection coefficient for optimally loaded octave antenna, $(R_{eff})_1$, and for unloaded antenna, $(R_{eff})_u$, with h/a as parameter. (b) Effective, R_{eff}, and maximal, R_{max}, reflection coefficient for optimally loaded half-octave antenna (solid lines) and octave antenna (dashed line) for h/a=54.3.

$(R_{eff})_u$ (with respect to its reference admittance), versus the lower frequency limit, f_1, with h/a as parameter. The difference between corresponding curves obviously represents a measure of improvement of matching obtained by the capacitive loading. It is also seen that it is more difficult to match thin antennas, which is natural, since VSWR of thin antennas when unloaded is also larger than for thick antennas, as seen from the figure.

Fig.8.14(b) shows the dependence of the effective reflection coefficient, R_{eff}, and the maximal reflection coefficient, R_{max}, for half-octave antennas on the lower frequency limit, f_1, viz. on the relative antenna length h/λ_{max}. For comparison, in dashed lines are also shown the values of R_{eff} and R_{max} for octave antennas. It is seen that an increase in bandwidth by increasing the upper frequency limit increases the reflection coefficient much less than by decreasing the lower frequency limit of the range. At the same time, this clearly indicates that the antenna length is a critical parameter for broadband matching of antennas of the type considered.

As the final example, Fig.8.15 shows the ratio $\left[(R_{eff})_l/(R_{eff})_u\right]^2$. This diagram indicates, just as that in Fig.8.14(b), that significant improvement in matching can only be obtained when the antenna length at the lower frequency limit is above about 0.3 or 0.4 wavelengths.

To analyse the influence on matching possibilities of the number of capacitive loadings, antennas were also optimized with a smaller number of loadings (4 and 3). It was concluded that the difference in the final results was relatively small for frequencies below 2 GHz, so that the results for 6 loadings given above can be considered as a practical upper limit of possibilities of the antenna type considered. At higher frequencies, however, the difference was found to be significant, which is undoubtedly due to a large distance (in wavelengths) between adjacent loadings in these cases.

The results presented above may be very useful for estimating necessary minimal size of capacitively loaded broadband cylindrical antennas which guarantees a desired level of the antenna matching in a desired frequency range.

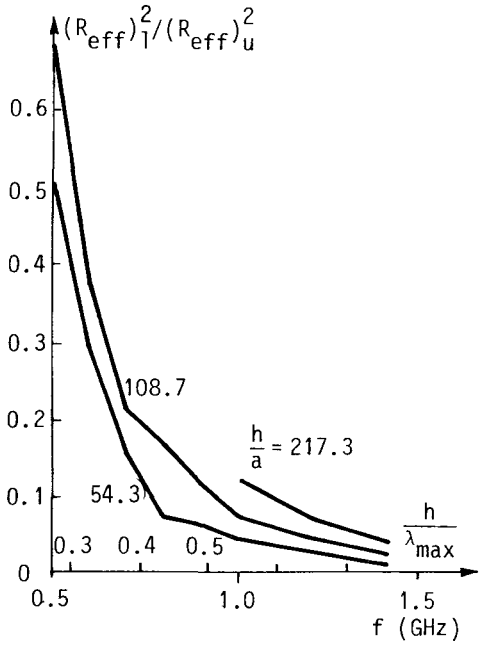

FIG.8.15. The ratio $[(R_{eff})_1/(R_{eff})_u]^2$ for octave antennas, versus frequency (or h/λ_{max}), with h/a as parameter.

8.5. OPTIMIZATION OF ADMITTANCE BY VARYING DISTRIBUTED AND CONCENTRATED LOADINGS[43]

We have seen in Subsection 4.2.1 that distributed resistive loading can result in cylindrical antennas with remarkably constant admittance and radiation pattern in a wide frequency range. We have also seen (Section 5.4) that addition of lumped capacitive loadings to distributed resistive loading can improve even further the antenna broadband properties, increasing at the same time its efficiency. In this section we shall explain a method for optimization of antennas with such combined loadings and present some theoretical and experimental results.

Note first that matching of broadband antennas to their feeders is a difficult task if classical single-frequency approach is adopted for matching the antenna by means of a reactive matching network. The reason is that, by Foster's reactance theorem, reactance (X) and susceptance (B=-1/X) of a linear reactive network always increase with

frequency, while the antenna susceptance does not generally decrease with frequency, and cannot in all cases be compensated by a reactive compensating network connected between the antenna terminals.

The present section is aimed at describing a simple method for obtaining a loaded broadband cylindrical antenna virtually perfectly matched to its feeder in a relatively wide frequency range, possibly by means of a broadband transformer, using a parallel reactance in the excitation zone. One way of achieving matching would be to analyse either experimentally or numerically the frequency behaviour of a number of antennas with the desired kind of loading. All those antennas having practically constant conductance, and a susceptance which decreases in a certain frequency range can, in principle, be matched in that frequency range to a feeder by means of a reactive compensating network (which has to be synthesized) connected between the antenna terminals, and possibly a broadband transformer. Unfortunately, this is usually not a simple task, particularly at microwave frequencies, because network synthesis and its realization at these frequencies are most often very intricate.

However, by varying the antenna loading, frequency dependence of its susceptance can be modified substantially. Therefore, basically opposite procedure is also possible, i.e., first to adopt a convenient simple reactive element with known frequency behaviour, and then to synthesize the loading along the antenna in order to obtain the antenna susceptance which compensates the reactive element susceptance. A certain insight into possibilities offered by variation of the loadings along an antenna in this case is of course necessary prior to adopting the reactive element, but for microwave antennas this method is nevertheless more appropriate, because synthesis and realization of a microwave broadband compensating reactive network is thereby avoided. It will be shown that in this manner loaded cylindrical antennas can be obtained having excellent broadband properties and quite small input susceptance in a relatively wide frequency range.

We have seen that the RC-loaded (as well as only C or R loaded) cylindrical antennas usually have positive susceptance. In accordance

with the method just outlined, an inductive coil connected in parallel with the antenna terminals was adopted as the compensating network, being the simplest for realization. Thus, theoretically,

$$B_{comp.net.} = -1/\omega L_c \ . \tag{8.47}$$

Following the proposed method, we next adopt the antenna dimensions, and determine the distributed and concentrated loadings along the antenna which minimize the optimization function

$$F = \int_{f_1}^{f_2} \left| B_{ant}(f) - \frac{1}{2\pi f L_c} \right| df \ . \tag{8.48}$$

In this equation L_c is also considered to be an unknown parameter to be determined from the optimization process, and f_1 and f_2, as before, are the lower and upper frequencies of the frequency range considered. In this manner both the loading along the antenna and the magnitude of the compensating coil inductance, which result in approximately real antenna admittance, are obtained. Of several optimization methods that can be used, a slight modification of the simplex method was adopted and found satisfactory.

Of particular interest in practice is that the antenna has as constant conductance as possible, in order that the broadband transformer matching can be applied. Therefore the optimization function given in eqn.(8.48) can be modified to require also that the antenna conductance be as close as possible to the average conductance in the frequency range $[f_1, f_2]$.

Although the method described above can be applied to any type of the loading along the antenna, and indeed to any type of antenna (not necessarily cylindrical), in practice it is restricted to cases which can more or less easily be realized. At microwave frequencies it is very difficult to obtain a pure concentrated or distributed inductive loading, as well as pure concentrated resistive loading or distributed capacitive loading. On the other hand, we know that concentrated capacitive loading can easily be obtained, and that it is not difficult to

realize a distributed resistive loading. An experimental model was therefore adopted similar to that shown in Fig.5.24. It consisted of a row of cylindrical resistors with metallic endings between which teflon discs were inserted to obtain lumped capacitors. The first segment was made of brass, i.e., having practically zero resistance per unit length. Contrary to the model described in Section 5.4, the present antenna was made as a self-supporting structure. To achieve this, a small hole was drilled along the axis of all the antenna elements, and the antenna parts were held together by means of a stretched nylon filament passing through the hole. By a simple device the nylon filament could be relaxed, the antenna dismounted, and then assembled again from new desired elements.

As a specific example, consider a cylindrical RC-loaded monopole antenna of diameter 2a=0.7 cm, made of four segments (i.e., three lumped capacitors), driven by a coaxial line of the inner diameter of the outer conductor 2b=1.38 cm. The values of the three lumped capacitors were considered as variables, as well as the length of the first brass segment and the values of the continuous resistive loadings of the other three segments, each of the length 4.8 cm. Available resistance values of the resistive segments were 50, 100, 200 and 400 Ω, i.e., about 1040, 2080, 4170 and 8330 Ω/m, respectively, which were incorporated into the optimization process as the only possible resistance values.

Numerical optimization was based on the method of antenna analysis outlined in Section 5.4. It resulted in the length of the first, brass segment equal to 3.11 cm, and in resistances of the other three segments of 100, 200 and 400 Ω, respectively. The optimal capacitances of the concentrated capacitors were found to be approximately 1.43 pF, 0.65 pF and 0.4 pF, counted from the excitation zone towards the antenna end. Finally, the optimal value of the compensating coil inductance was found to be approximately L_c=15 nH. The compensating coil was made in the form of few turns of very thin wire (of diameter 0.09 mm), wound on a short styrofoam cylinder of radius 4 mm. At both ends of the coil very small metallic contacts were made and the coil was fixed at the coaxial-line opening, between the antenna rod and the outer coaxial-

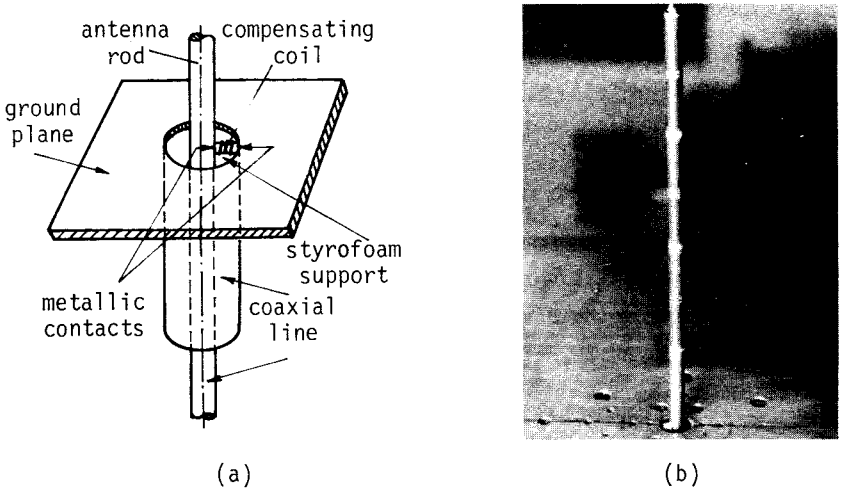

FIG.8.16. (a) Sketch of monopole-antenna excitation zone with compensating element. (b) Photograph of assembled RC-loaded antenna with compensating element.

line conductor (Fig.8.16). By a rough calculation it was found that the coil should have approximately 2 turns of the wire, but the accuracy of this result was quite doubtful. Therefore several coils were made and the optimal one, having approximately 1.75 turns, was determined experimentally.

Shown in Fig.8.17 are the computed and measured antenna conductance (G) and susceptance (B), versus frequency. For comparison, curves are also shown for under-compensation (too high value of L_c, approximately 3 turns) and over-compensation (too small value of L_c, approximately 1 turn), as well as the measured results without compensation. Excellent broadband properties of the optimally compensated antenna can be observed, comparable to those of a much more complicated structure like a log-periodic dipole antenna with seven elements.[89] Fig.8.18 shows radiation patterns of the antenna at three frequencies. The patterns have the expected shapes, typical for travelling-wave cylindrical wire antennas, and are quite stable in a wide frequency range.

By comparing theoretical and experimental susceptance curves it is

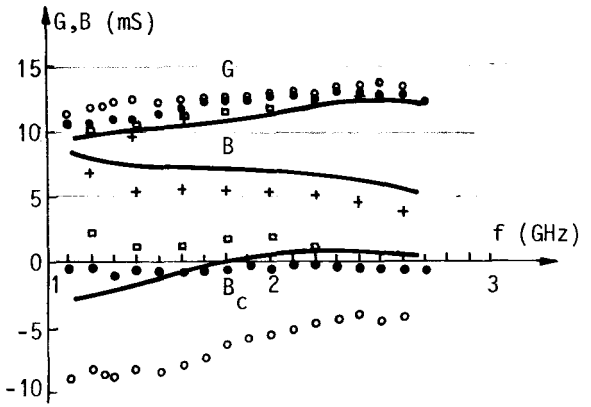

FIG.8.17. Conductance (G), susceptance (B) and compensated susceptance (B_c) of the RC-loaded cylindrical monopole antenna versus frequency; a=3.5 mm, h=17.75 cm; ——— theoretical; + + + experimental, without compensation; • • • experimental, optimally compensated; □ □ □ experimental, under-compensated; o o o experimental, over-compensated.

obvious that the compensating coil susceptance does not vary with frequency exactly as $(-1/\omega L_c)$. Also, in all the cases with compensating element the measured G-curves are affected as well. Fortunately, actual frequency behaviour of the coil appears to be more favourable for the present purpose than the theoretical one.

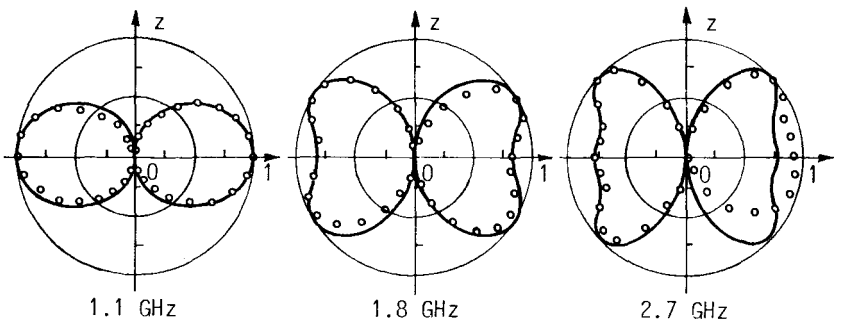

FIG.8.18. The optimal RC-loaded dipole-antenna radiation pattern in electric-field strength; o o o experimental; ——— theoretical.

For convenience, Table 8.3 summarizes some of the results shown in Fig.8.17 in a different form. The voltage standing-wave ratios and the reflection coefficients were computed corresponding to the average values of conductance G in the frequency range considered. It should also be noted that theoretically obtained efficiency of the antenna was over 80% in the whole frequency range. If a higher antenna efficiency is required, the optimization function can, of course, be modified to include efficiency as a parameter to be optimized. However, to achieve performances comparable to those of the antenna described above, a smaller frequency range than in the present example should be adopted.

TABLE 8.3. Theoretical and experimental average (arithmetic mean) parameters of RC-loaded cylindrical monopole antennas.

	Without compensation		Optimal compensation	
	theory	experiment	theory	experiment
Frequency range (GHz)	1.1-2.7	1.2-2.6	1.1-2.7	1.1-2.7
Average (reference) admittance (mS)	11.04+j6.84	11.29+j5.25	11.04-j0.52	12.07-j0.51
Average reflection coefficient (%)	30.0	23.1	6.74	3.94
Average VSWR	1.86	1.60	1.14	1.08

8.6. OPTIMIZATION OF ADMITTANCE BY MODIFICATION OF ANTENNA SHAPE[90,91]

In the case of antennas of fixed geometry, the only means of varying their properties is to load them with distributed and/or concentrated loadings. Although the antenna parameters can in this manner be varied in a relatively wide range, they are rather limited, essentially by the antenna size. For example, we have seen in Subsection 8.4.2 that if we wish to make a capacitively loaded cylindrical antenna broadband by loading it with lumped loadings, the lower limit of the frequency band is determined basically by the antenna length.

This section is devoted to synthesis of antenna admittance by modification of the antenna shape, instead of by varying the loadings along

it. Although synthesis of antennas with variable both shape and loadings is possible in principle, only perfectly conducting unloaded structures will be considered. This will be done because analysis of a single general case tends to be quite lengthy, so that synthesis of such structures is rather uneconomical from the computer-time point of view. Conceptually, however, it is a relatively simple matter to synthesize such general wire-antenna structures.

Since the general principles of synthesis of antennas with respect to their admittance have already been explained, here we shall only mention some details relevant to the examples presented in the following subsections. These examples are fairly simple, but it is believed that they will serve the purpose of demonstrating usefulness of numerical antenna synthesis in the case of variable antenna shape, because they all were realized, their properties measured and compared with theoretically predicted properties.

In all the cases, monopole antennas driven by a coaxial line with a=3 mm and b/a=2.3 (i.e., Z_c=50 Ω) were considered. The radius of all structure wires was equal to a, i.e., 3 mm. The lengths of theoretically synthesized optimal antennas were determined with accuracy of about 1 mm. The experimental models, however, for practical reasons differed somewhat from the optimal antennas. In these cases the experimental model was analyzed theoretically, and these results compared with experimental results.

For analysis, either the Hallén-type equation or the two-potential equation were used, with magnetic-current frill or belt-generator approximation to coaxial-line excitation, and with piecewise polynomial approximation for current distribution. In synthesizing broadband antennas, the reference admittance was assumed in the form

$$Y_{cref} = \frac{1}{n_f} \sum_{i=1}^{n_f} G_i \ , \tag{8.49}$$

i.e., in the form of the arithmetic mean of the antenna conductance at n_f frequencies in the range considered, if not stated otherwise. In all cases (where applicable), the modulus of the reflection coeffi-

cient, $|R|$, given in eqn.(8.1), was computed as a function of frequency and used for forming the optimization function.

In all the examples presented in this section the optimization parameters were taken to be the rectangular coordinates of the antenna nodes, because they are the simplest parameters which can define the antenna geometry in the general case.

Concerning the optimization method, a combination of essentially two different techniques was found to be most suitable in the majority of cases. At the very beginning of synthesis, when almost nothing is known about the function behaviour, it seemed convenient to apply several steps of random or interactive search in the whole region of the optimization parameters, in order to gain some insight into the realizable antenna properties. The best point in the parameter space out of these was then adopted as the starting point, and an optimization method used for determining the local optimum. By extensive comparisons it was concluded that the simplex algorithm,[80] with minor modifications, outlined in Appendix 7, appeared to be the most suitable in almost all examples. It was found to be sometimes far superior to other methods examined, such as coordinate search, pattern search and some variants of steepest descent.

In order to provide realizability of the antenna, to prevent possible crossings of the wire segments during optimization and to limit the antenna marginal dimensions, certain constraints were introduced, in the form of simple inequalities. Since in some cases the violation of these inequalities leads to an impossible antenna structure, or the method for analysis fails (e.g., wire segments penetrating into the conducting plane, or are too short), these inequalities were made intransitive in such a way that the optimization function was set to a large positive value whenever a constraint was violated. Thus the simplex was forced to contract back into the admissible region.

At the beginning, it is necessary to specify a convenient initial structure (by an educated guess, or based on previous knowledge), and to specify the desired properties of the final, optimal structure. The initial structure is determined by the number of wire segments and the

way they are interconnected. The computer takes over the rest of the work, trying to optimize the given structure. Naturally, there is no guarantee in advance that the proposed structure can fulfil the requirements, nor there is a general method for estimating in advance the characteristics which can be obtained from a structure. As usual, a good initial guess can sometimes be essential for obtaining satisfactory results, since the optimization function is often multimodal.

8.6.1. Synthesis of broadband folded monopole antenna. Consider a folded monopole antenna sketched in Fig.8.19. We assume that the height h of the monopole and the distance d between the two monopole arms are variable. The aim is to synthesize the antenna so that it be optimally matched (in the described sense) to the reference admittance given in eqn.(8.49) between f_1=1.0 GHz and f_2=1.2 GHz.

Since the frequency range is relatively narrow, it was adopted that n_f=2. No random search was used in this case to obtain initial values of the parameters. They were adopted to be h=75 mm (approximately quarter-wavelength) and d=20 mm. Using the two-potential equation, after only 5 iterations, which amounted to 12 optimization function computations, an optimal antenna was obtained with h=62 mm and d=21

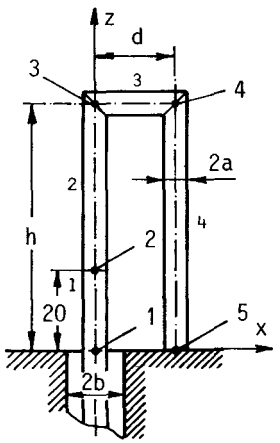

FIG.8.19. Sketch of a folded monopole antenna. Larger numbers indicate nodes, and smaller the segments. The length of the first segment is given in millimeters, a=3 mm and b/a=2.3.

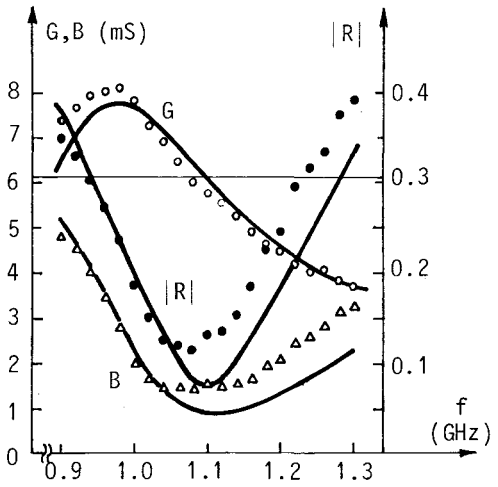

FIG.8.20. Conductance (G), susceptance (B) and modulus of the reflection coefficient ($|R|$) with respect to Y_{cref}=6.1 mS, for the folded monopole antenna in Fig.8.19, versus frequency; a=3 mm, h=61.5 mm, d=20.4 mm; ——— theory; oo, ΔΔ, •• experiment.

mm. Modulus of the reflection coefficient at f_1 and f_2 was found to be about 0.19, with respect to the reference admittance Y_{cref}=6.1 mS. The experimental model was somewhat different, with h=61.5 mm and d=20.4 mm. Theoretical and experimental conductance and susceptance of that antenna, as well as the modulus of the reflection coefficient (with respect to Y_{cref}=6.1 mS), are shown in Fig.8.20.

8.6.2. Synthesis of broadband monopole antenna with parasitic elements.[92] Already for some time it has been known that by adding two parasitic elements at a small distance from and parallel to a cylindrical monopole antenna near resonance a relatively good broadband antenna could be obtained.[93,94] The synthesis problem of determining the optimal dimensions of such an antenna by an optimization procedure has not, however, been considered. The present subsection is aimed at describing an optimal monopole antenna with two symmetrical, closely-spaced parasitic elements with respect to the monopole admittance.

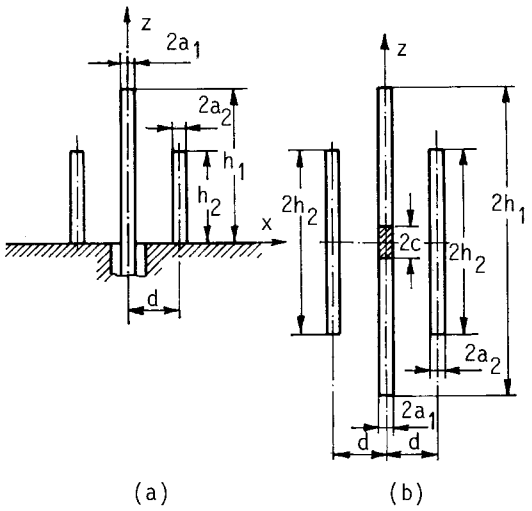

FIG.8.21. Sketch of antenna with two identical parasitic elements. (a) Coaxial-line feed; (b) belt-generator feed of equivalent dipole. (Ref. 92)

Consider the monopole antenna driven by a coaxial line and with two identical, symmetrically positioned parasitic elements, shown in Fig. 8.21(a). The equivalent dipole antenna with two parasitic elements, driven by a belt generator, is shown in Fig.8.21(b).

The Hallén-type simultaneous integral equations for currents $I_1(z)$ and $I_2(z)$ along the driven and the parasitic dipole elements have the following form:

$$\begin{aligned} \int_{-h_1}^{h_1} I_1(z')\, G_{11}(z,z')\, dz' + \int_{-h_2}^{h_2} I_2(z')\, G_{12}(z,z')\, dz' &= F_g(z) \\ \int_{-h_1}^{h_1} I_1(z')\, G_{21}(z,z')\, dz' + \int_{-h_2}^{h_2} I_2(z')\, G_{22}(z,z')\, dz' &= 0. \end{aligned} \tag{8.50}$$

The kernels $G_{mn}(z,z')$ are known functions, and $F_g(z)$ is a function describing the belt-generator excitation. This system of integral equations was approximately solved by assuming current distribution in the form of polynomials with unknown complex coefficients and applying the point-matching method. On the driven element the current was approxi-

mated by two polynomials (one along the belt generator, and the other along the rest of the antenna), with constraints that values of the polynomials and their first derivatives at z=c be equal, and that $I_1(h_1)=0$. Along the parasitic elements it was adopted simply that

$$I_2(z) = I_p\,(1 - z^2/h_2^2)\,, \tag{8.51}$$

because the parasites are electrically short. A higher-order approximation for current distribution along the parasitic elements was found to be unnecessary.

Of particular interest in the present case was to synthesize an antenna with approximately real and constant admittance in a given frequency range. To that aim, first for n_f frequencies in the desired frequency range the antenna conductances were computed, their geometric mean value determined, and that value used as the reference admittance,

$$Y_{cref} = \left(\prod_{i=1}^{n_f} G_i\right)^{1/n_f}\,. \tag{8.52}$$

The moduli $|R_i|$, $i=1,2,\ldots,n_f$, of the reflection coefficients were then found at the n_f frequencies with respect to the reference admittance, and the corresponding voltage standing-wave ratios, Γ_i, calculated. The mean value of the voltage standing-wave ratio was then defined as

$$\Gamma_{mean} = \left(\frac{1}{n_f}\sum_{i=1}^{n_f}\Gamma_i^m\right)^{1/m}\,, \tag{8.53}$$

which served as the optimization function, with m=8. Note that Γ_{mean} tends to $\max(\Gamma_i)$ when $m\to\infty$.

Determination of $(\Gamma_{mean})_{min}$ was performed by the pattern search[79] in the plane of the variables d and h_2, with $a_1=a_2=a=0.3$ cm and $h_1=7.5$ cm kept constant, for $n_f=3$, with $f_i=[1+(i-1)\cdot 0.1]$ GHz, i=1,2,3. The search was programmed to terminate when simultaneously the step size in d was less than 1.6 mm and in h_2 less than 2.5 mm. Optimization resulted in d=1.9 cm and $h_2=4.7$ cm, with $(\Gamma_{mean})_{min}=1.09$, with respect to $Y_{cref}=$

21.9 mS. (If a wider frequency range is required, however, VSWR cannot be kept so low.)

The elements of the antenna considered are relatively thick with respect to their lengths and distances between them. For example, in the present case $(d/a)\approx 6$, $(h_1/a)\approx 25$ and $(h_2/a)\approx 15$. Therefore certain corrections to account for the end and proximity effects were considered to be necessary when comparing theoretical and experimental results.

Concerning the end effect, the simplest correction was used, by adopting the experimental antenna length to be for a/2 shorter than that of the theoretical antenna (see Subsection 1.3.2).

It was more difficult to decide on the kind of the proximity-effect correction. Preliminary theoretical results indicated the currents in the driven and the parasitic elements to be approximately opposite in phase. Therefore the quasi-static approximation for the equivalent distance between the conductors of a two-wire line was adopted, which amounted to taking somewhat larger d in the theoretical model.

In the experimental model, both the driven and the parasitic elements were made of several cylindrical pieces of radius a=3 mm screwed one into the other. In this manner it was possible to change the lengths of the elements in steps of $\Delta h=0.5$ mm. The parasitic elements were mounted onto thin strips which could slide along a radial slot made in the ground plane.

The synthesized antenna was realized and checked experimentally. The results are shown in Fig.8.22. Good agreement between theoretical and experimental results can be observed. For comparison, theoretical results are also plotted for the antenna without correction of the end and proximity effects, showing worse agreement with experimental data than those with corrected effects, as well as for the antenna without parasitic elements.

The radiation pattern of the antenna was found to be practically identical with that of a half-wave dipole in the whole frequency range, as expected. Thus, a moderately broadband antenna in both the admittance and the radiation pattern was obtained.

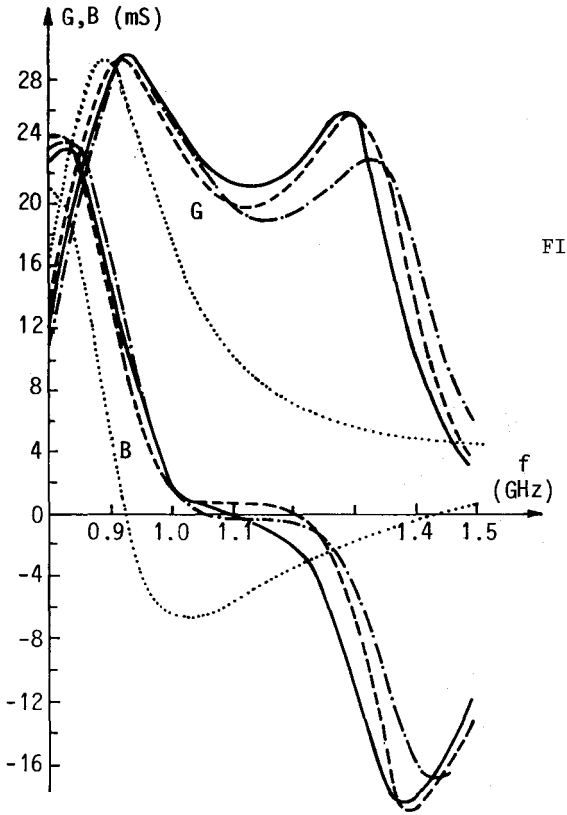

FIG.8.22. Conductance (G) and susceptance (B) of the monopole antenna shown in Fig.8.21(a), with $a_1=a_2=$ 0.3 cm. ——— experimental, $h_1=7.35$ cm, $h_2=4.55$ cm, d=2 cm; — — — computed, $h_1=$ 7.5 cm, $h_2=4.7$ cm, d=1.9 cm; — • — computed, $h_1=7.35$ cm, $h_2=4.55$ cm, d=2 cm; ····· computed, $h_1=7.5$ cm, $h_2=0$ (antenna without parasitic elements). (Ref.92)

Several other similar cases were synthesized theoretically, and checked experimentally, all of them showing the same degree of agreement between theory and experiment.

8.6.3. Synthesis of cactus-like antenna matched to feeder at two frequencies. In various practical situations an antenna is needed which is matched to its feeder at two or more arbitrary, relatively close frequencies. There are many possibilities for solving that problem, for example by optimizing an antenna with several parasitic elements of different lengths. The authors considered also the antenna shown in Fig.8.23, in the form of a saguaro-cactus with two or three branches. As an example, we shall consider the structure with two branches.

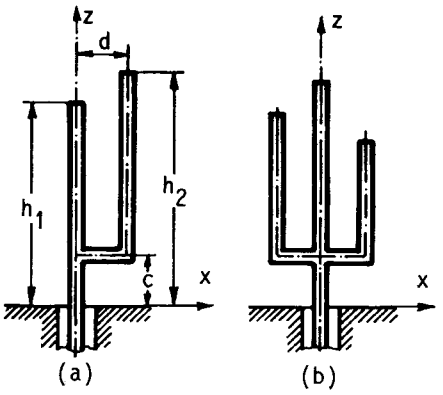

FIG.8.23. Sketch of cactus-like antennas with (a) two branches, and (b) three branches.

The antenna optimization parameters were the lengths h_1 and h_2 of the two branches, with c and d arbitrarily adopted to be equal, c=d= 20 mm. It was required that the antenna be optimally matched to a coaxial-line feeder of characteristic impedance Z_c=50 Ω at frequencies

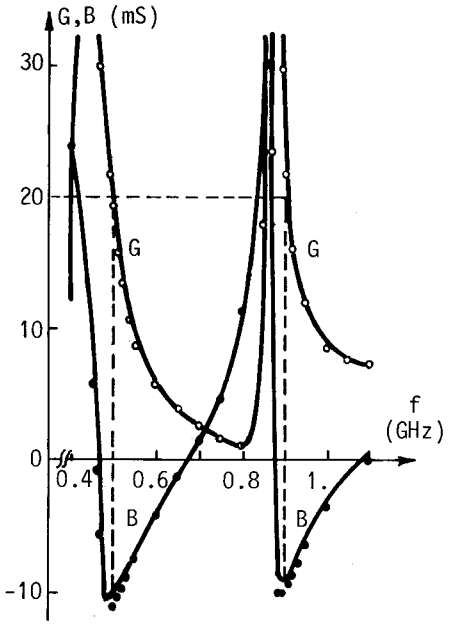

FIG.8.24. Conductance (G) and susceptance (B) of the antenna sketched in Fig.8.23(a), versus frequency; h_1=90 mm, h_2=144.2 mm, c=21 mm, d=22.5 mm; ——— theory; oo, •• experiment.

f_1=0.5 GHz and f_2=0.9 GHz.

The initial configuration for simplex optimization was adopted with $h_1=h_2$=100 mm. After 11 iterations, i.e., 26 computations of the optimization function, using the two-potential equation, optimal antenna was obtained with h_1=89 mm and h_2=142 mm. Modulus of the reflection coefficient at both frequencies was found to be 0.22. The experimental model differed somewhat from the optimal theoretical antenna, its dimensions being h_1=90 mm, h_2=144.2 mm, c=21 mm and d=22.5 mm. Theoretical and experimental results for admittance of this antenna versus frequency are shown in Fig.8.24.

8.6.4. Synthesis of vertical monopole antenna with susceptance-compensating element. As the last example, consider a vertical monopole antenna sketched in Fig.8.25. The horizontal segment, with its image, represents an open-circuited two-wire line. By choosing its length appropriately, it should be possible to compensate the antenna susceptance. Of course, this can also be done by a lumped reactive element, but at microwave frequencies it is not simple to do that. On the other hand, if the compensating conductor is adopted to be relatively far from the ground plane and short in terms of the wavelength, it cannot be accurately designed on the basis of the transmission-line theory. Therefore it must be considered as an integral part of the antenna.

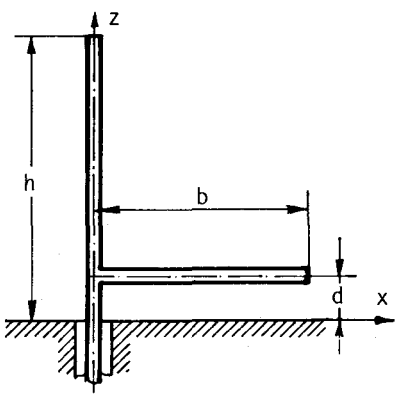

FIG.8.25. Sketch of vertical monopole antenna with a horizontal segment added for compensation of the monopole susceptance.

If we assume that h=λ/4 and a=0.01 λ, the monopole without compensation has an admittance Y≈(18-j7) mS. By compensating the susceptance in this case, an antenna is obtained matched almost perfectly to a 50 Ω (20 mS) coaxial line. Since we adopted a=3 mm, frequency was set to 1 GHz, d was adopted to be 10 mm, and h and b were considered as optimization parameters. The initial values of the parameters, with which the simplex optimization process was started, were h=75 mm (i.e., λ/4) and b=40 mm (approximately the length of the line having susceptance which, according to the electrostatic approximation, would compensate the -j7 mS monopole susceptance). After 8 iterations, i.e., 18 computations of the optimization function, the optimal antenna was obtained having h=82 mm and b=55 mm. (Note considerable difference between the optimal and the initial values of h and b.) The theoretical reflection coefficient of this antenna, with respect to a 50 Ω line, was found to be only 0.02 (i.e., the VSWR only 1.04).

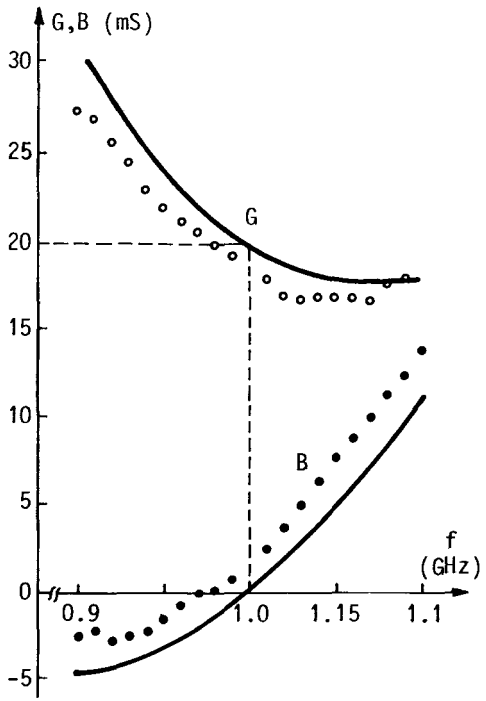

FIG.8.26. Conductance (G) and susceptance (B) of the antenna shown in Fig.8.25, with a=3 mm, h=81.5 mm, b=54.2 mm and d=9.5 mm; ——— theory; oo, •• experiment.

The experimental model differed somewhat from the optimal antenna, having h=81.5 mm, b=54.2 mm and d=9.5 mm. The theoretical and experimental results for this antenna are shown in Fig.8.26.

8.7. CONCLUSIONS

In this chapter some methods of synthesis of wire antennas with respect to the antenna admittance were explained and illustrated by examples, most of which were analysed also experimentally. The general conclusion might be that wire-antenna synthesis with respect to their admittance is a reliable and efficient method of designing such antennas.

All the examples of antennas considered were such that their radiation pattern was at least approximately known in advance, because the length and/or the complexity of the structures were not large. Almost only cylindrical structures were synthesized, possibly with additional elements which do not influence considerably the basic radiation pattern of a single cylindrical antenna. Therefore it was not necessary to consider the radiation pattern of the antenna as unknown.

It was shown that efficient optimization of wire-antenna admittance can be performed by varying distributed and/or concentrated loadings along it, as well as by varying the antenna shape and size. The combined, general case of optimization, of varying simultaneously the antenna loadings and shape, was not considered, because a large number of optimization parameters is then involved, making the optimization process quite lengthy. In principle, however, it is quite simple to optimize an antenna in that general case also, following the lines of reasoning presented in connection with optimization of the three special cases.

It was pointed out at several places in the chapter that optimization of wire antennas is not a single-valued process in many respects: in the choice of optimization function, in the choice of optimization method, in the choice of optimization parameters, and, in particular, in the choice of initial values of these parameters. It seems that very little can be suggested concerning the best possible choice of

these quantities, and that the only basis on which numerical synthesis can efficiently be built is a certain amount of experience. The authors hope that this chapter, summarizing the larger part of their knowledge and experience in synthesis of wire-antenna structures, may be of some help in that respect both to those who are interested merely in possibilities of this modern approach to wire-antenna design, and to those who have been using the numerical synthesis method for antenna design for some time. In particular, the authors feel that the material presented in Subsection 8.4.2 might serve as a useful basis for estimating potential broadband properties of antennas limited to a given volume.

Frequently a wire antenna has to be designed satisfying as closely as possible certain requirements relating to both its admittance and radiation pattern, or, sometimes, to its radiation pattern only. Optimization of wire antennas with respect to radiation pattern, and combined optimization of pattern and admittance, is the topic of the next, last chapter of the monograph.

CHAPTER 9
Optimization of Antenna Radiation Pattern

9.1. INTRODUCTION

The radiation pattern of an antenna situated in a homogeneous medium and bounded by the surface S is uniquely determined by distribution of currents inside S. The classical methods of pattern synthesis were aimed at determining current distribution in S resulting in a desired pattern. The other, more difficult problem, how such a distribution of current can be obtained, and whether it can be obtained at all, was not considered. In contrast to this, the method of pattern synthesis to be outlined below is always associated with a real antenna structure, which is modified until a radiation pattern of the structure is obtained which is as close as possible to a desired pattern.

As a rule, modification of the antenna structure in order to modify the radiation pattern influences also the antenna admittance. In fact, we know that admittance is usually much more sensitive to variations of the antenna shape or loading than radiation pattern. Therefore optimization of the antenna radiation pattern alone is frequently not advantageous. Instead, simultaneous optimization of the radiation pattern and admittance seems to be a better design approach. For this reason, the stress in this chapter will be on simultaneous optimization of admittance and pattern, although some attention will also be paid to optimization of the radiation pattern alone.

Concerning possible optimization functions when optimizing simultaneously radiation pattern and admittance, they may be of the form

$$F = w_a F_a + w_p F_p \ , \tag{9.1}$$

where F_a and F_p are convenient optimization functions incorporating the antenna admittance and radiation pattern alone, respectively, and w_a and w_p are weighting coefficients. The function F_a can be any of the functions used in the preceding chapter (or some other convenient function for admittance optimization). The function F_p can be of various forms, some of which are briefly described below. Of course, the form of the optimization function F can also be different from that given in eqn.(9.1).

A frequent requirement on the radiation pattern is that the antenna gain be maximal possible in a given direction. The optimization function in that case could be any function which decreases with increasing antenna directive gain, g_d (or power gain in the case of lossy antenna structures). A simple choice of the optimization function could be

$$(F_p)_1 = 1/g_d \ . \tag{9.2}$$

Alternatively, it can be required that the antenna gain in a given direction be as small as possible, which amounts to postulating that in a certain direction the antenna radiation pattern has a null. The optimization function in that case might be

$$(F_p)_2 = g_d \ . \tag{9.3}$$

In some engineering applications we can require that the antenna directive gain in certain directions be equal or larger than a prescribed value, while in other directions be smaller than a given value. If the antenna properties are of interest in a certain range of frequencies, the optimization function can be of the form

$$(F_p)_3 = \frac{1}{n_f n_d} \sum_{i=1}^{n_f} \sum_{j=1}^{n_d} D_{ij} \ , \tag{9.4}$$

where n_f is the number of discrete frequencies in the range considered, and n_d is the number of directions in which the antenna gain is specified. D_{ij} should be positive functions which rapidly tend to zero if the antenna directive gain in the specified direction is better than

required, and have large positive values otherwise. Of course, these functions can have various forms. Since the antenna gain is usually specified in decibels, one possible choice of the functions D_{ij} is

$$D_{ij} = \left(\frac{t_{ij} + |t_{ij}| + 1}{t_{ij} - |t_{ij}| - 1} \right)^2 , \tag{9.5}$$

where

$$t_{ij} = A\,(G_{d0j} - G_{dij}) \tag{9.6}$$

when directive gain in decibels G_{dij} larger than G_{d0j} is required, and

$$t_{ij} = A\,(G_{dij} - G_{d0j}) \tag{9.7}$$

when directive gain G_{dij} smaller than G_{d0j} is required. The quantity A is a constant which determines the steepness of the D_{ij} functions. In all the examples presented in this chapter in which eqn.(9.4) was used, A was arbitrarily set to be $0.1 \cdot \ln 10$, so that t_{ij} represents double difference of the prescribed and the attained directive gain in the direction j, expressed in nepers.

The final example of the optimization function F_p is for the case when the antenna is required to have a specified shape of the radiation pattern in a given plane, at a single frequency. Most often, only relative intensities of the far-zone field are of interest, and not the phases. If we assume that the desired radiation pattern is specified at a (usually large) number of directions, determined by angles ϕ_i in the plane considered, instead of eqn.(9.4) the optimization function can be chosen in the form

$$(F_p)_4 = \max_i \left| \ln \left[|\vec{E}_n(\phi_i)| / |\vec{E}_{0n}(\phi_i)| \right] \right| , \tag{9.8}$$

where $|\vec{E}_n(\phi_i)|$ is the normalized electric-field intensity in the direction determined by ϕ_i, and $|\vec{E}_{0n}(\phi_i)|$ the desired normalized intensity in that direction. The normalizations can be various. For example, the electric field can be normalized so that the maximal intensity of both the prescribed and attained fields be unity in a certain direction.

Of course, other optimization functions can be constructed, e.g., those which would take care of the polarization of the electric field, phase variations, those aimed at maximizing the front-to-back ratio, or maximizing the signal-to-noise ratio.[95]

Note that determination of the radiation pattern is numerically a simple task once the antenna current distribution has been determined, as outlined in Appendix 3. Therefore even complicated optimization functions F_p usually do not have too high computer-time requirements, except if the far-zone field has to be computed at a very large number of directions.

It should also be noted that considerable insight into radiation possibilities of an antenna structure is needed before constructing the optimization function. For example, if a relatively short cylindrical antenna is optimized (shorter than about one half-wavelength), no resistive or capacitive loading can make the antenna to have a zero radiation at an angle of 45° with respect to the antenna axis (and, indeed, at any angle except 0°). Therefore, whenever optimizing the pattern of a novel antenna type, it is highly recommendable to analyse the pattern in a number of cases prior to introducing requirements into the optimization function.

Finally, in simultaneous optimization of admittance and pattern it should be kept in mind that the requirements on the two quantities might be to some extent contradictory, without our knowing it. Appropriate choice of the weighting coefficients w_a and w_p in eqn.(9.1) can be of considerable help in compromizing possible contradictory requirements.

In the following sections a number of simple examples of optimization of the radiation pattern will be presented. These cases include optimization of the driving voltages of antenna-array elements, of the loading impedances, or of the antenna shape and dimensions, in order to obtain a desired radiation pattern, or to maximize the directive gain and the front-to-back ratio.

9.2. OPTIMIZATION OF RADIATION PATTERN BY VARYING DRIVING VOLTAGES OF ANTENNA-ARRAY ELEMENTS

The simplest case of radiation pattern optimization is to determine driving voltages of antenna-array elements in order to obtain a specified radiation pattern. This problem has been extensively treated in many papers using the classical array design techniques. Review of these methods can be found in References 96 and 97. Most of these techniques are based on methods of linear algebra, usually involving matrix calculus. In some more recently published papers iterative[98] or optimization methods[99,100,101] are used. However, only in few existing papers mutual coupling between the array elements is correctly taken into account.[102] In this section we shall present a simple example of determining the driving voltages of array elements for given dimensions and positions of these elements, taking rigorously into account the coupling between the antennas.

Consider a circular array of three identical equidistantly spaced half-wavelength monopole antennas, of radius 0.01 λ, located along a circle of radius 0.25 λ, as sketched in Fig.9.1. The desired electric-field radiation pattern of the array in the horizontal (xOy) plane is shown in Fig.9.2 by the dashed line.

For the purpose of optimization, the radiation pattern was sampled at angles $\phi_i = (i-1)\pi/6$, $i=1,2,\ldots,12$, and the optimization function

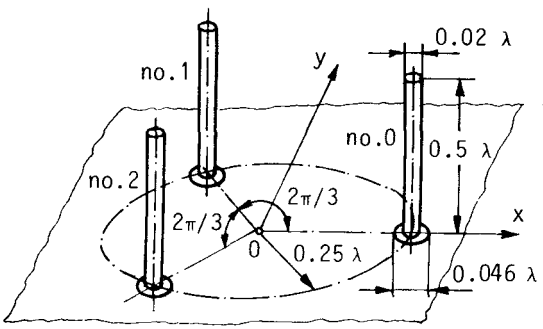

FIG.9.1. Sketch of a circular array of three half-wavelength monopole antennas, located above a perfectly conducting ground plane.

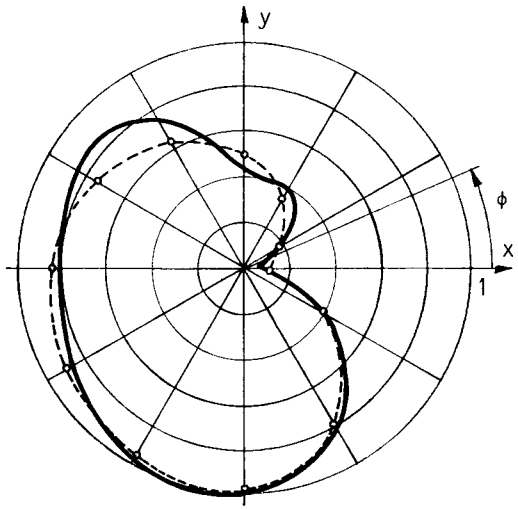

FIG.9.2. Specified radiation pattern in electric-field strength of the array sketched in Fig.9.1 (dashed line) and optimized pattern (solid line).

$(F_p)_4$, given in eqn.(9.8), was adopted. Both the desired and attained radiation patterns were normalized so that $|E_n(3\pi/2)|=1$. In order to expedite evaluation of the radiation pattern, the far-zone electric field at the angles ϕ_i was expressed in the form

$$E(\phi_i) = \sum_{j=0}^{n} T_j(\phi_i)\, V_j \,, \tag{9.9}$$

where n=2, V_j are the antenna driving voltages, and $T_j(\phi_i)$ are transmission coefficients. These coefficients can be determined knowing the far-zone electric field for three independent driving conditions of the array, in a similar manner as were determined the Y-parameters in the case of antennas with concentrated loadings (Section 8.4). Note that, due to symmetry, in the present case many of the coefficients $T_j(\phi_i)$ are identical. In this example the two-potential equation was used to analyse the array.

Fixing the driving voltage V_0 at V_0=1 V, the simplex optimization procedure was used, to obtain the optimal values of the driving voltages $V_1=(0.099 - j0.134)$ V and $V_2=(0.207 - j0.874)$ V. The corresponding radiation pattern is shown by solid line in Fig.9.2. Note that the

largest difference between the specified and the optimal radiation pattern, of about 1.3 dB, occurs at several angles ϕ_i, which results from the adopted minimax optimization. This example clearly illustrates that it is in general very difficult to approach an arbitrarily specified radiation pattern if we have only a small number of variable parameters.

9.3. OPTIMIZATION OF RADIATION PATTERN BY VARYING ANTENNA LOADINGS

Antenna loadings can in some cases have a large influence on the radiation pattern, and can thus be efficiently used for optimization of the antenna radiation properties, as proposed by Harrington and Mautz.[103,104] For practical applications it is usually desirable to optimize also the antenna admittance in order to match the antenna to the feeder. In this section we shall present an example of simultaneous optimization of the radiation pattern and the admittance of an Uda-Yagi array.

Consider an electrically-small, three-element, symmetrical Uda-Yagi array, sketched in Fig.9.3. The dipoles are loaded by concentrated inductive loadings, of admittances Y_1, Y_2 and Y_3, and an additional loading, of admittance Y_0, is provided in parallel with the antenna

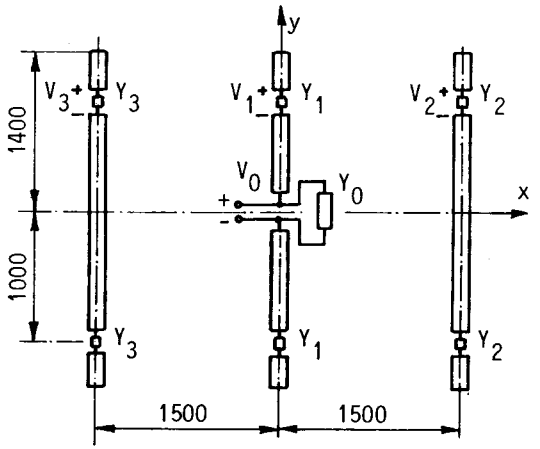

FIG.9.3. Sketch of loaded Uda-Yagi array. All dimensions are in millimeters. Wire diameter is 22 mm.

input terminals in order to compensate the antenna susceptance. The array is to be designed for a narrow-band operation at a frequency f=27 MHz (at which the dipole lengths are only about $\lambda/8$) with the following requirements: (1) the antenna forward directive gain, g_{df}, should be as large as possible, (2) the array backward directive gain, g_{db}, should be as small as possible, and (3) the array should be well matched to a reference admittance Y_{cref}=5 mS (so that it can easily be matched to a 20 mS coaxial line by means of a 4:1 balun). The antenna synthesis was performed for fixed antenna dimensions (including the loading positions), by varying the magnitudes of the loadings only. The optimization function was constructed so to combine the reflection coefficient, R, of the antenna (together with the compensating admittance Y_0) with respect to Y_{cref}, and the optimization functions $(F_p)_1$ and $(F_p)_2$, given by eqns.(9.2) and (9.3), in a quasi-minimax way, i.e.,

$$F(Y_1,Y_2,Y_3) = \left[(100\,|R|)^8 + (2/g_{df})^8 + (5\,g_{db})^8\right]^{1/8} , \qquad (9.10)$$

with arbitrarily adopted weighting coefficients (100, 2 and 5). The admittance Y_0 was always chosen so that the antenna admittance be real. The antenna dimensions being fixed, the Y-parameters describing the antenna with respect to its input and loading terminals, as given in eqn.(8.43), can be found as outlined in Section 8.4. The antenna far-zone electric field can be expressed in terms of the transmission T-coefficients as given in eqn.(9.9), where now n=3, V_0 is the antenna driving voltage, and V_j, j=1,2,3, are the voltages across the loading terminals. The T-parameters can easily be evaluated in a similar manner as the Y-parameters.

The Y- and T-parameters known, the loading voltages and the input admittance can be evaluated from eqns.(8.45), and the far-zone electric field can be computed from eqn.(9.9). Therefore the optimization function can be determined very rapidly. The simplex optimization procedure yielded the optimal loadings Y_1=-j1.91 mS, Y_2=-j2.00 mS, Y_3=-j1.85 mS and the compensating admittance Y_0=-j14.7 mS. For this set of loadings the antenna forward directive gain is g_{df}=5.2 (i.e., 7.2 dB), the backward directive gain is g_{db}=0.056 (i.e., -12.5 dB), whence the front-to-

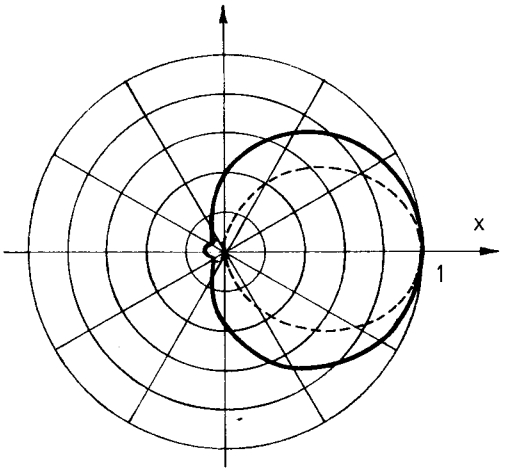

FIG.9.4. Electric-field radiation pattern of the optimal Uda-Yagi array sketched in Fig.9.3 in the xOz, or H-plane (———), and in the xOy, or E-plane (– – –).

back ratio is 19.7 dB, and the modulus of the reflection coefficient is less than 0.001. The array electric-field pattern is plotted in Fig. 9.4. It should be noted that the synthesized array is, actually, almost a supergain array, and that it is very sensitive to variations of any dimensions, loading magnitudes and frequency. Of course, this is not unexpected, because the array dimensions are relatively small when compared with the wavelength.

9.4. OPTIMIZATION OF RADIATION PATTERN BY VARYING ANTENNA SHAPE[90,91]

Theoretical antenna optimization by modifying its shape and size has been treated in only few papers.[90,105-109] In the following subsections some examples will be presented to illustrate either optimization of the radiation pattern only, or simultaneous optimization of radiation pattern and admittance of wire-antenna structures. In all the cases optimization function of the form given in eqn.(9.1) was used, with function F_a being the effective reflection coefficient, defined by eqn.(8.5), and the function $F_p=(F_p)_3$ given by eqns.(9.4)-(9.7). Radiation-pattern optimization was not aimed at synthesizing the whole pattern. Rather, it was used either to obtain antenna directivity larger than some prescribed value, or the best possible front-to-back ratio.

As in other examples of antenna synthesis presented in this monograph, care had to be exercised that the requirements on the pattern and admittance be realistic and not contradictory, and that the weighting coefficients w_a and w_p be chosen appropriately.

9.4.1. Synthesis of Uda-Yagi arrays with one and two directors and two reflectors. We shall illustrate synthesis of antennas with respect to their radiation pattern alone by varying the antenna geometry on two examples of small Uda-Yagi arrays. Such arrays are of interest in the lower range of very high frequencies (of the order of 100 MHz), because at these frequencies the antenna elements tend to be large and the whole structure clumsy and heavy if the antenna has a larger number of elements.

We shall consider an antenna with a driven element, two symmetrically positioned reflectors and a single director, and the same antenna with one more director added. In order to meet the requirements imposed by the available experimental equipment, used to verify the theoretical results, both antennas were analysed at 1 GHz. (Using the theorem of electromagnetic similitude,[5] the antenna can always be scaled to lower or higher frequencies.) It was required that both antennas have maximal possible directivity and highest possible front-to-back ratio (FBR). In order to reduce the number of optimization parameters, the size of the driven element was fixed, at h_1=70 mm, as well as the distances c_1=c_2=40 mm of the two reflectors from the antenna plane of symmetry. As the optimization parameters, the heights of all passive elements and their distances from the driven element were considered.

The first case, of Uda-Yagi array with two reflectors and a single director, is sketched in Fig.9.5. It was adopted that G_{d01}=8 dB* (the main beam, in the direction of x-axis), and G_{d02}=-4 dB (back radiation, in the opposite direction). The initial values of the optimization parameters were h_2=65 mm, h_3=h_4=80 mm and d_1=d_2=75 mm (i.e., $\lambda/4$). These values were based on an educated guess. After 10 simplex itera-

* With respect to a semi-isotropic radiator, as in other examples of monopole-antenna synthesis.

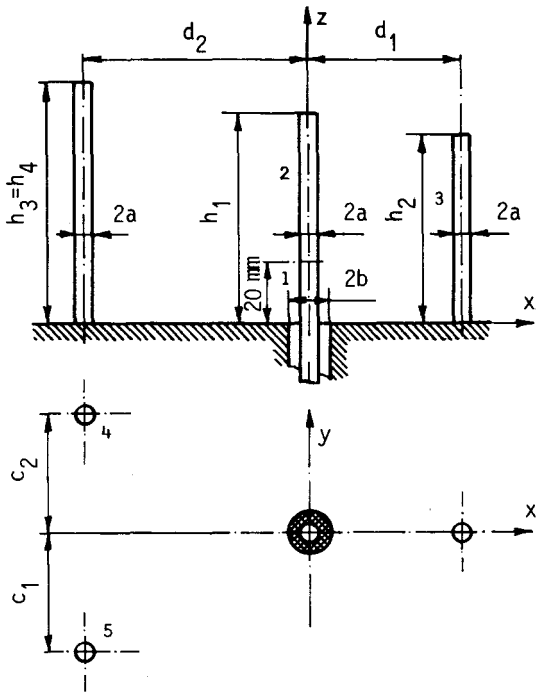

FIG.9.5. Sketch of an Uda-Yagi array with two reflectors and a single director; a=3 mm, b/a=2.3.

tions, which amounted to 32 optimization function computations, an antenna was obtained with h_1=70 mm (prefixed), h_2=63 mm, $h_3=h_4$=81 mm, $c_1=c_2$=40 mm (prefixed), d_1=52 mm and d_2=77 mm. Directivity of this antenna (in the direction of the x-axis) was found to be 9 dB, while directive gain in the opposite direction was -9.7 dB, so that FBR was 18.7 dB. The admittance of the antenna (which was not optimized) was Y=(42 - j33) mS. The experimental model used for measurement of the radiation pattern was practically the same as the theoretical, except that symmetrical antenna was made. Theoretical and experimental results for the radiation pattern in the xOy and xOz planes are shown in Fig. 9.6. Theoretical analysis was performed using the two-potential equation and polynomial approximation for current distribution, with n_1=3, n_2=4, and $n_3=n_4=n_5$=3. (Labels of the antenna segments are given in

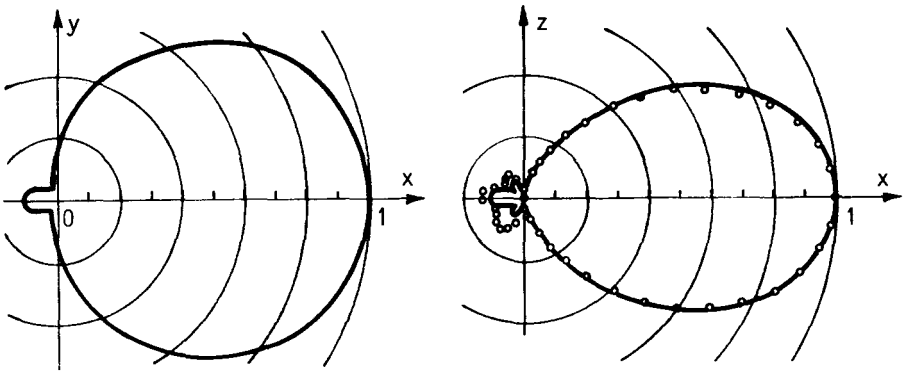

FIG.9.6. Radiation pattern in electric-field strength of symmetrical equivalent of the optimal Uda-Yagi array sketched in Fig.9.5. The dimensions of the array are given in the text, and frequency f=1 GHz. ——— theory; o o o experiment.

Fig.9.5.)

Shown in Fig.9.7 is a sketch of an Uda-Yagi array with two directors and two reflectors. It was expected that this structure would have a higher directivity than the antenna with a single director, shown in Fig.9.5. The same values of G_{d01} and G_{d02} were adopted as in the preceding example. The initial values of the optimization parameters were $h_2=h_3=65$ mm, $h_4=h_5=80$ mm, $d_1=d_3=75$ mm and $d_2=150$ mm.

The optimal antenna was obtained by the simplex method, which resulted in the following dimensions of the optimal antenna: $h_1=70$ mm (prefixed), $h_2=68$ mm, $h_3=60$ mm, $h_4=h_5=85$ mm, $d_1=37$ mm, $d_2=113$ mm, $d_3=80$ mm and $c_1=c_2=40$ mm (prefixed). Directivity of the antenna (in the direction of the x-axis) was 9.9 dB, and the front-to-back ratio was about 24 dB, which is somewhat better than in the preceding example. The experimental pattern was obtained on a model practically identical with the optimal antenna (except that it was symmetrical), and is shown in Fig.9.8, together with the theoretical pattern. The degrees of the polynomial approximation of current used were $n_1=3$, $n_2=4$, $n_3=n_4=n_5=n_6=3$. The theoretical admittance of the optimal antenna sketched in Fig.9.7 was found to be $Y=(33-j43)$ mS.

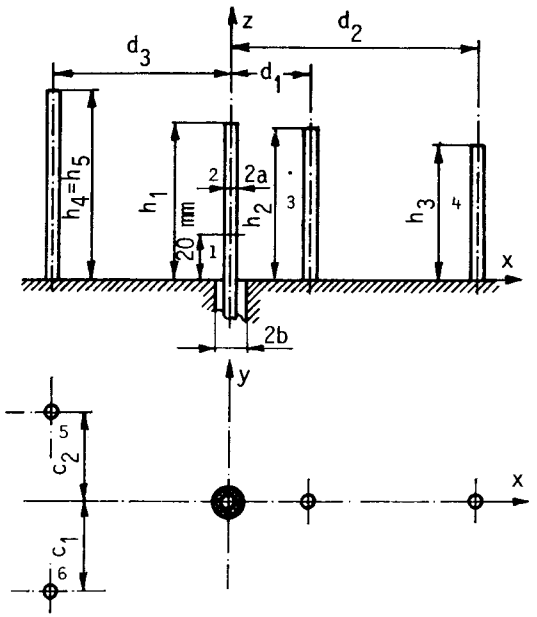

FIG.9.7. Sketch of an Uda-Yagi array with two reflectors and two directors; a=3 mm, b/a=2.3.

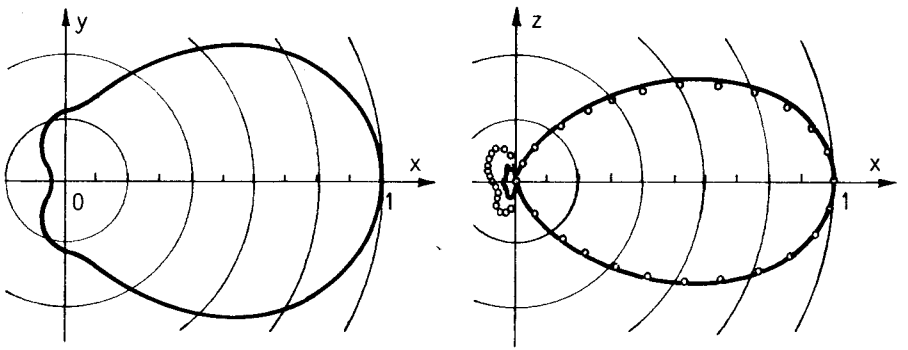

FIG.9.8. Radiation pattern in electric-field strength of symmetrical equivalent of the optimal Uda-Yagi array sketched in Fig.9.7. The dimensions of the array are given in the text, and frequency f=1 GHz. ——— theory; o o o experiment.

9.4.2. Synthesis of inclined monopole antenna. As the next example, consider the following design task: it is necessary to synthesize a single monopole antenna which is well matched to a 20 mS coaxial feeder at 0.975 GHz and has directive gain of at least 5 dB in one direction in the horizontal plane. The simplest structure which could fulfil these requirements seemed to be an inclined monopole antenna. Such an antenna, sketched in Fig.9.9, was therefore considered and optimized.

The length of the vertical segment of the antenna was fixed at c=20 mm, and the coordinates d and h of the antenna end were considered as optimization parameters. The weighting coefficients in the optimization function F were adopted to be equal, $w_a=w_p$. The reference admittance was adopted to be $Y_{cref}=20$ mS, and the optimization function F_a in this case is simply equal to $|R|$, because in eqn.(8.5) $n_f=1$. The value of G_{d01} was adopted to be $G_{d01}=5$ dB in the direction of the x-axis.

It was fairly obvious that the initial total length of the monopole should be $\lambda/4$, $3\lambda/4$, etc. With monopole length of $\lambda/4$, the simplex

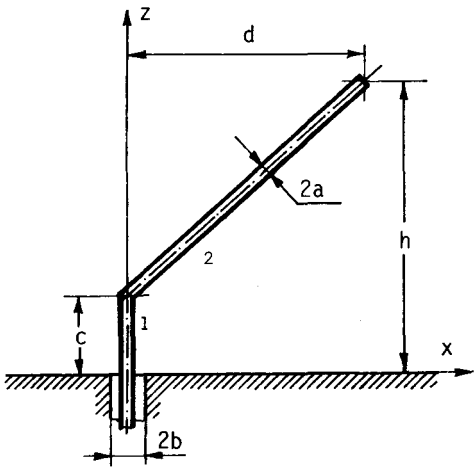

FIG.9.9. Sketch of an inclined monopole antenna; a=3 mm, b/a=2.3.

optimization resulted in a practically vertical monopole with insufficient directive gain in the x-axis direction of G_{d1}=2.2 dB. For the initial monopole length of $3\lambda/4$, after about 50 evaluations of the optimization function the simplex optimization resulted in an antenna with h=205 mm and d=98 mm. The optimal antenna had VSWR equal to 1.09, and sufficient directive gain in the x-axis direction of G_{d1}=6.27 dB. Theoretical and experimental results for the antenna admittance versus frequency are presented in Fig.9.10. Theoretical and experimental results are slightly shifted due to the end effect, which was not included in the theoretical model. Minimal experimental value of the VSWR was 1.06 at 0.96 GHz, which agrees well with the result of synthesis. The degrees of the polynomial approximation for current were n_1=3 and n_2=6.

9.4.3. Synthesis of Uda-Yagi array with folded monopole as a driven element. Consider next the Uda-Yagi array with two directors, one reflector and a folded monopole as the driven element, sketched in Fig.9.11. It was required for the array to have directive gain in the

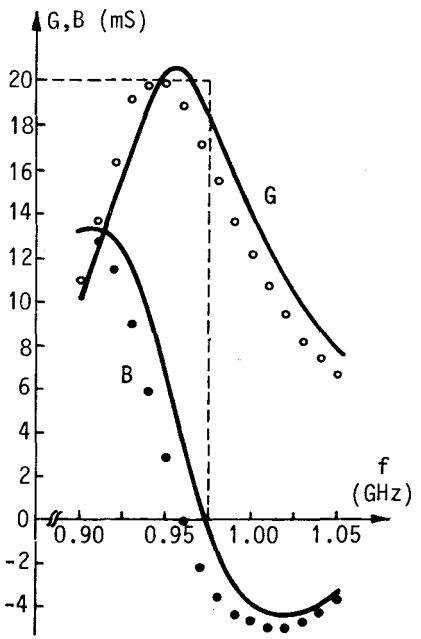

FIG.9.10. Conductance (G) and susceptance (B) of the optimal inclined monopole antenna sketched in Fig.9.9, with a=3 mm, b/a=2.3, h=205 mm and d=98 mm. ——— theory; oo, •• experiment.

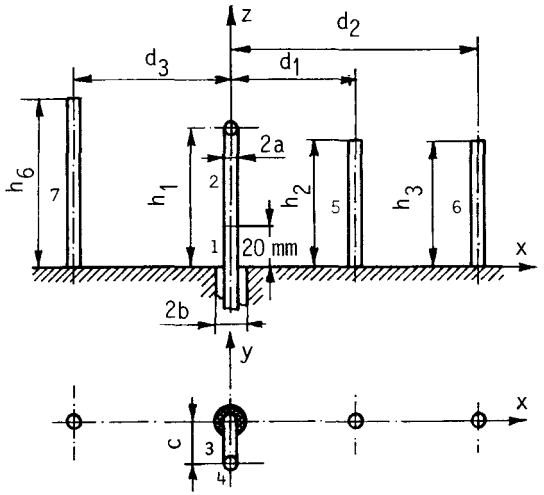

FIG.9.11. Sketch of an Uda-Yagi array with two directors, one reflector and folded monopole as the driven element; a=3 mm, b/a=2.3.

forward direction (x-direction) of at least G_{df}=9 dB, that in the backward direction of at most G_{db}=-4 dB, and to have approximately real admittance at f=1 GHz. The dimensions of the active element were fixed at h_1=70 mm and c=20 mm. The positions and lengths of the passive elements were considered as optimization parameters. The weighting coefficients in the optimization function (9.1) were adopted to be w_a=10 and w_p=1, with Y_{cref}=Re(Y), G_{d01}=9 dB (in the direction of x-axis) and G_{d02}=-4 dB (in the opposite direction).

Using the simplex method, the optimal structure was obtained with director lengths h_2=h_3=64 mm, reflector length h_4=84 mm, and director and reflector positions d_1=64 mm, d_2=126 mm and d_3=81 mm. The forward directive gain was 9.5 dB, and FBR was 19 dB. The antenna admittance was Y=(7.9 + j0.0) mS.

The experimental model dimensions for admittance measurements were the following: h_1=69.2 mm, h_2=63.2 mm, h_3=62.9 mm, h_4=84.2 mm, c=21.2 mm, d_1=64.2 mm, d_2=126.4 mm and d_3=81.2 mm. The theoretical and expe-

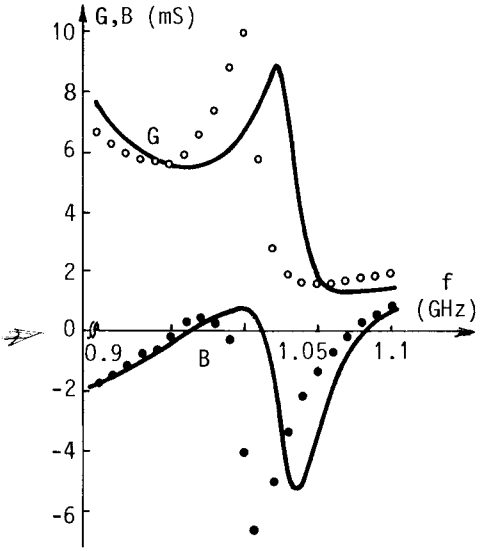

FIG.9.12. Conductance (G) and susceptance (B) of approximately optimal Uda-Yagi array sketched in Fig.9.11; a=3 mm, b/a=2.3, the other dimensions are given in the text. ——— theory; oo, •• experiment.

rimental antenna conductance and susceptance, versus frequency, are shown in Fig.9.12.

The experimental model for pattern measurements (the symmetric equi-

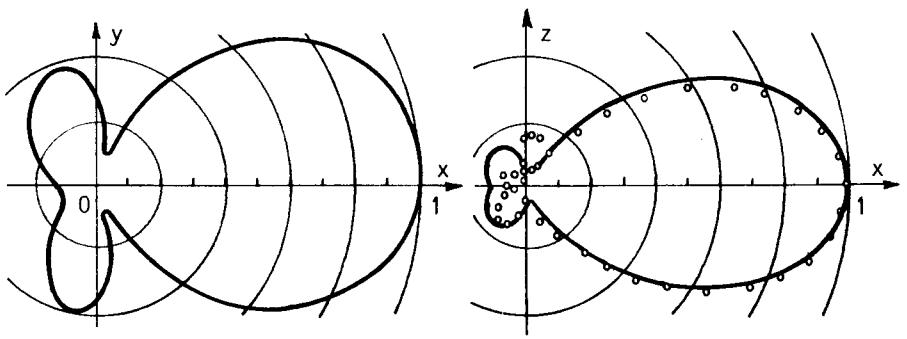

FIG.9.13. Radiation pattern in electric-field strength of symmetrical equivalent of the optimal Uda-Yagi array sketched in Fig.9.11, with a=3 mm, b/a=2.3 and other dimensions given in the text. ——— theory; o o o experiment.

valent of the antenna sketched in Fig.9.11) was practically identical with the optimal antenna. The theoretical and experimental radiation patterns in the xOy and xOz planes are shown in Fig.9.13.

9.4.4. Synthesis of moderately broadband Uda-Yagi array.[110] In principle, Uda-Yagi arrays are narrow-band antennas, because they consist of basically resonant elements. Theoretical optimization of such arrays with respect to their radiation pattern at a single frequency was considered in References 105, 106 and 107, and increase in bandwidth was demonstrated in Reference 108, but it seems that no attempt has been made to optimize the Uda-Yagi array so that it be to some extent broadband in its radiation pattern and admittance. This example is aimed at demonstrating that such a synthesis is possible, and that the results are quite acceptable for practical applications.

There was a need for a rugged, simple symmetrical antenna, well-matched to a 20 mS coaxial feeder (with VSWR less than 1.4) in a frequency range from 440 MHz to 470 MHz, having directivity larger than 9 dB and FBR not less than 15 dB. Since the frequency range was relatively narrow (about 10%), a solution was sought in the form of an Uda-Yagi

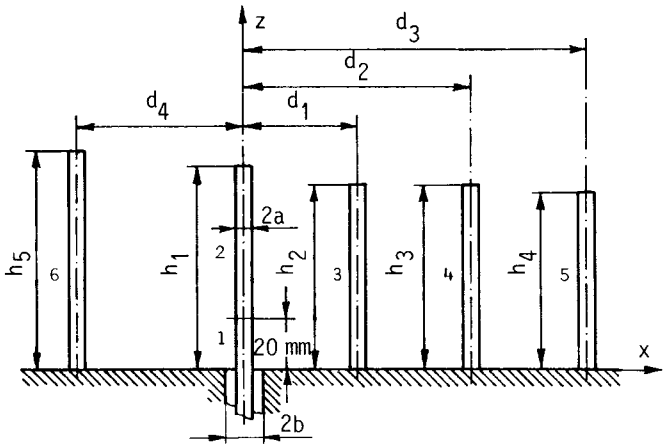

FIG.9.14. Sketch of Uda-Yagi array with three directors, one reflector and simple monopole as driven element; a=3 mm, b/a=2.3.

array. For practical reasons, asymmetrical equivalent of the antenna was considered, and frequency in theoretical analysis and synthesis was doubled, as well as in later experiments, so that the range between 0.88 and 0.94 GHz was of interest. An array with three directors, a single reflector and a driven element in the form of a simple monopole, shown in Fig.9.14, was considered as the initial structure, with a possibility of increasing the number of elements if needed.

The initial synthesis was performed using the interactive search, to obtain a reasonable starting point for simplex optimization, with $n_f=3$ ($f_1=0.88$ GHz, $f_2=0.91$ GHz and $f_3=0.94$ GHz). The approximately optimal antenna thus obtained had the following dimensions: $h_1=74.8$ mm, $h_2=h_3=68$ mm, $h_4=65.8$ mm, $h_5=80.5$ mm, $d_1=43$ mm, $d_2=86$ mm, $d_3=129$ mm and $d_4=63$ mm. The VSWR of the antenna (with respect to $Y_{cref}=43$ mS) was less than 1.35 in the whole frequency range, its directivity larger than 9.7 dB, and FBR larger than 9 dB. This antenna was realized, and its properties measured. The results are shown in Fig.9.15.

This antenna was then used as a starting point for further optimization, using the two-potential equation and the optimization function in eqn.(9.1), with Y_{cref} as given in eqn.(8.49), $w_a=1$, $w_p=0.1$, $G_{d01}=9.5$ dB (in the x-axis direction) and $G_{d02}=-0.5$ dB (in the opposite direction). The simplex optimization resulted in somewhat better antenna, having the following dimensions: $h_1=74.9$ mm, $h_2=h_3=68.4$ mm, $h_4=65.9$ mm, $h_5=83.3$ mm, $d_1=43$ mm, $d_2=84$ mm, $d_3=134$ mm and $d_4=65$ mm. The VSWR of this optimal antenna was less than 1.25 (with respect to $Y_{cref}=42$ mS) in the whole frequency range, its directivity (in the x-axis direction) larger than 9.7 dB, and FBR larger than 11.5 dB. These parameters versus frequency are shown in Fig.9.15 in dashed lines. The degrees of polynomials used for current approximation were $n_1=3$, $n_2=4$ and $n_3=n_4=n_5=n_6=3$.

The simple antenna shown in Fig.9.14 was thus not able to fulfil all the requirements (its FBR was only 11.5 dB, as compared with the desired 15 dB). Another director was therefore added to the structure, and a folded dipole incorporating a $\lambda/4$ coaxial transformer (serving to obtain a better match) was adopted as the driven element.[111] The resulting antenna, shown in Fig.9.16, did satisfy all the requirements,

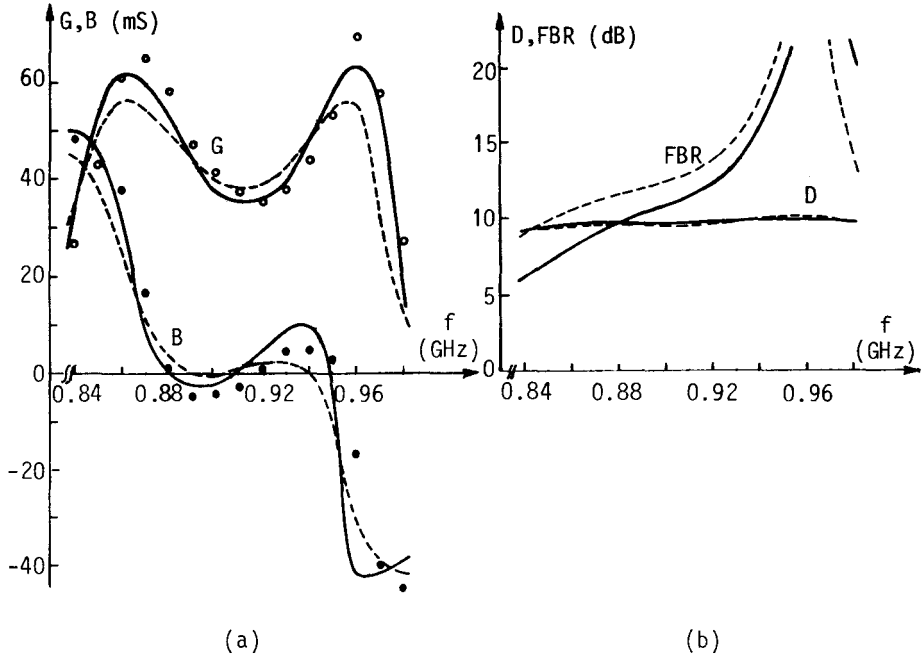

FIG.9.15. (a) Conductance (G) and susceptance (B), and (b) directivity (D) and FBR of the antenna sketched in Fig.9.14, versus frequency. ——— theory, approximately optimal antenna of dimensions given in the text; oo, •• experiment, approximately optimal antenna; — — — the optimal antenna, of dimensions given in the text.

but its optimization was done partly theoretically, partly experimentally, because the available computer was not able to synthesize larger structures than approximately that shown in Fig.9.11.

9.5. CONCLUSIONS

This, last chapter of the monograph dealt with some general principles of synthesis of wire-antenna structures with respect to their radiation pattern, and with respect to simultaneously their radiation pattern and admittance. Relatively large number of examples of optimization presented as illustrations were given, most of which were checked experimentally. They indicated that the proposed methods of wire-antenna

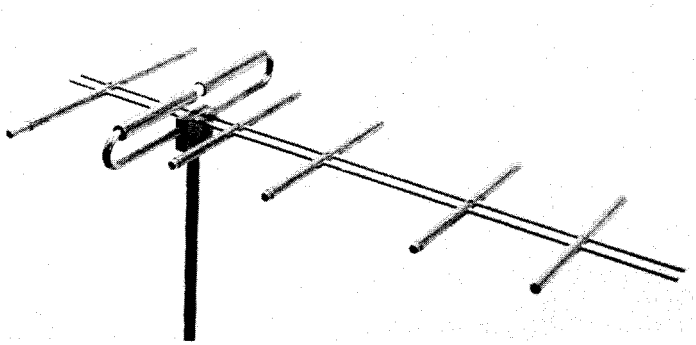

FIG.9.16. Photograph of experimental model for optimization of Uda-Yagi array with four directors, one reflector and a driven folded monopole, which incorporates a matching network. Lengths and positions of parasitic elements are variable.

synthesis may be considered as reliable engineering methods for modern design of such antenna structures. However, it was also obvious that considerable insight, or previous knowledge, was necessary for deciding both on initial values of the optimization parameters, and for adopting the desired antenna parameters. This is, perhaps, of particular importance when simultaneous optimization of radiation pattern and admittance is desired, because requirements on the radiation pattern and admittance can to some extent be contradictory.

Obviously, this and the preceding shapters presented only some basic details of the broad field of computer-aided antenna synthesis. In the authors' opinion, this novel approach to design of wire antennas is, in many respects, still in a relatively early stage of development.

APPENDIX 1

Notes on Evaluation of Integrals Encountered in Analysis of Wire Structures Assembled from Straight Wire Segments

Consider a straight current-carrying wire segment, located on the s-axis, as shown in Fig.A1.1. We wish to determine the p-component of the electric field due to this segment at the field point P in the case when the current distribution along the segment is approximated by a power-series expansion, as given in eqn.(1.16). Substituting this expansion into eqn.(1.14) and multiplying both sides of the equation thus obtained by the unit vector $\vec{i}_p$, we obtain for the p-component

$$E_p = -j\omega\mu \sum_{m=0}^{n} I_m \int_{s_1}^{s_2} (\vec{i}_p \cdot \vec{i}_s s^m + \frac{m}{k^2} s^{m-1} \frac{\partial}{\partial p}) g(r_a)\,|_{p=0}\, ds \,, \qquad (A1.1)$$

since $\vec{i}_p \cdot \text{grad} = \partial/\partial p$, where

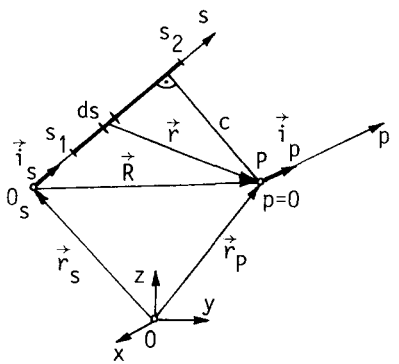

FIG.A1.1. Straight current-carrying wire segment and the field point P.

$$r_a = (r^2 + a^2)^{\frac{1}{2}}, \tag{A1.2}$$

a is the wire radius and

$$\vec{r} = \vec{r}_p + p\vec{i}_p - \vec{r}_s - s\vec{i}_s \ . \tag{A1.3}$$

The auxiliary p-coordinate was introduced to perform the differentiation involved in eqn.(A1.1). If we assume that all lengths are in electrical units (i.e., k times the real lengths), we obtain that the integrals in eqn.(A1.1) have the common form

$$P_m = \int_{s_1}^{s_2} (\vec{i}_p \cdot \vec{i}_s \, s^m + m s^{m-1} \frac{\partial}{\partial p}) \frac{\exp(-jr_a)}{r_a} \Big|_{p=0} ds \ , \quad m=0,\ldots,n \ . \tag{A1.4}$$

The length of the integration interval (s_1, s_2) is usually of the order of magnitude 1. When a matching point is in the vicinity or on the segment considered, r_a can be as small as the wire radius, which is typically of the order of magnitude 10^{-4} to 10^{-2}. Hence the integrals P_m can be pseudosingular, and therefore their numerical integration should be performed carefully.

Using elementary transformations, the integrals P_m can be expressed in terms of the integrals

$$G_m = \int_{s_1-t}^{s_2-t} u^m \frac{\exp(-jr_a)}{r_a} du \ , \quad m=0,\ldots,n \tag{A1.5}$$

and

$$S_0 = \int_{s_1-t}^{s_2-t} \frac{1}{r_a} \frac{d}{dr_a} \left[\frac{\exp(-jr_a)}{r_a} \right] du \ , \tag{A1.6}$$

where

$$t=\vec{i}_s \cdot \vec{R} \ , \quad \vec{R}=\vec{r}_p-\vec{r}_s \ , \quad u=s-t \ , \quad r_a=(u^2+c^2+a^2)^{\frac{1}{2}} \ , \quad c=(R^2-t^2)^{\frac{1}{2}} \ . \tag{A1.7}$$

The integral G_1 can be evaluated explicitly. The integrands in eqns. (A1.5) and (A1.6) have poles in the complex u-plane at

$$u = \pm j(c^2 + a^2)^{\frac{1}{2}} \quad . \tag{A1.8}$$

The integrands of G_m, m=2,...,n, have a m-fold zero at u=0, which softens the influence of the poles on the real u-axis. To integrate these integrals numerically it is very convenient to extract the pseudo-singularities. To that purpose the term $(1/r - 0.5\,r)$ should be subtracted from the integrand of G_0, the term u^m/r from the integrand of G_m ($m \geq 2$), and the term $(1/r^3 - 0.5/r + 0.125\,r)$ from the integrand of S_0. The subtracted terms can be integrated explicitly, and the remaining parts can be integrated numerically using the Gauss-Legendre quadrature formula. It appeared that the five-point formula (for $n \leq 6$) on subsegments not longer than about 1 was efficient. If the poles, given by eqn.(A1.8), are distant from the integration segment considered, this integration formula can be applied directly to the P_m integrals. All the integrals, either in eqns.(A1.4), (A1.5) or (A1.6), should be integrated simultaneously, in order to avoid repeated calculations of the same trigonometric or square-root functions (which require about five to ten times as much computing time as algebraic operations). It is possible to reduce in this manner the average c.p.u. time necessary for evaluation of one integral P_m to approximately only ten times that necessary for evaluation of a single square root.

APPENDIX 2

Notes on Hallén's Equation

We shall prove here that F(z) given by eqn.(1.25) is the general solution of eqn.(1.24) for an arbitrary constant z_0.

Let

$$w(z) = \int_{t_1(z)}^{t_2(z)} v(z,z')\,dz' \,. \tag{A2.1}$$

Then, according to the known rule of differentiation,

$$\frac{dw(z)}{dz} = \int_{t_1(z)}^{t_2(z)} \frac{\partial v(z,z')}{\partial z}\,dz' + v\left[z,t_2(z)\right]\frac{dt_2(z)}{dz} - v\left[z,t_1(z)\right]\frac{dt_1(z)}{dz} \,. \tag{A2.2}$$

If we set $v(z,z')=kS(z')\sin k(z-z')$, $t_1(z)=z_0$ (z_0=arbitrary constant) and $t_2(z)=z$, w(z) becomes precisely the last term in eqn.(1.25). By using the above rule twice to obtain dw/dz and d^2w/dz^2, it is a simple matter to show that

$$\frac{d^2w(z)}{dz^2} = -k^2w(z) + k^2S(z) \,. \tag{A2.3}$$

Substituting the adopted w(z) and the above found d^2w/dz^2 into eqn. (1.24) we immediately find that, indeed, the last term in eqn.(1.25) represents the particular solution of eqn.(1.24). Since $C_1\cos kz$ and $C_2\sin kz$ both satisfy the homogeneous equation $(k^2+d^2/dz^2)F(z)=0$ and

are mutually independent, eqn.(1.25) is the general solution of eqn. (1.24).

For a given set of two independent conditions and the value of z_0 the constants C_1 and C_2 can be found, thus obtaining the particular solution of eqn.(1.24) corresponding to these conditions. Suppose that a new constant, z_{01}, is adopted instead of z_0. In that case we have

$$\int_{z_0}^{z} S(z') \sin k(z-z')\, dz' = \int_{z_0}^{z_{01}} S(z') \sin k(z-z')\, dz' + \int_{z_{01}}^{z} S(z') \sin k(z-z')\, dz' . \qquad \text{(A2.4)}$$

The sine in the first term on the right-hand side of this equation can be written in the form $(\sin kz \cos kz' - \cos kz \sin kz')$, and then $\sin kz$ and $\cos kz$ taken in front of the two integrals thus obtained. These integrals do not contain z any more, so they are both equal to constants. Therefore, a change in z_0 is actually absorbed in the constants C_1 and C_2, so that z_0 can indeed be chosen arbitrarily.

APPENDIX 3

Evaluation of Thin-Wire Antenna Radiation Pattern and Induced Electromotive Force

The most involved part of the antenna analysis is to determine the current distribution along the antenna. Once this distribution is known, other antenna characteristics can be computed with relative ease. Evaluation of one very important antenna characteristic, the antenna admittance or impedance, is presented in Chapter 2. (The admittance is known to be the same in the antenna transmitting and receiving modes.) This appendix deals with evaluation of two other important antenna characteristics, the antenna radiation pattern and emf induced in the antenna when it is situated in an arbitrary impressed electric field. Both evaluations are based on the known current distribution along the antenna when it operates in the transmitting mode.

A3.1. EVALUATION OF RADIATION PATTERN

Consider an arbitrary thin-wire antenna, located in a homogeneous medium and excited by a suitable generator, as sketched in Fig.A3.1. In the far-field zone, i.e., for r_0 much greater than the wavelength and the overall antenna dimensions, the electric-field vector, $\vec{E}$, due to the antenna currents is transverse to the radius $\vec{r}_0$, and can be expressed in terms of the magnetic vector-potential as (see, for example, Reference 96, p.39)

$$\vec{E}(\vec{r}_0) = j\omega\vec{i}_{ro}\times[\vec{i}_{ro}\times\vec{A}(\vec{r}_0)] \ , \qquad \text{(A3.1)}$$

where $\vec{i}_{ro}=\vec{r}_0/r_0$ is the unit vector directed from the coordinate origin towards the field point. The radiated magnetic-field vector is given

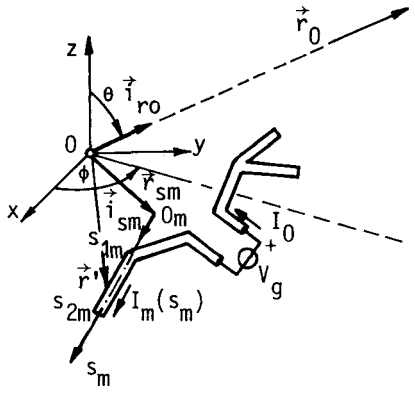

FIG.A3.1. Coordinate system for evaluation of far-zone field of a transmitting antenna.

by

$$\vec{H}(\vec{r}_0) = \frac{1}{\zeta} \vec{i}_{ro} \times \vec{E}(\vec{r}_0) \ , \tag{A3.2}$$

where $\zeta=\sqrt{\mu/\varepsilon}$ is the intrinsic impedance of the medium.

The dimensions of the wire cross-section being much smaller than the wavelength, when computing the far-field magnetic vector-potential the total current in the wire can be assumed to be along the wire axis. Thus the far-field magnetic vector-potential can be expressed approximately as

$$\vec{A}(\vec{r}_0) = \mu\, g(r_0) \sum_{m=1}^{N} \int_{s_{1m}}^{s_{2m}} \vec{i}_{sm}\, I_m(s_m) \exp(jk\vec{r}' \cdot \vec{i}_{ro})\, ds_m \ , \tag{A3.3}$$

where, as explained in Section 1.2, the antenna is assembled from N (generally curved) segments, $\vec{i}_{sm}$ is the unit vector locally tangential to the wire axis, $\vec{r}'$ is the distance from the coordinate origin to the element ds_m, and $g(r_0)$ is Green's function, given in eqn.(1.5). If the wire segments are straight instead of curved, $\vec{r}'=\vec{r}_{sm}+s_m\vec{i}_{sm}$, where $\vec{r}_{sm}$ is the distance between the coordinate origin and the s_m-axis origin. From eqns.(A3.1) and (A3.3) we thus obtain for wire antennas assembled from straight segments

$$\vec{E}(\vec{r}_0) = -jk\zeta g(r_0) \sum_{m=1}^{N} [\vec{i}_\theta(\vec{i}_\theta \cdot \vec{i}_{sm}) + \vec{i}_\phi(\vec{i}_\phi \cdot \vec{i}_{sm})] \exp(jk\vec{r}_{sm} \cdot \vec{i}_{ro}) \cdot$$

$$\cdot \int_{s_{1m}}^{s_{2m}} I_m(s_m) \exp(jks_m \vec{i}_{sm} \cdot \vec{i}_{ro})\, ds_m \,, \qquad \text{(A3.4)}$$

where $\vec{i}_\theta$ and $\vec{i}_\phi$ are the unit vectors of the spherical coordinate system. If $I_m(s_m)$ is approximated by a polynomial, as given in eqn.(1.16), or by a combined trigonometric and polynomial expansion, as in eqn.(1.30), the integrals involved in eqn.(A3.4) can be evaluated explicitly. However, when $|\vec{i}_{sm} \cdot \vec{i}_{ro}| \ll 1$, i.e., when the field point is close to the wire-segment equatorial plane, these explicit formulas are inconvenient because they involve subtraction of almost-equal terms, which results in significant numerical errors. Fortunately, the integrands in eqn. (A3.4) are well-behaved functions and the integrals can easily be evaluated numerically.

If the far-zone electric field is known, the antenna directive gain is given by

$$g_d(\vec{i}_{ro}) = \frac{|E(\vec{r}_0)|^2/\zeta}{P_r/(4\pi r_0^2)} \,, \qquad \text{(A3.5)}$$

or, in decibels,

$$G_d(\vec{i}_{ro}) = 10 \log_{10} g_d(\vec{i}_{ro}) \quad \text{(dB)} \,, \qquad \text{(A3.6)}$$

where

$$P_r = \eta P_{input} \qquad \text{(A3.7)}$$

is the radiated power, P_{input} the power fed to the antenna and η the antenna efficiency, which can be computed from eqns.(5.11)-(5.13). The antenna radiation pattern, if plotted in decibels, is determined by eqn.(A3.6). The antenna directivity is, by definition,

$$D = \max\{g_d(\vec{i}_{ro})\} \,, \qquad \text{(A3.8)}$$

and the antenna power gain is given by

$$g(\vec{i}_{ro}) = \eta g_d(\vec{i}_{ro}) \ . \qquad \text{(A3.9)}$$

Both the directive and power gains, given in eqns.(A3.5) and (A3.9), are defined with respect to an isotropic radiator radiating uniformly into the whole space. In the case of antennas above an infinite, perfectly conducting ground plane, driven at one or more points at the plane, both gains can be defined with respect to a semi-isotropic radiator, radiating uniformly only into the upper half-space. In that case the monopole-antenna gain is equal to the gain of the equivalent symmetrical dipole antenna.

A3.2. EVALUATION OF ELECTROMOTIVE FORCE INDUCED IN A RECEIVING WIRE ANTENNA

Consider a wire antenna having only one pair of closely spaced terminals, as sketched in Fig.A3.2. Let the antenna be situated in an arbitrary impressed electric field, $\vec{E}_i$, due to some distant sources. If the antenna terminals are open, a voltage V_o will appear between them, equal to the emf E_{ind} induced in the antenna (i.e., $V_o = E_{ind}$, where V_o and E_{ind} are determined with respect to the reference directions shown in Fig.A3.2). Assume that an ideal voltage generator, of voltage $V_g = V_o$, is connected between the antenna terminals, in opposition to the emf induced in the antenna [see Fig.A3.3(a)]. Obviously, no current will flow through the antenna terminals. We can represent this case as a superposition of two cases: (1) the impressed electric field, $\vec{E}_i$, present, the antenna terminals short circuited [Fig.A3.3(b)], and (2)

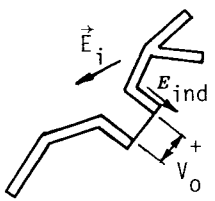

FIG.A3.2. Receiving antenna in arbitrary impressed electric field.

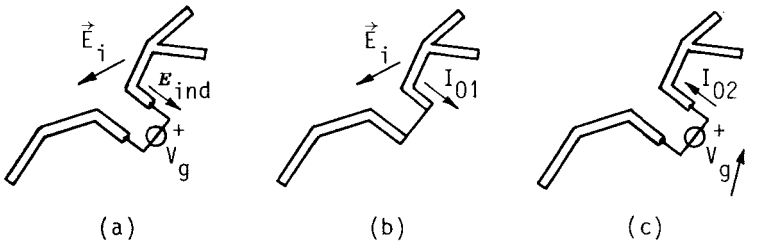

FIG.A3.3. (a) Ideal voltage generator connected between antenna terminals in opposition to emf induced in antenna. This case can be regarded as superposition of two cases denoted as (b) and (c).

the impressed electric field, $\vec{E}_i$, not present, the antenna connected to the voltage generator V_g [see Fig.A3.3(c)]. Let the current in the antenna terminals in the first case be I_{01}, and in the second case $I_{02}=I_0$, with respect to the reference directions shown in Fig.A3.3. Obviously, $I_{01}=I_{02}=I_0$. Using the reciprocity theorem specialised for the case of line currents,[112]

$$\int_L \vec{E}_{i1}\cdot(I_2 d\vec{l}) = \int_L \vec{E}_{i2}\cdot(I_1 d\vec{l}) \ , \tag{A3.10}$$

where $\vec{E}_{i1}$ is the impressed electric field in the first case, I_1 the corresponding antenna current, and $\vec{E}_{i2}$ and I_2 the impressed electric field, namely antenna current in the second case, we can easily obtain the equation

$$-V_g I_{01} = \sum_{m=1}^{N} \int_{s_{1m}}^{s_{2m}} I_m(s_m)\, \vec{i}_{sm}\cdot\vec{E}_i(\vec{r}')\, ds_m \ , \tag{A3.11}$$

where $I_m(s_m)$ is the current along the antenna when it operates in the transmitting mode, driven by the generator of voltage V_g. Hence we finally obtain

$$E_{ind} = \frac{-1}{I_0} \sum_{m=1}^{N} \int_{s_{1m}}^{s_{2m}} I_m(s_m)\, \vec{i}_{sm} \cdot \vec{E}_i(\vec{r}')\, ds_m \ . \qquad \text{(A3.12)}$$

In the special case when $\vec{E}_i$ is the electric field of a plane wave travelling in the direction of a unit vector $\vec{n}$, i.e., when $\vec{E}_i(r') = \vec{E}_{io} \exp(-jk\vec{r}' \cdot \vec{n})$, where $\vec{E}_{io}$ is the impressed electric field in the coordinate origin, we obtain

$$E_{ind} = -\vec{E}_{io} \cdot \left[\frac{1}{I_0} \sum_{m=1}^{N} \int_{s_{1m}}^{s_{2m}} \vec{i}_{sm}\, I_m(s_m) \exp(-jk\vec{r}' \cdot \vec{n})\, ds_m \right] . \qquad \text{(A3.13)}$$

Note that the term in brackets in eqn.(A3.13) is actually independent of the current I_0, and that the sum in this term is equal to the corresponding sum in eqn.(A3.3), provided that $\vec{n} = -\vec{i}_{ro}$.

APPENDIX 4

Notes on TEM Magnetic-Current Frill Approximation of Coaxial-Line Excitation

This appendix deals with the following topics related to the TEM magnetic-current frill approximation of coaxial-line excitation: with evaluation of near-zone and far-zone fields due to the TEM frill, with a method for determining the antenna admittance based on the complex power of magnetic currents [which is an alternative to eqn.(2.27)], and, finally, with the antenna admittance correction which is necessary in the case when boundary conditions in the excitation region are not satisfied adequately.

A4.1. NEAR-ZONE FIELD OF TEM MAGNETIC-CURRENT FRILL

The near-zone electric field due to the TEM magnetic-current frill can be determined starting from eqn.(2.4). Let, for simplicity, the annular magnetic-current frill be located in the xOy plane, and the field point P in the xOz plane, as shown in Fig.A4.1. In the case considered, the surface magnetic currents are circular, of density

$$\vec{J}_{ms} = \frac{-2V}{\rho \ln(b/a)} \vec{i}_{\phi} , \tag{A4.1}$$

according to eqns.(2.16) and (2.17), and Fig.2.6. From Fig.A4.1 we have $r=(x^2+z^2+\rho^2-2x\rho\cos\phi)^{\frac{1}{2}}$, $dS=\rho\, d\rho\, d\phi$ and $\vec{i}_{\phi}\times\vec{i}_r=(\vec{i}_z\times\vec{i}_{\rho})\times\vec{i}_r=\vec{i}_{\rho}(\vec{i}_r\cdot\vec{i}_z)-\vec{i}_z(\vec{i}_r\cdot\vec{i}_{\rho})$. Noting that $\operatorname{grad} g(r)=\frac{dg(r)}{dr}\vec{i}_r$, $\vec{i}_r\cdot\vec{i}_z=z/r$ and $\vec{i}_r\cdot\vec{i}_{\rho}=\cos\psi$, from eqn.(2.4) we obtain for the elemental electric field

$$d\vec{E}_i = J_{ms}\left(\frac{z}{r}\vec{i}_{\rho} - \cos\psi\,\vec{i}_z\right)\frac{dg(r)}{dr}\,\rho\, d\rho\, d\phi . \tag{A4.2}$$

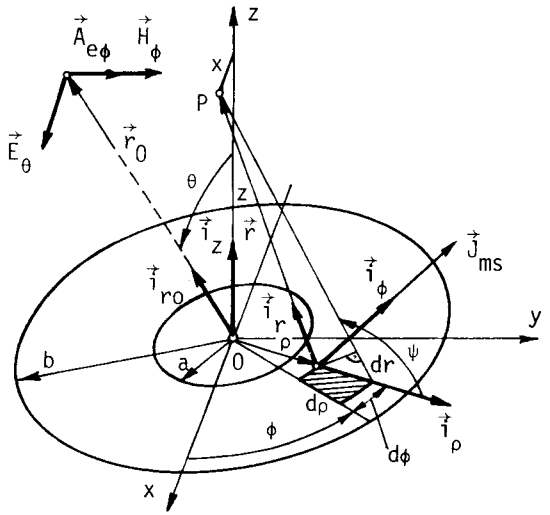

FIG.A4.1. Coordinate system for evaluating near-zone and far-zone electric field due to annular magnetic-current frill.

From Fig.A4.1 we also have $\vec{i}_\rho = \cos\phi\,\vec{i}_x + \sin\phi\,\vec{i}_y$, and $\cos\psi\,d\rho = -dr$. Due to symmetry, the y-component of the resultant field, E_{iy}, is zero, and for the other two components we obtain

$$E_{ix}(x,z) = 2z \int_0^\pi \int_a^b \cos\phi\ \rho J_{ms}(\rho)\ \frac{1}{r}\frac{dg(r)}{dr}\,d\rho\,d\phi \tag{A4.3}$$

and

$$E_{iz}(x,z) = 2\int_0^\pi \int_{\rho=a}^b \rho J_{ms}(\rho)\,dg(r)\,d\phi = 2\int_0^\pi \rho J_{ms}(\rho)\,g(r)\Big|_{\rho=a}^b d\phi -$$

$$- 2\int_0^\pi \int_a^b \frac{\partial}{\partial\rho}\left[\rho J_{ms}(\rho)\right] g(r)\,d\rho\,d\phi\ . \tag{A4.4}$$

From eqn.(A4.1) $\rho J_{ms}(\rho) = -2V/\ln(b/a)$, so that from eqns.(A4.3) and (A4.4) we finally obtain eqns.(2.18) and (2.19).

A4.2. RADIATION FIELD OF TEM MAGNETIC-CURRENT FRILL

The far-zone field due to the TEM magnetic-current frill can be determined in terms of the electric vector-potential, $\vec{A}_e$. This vector has only the ϕ-component (see Fig.A4.1) and the magnetic field due to the frill in the far zone has also only this component,

$$H_\phi(r_0,\theta) = -j\omega A_{e\phi} \ . \tag{A4.5}$$

Note that this equation is dual to eqn.(A3.1) in Appendix 3. The electric field has only the θ-component,

$$E_\theta(r_0,\theta) = \zeta \, H_\phi(r_0,\theta) \ , \tag{A4.6}$$

where $\zeta=\sqrt{\mu/\varepsilon}$ is the intrinsic impedance of the medium. The far-zone electric vector-potential can be evaluated as

$$\vec{A}_e = \varepsilon g(r_0) \int_S \vec{J}_{ms} \exp(jk\rho \vec{i}_\rho \cdot \vec{i}_{ro}) \, dS \ , \tag{A4.7}$$

which is, essentially, an equation dual to eqn.(A3.3) in Appendix 3. In eqn.(A4.7), $\vec{r}_0$ is the distance between the frill center and the field point, S is the surface of the frill, $\vec{J}_{ms}$ is given by eqn.(A4.1) and $\vec{i}_{ro}=\sin\theta \, \vec{i}_x + \cos\theta \, \vec{i}_z$, where, for simplicity, the field point is taken to be located in the xOz plane. Hence we have

$$A_{e\phi} = \varepsilon g(r_0) \int_{-\pi}^{\pi} \int_a^b \frac{-2V}{\rho \, \ln(b/a)} \cos\phi \exp(jk\rho \cos\phi \sin\theta) \, \rho \, d\rho \, d\phi \ . \tag{A4.8}$$

The integration over ρ in eqn.(A4.8) can be performed explicitly, to obtain

$$A_{e\phi} = \varepsilon g(r_0) \frac{4\pi V}{\ln(b/a)} \frac{j}{k \sin\theta} \left[\frac{1}{2\pi} \int_{-\pi}^{\pi} \exp(jk\rho \cos\phi \sin\theta) d\phi \right] \Bigg|_{\rho=a}^{b} \ . \tag{A4.9}$$

The integral in brackets in eqn.(A4.9) is, essentially, the zeroth-order Bessel function of the first kind. Hence E_θ is finally given by

$$E_\theta(r_0,\theta) = - \frac{4\pi V}{\ln(b/a)} \frac{J_0(ka \sin\theta) - J_0(kb \sin\theta)}{\sin\theta} g(r_0) \ . \tag{A4.10}$$

Noting that, for a small argument t, $J_0(t) \simeq 1-t^2/4$, an approximate far-field expression is obtained. It is essentially the same as that presented in Reference 21, and is also valid only if kb<<1.

A4.3. DETERMINATION OF ANTENNA ADMITTANCE FROM POWER GENERATED BY MAGNETIC-CURRENT FRILL

A rigorous method for determining the antenna admittance in terms of the coaxial-line TEM mode must take higher-order modes into account (see Subsection 2.3.3). All other procedures necessarily involve certain approximations, and therefore introduce an error in the theoretical results for the antenna admittance. Since eqn.(2.27) is based on approximation of *both* the electric and magnetic field at the coaxial-line opening (Fig.2.5) by the TEM mode, it is, also, theoretically incorrect. A somewhat different approach to determining the antenna admittance is presented in this section. It is based on the TEM approximation of the electric field in Fig.2.5, while the magnetic field is, essentially, assumed to contain higher-order modes.

The TEM approximation of the electric field results in the equivalent system shown in Fig.2.6(b), where the density of the magnetic currents is given by eqn.(A4.1). Once the antenna current distribution is obtained, the monopole-antenna admittance is computed as

$$Y = S^*_{frill}/(2|V|^2) \ , \tag{A4.11}$$

where S_{frill} is the complex power of the magnetic-current frill in Fig. 2.6(b), and the asterisk denotes the complex conjugate. The frill complex power can be computed as

$$S_{frill} = - \int_{frill} \vec{J}_{ms} \cdot \vec{H}^*_{total} \, dS \ , \tag{A4.12}$$

where

$$\vec{H}_{total} = \frac{1}{\mu} \, curl \, \vec{A} - j\omega \vec{A}_e \ . \tag{A4.13}$$

$\vec{A}$ is the magnetic vector-potential due to the antenna currents, given in eqn.(1.3), and $\vec{A}_e$ the electric vector-potential due to the magnetic currents, given in eqn.(2.3).

In the case of the cylindrical antenna shown in Fig.2.6(b), $\vec{H}_{total}$ has only the ϕ-component, which is independent of the ϕ-coordinate, due to symmetry. Thus from eqns.(A4.1), (A4.11) and (A4.12) we obtain

$$Y = \frac{2\pi}{V \ln(b/a)} \int_a^b H_{\phi\ total}(\rho)\, d\rho \ . \tag{A4.14}$$

According to Maxwell's equations, $H_{\phi\ total}(\rho)$ is determined by I(0) *and* the displacement current (i.e., by the flux of the vector $j\omega\vec{D}$) through the annular ring of radii a and ρ. At lower frequencies and/or when $a \simeq b$, the displacement current can be neglected, and we have, approximately, $H_{\phi\ total}(\rho) = I(0)/(2\pi\rho)$, so that eqn.(A4.14) is reduced to $Y = I(0)/V$. If the displacement current is not negligible [for example, at higher frequencies or for monopole lengths comparable with (b-a)], eqn.(A4.14) yields different results from eqn.(2.27).

Eqn.(A4.14) can be obtained also using another approach, as follows. The antenna admittance is defined in terms of the TEM mode at the coaxial-line opening as

$$Y = \frac{I_{TEM}(0)}{V} \tag{A4.15}$$

(see Subsection 2.3.3), where $I_{TEM}(0) = 2\pi\rho H_{TEM}(\rho) \neq I(0)$, and $\vec{H}_{TEM}$ is the TEM component of the total magnetic field at the coaxial-line opening. If we recall the orthogonality property of the TEM and higher-order modes in the coaxial line,

$$\int_{frill} \vec{H}_{TEM} \cdot \vec{H}_{total}\, dS = \int_{frill} H_{TEM}^2\, dS \ , \tag{A4.16}$$

substitute H_{TEM} by $I_{TEM}(0)/(2\pi\rho)$ and evaluate the integral on the right-hand side of the last equation, we obtain

$$I_{TEM}(0) = \frac{1}{\ln(b/a)} \int_{frill} \frac{1}{\rho} \vec{i}_\phi \cdot \vec{H}_{total} \, dS = \frac{2\pi}{\ln(b/a)} \int_a^b H_{\phi\, total}(\rho) \, d\rho \, . \tag{A4.17}$$

Combining eqns.(A4.15) and (A4.17) we obtain again eqn.(A4.14). Although this extraction of the TEM magnetic-field mode from the total field at the coaxial-line opening resembles the approach in Subsection 2.3.3, and eqn.(A4.14) is correct, the result is still only an approximation. We make here an error in computing $\vec{H}_{total}$, because we assume that the electric field at the coaxial-line opening is given solely by the TEM mode, thus neglecting higher-order electric-field modes.

If the radial currents at the antenna ends are neglected (which cannot be done only when the antenna is very short), the magnetic vector-potential, $\vec{A}$, at the magnetic-current frill has but the z-component, which depends on ρ and z only. Hence, $\text{curl}\, \vec{A} = -(\partial A_z/\partial\rho)\vec{i}_\phi$. Since the electric vector-potential, $\vec{A}_e$, has only the ϕ-component, from eqns. (A4.13) and (A4.14) we obtain for the antenna admittance

$$Y = \frac{2\pi}{V \ln(b/a)} \left\{ \frac{1}{\mu} [A_z(\rho=a) - A_z(\rho=b)] - j\omega \int_a^b A_{e\phi} \, d\rho \right\}_{|z=0} . \tag{A4.18}$$

Essentially, this equation is simpler than eqn.(A4.14), because $\vec{H}_{total}$ in eqn.(A4.14) must be computed as the curl of the magnetic vector-potential.

As an illustration, consider a quarter-wavelength monopole of radius a=0.01 λ, driven by a coaxial line with b/a=2.3. Eqn.(2.27) yields for the antenna admittance I(0)/V=(17.7975 - j6.4388) mS. The first term in eqn.(A4.18), corresponding to the difference of the two magnetic vector-potentials, equals (17.7939 - j7.5286) mS, and the total result according to eqn.(A4.18) is (17.7942 - j6.5919) mS. As it can be seen, eqn. (A4.18) yields practically the same result for the antenna conductance as eqn.(2.27), while the susceptance given by eqn.(A4.18) is smaller for 0.1531 mS, which corresponds to a negative capacitance. Numerical experiments have shown that this capacitance depends practically only

on the physical dimensions of the coaxial-line cross-section, and is independent of the antenna length and frequency. Eqn.(A4.18) yields results which are between those obtained by eqn.(2.27) and those presented in Subsection 2.3.3. It should be noted, however, that evaluation of the right-hand side expression in eqn.(A4.18) is very difficult because the magnetic vector-potential must be computed without approximations (which involves numerical evaluation of double integrals, one of which is singular for $\rho=a$), and computation of the term containing the electric vector-potential involves a triple singular integral. Since the final correction is practically most often insignificant, eqn.(2.27) is preferred to eqn.(A4.18).

A4.4. ANTENNA ADMITTANCE CORRECTION WHEN BOUNDARY CONDITIONS ARE SATISFIED INADEQUATELY

If the boundary conditions are not satisfied adequately, the electric currents in the equivalent system shown in Fig.2.6(c) are situated in a non-zero axial electric field. Therefore they generate non-zero complex power, in addition to the power generated by the magnetic-current frill. Taking into account the total generated power, a method is developed in this section for estimating and, to some extent, for correcting the error introduced into the antenna admittance when calculated from eqns. (2.27) and (A4.14).

We shall assume that the coaxial-line dimensions, a and b, are much smaller than the wavelength, and that the boundary conditions are inadequately satisfied only in the excitation region, in a zone which, measured along the z-axis, is much shorter than the wavelength. The complex power generated by the electric currents can be computed as

$$S_e = - \int_{\text{antenna}} (\vec{E}+\vec{E}_i)\cdot\vec{J}_s^{*}\, dS \ . \qquad \text{(A4.19)}$$

As can be seen from Fig.2.7, the z-component of the total electric field at the antenna surface is practically identical to that at the z-axis. Therefore eqn.(A4.19) can be approximated by

$$S_e \simeq -\int_L (E_z + E_{iz})\, I(z)^*\, dz \ , \tag{A4.20}$$

where L is a path along the z-axis in the excitation region, from z=-d to z=d. This path being relatively short, the antenna current intensity, I(z), can be approximately taken to be constant in this region and equal to I(0). Thus we have

$$S_e \simeq -I(0)^* \int_{-d}^{d} (E_z + E_{iz})\, dz = 2\Delta V\, I(0)^* \ , \tag{A4.21}$$

where

$$\Delta V = -\int_0^d (E_z + E_{iz})\, dz \ . \tag{A4.22}$$

From eqns.(A4.11) and (A4.12) and the discussion following eqn.(A4.14) we can deduce that for kb<<1 the power generated by the magnetic-current frill is very closely equal to $2V\, I(0)^*$. Thus the total power generated by the electric and magnetic currents is

$$S_{frill} + S_e = 2(V + \Delta V)\, I(0)^* \ . \tag{A4.23}$$

Suppose now that we retain the approximate electric-current distribution along the antenna, while we seek for a new voltage instead of V, which would give correct results for the total generated power, and thus also for the antenna admittance. It is obvious from eqn.(A4.23) that $(V + \Delta V)$ is exactly what we need. Therefore we have for the monopole-antenna admittance

$$Y = \frac{I(0)}{V + \Delta V} \simeq \frac{I(0)}{V}\left(1 - \frac{\Delta V}{V}\right) \tag{A4.24}$$

if $|\Delta V/V| << 1$. Although approximate, eqn.(A4.24) can be used successfully to correct errors of the order of few percents in the monopole-antenna admittance due to inadequate satisfaction of the boundary conditions in the excitation region (i.e., due to inaccurate approximation of the current distribution). However, the integral in eqn.(A4.22) is

very time-consuming to compute, and it is therefore always more efficient to provide in advance a sufficiently accurate approximation of the antenna current distribution.

It should be noted that the ratio $|\Delta V/V|$ can be used as a very good measure of accuracy of the approximate antenna current distribution, because the smaller is this ratio, the better is the approximation.

APPENDIX 5

Admittance of Monopole Antennas Driven by Coaxial Line

In this appendix plots are presented showing conductance and susceptance of the monopole antenna sketched in Fig.2.5, located above an infinite, perfectly conducting ground plane and fed in that plane by means of a coaxial line, versus monopole radius, a, and height, h. The medium is assumed to be a vacuum both above the perfectly conducting plane and in the coaxial line. These results were obtained by the two-potential equation, formulated to include the end effect, according to Section 3.4. The coaxial-line excitation was approximated by a TEM magnetic-current frill, as explained in Subsection 2.3.1. No higher-order mode correction was included. In Figs.A5.1-A5.3 the monopole admittance is shown plotted versus the normalized monopole height h/λ (which includes the hemispherical end cap), for $a/\lambda=0.0001$, 0.001 and 0.01, and a coaxial line of characteristic admittance $Y_c=20$ mS (i.e., characteristic impedance $Z_c=50\ \Omega$), which corresponds to $b/a=2.3$, where b is the outer coaxial-line radius. To make these plots applicable for other coaxial-line dimensions, shown in Fig.A5.4 is the correction in susceptance, ΔB (which should be added to the values shown in Figs. A5.1-A5.3), versus the coaxial-line characteristic impedance. The conductance is practically independent of the coaxial-line dimensions.

Accuracy of the theoretical results presented in the plots is believed to be better than 5% when compared with the best available experimental results, except for values of susceptance (B) less than about 1 mS.

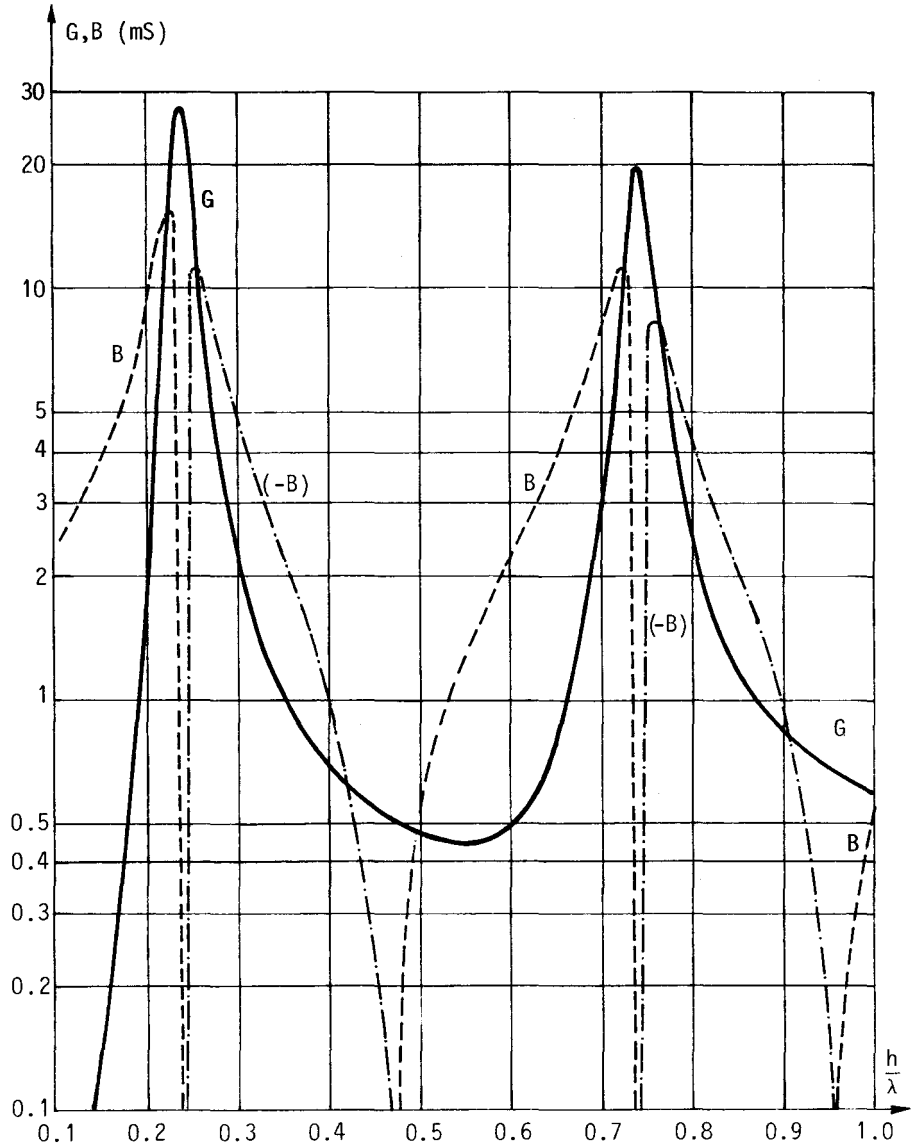

FIG.A5.1. Monopole conductance (G) and susceptance (B) versus normalized monopole height, for $a/\lambda=0.0001$.

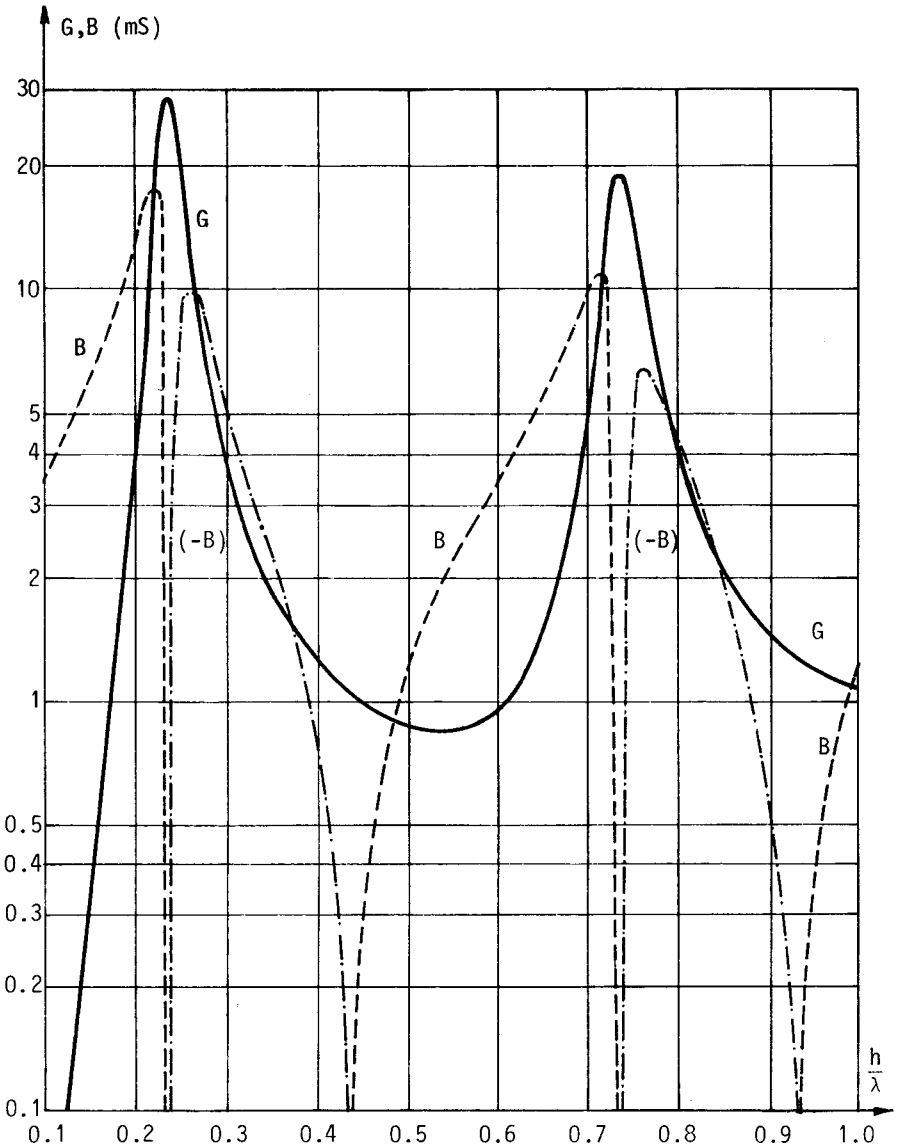

FIG.A5.2. Monopole conductance (G) and susceptance (B) versus normalized monopole height, for $a/\lambda=0.001$.

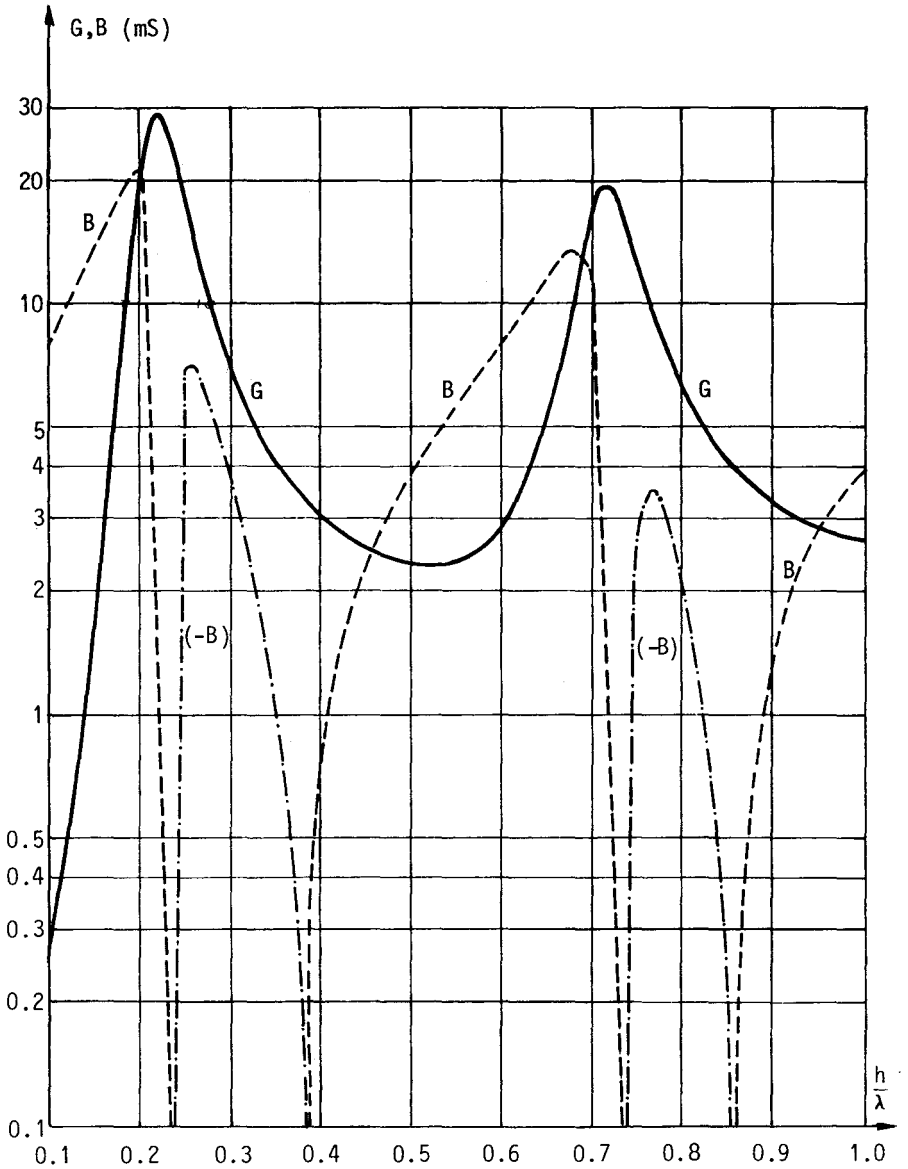

FIG.A5.3. Monopole conductance (G) and susceptance (B) versus normalized monopole height, for $a/\lambda=0.01$.

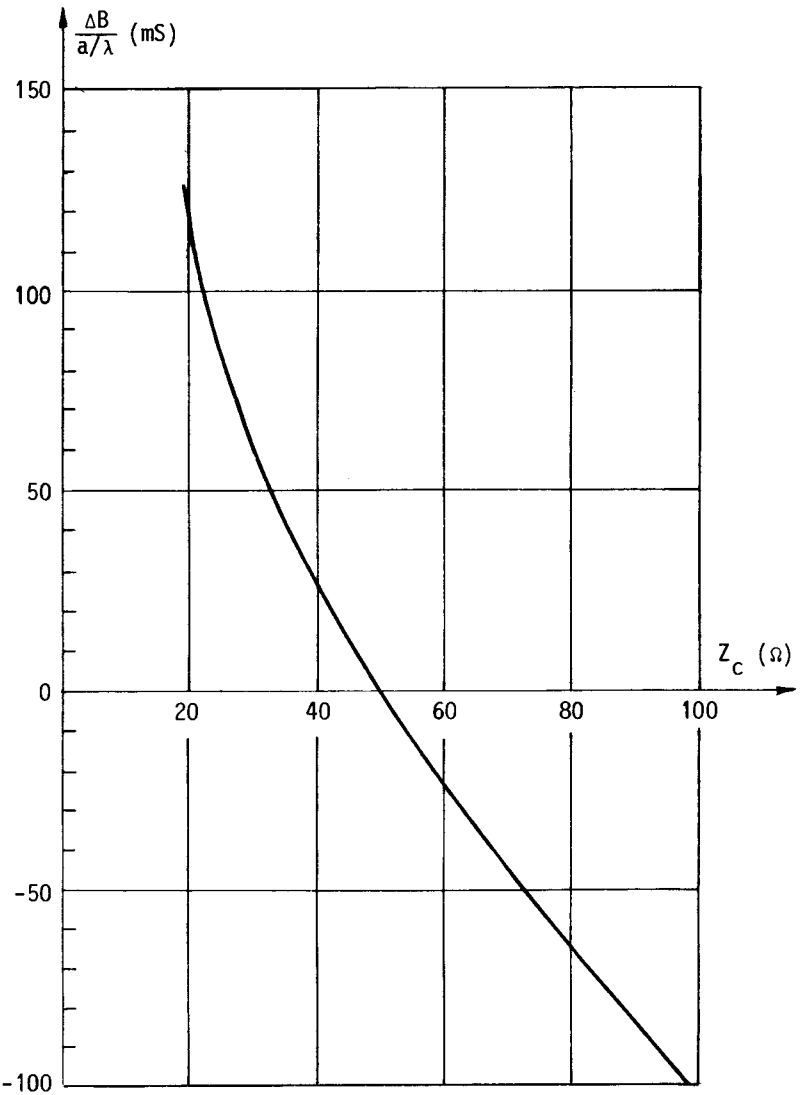

FIG.A5.4. Susceptance correction (ΔB) versus coaxial-line characteristic impedance, Z_c.

APPENDIX 6

Field Intensity Versus Radiated Power, Height and Thickness of a Vertical Monopole Antenna Above Perfectly Conducting Ground Plane[113]

Of considerable interest to communications engineers is the electric field intensity at a required distance from the transmitting antenna, for a given power radiated by the antenna. This field can be calculated relatively easily for wire-antenna structures once current distribution in the antenna is known, using the formulas derived in Appendix 3. However, for the frequently used cylindrical symmetrical wire antenna, or its asymmetrical equivalent above ground plane, it is very useful to have these results in the form of a diagram. Such a diagram is presented in this appendix.

Shown in Fig.A6.1 is a diagram representing unattenuated radiated electric-field intensity of vertical cylindrical monopole antennas, at a point on the ground at a reference distance of 1 km from the antenna radiating a reference power of 1 kW, versus the antenna electrical height, kh, with the antenna height-to-diameter ratio, h/2a, as parameter. The diagram was obtained by assuming current distribution along the antennas of the form (Reference 3, p.254)

$$I(z) = V\{A \sin k(h-z) + B[1 - \cos k(h-z)]\} , \qquad (A6.1)$$

where V is the driving monopole voltage, and power radiated was calculated as the flux of the Poynting vector through a large hemisphere centered at the monopole. Since the radiation pattern of antennas with current approximation as in eqn.(A6.1) is known to be quite accurate,[114] there was no need to use a better approximation for current distribution. Note that the commonly used diagram corresponding to that in Fig.A6.1 is based on the sinusoidal distribution of current,

and therefore does not take into account the thickness of the antenna.[115] (This classical curve coincides with the curve labelled $h/2a \to \infty$ in Fig.A6.1.) Fig.A6.1 shows that thickness of the antenna becomes an important factor for monopole electrical heights larger than about 190°.

For a power of P kW radiated by a monopole antenna and for a distance of d km from the antenna, the value of E from the diagram should be multiplied by $\sqrt{P}/d$. If the radiated field in the plane of symmetry of a symmetrical antenna is needed instead, P should be substituted by $P_{dipole}/2$.

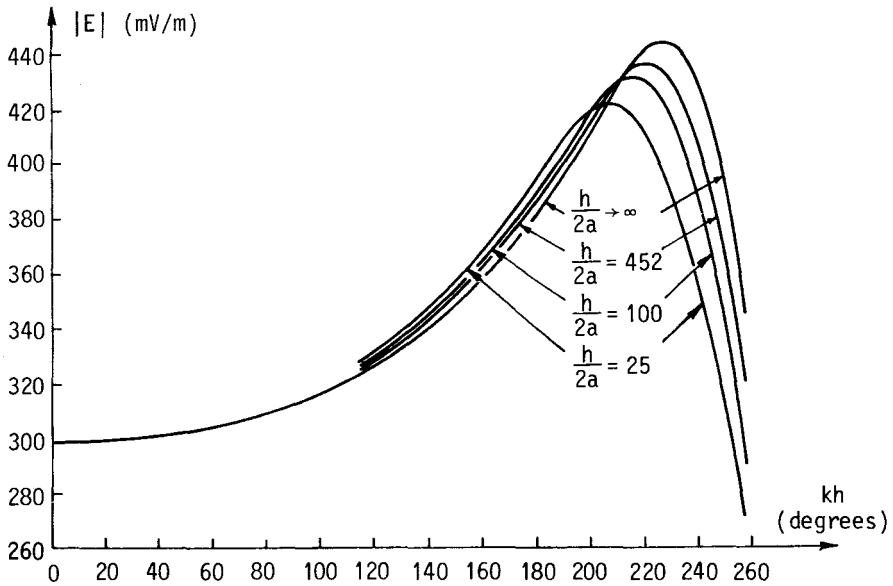

FIG.A6.1. Unattenuated electric-field intensity on the ground, at 1 km from a ground-based vertical cylindrical monopole antenna, per kilowatt radiated power, with height-to-diameter ratio h/2a as parameter. (Ref.113)

APPENDIX 7

Simplex Optimization Procedure[80]

Let $X=(x_1,\ldots,x_n)$ be a vector in the n-dimensional space, and f(X) a real function of X. We wish to search for a local minimum of f(X) using the simplex optimization procedure. We shall refer to simplex as to a polyhedron in the n-dimensional space, having (n+1) vertices at points X_i, i=0,...,n. This procedure can be divided into the following steps:

1. Given the starting point $X_0=(x_{01},\ldots,x_{0n})$ and the initial step S, form the initial regular simplex, consisting of points $X_0,X_1,\ldots,X_n$, the coordinates of which are

$$x_{ik} = \left\{ \begin{array}{ll} \dfrac{\sqrt{n+1}-1}{n\sqrt{2}} S + x_{0k}, & k\neq i \\ \dfrac{\sqrt{n+1}+n-1}{n\sqrt{2}} S + x_{0k}, & k=i \end{array} \right\}, \quad i,k=1,\ldots,n, \tag{A7.1}$$

and compute values $y_i=f(X_i)$, i=0,...,n .

2. Search the set $\{y_i\}$ to find the maximal, second maximal and the minimal value, i.e.,

$$y_h = f(X_h) = \max_i\{y_i\}, \quad y_s = f(X_s) = \max_{i\neq h}\{y_i\}, \quad y_l = f(X_l) = \min_i\{y_i\}, \tag{A7.2}$$

and test for termination of the optimization procedure.

3. Determine the centroid of the points X_i, $i\neq h$,

$$X_c = \frac{1}{n} \sum_{\substack{i=0 \\ i\neq h}}^{n} X_i . \tag{A7.3}$$

4. Reflect the point X_h with respect to X_c to obtain

$$X_r = 2X_c - X_h \ , \tag{A7.4}$$

and compute $y_r=f(X_r)$.

If $y_r<y_1$ proceed to step 5.

If $y_1<y_r<y_s$ replace X_h by X_r and y_h by y_r and return to step 2.

If $y_s<y_r<y_h$ replace X_h by X_r and y_h by y_r and proceed to step 6.

If $y_h<y_r$ proceed to step 6.

5. Expand the point X_r with respect to X_c to obtain

$$X_e = 2X_r - X_c \ , \tag{A7.5}$$

and compute $y_e=f(X_e)$.

If $y_e<y_1$ replace X_h by X_e and y_h by y_e and return to step 2.

If $y_1<y_e$ replace X_h by X_r and y_h by y_r and return to step 2.

6. Contract the point X_h with respect to X_c to obtain

$$X_k = 0.5(X_h + X_c) \ , \tag{A7.6}$$

and compute $y_k=f(X_k)$.

If $y_k<y_h$ replace X_h by X_k and y_h by y_k and return to step 2.

If $y_h<y_k$ replace X_i, $i\neq1$, by

$$X_i' = 0.5(X_i + X_1), \quad i=0,\ldots,n \ , \quad i\neq1 \ , \tag{A7.7}$$

whereby the simplex is reduced towards the "lowest" point X_1. Compute $y_i=f(X_i)$, $i\neq1$, and return to step 2.

In the original Nelder-Mead's algorithm, criterion for termination of the simplex optimization procedure is based on comparison of the values y_i, $i=0,\ldots,n$, and the computed value at the centroid, $y_c=f(X_c)$. However, such a test requires in each iteration one additional evaluation of $f(X)$, for $X=X_c$. By avoiding the computation of $f(X_c)$ the c.p.u. time can be significantly reduced (on average for more than 30%) if the computation of $f(X)$ is time-consuming, such as is the case in an-

tenna optimization. Therefore other tests for termination of the optimization procedure can be adopted, such as:

1. The largest distance between any two points X_i and X_j is smaller than a prescribed value.

2. The difference $y_h - y_l$ is smaller than a prescribed value.

3. The maximal prescribed number of iterations is attained.

4. $f(X_l)$ is smaller than a prescribed value (i.e., the antenna performance is satisfactory, although the local optimum is not attained).

References

1. Pocklington, H.E., "Electrical oscillations in wires", Cambridge Phil. Soc. Proc., Vol. 9, 1897, pp.324-332.

2. Hallén, E., "Theoretical investigation into the transmitting and receiving qualities of antennae", Nova Acta Soc. Sci. Upsal., 1938, pp.1-44.

3. King, R.W.P., *The Theory of Linear Antennas* (Harvard University Press, 1956).

4. Newman, E.H., Schrote, M.R., Djordjević, A.R., Popović, B.D. and Dragović, M.B., "Some effects of the circumferential polarization of current on thin-wire antennas", IEEE Trans., AP-29, 1981, pp.815-817.

5. Popović, B.D., "Electromagnetic field theorems (a review)", Proc. IEE, Part A, 1981, pp.47-63.

6. Imbraile, W.A., "Applications of the method of moments to thin-wire elements and arrays", in Mittra, R. (Ed.), *Numerical and Asymptotic Techniques in Electromagnetics* (Springer-Verlag, Berlin, 1975).

7. Waterman, P.C., "New formulation of acoustic scattering", J. Acoust. Soc. Am., Vol.45, 1969, pp.1417-1429.

8. Djordjević, A.R., Popović, B.D. and Dragović, M.B., "A rapid method for analysis of wire-antenna structures", Archiv für Elektrotechnik, Vol. 61, 1979, pp.17-23.

9. Harrington, R.F., *Field Computation by Moment Methods* (Macmillan, New York, 1968).

10. Popović, B.D., "Polynomial approximation of current along thin symmetrical cylindrical dipoles", Proc. IEE, Vol. 117, 1970, pp. 873-878.

11. Popović, B.D., "Theory of cylindrical antennas with lumped impedance loadings", The Radio and Electronic Eng., Vol. 43, 1973, pp.243-248.

12. Harrington, R.F., "Straight wires with arbitrary excitation and loadings", IEEE Trans., AP-15, 1967, pp.502-515.

13. Boyce, E.W. and DiPrima, R.C., *Elementary Differential Equations and Boundary Value Problems* (John Wiley and Sons, New York, 1977), p.126.

14. Schelkunoff, S.A., *Advanced Antenna Theory* (John Wiley and Sons, New York, 1952), p.130.

15. Dragović, M.B. and Popović, B.D., "Combined trigonometric and polynomial expansion for current along cylindrical antennas of large length", Proc. 1st ICAP, London, 1978 (IEE Conf. Publ. No. 169), pp.408-412.

16. Dragović, M.B., "On synthesis of cylindrical antennas with concentrated loadings", D.Sc. Thesis, Univ. of Belgrade, Dept. of El. Eng., 1979 (in Serbo-Croatian).

17. Mack, R.B., "A study of circular arrays", Cruft Lab., Harvard University, Techn. Reports 382 and 383, 1963.

18. Popović, B.D., "Analysis of two identical arbitrarily located thin asymmetrical antennas", Proc. IEE, Vol. 117, 1970, pp.1735-1740.

19. Popović, B.D., "On polynomial approximation of current along thin asymmetrical cylindrical dipoles", IEEE Trans., AP-19, 1971, pp. 117-120.

20. Popović, B.D. and Surutka, J.V., "A variational solution to the problem of an asymmetrical cylindrical dipole", IEEE Trans., AP-19, 1971, pp.17-22.

21. Tsai, L.L., "A numerical solution for near and far fields of an annular ring of magnetic current", IEEE Trans., AP-20, 1972, pp. 569-576.

22. Thiele, G.A., "Wire antennas", in Mittra, R. (Ed.), *Computer Techniques for Electromagnetics* (Pergamon Press, Oxford, 1973).

23. Miller, E.K. and Deadrick, F.J., "Some computational aspects of thin-wire modelling", in Mittra, R. (Ed.), *Numerical and Asymptotic Techniques in Electromagnetics* (Springer-Verlag, Berlin, 1975).

24. Dragović, M.B., Djordjević, A.R. and Popović, B.D., "Analysis of extended boundary conditions in cylindrical antennas", Proc.

XXI Yugosl. ETAN Conf., Banja Luka, 1977, pp.II.227-II.284 (in Serbo-Croatian).

25. Dragović, M.B. and Djordjević, A.R., "Analysis of current distribution in excitation zone of cylindrical antennas", Proc. XXV Yugosl. ETAN Conf., Mostar, 1981, pp.II.583-II.590 (in Serbo-Croatian).

26. Popović, B.D., "Thin monopole antenna: finite-size belt-generator representation of coaxial-line excitation", Proc. IEE, Vol. 120, 1973, pp.544-550.

27. Landstorfer, F., "Admittanz und Stromverteilung bei linearen zylindrischen Antennen", Arch. Elec. Übertrag., Vol. 23, 1969, pp.61-69.

28. Surutka, J.V. and Popović, B.D., "A simple method for determining admittance of monopole antennas driven by a coaxial line", Arch. Elec. Übertrag., Vol. 26, 1972, pp.397-402.

29. Djordjević, A.R. and Dragović, M.B., "Analysis of excitation zone of cylindrical antennas driven by a coaxial line", Proc. XXII Yugosl. ETAN Conf., Zadar, 1978, pp.II.377-II.384 (in Serbo-Croatian).

30. Chang, D.C., "Input admittance and complete near-field distribution of an annular aperture antenna driven by a coaxial line", IEEE Trans., AP-18, 1970, pp.610-616.

31. Smythe, W.R., *Static and Dynamic Electricity* (McGraw-Hill, New York, 1968), p.84.

32. Markuwitz, N. (Ed.), *Waveguide Handbook* (McGraw-Hill, New York, 1951), p.72.

33. Surutka, J.V. and Veličković, D.M., "Theory of V-dipole antenna driven by a two-wire line", Publ. Elektrot. Fak., Univ. of Belgrade, No.109-113, Belgrade, 1976, pp.31-41.

34. Dragović, M.B. and Surutka, J.V., "Measurement of input impedance of symmetrical antennas by means of a slotted coaxial line", Proc. XIX Yugosl. ETAN Conf., Ohrid, 1975, pp.413-420 (in Serbo-Croatian).

35. Popović, B.D., *Introductory Engineering Electromagnetics* (Addison-Wesley, Reading, 1971), pp.291-292.

36. Silvester, P. and Chan, K.K., "Analysis of antenna structures assembled from arbitrarily located straight wires", Proc. IEE, Vol. 120, 1973, pp.21-26.

37. Butler, C.M., "Evaluation of potential integral singularity of

exact kernel in thin-wire calculations", IEEE Trans., AP-23, 1975, pp.293-295.

38. Taylor, C.D. and Wilton, D.R., "The extended boundary condition solution of dipole antenna of revolution", IEEE Trans., AP-20, 1972, pp.772-776.

39. Barker, T.H., *The Numerical Treatment of Integral Equations* (Oxford Univ. Press, 1977), p.68.

40. Shen, L.C., "An experimental study of imperfectly conducting dipoles", IEEE Trans., AP-15, 1967, pp.782-784.

41. Shen, L.C., "An experimental study of the antenna with non-reflecting resistive loading", IEEE Trans., AP-15, 1967, pp.606-611.

42. Popović, B.D., Dragović, M.B. and Paunović, Dj.S., "Broadband cylindrical antenna with continuous resistive and concentrated capacitive loadings", Electronics Letters, Vol. 11, 1975, pp.611-613.

43. Paunović, Dj.S. and Popović, B.D., "Broadband RC-loaded microwave cylindrical antenna with approximately real input admittance", The Radio and Electronic Eng., Vol. 47, 1977, pp.225-228.

44. Popović, B.D. and Paunović, Dj.S., "Experimental and theoretical analysis of cylindrical RC-antennas", Proc. 1st ICAP, London, 1978 (IEE Conf. Publ. No. 169), pp.331-335.

45. Hallén, E., *Electromagnetic Theory* (Chapman & Hall, London, 1962), pp.501-504.

46. Rao, B.L.J., Ferris, J.E. and Zimmerman, W.E., "Broadband characteristics of cylindrical antennas with exponentially tapered capacitive loading", IEEE Trans., AP-17, 1969, pp.145-151.

47. Popović, B.D. and Dragović, M.B., "Simple broadband cylindrical antenna with quasidistributed capacitive loading", Electronics Letters, Vol. 8, 1972, pp.148-149.

48. Popović, B.D. and Dragović, M.B., "Cylindrical antennas with constant capacitive loading", Electronics Letters, Vol. 8, 1972, pp. 396-398.

49. Popović, B.D., "Theory of imperfectly conducting thin cylindrical dipoles", Proc. IEE, Vol. 117, 1970, pp.2205-2208.

50. Popović, B.D., "Theory of cylindrical antennas with arbitrary impedance loading", Proc. IEE, Vol. 118, 1971, pp.1327-1332.

51. Wu, T.T. and King, R.W.P., "The cylindrical antenna with nonreflecting resistive loading", IEEE Trans., AP-13, 1965, pp.369-373.

52. Shen, L.C. and King, R.W.P., "Correction to 'The cylindrical antenna with nonreflecting resistive loading'", IEEE Trans., AP-13, 1965, p.998.

53. Popović, B.D., Djordjević, A.R. and Kirćanski, N.M., "Simple method for analysis of dielectric-coated wire antennas", The Radio and Electronic Eng., Vol. 51, 1981, pp.141-145.

54. Djordjević, A.R., Popović, B.D. and Kirćanski, N.M., "Analysis of ferrite-coated wire antennas", Proc. XXV Yugosl. ETAN Conf., Mostar, 1981, pp.II.551-II.558 (in Serbo-Croatian).

55. Richmond, J.H. and Newman, E.H., "Dielectric coated wire antennas", Radio Sci., Vol. 11, 1976, pp.13-20.

56. James, J.R. and Henderson, A., "Electrically short monopole antennas with dielectric or ferrite coating", Proc. IEE, Vol. 125, 1978, pp.793-803.

57. James, J.R. and Henderson, A., "Investigation of electrically small VHF and HF cavity-type antennas", Proc. 1st ICAP, London, 1978 (IEE Conf. Publ. No. 169), pp.322-326.

58. Lamensdorf, D., "An experimental investigation of dielectric-coated antennas", IEEE Trans., AP-15, 1967, pp.767-771.

59. Altshuler, E.E., "The travelling-wave linear antenna", IRE Trans., AP-9, 1961, pp.324-329.

60. Popović, B.D. and Dragović, M.B., "Capacitively loaded thin cylindrical antenna", Proc. IEE, Vol. 121, 1974, pp.101-108.

61. Nyquist, D.P. and Chen, K.M., "The travelling-wave linear antenna with nondissipative loading", IEEE Trans., AP-16, 1968, pp.21-31.

62. Popović, B.D. and Dragović, M.B., "Nonreflecting broadband capacitive termination for thin-wire antennas", Electronics Letters, Vol. 10, 1974, pp.314-315.

63. Popović, B.D., "Theory of cylindrical monopole antennas immersed in conducting media", Proc. IEE, Vol. 121, 1974, pp.252-254.

64. Popović, B.D., "Theory of cylindrical antennas in conducting media", Proc. IEE, Vol. 118, 1971, pp.507-510.

65. Iizuka, K. and King, R.W.P., "An experimental study of the properties of antennas immersed in conducting media", Cruft Lab., Harvard Univ., Sc. Report No.2, 1962.

66. Iizuka, K. and King, R.W.P., "An experimental study of the insulated dipole antenna immersed in a conducting medium", Cruft Lab., Harvard Univ., Sc. Report No.3, 1962.

67. Iizuka, K. and King, R.W.P., "The dipole antenna immersed in a homogeneous conducting medium", IEEE Trans., AP-10, 1962, pp. 384-392.

68. Popović, B.D. and Gavrilov, T.S., "Simple method for analysis of cylindrical antennas at the interface between two media", The Radio and Electronic Eng., Vol. 46, 1976, pp.553-554.

69. Coleman, B.L., "Propagation of electromagnetic disturbances along a thin wire in a horizontally stratified medium", Phil. Mag., Vol. 41, 1950, pp.276-288.

70. Iizuka, K., "An experimental investigation of the behaviour of the dipole antenna near the interface between the conducting medium and free space", Cruft Lab., Harvard Univ., Sc. Report No.4, 1963. Condensed report, under the same title, was published in IEEE Trans., AP-12, 1964, pp.27-35.

71. Sommerfeld, A.N., "Über die Ausbreitung der Wellen in der Drahtlosen Telegraphie", Ann. der Physik, Vol. 28, 1909, pp.665-736.

72. Baños, A., *Dipole Radiation in the Presence of a Conducting Half-Space* (Pergamon Press, New York, 1966).

73. Sarkar, T.K., "Analysis of arbitrarily oriented thin wire antennas over a plane imperfect ground", Arch. Elec. Übertrag., Vol. 31, 1977, pp.449-457.

74. Mitić, D.N., "Influence of finite ground conductivity on properties of horizontal wire antennas", D.Sc. Thesis, Dept. of Electronics, Univ. of Niš, 1980 (in Serbo-Croatian).

75. Fanson, P.L. and Chen, K.M., "Modification of antenna radiating characteristics with multi-impedance loading", IEEE Trans., AP-21, 1973, pp.715-721.

76. Popović, B.D., "Synthesis of cylindrical antennas with continuous impedance loading", Proc. IEE, Vol. 124, 1977, pp.425-428.

77. Poggio, A.J. and Mayes, P.E., "Bandwidth extension for dipole antennas by conjugate reactance loading", IEEE Trans., AP-19, 1971, pp.544-547.

78. Jacoby, S.L.S., Kowalik, J.S. and Pizzo, J.T., *Iterative Methods for Nonlinear Optimization Problems* (Prentice-Hall, Englewood Cliffs, 1972).

79. Adby, P.R. and Dempster, M.A.H., *Introduction to Optimization Methods* (Chapman & Hall, London, 1974).

80. Nelder, J.A. and Mead, R., "A simplex method for function minimization", Comp. Journal, Vol. 7, 1965, pp.308-313.

81. Panther, P.F., *Communication Systems Design: Line-of-Sight and Tropo-Scatterer Systems* (McGraw-Hill, New York, 1972), Sect.7.7.

82. Popović, B.D., "Synthesis of parallel cylindrical antennas with minimal mutual coupling", Bul. Serbian Acad. of Sci. and Arts, T.LXXIII, Techn. Sci. No. 16, Belgrade, 1980.

83. Popović, B.D., Paunović, Dj.S. and Gavrilov, T.S., "Theoretical and experimental analysis of cylindrical dipoles with minimal mutual coupling", Proc. 2nd ICAP, York, 1981 (IEE Conf. Publ. No. 195), pp.508-512.

84. Dragović, M.B., Popović, B.D. and Jensen, N.E., "Some experimental results for a capacitively loaded V-antenna", Electronics Letters, Vol. 9, 1973, pp.45-46.

85. Dragović, M.B. and Popović, B.D., "Inclined monopole antenna with nonreflecting capacitive termination", Proc. XVIII Yugosl. ETAN Conf., Ulcinj, 1974, pp.369-375 (in Serbo-Croatian).

86. Popović, B.D., Dragović, M.B. and Djordjević, A.R., "Optimal broadband cylindrical antenna with one and two lumped capacitive loadings", Electronics Letters, Vol. 11, 1975, pp.99-100.

87. Dragović, M.B. and Popović, B.D., "Limits of VSWR for optimal broadband capacitively loaded cylindrical antennas versus their length", Proc. 2nd ICAP, York, 1981 (IEE Conf. Publ. No. 195), pp.343-347.

88. Popović, B.D. and Dragović, M.B., "A new concept of sources of the electromagnetic field and some applications", Bul. Serbian Acad. of Sci. and Arts (to be published).

89. Stutzman, W.L. and Thiele, G.A., *Antenna Theory and Design* (John Wiley and Sons, New York, 1981), p.298.

90. Djordjević, A.R. and Popović, B.D., "Synthesis of thin-wire antennas assembled from arbitrarily interconnected straight segments", Proc. 1st ICAP, London, 1978 (IEE Conf. Publ. No. 169), pp. 403-407.

91. Djordjević, A.R., "On synthesis of thin-wire antennas", D.Sc. Thesis, Univ. of Belgrade, Dept. of El. Eng., 1979 (in Serbo-Croatian).

92. Popović, B.D., Dragović, M.B. and Djordjević, A.R., "Synthesis of broadband cylindrical monopole antenna with parasitic elements", The Radio and Electronic Eng., Vol. 47, 1977, pp.229-231.

93. Weeks, W.L., *Antenna Engineering* (McGraw-Hill, New York, 1968), p.265.

94. Surutka, J.V. and Veličković, D.M., "Theoretical and experimental analysis of a broadband antenna", Proc. XVIII Yugosl. ETAN Conf., Ulcinj, 1974, pp.359-365 (in Serbo-Croatian).

95. Winkler, L.P. and Schwartz, M., "A fast numerical method for determining the optimum SNR of an array subject to Q-factor constraint", IEEE Trans., AP-20, 1972, pp.503-505.

96. Collin, R.E. and Zucker, F.J. (Editors), *Antenna Theory, Part 1* (McGraw-Hill, New York, 1969).

97. Cheng, D.K., "Optimization techniques for antenna arrays", Proc. IEEE, Vol. 59, 1971, pp.1664-1674.

98. Mautz, J.R. and Harrington, R.F., "Computational methods for antenna pattern synthesis", IEEE Trans., AP-23, 1975, pp.507-512.

99. Perini, J. and Idselis, M., "Note on antenna pattern synthesis using numerical iterative methods", IEEE Trans., AP-19, 1971, pp.284-286.

100. Voges, R.C. and Butler, J.K., "Phase optimization of antenna array gain with constrained amplitude excitation", IEEE Trans., AP-20, 1972, pp.432-436.

101. Sarkar, T.K. and Strait, B.J., "Optimization methods for arbitrarily oriented arrays of antennas in any environment", Radio Sci., Vol. 11, 1976, pp.959-967.

102. Sahalos, J., "Synthesis and optimization for arrays of non-parallel wire antennas by the orthogonal method", IEEE Trans., AP-26, 1978, pp.886-891.

103. Harrington, R.F. and Mautz, J.R., "Pattern synthesis for loaded N-port scatterers", IEEE Trans., AP-22, 1974, pp.184-190.

104. Harrington, R.F. and Mautz, J.R., "Optimization of radar cross section of loaded N-port scatterers", IEEE Trans., AP-22, 1974, pp.697-701.

105. Bojsen, J.H., Shaer-Jacobsen, H., Nilsson, E. and Andersen, J.B., "Maximum gain of Yagi-Uda arrays", Electronics Letters, Vol. 7, 1971, pp.531-532.

106. Cheng, D.K. and Chen, C.A., "Optimum element spacing for Yagi-Uda arrays", IEEE Trans., AP-21, 1973, pp.615-623.

107. Chen, C.A. and Cheng, D.K., "Optimum element lengths for Yagi-Uda arrays", IEEE Trans., AP-23, 1975, pp.8-15.

108. Kajfež, D., "Nonlinear optimization reduces the sidelobes of Yagi antenna", IEEE Trans., AP-21, 1973, pp.714-715.

109. Kajfež, D., "Nonlinear optimization extends the bandwidth of Yagi antenna", IEEE Trans., AP-23, 1975, pp.287-289.

110. Popović, B.D. and Djordjević, A.R., "Theoretical and experimental synthesis of a broadband Yagi antenna", Proc. XXII Yugosl. ETAN Conf., Zadar, 1978, pp.II.351-II.358 (in Serbo-Croatian).

111. Dragović, M.B. and Popović, B.D., "Experimental optimization of coaxially driven Yagi antenna with a symmetrizing folded dipole", Proc. XXII Yugosl. ETAN Conf., Zadar, 1978, pp.II.359-II.366 (in Serbo-Croatian).

112. Jordan, E.C., *Electromagnetic Waves and Radiating Systems* (Prentice-Hall, New York, 1950), p.328.

113. Surutka, J.V. and Popović, B.D., "Field intensity versus radiated power, height and thickness of a linear antenna", Proc. IEE, Vol. 114, 1967, pp.923-924.

114. Surutka, J.V., "Influence of driving conditions on the vertical radiation characteristics of antifading antennas", Publ. Elektrot. Fak., Univ. of Belgrade, No.12, 1959.

115. CCIR, *Diagrammes d'Antenne* (Union Internationale des Télécommunications, Genéve, 1953), p.8.

Index

Admittance of cylindrical antennas, 32-33
  graphs of, 279-283
  measured values, 32, 48
Altshuler's antenna, 114
Antenna admittance, 53, 54, 273, 274
  corrective terms, 54-55, 275
  defined, 25, 31, 40
  determination of, 272
  measurement of, 63-65
  reference, *see* reference feeder admittance
Antenna efficiency, 142
  of resistive antennas, 139, 142, 220
Antenna synthesis
  defined, 168
  principles of, 169-170
Antennas as two-terminal networks, 24
Antennas for two frequencies, 228

Belt generator, 44
  and TEM frill, 48-49
Boundary conditions in approximate solution, 41-43
Broadband antenna, 97
  and antenna size, 212-214
  capacitive, 99, 125-128
  folded monopole, 223-224
  half-octave, 209-213
  monopole with parasites, 224-228
  octave, 209-214
  resistive, 114
  resistive-capacitive, 214-220
  Uda-Yagi, 252-254

Capacitive loading, 118
  construction of, 119, 137, 208
  measurement of, 129-132
  quasidistributed, 98-100
  values of, 132, 137
Circumferential distribution of current, 6
Coating over antennas, 100-108
  dielectric, 100-108
  ferrite, 100-108
Coaxial excitation
  approximations of, 34
    TEM frill, 35
    belt generator, 44
    higher-order modes, 48
Compensation of susceptance, 207, 214, 230
Concentrated loadings
  capacitive, 118-128
    measured values, 132
  defined, 109-111
  delta-function, 112
  influence of the number of, 123
  inductive, 136
    measured values, 138
  mixed with distributed, 139
  other approximations, 113
  resistive, 114
  used to approximate continuous, 115-117
Current approximation
  simple polynomial, 11
  trigonometric-polynomial, 19

various polynomials, 12
Curved segments, 8, 104, 264
Curved wires, 13
Cylindrical antennas
equations for, 13-20
long, 20, 88
tubular, 80-81
with flat ends, 80, 85
with hemispherical ends, 80, 84, 279

Delta-function generator
and Hallén's equation, 29
defined, 25-29
Dielectric-coated antennas, 100-108
Directive gain, expression for, 265
Directivity, 265
Discontinuities, defined, 3
Distributed loadings
approximation by lumped, 115-117
capacitive (quasidistributed), 99
defined, 93
ensuring minimal coupling, 197
in the form of coatings, 100
mixed with concentrated, 139
resistive, 96-98
stepwise approximation of, 201

Effective reflection coefficient, defined, 181
Electric field
of general wire structures 265
of magnetic-current frill, 269-271
of magnetic-current ring, 27
of monopoles, 285
Electric scalar-potential, 7, 155-161
Electric vector-potential, 27, 161, 271, 273
End effect, 41-42, 79-88
correction of, 17, 227
Equivalence theorem, 7, 26, 36
Equation of continuity, 8, 38
Excitation of antennas, 23-24
coaxial line, 34
delta-function generator, 25
two-wire line, 56-63
Excitation of wire structures, 3-4
Excitation region, defined, 3, 4, 23
Extended boundary conditions, 9, 13, 27, 47, 82, 95

Ferrite-coated antennas, 100-108

Half-octave antennas, 209-213
Hallén's equation
and delta-function generator, 29
existence of solution, 30
and two-wire line excitation, 57-58
derived, 16
end effect with, 17
for antennas above ground, 163
for antennas with concentrated loadings, 112
for antennas with distributed loadings, 95, 184
for coupled antennas, 195, 225
general solution of, 261
Homogenization of the medium, 7, 26, 37, 93

Impressed field
defined, 4
of belt generator, 46
and TEM frill, 49
of magnetic-current frill, 37
and belt generator, 49
of magnetic-current ring, 27
rapidly varying, 23
Inductive loading, 136, 241
construction of, 137
values of, 138
Internal impedance, 93

Junction
constraints on currents, 70-73
constraints on field, 73-78
definition of, 3, 69

Kirchhoff's law
first, 7, 70
second, 74

Loaded antenna, defined, 91

Loadings, definitions of, 91-92
see also capacitive loading, inductive loading, resistive loading

Magnetic vector-potential, 7
155-161, 263-264, 273
Matching points, adoption of, 11, 31, 149
Moment method, 10
Monopole
folded, 223
inclined, 248

Nonreflecting
capacitive termination, 128
resistive loading, 97, 189

Octave antennas, 209-211
Optimal broadband antennas, 206
folded monopole, 223
half-octave, 209-211
limits of VSWR of, 212-214
octave, 209-211
RC, 214-220
Uda-Yagi, 252-254
with distributed loadings, 188-192
with parasitic elements, 224
Optimization
of admittance, 179
by varying antenna shape, 220-232
by varying concentrated loadings, 202-214
by varying distributed loadings, 183-192
by varying mixed loadings, 214-220
of mutual admittance, 192-202
of radiation pattern, 235
by varying antenna shape, 243-254
by varying driving voltages, 239-241
by varying loadings, 241-243
simultaneously with admittance, 235-236, 241, 248, 250, 252
Optimization function, examples, 170, 180, 181, 186, 187, 196, 216, 236, 237, 242
Optimization methods, 173
complete search, 175
gradient, 175
simplex, 177, 287
Optimization parameters, 172

Pocklington's equation, 18
for antennas with distributed loadings, 95
Point-matching method, described, 10-11
Polynomial current approximation, 11, 12, 31
discussion of, 12
Power gain, expression for, 266
Proximity effect, correction of, 227

Quasi-distributed capacitive loading, 98

Radiation pattern, 4, 40, 265
evaluation of, 263
optimization of, *see* optimization of radiation pattern
Receiving antenna, 4, 24
emf of, 24, 266
Reference feeder admittance, 183, 192, 221, 226
Resistive loading, 96-97
construction of, 140
nonreflecting, 97, 189
stepwise approximation of, 97, 139, 201

Schelkunoff's equation, 18, 39
for antennas with distributed loadings, 95
Steplike loading, 97
Synthesis of antennas
defined, 168
general principles of, 169

TEM frill
condition for electric current imposed by, 38
field of, 37, 269-272
near zone, 269-270
radiation, 271
Transmitting antenna, 3, 24
Travelling-wave antenna
capacitive, 128, 190

resistive, 114, 139, 189
Two-potential equation
approximate solution of, 10-13
derived
for antennas above ground, 162
for antennas with distributed loadings, 95
for arbitrary structures, 5-9
for cylindrical antennas, 14, 82

Uda-Yagi array
broadband, 252
loaded, 241
with folded monopole, 249
with two reflectors, 244

Vector-potential equation, 14
for antennas with distributed loadings, 95

Wire antennas
above ground, 154
defined, 3
in homogeneous lossless media, 5
in homogeneous lossy media, 146
on the interface of two media, 150
Wire
defined, 3
thin, 3
Wire ends, 3, 69, 79
treatment of, 79-88

ELECTRONIC & ELECTRICAL ENGINEERING RESEARCH STUDIES

ANTENNAS SERIES

Series Editor: **Professor J. R. James,** *Royal Military College of Science, England*

1. **Flat Radiating Dipoles and Applications to Arrays**
   G. Dubost
2. **Analysis and Synthesis of Wire Antennas**
   B. D. Popović, M. B. Dragović *and* A. R. Djordjević

Of related interest:

ELECTRONIC CIRCUITS AND SYSTEMS SERIES

1. **Broadband Feedback Amplifiers**
   D. J. H. Maclean

ELECTRONIC DEVICES AND SYSTEMS SERIES

1. **Microwave Field-Effect Transistors—Theory, Design and Applications**
   Raymond S. Pengelly

PATTERN RECOGNITION AND IMAGE PROCESSING SERIES

1. **Statistical Pattern Classification using Contextual Information**
   K-S Fu *and* T. S. Yu
2. **Kernel Discriminant Analysis**
   D. J. Hand
3. **Nonlinear Maximum Entropy Spectral Analysis Methods for Signal Recognition**
   C. H. Chen

RESEARCH STUDIES PRESS
A DIVISION OF JOHN WILEY & SONS LTD
Chichester · New York · Brisbane · Toronto · Singapore

ISBN 0 471 90008 7